SINGLE-NUCLEON TRANSFER REACTIONS IN Br AND Mo ISOTOPES

A B S T R A C T

"SINGLE-NUCLEON TRANSFER REACTIONS IN Br AND Mo ISOTOPES"

by

Hay Chiu Cheung

Foster Radiation Laboratory — Ph.D.

Physics Department — November 1972

The $^{94,96,98,100}Mo(^{3}He,d)^{95,97,99,101}Tc$ and $^{79,81}Br(d,p)^{80,82}Br$ reactions are investigated with an 18 MeV ^{3}He beam and a 12 MeV deuteron beam, respectively, from tandem accelerators. Measurements are performed using ΔE-E silicon detector telescopes and Enge split-pole magnetic spectrograph. For the detector telescope method, techniques of 'range-energy' electronic charged particle identification are employed. A total of 198 low-lying states in $^{95,97,99,101}Tc$ and $^{80,82}Br$ are identified. Most of these states are observed for the first time. The differential cross section angular distributions of 127 of the observed states are analysed with the DWBA theory; the ℓ-transfer values, spectroscopic factors and spin-parity assignments for the levels are deduced. The results are interpreted in terms of the shell model using the spectroscopic sum rules. The observed nuclear systematics and the deduced target nucleus configurational structure are discussed.

SINGLE-NUCLEON TRANSFER REACTIONS IN Br AND Mo ISOTOPES

SINGLE-NUCLEON TRANSFER REACTIONS IN Br AND Mo ISOTOPES

by

Hay Chiu Cheung

A Thesis

Submitted to the Faculty of

Graduate Studies and Research

in Partial Fulfilment of the Requirements

for the Degree of

Doctor of Philosophy

Foster Radiation Laboratory

McGill University

November 1972

ABSTRACT

The $^{94,96,98,100}Mo(^{3}He,d)^{95,97,99,101}Tc$ and $^{79,81}Br(d,p)^{80,82}Br$ reactions are investigated with an 18 MeV ^{3}He beam and a 12 MeV deuteron beam, respectively, from tandem accelerators. Measurements are performed using Δ E-E silicon detector telescopes and Enge split-pole magnetic spectrograph. For the detector telescope method, techniques of 'range-energy' electronic charged particle identification are employed. A total of 198 low-lying states in $^{95,97,99,101}Tc$ and $^{80,82}Br$ are identified. Most of these states are observed for the first time. The differential cross section angular distributions of 127 of the observed states are analysed with the DWBA theory; the ℓ-transfer values, spectroscopic factors and spin-parity assignments for the levels are deduced. The results are interpreted in terms of the shell model using the spectroscopic sum rules. The observed nuclear systematics and the deduced target nucleus configurational structure are discussed.

ACKNOWLEDGEMENTS

It is a pleasure to express my gratitude to Dr. S.K. Mark, Director of the Foster Radiation Laboratory, for his guidance, instruction and encouragement throughout the course of this work. His careful attention to detail and insight into many of the experimental and theoretical aspects of this research, and his patience in correcting this manuscript are deeply appreciated.

I would like to thank Dr. J.E. Kitching for his instruction and advice, particularly in the theoretical analysis of this work. Thanks are also due to Dr. J.K.P. Lee and Dr. P.F. Hinrichsen for their valuable assistance and many illuminating discussions. I am also indebted to Mr. J.L. Schoonover for the long periods of continuous cooperation in the experiments and the many hours he has devoted to proof-reading this thesis.

Acknowledgements are also due to Dr. P. Depommier, Director of Laboratoire de Physique Nucleaire, Université de Montréal and Dr. J.A. Kuehner, Director of Tandem Accelerator Laboratory, McMaster University for their hospitality toward the McGill Nuclear Physics Group; and, the staffs of these two laboratories, for their technical help during the experiments. I would also like to thank Dr. S.I. Hayakawa and Dr. J. Waddington for their help in the experiment of $^{98}Mo(^{3}He,d)^{99}Tc$, and to thank Dr. T.Y. Li

for his assistance during the work of the (d,p) reactions.

Thanks are also due to Mrs. P. Grier for her typing this thesis, and Mr. G. Popow and Mr. G. Sham for preparing the diagrams for me.

Finally, the financial support provided by the J.W. McConnell Memorial Fellowships (1969-72) and by the Laboratory on behalf of the Atomic Energy Control Board of Canada are gratefully acknowledged.

TABLE OF CONTENTS

LIST OF TABLES

LIST OF FIGURES

CHAPTER I

INTRODUCTION

The studies of nuclear reactions involving a beam of projectiles impinging upon a target nucleus can yield information on the nuclear interactions, reaction mechanisms, and the structural properties of the nuclear system. There are two basic nuclear reaction mechanisms known to-date: the compound nucleus reaction and direct reaction (Austern 1969). A reaction is said to proceed via the compound nucleus process when it involves a complicated excitation of many degrees of freedom in the whole nuclear system. It occurs if the incident projectile enters the target nucleus, distributes its energy to many nucleons through multiple internal collisions and finally loses its identity to form a compound system. This intermediate state decays subsequently, independent of its mode of formation, via as many channels as there are available, in the emission of one or more particles or radiations. A reaction is said to proceed through the direct reaction process when it involves the excitation of only a few degrees of freedom of the nuclear many body system and the other parts of the nuclear system remain effectively passive. This process occurs quickly ($\sim 10^{-22}$ sec.) with a minimum of rearrangement of the internal structure

of the colliding particles. Since there are no intermediate states formed, the direct reaction provides a close overlap between the target state and residual nuclear state, leading to interesting information on the properties of the states involved. There is no clear-cut division between these direct reactions and those processes which proceed through intermediate compound nucleus formation. The general guideline is that if the incident projectiles pass through the region of interaction in a time which is short compared to the Fourierperiod of the nuclear wavefunction, the induced reaction will proceed via the direct mechanism and, otherwise, the reaction will proceed by the compound mode. However, direct reactions have been observed to occur at a fairly low incident projectile energy (few MeV). These reactions most probably arise from direct interactions near the target nuclear surface region where the nucleon density is relatively low.

In the class of direct reactions, the single-nucleon transfer reactions are the ones which have been receiving the greatest theoretical and experimental attention. They constitute a major source of nuclear spectroscopic information over the past two decades. The single nucleon transfer reactions are subdivided into the stripping reactions, wherein a proton (neutron) is captured from the incident projectile by the target nucleus, and the pick-up reactions, wherein a proton (neutron) is

captured from the incident projectile by the target nucleus, and the pick-up reactions, wherein a proton (neutron) is 'snatched' away by the projectile from the target nucleus. They can be symbolically represented in the following manner. If 'T' denotes the target nucleus, 'a' the incoming particle (projectile), 'R' the residual nucleus, 'b' the outgoing particle and 'x' the transferred nucleon, the reaction $a + T \rightarrow b + R$, abbreviated as $T(a,b)R$, has the relations: $a = b + x$, $R = T + x$ for stripping reactions and $b = a + x$, $T = R + x$ for pick-up reactions.

Extensive studies of single-nucleon transfer reactions started about two decades ago with deuteron stripping reactions. Burrow (1950) and Holt (1950) were among the first to observe the angular distributions of the outgoing protons in their study of the (d,p) reactions in light nuclei. These angular distributions exhibited a pronounced oscillatory structure. It triggered a furor of experimental and theoretical research activities on the study of stripping and pick-up reactions in the years to follow. In the Butler theory (1951), the incoming and the outgoing projectiles are described by plane waves so that the transition amplitude is the Fourier transform of the bound state wavefunction. The theory enjoyed a reasonable success in predicting the shape of the angular distribution of the outgoing particles, but failed to predict the magnitude of

the differential cross sections. Nevertheless, it set the early stage of development in the theoretical interpretation of single-nucleon transfer reactions (Lane 1953, Satchler 1954, Auerbach and French 1955, French and Raz 1956).

The potential usefulness of the single-nucleon transfer reactions was not realized until the early 60's when good energy resolution detectors, electronics systems, and high energy, good resolution particle accelerators became available, rendering the properties of the individual nuclear states susceptible to detailed investigations. With the advent of large digital computers, the theory of direct reaction for the single-nucleon reactions had been refined to a state where useful nuclear spectroscopic information could be extracted from experimental data. The theory which is commonly used for the analysis of the direct single-nucleon transfer reactions is called the distorted wave Born approximation (DWBA). Many excellent review articles have been written on this subject (for examples: Tobocman 1961, Satchler and Tobocman 1960, Satchler 1964 and 1965, Glendenning 1963, Bassel et al. 1962, Austern et al. 1964, Austern 1963 and 1969). In this theory, the incident waves are first permitted to interact with the nuclear field as a whole, inflicting a distortion in the otherwise plane waves. A nucleon is then transferred to (from) a specific

orbital of the target nucleus from (to) the incident particle, and the outgoing particle again suffers a distortion upon its leaving the nuclear field. The target and residual nuclear fields are represented by absorptive potentials, called optical potentials, to account for the loss of particles to the other reaction channels.

The basic information that is obtainable from the single-nucleon transfer reactions may be inferred from the conservation laws. Since the final products are in two separate pieces and the lighter one (the outgoing particle) such as proton, deuteron etc., usually has no excited bound state. A measurement of the energies of the outgoing particle groups will give direct information about the Q-values of the reaction leading to the various states in the residual nucleus. From the angular distribution of the outgoing particles, the orbital angular momentum, ℓ, of the transferred nucleon can be deduced, hence its total angular momentum $j = \ell \pm 1/2$. If the initial and final nuclear states are characterized by the spin-parity $J_i^{\pi_i}$ and $J_f^{\pi_f}$, respectively, the relations $|J_i - j| \leq J_f \leq J_i + j$, $\pi_i \pi_f = (-1)^{\ell}$ are provided by the conservation of angular momentum and parity.

The differential cross section as given by the DWBA theory for the transition from an initial state to a final state with the transfer of a nucleon to or from a

specific single particle orbital (ℓ, j) may be written as

$$\frac{d\sigma}{d\Omega}(\ell,j) \propto S(\ell,j)\cdot\sigma(\theta) \qquad (1\text{-}1)$$

where S(ℓ, j) is called the spectroscopic factor as defined by MacFarlane and French (1960) and $\sigma(\theta)$ is the transition amplitude. The quantity $\sigma(\theta)$ determines the angular distribution of the differential cross sections and it is a measure of the probability of forming a single particle (for stripping) or a single hole (for pick-up) state characterized by (ℓ, j). The quantity S(ℓ, j) is a measure of the transition strength reflecting the probability of finding the target in such a state that when it combines with the orbital (ℓ, j) will produce the final state. Thus, S(ℓ, j) measures the degree of overlap to which the passive nucleons occupy the same configuration in the initial and final states of the reaction, and it determines directly the single particle or single hole component in the final nuclear state. Therefore, the spectroscopic factors determined experimentally for all the excited states of the residual nucleus will yield information about the distribution and fragmentation of each single particle and single hole state. Furthermore, by examining the sum of the spectroscopic factors of all the states to which a given (ℓ, j) orbital contributes, one can obtain information on the occupation and unocu-

pation probabilities of the single particle or hole state in the target. Indeed, the spectroscopic factor carries the dynamical properties of the nuclear states involved, and it reflects directly the validity of the wave functions of the states predicted by different nuclear model calculations.

This dissertation describes the results of a study of the $^{94,96,98,100}Mo(^{3}He,d)^{95,97,99,101}Tc$ and $^{79,81}Br(d,p)^{80,82}Br$ reactions.

There is much physics to be learned from a study of the (^{3}He,d) reactions in the targets of Mo-94,96,98 and 100. Nuclei in the mass region of $A \sim 90$ which are characterized by the closure of $N = 50$ neutron shell, have been extensively studied both experimentally and theoretically in the past few years. The low-lying states of these nuclei have been shown to subscribe reasonably well to the description within the context of spherical shell model (Talmi and Unna 1960, Bhatt and Ball 1965, Auerbach and Talmi 1965, Vervier 196 , Cohen et al. 1964). Recently, experimental evidence obtained from nuclei in the mass region of $A \gtrsim 100$ revealed the rotational-like behavior in the structure of the very neutron rich even-even Zr, Mo, Ru and Pd isotopes (Cheifetz et al. 1970, Castern et al. 1972), in accordance with the prediction of a new region of stable deformation existing

in the region of $28 < Z < 50$ and $50 < N < 82$ (Johanssen 1965, Arseniev et al. 1969). The nuclei in the neighborhood of $A = 100$, therefore, may exhibit a transitional character in their structure varying from near spherical shape to deformed shape.

The ^{95,97,99,101}Tc nuclei fall within this region. Therefore, it has been chosen in this work to investigate the structural properties of the low-lying states of these nuclei through the (^{3}He,d) reactions in the ^{94,96,98,100}Mo nuclei. In this study, the results will not only lead to information about the Tc nuclei, but also provides valuable knowledge about the ground state properties of the Mo target nuclei. Since the ^{92}Mo(^{3}He,d)^{93}Tc reaction has been studied by Picard and Bassani(1969) and Kozub and Youngblood (1971), the present work will complete a systematic investigation of the odd mass Tc isotopes using the (^{3}He,d) reactions in all even mass Mo isotopes.

The present study of the ^{79,81}Br(d,p)^{80,82}Br reactions has been undertaken to obtain information on the proton and neutron configurations which participate in the formation of the various states of the ^{80}Br and ^{82}Br nuclei, and the orbital distribution of the neutrons in the ground states of ^{79}Br and ^{81}Br. Since the (d,p) reactions select preferentially those final states associated with

configurations of a single neutron coupled with the target nucleus, the results of the present measurements should be complimentary to those obtained from the (p,n) reactions by Finckh *et al.* (1970), which are most likely proceeded via the compound nuclear reactions. The ^{79}Br and ^{81}Br nuclei consist of 35 protons and 44 and 46 neutrons, respectively. From the nucleon orbital filling of the shell model, the lowest-lying states to be observed in the present study are expected to arise from the coupling of the $1g_{9/2}$ and $2p_{1/2}$ neutrons with the $2p_{3/2}$ protons. Therefore, with the use of the sum rules, angular distribution patterns and the $2J+1$ dependence of the spectroscopic strength one may be able to make spin-parity J^{π} assignments to the levels. These results should be comparable with those obtained experimentally in the neighboring nuclei.

CHAPTER II

EXPERIMENTAL TECHNIQUES AND APPARATUS

2.1 Preamble

To study the structure of medium mass nuclei such as technetium and bromine by means of proton or neutron stripping reactions, a particle beam of good energy resolution and high intensity is needed because of their relatively high energy level density. In addition, the particle energy should be sufficiently high to overcome the Q-value of the reaction and the Coulomb barrier of the nucleus under study. The 12 MeV deuteron beam and the 18 MeV helium-3 beam from the EN tandem Van de Graaff accelerator at the Laboratoire de Physique Nucleaire, Université de Montréal, and the 18 MeV helium-3 beam from the FN tandem Van de Graaff accelerator at McMaster University meet the above criteria and are readily accessible to the Nuclear Physics Group at McGill University. This thesis describes the results of a study on the structure of ^{79}Br and ^{81}Br using the (d,p) reactions on ^{80}Br and ^{82}Br, and of ^{95}Tc, ^{97}Tc, ^{99}Tc and ^{101}Tc through the (^{3}He,d) reactions on

^{94}Mo, ^{96}Mo, ^{98}Mo and ^{100}Mo. All experiments, except the $^{98}Mo(^{3}He,d)^{99}Tc$ reaction, were performed at the Université de Montréal using either the 12 MeV deuteron beam or the 18 MeV helium-3 beam from the EN tandem accelerator. The measurement on the $^{98}Mo(^{3}He,d)^{99}Tc$ reaction was performed at McMaster University using the 18 MeV helium-3 beam from the FN tandem accelerator and the Enge-type broad range magnetic spectrograph.

One of the major difficulties which is normally encountered in such experiments is the detection and identification of the desired product particles in the presence of a large flux of the incident particles (scattered) and other reaction product particles. With the use of a magnetic spectrograph this difficulty is not a problem because normally the kinematics of the reaction and the particle magnetic rigidity permit the selection of a particular type of charged particles with a given momentum range. On the other hand, with the use of a conventional solid state detector system without any pre-selection of particles, which is how the measurements were performed at the University of Montreal, a scheme must be adopted to identify and select the desired reaction products.

The method commonly used for charged particle identification is based on the range-energy relationship

of the particle passing through matter coupled with the use of a transmission-plus-total absorption (ΔE-E) detector telescope system. Such a system has been adopted for the present work and will be described in detail in section 2.4 of this chapter. For reasons of good energy resolution and ease in handling, solid state silicon detectors have been chosen for the experiments described here. Furthermore, because of the particular range-energy relationship for charged particles, such as proton, deuteron, triton, ^{3}He and alpha, passing through silicon, this choice of detectors facilitates the design of a high speed electronic circuit to perform the particle identification.

The second problem lies in the accelerator beam time required to carry out the reactions on all desired targets (^{79,81}Br and ^{94,96,98,100}Mo). The maximum differential cross section for the (d,p) and (^{3}He,d) reactions in these nuclei has been estimated to be of the order of one millibarn. To attain good angular resolution and a statistically significant number of events in the various peaks of the excitation spectrum, a sufficiently long counting period per angle is necessary. One must not use too thick a target since the variation in the energy degradation of the charged particles in the target significantly affects the experimental energy resolution. One must also pay special attention to the instantaneous

count rates in the detectors so that deterioration in energy resolution due to pulse pile-up will not be an important factor and counting losses due to electronics deadtime will not be intolerable.

After optimizing the various factors mentioned above, the average counting time per angle setting is about 8 hours for an incident beam of about 10^{12} to 10^{13} particles per second. There are about 15 angles per angular distribution for each target. If employing only one detection system, each target would require five 24-hour days to complete all the measurements. To this time one must also add 25 to 30% time lost due to accelerator, electronics and detector breakdowns. This would amount to about six and one-half 24-hour days per target and six targets would require about thirty-nine 24-hour days accelerator beam time, putting a severe strain on the manpower to "run" the experiments. To minimize this problem, it has been decided to use two detector telescope systems set at two different angles simultaneously. Because of the difference in differential cross section at the two different angles and the necessity to normalize the detection efficiency of the two detector systems, the two-telescope arrangement will not reduce the beam time requirement by a factor of 2, but should be somewhere between 1.5 and 2.

In general the experimental techniques involved in the measurements of the two types of reactions, (^{3}He,d) and (d,p), are fairly straight forward and they will be described in the subsequent sections of this chapter. Since most of the experimental work was conducted at the University of Montreal more attention will be devoted to that part of the work.

2.2 Scattering Chamber and Detection System

There were two basic experimental set-ups used in this work: one at l'Université de Montréal for the measurements of the ^{79,81}Br(d,p)^{80,82}Br and ^{94,96,100}Mo (^{3}He,d) ^{95,97,101}Tc and the other at McMaster University for the measurements of the ^{98}Mo (^{3}He,d) ^{99}Tc reaction. The set-up at the University of Montreal is housed in the $+45^{o}$ beam line employing a conventional scattering chamber and solid state silicon detector ΔE-E telescope systems. The layout of this beam line, including its vacuum systems, beam transport and closed circuit television facilities, has been described elsewhere (Rabin, 1971). The details of the scattering chamber assembly have been presented by Brien (1971). It is a general purpose charged particle scattering chamber of 28 inches in diameter and 8 inches in depth made of aluminium. Inside the chamber there are

two independently rotatable aluminium plates, one in the top and the other in the bottom, whose angular positions can be manipulated from outside. The detector systems were mounted on these plates so that their angular positions could be changed without disturbing the vacuum system of the chamber. The target holder assembly, which can house four targets at a time in a vertical column, is mounted from outside at the bottom of the chamber so that the target can be inserted into the center of the chamber through a vacuum gate. The target holder is rotatable to permit the change of the angle between the target and the incident beam. A 2 mm diameter beam collimator made of tantalum is placed at the entrance port of the chamber and the unscattered beam is received by a Faraday cup connected to the exit port of the chamber. During the experiments, the entire chamber assembly was kept under vacuum of about 10^{-6} mm Hg.

To reduce the beam time requirement in the present work, two ΔE-E detector telescope systems were used simultaneously. For the measurements of the (^{3}He,d) reaction, the ΔE detectors used were totally depleted diffused junction silicon detectors of thickness 100 μm and area 100 mm^2 supplied by Simtec Ltd. of Montreal, while for the measurements of the (d,p)

reaction they were surface barrier silicon detectors of thickness 200 μm and area 50 mm^2 supplied by Ortec, U.S.A. In both cases the E detectors employed were partially depleted surface barrier silicon detectors of thickness 2000 μm and area 50 mm^2 supplied by Ortec. The thickness of the ΔE detectors, in each case, was chosen so that the most energetic charged particle of interest will induce no more than 20% fluctuation (Landau 1944) in its energy loss when traversing them. The thickness of the E detectors was selected to stop completely the most energetic reaction products of interest in both cases.

Each detector telescope system was aligned so that its axis intersected the incident particle beam at the target center. The solid angle $\Delta\Omega$ of each detector system subtended at the target was defined by a collimator of circular aperture. The solid angle used for each detector system varied from target to target and its value will be given later in the sections describing the experimental procedures for the different reactions. To avoid detecting the high flux of delta rays ejected from the target by the incident beam, a small magnet was installed at the entrance of each telescope.

The measurements on the $^{98}Mo(^{3}He,d)^{99}Tc$ reaction were performed at McMaster University using the -45° beam line which was equipped with an Enge split-pole magnetic

spectrograph coupled to a scattering chamber through a rotating seal (windowless coupling). The chamber was about 12 inches in diameter and 6 inches in depth. The target was placed at the center of the chamber and the incident beam intensity was monitored by a silicon detector placed at 90^{o} to the beam direction and calibrated against the elastic scattering events from the target. At each angle setting the magnetic field of the spectrograph, which was regulated by a nuclear magnetic resonance system (NMR), was adjusted to select deuterons of a given momentum band. These outgoing deuterons were focused and momentum analysed by the spectrograph and recorded in a set of nuclear emulsion plates placed at the focal plane. The emusion plates were covered with thin sheets of aluminium of thickness ranging from 8 to 20 mils. The purpose of this shield was to prevent heavy charged particles such as alpha particles of the same magnetic rigidity as the desired deuterons from striking the emulsion plates. After processing, the plates were scanned with a microscope in quarter millimeter swaths across the width of each plate and the number of deuteron tracks were recorded.

The structure of the type of spectrograph used has been described by Enge and Smith (1966) in detail. The instrument consists of two separate pole pieces enveloped

by a single coil. The split between these poles provides a second order double focusing over a wide range of energies. Using the fringing field associated with four pole boundaries, two dimensional focusing can be obtained. The advantage of this type spectrograph over the others is the high resolving power obtainable with a large acceptance solid angle while the Doppler broading (kinematic broadening) can be corrected for at the same time. The entire assembly is mounted so that it can rotate about an axis through the position of the target.

The performance of a split-pole magnetic spectrograph for nuclear reaction studies is superior to that of ΔE-E detector telescopes in many respects: (1) the outstanding energy resolution; (2) no dead time loss and pile-up problems involved so that high beam current and large solid angle can be employed; (3) measurements at small forward scattering angles may be performed with a small scattering chamber which otherwise would be prohibited with the use of solid state detectors; and (4) the momentum selection in the magnetic fields gives the particle identification without further electronic processing. However, most spectrographs suffer the drawbacks in that the events are recorded in a set of photo emulsion plates, no instant display can be obtained and the time information of individual reaction events is

also lost. A detector placed at fixed position relative to the target is necessary to monitor the beam current.

2.3 Target Preparation

Thin film targets were prepared by the techniques of evaporation in high vacuum. Target materials which are isotopically enriched were obtained from the Oak Ridge National Laboratories. The isotopic composition of the molydenum and bromine are listed in table 1, as provided by the supplier. The bromine isotopes were procured in the form of NaBr compound, which has an evaporation temperature of 800° C (Arnison 1967). This compound was selected for target material over pure bromine because the latter is in liquid form at room temperature and has a boiling point 58.78° C, and a pure bromine target would disintegrate under the bombardment of a few hundred nanoamperes of deuteron beam. The presence of the sodium isotopes in the bromine targets does not interfere with the present measurements because their effects are easily recognizable. The proton spectrum resulting from the (d,p) reactions in the sodium isotopes is quite different from that of the bromine isotopes and it has a remarkable kinematic shift from one angle to another.

The molydenum isotopes were purchased in the form

of pure metal. Since molydenum metal has a high melting point 2610° C, it was decided to convert all isotopically enriched molydenum metals, except ^{98}Mo, into oxides of the form MoO_x with x = 2 and 3. The MoO_3 has a evaporation temperature of 1000° C (Arnison 1967) and thus can be vaporized in a moderate power vacuum evaporator. The oxidation processes were carried out in the Chemistry Department, McGill University. Like the sodium in the bromine targets, the presence of the oxygen in the molydenum targets does not cause any problem in the present measurements, because of the difference in Q-value and kinematic shift of the (^3He,d) reactions in the two elements.

The targets of NaBr enriched in ^{79}Br and ^{81}Br and of oxides of ^{96}Mo and ^{100}Mo were fabricated in a vacuum evaporator manufactured by Mikros Inc., Model VE-10. This apparatus was equipped with a continuously controllable 1 kW AC power supply. The target material to be evaporated was contained in a tantalum dimple boat connected between the two output terminals of the power supply inside a vacuum belt-jar. The tantalum was chosen as the refractory material for the boat because it is ductile, and can be spot welded and also it has an evaporation temperature of 2800° C, a value which is substantially higher than that for either NaBr or $MoO_{2,3}$. However, recently the laboratory installed a new vacuum

evaporator equipped with a 2 kW electron gun supplied by Varian Inc., Model 980-0001. The ^{94}Mo oxide target and the ^{98}Mo pure metal target were fabricated in this new instrument. In this case the material to be vaporized by the beam from the electron gun was contained in a highly thermo-conductive metallic crucible.

The target material for each isotope was evaporated onto a thin carbon backing for mechanical strength. The carbon foils used were YISSUM type of S-20 and S-30, supplied by Yissum Research Development Co., Israel, of thickness 20 and 30 $\mu g/cm^2$, respectively. These carbon backings were prepared by sublimation of carbon onto glass slides, treated with teepol, which acts as a release agent in water. The carbon-coated glass slide was placed a few inches above the evaporation point. In order for vapor molecules to reach the carbon substrate, it was found that the evaporation chamber must be held at pressure of about 10^{-5} to 10^{-6} mm Hg. After evaporation, the thin film of target together with the carbon backing was stripped off by slowly submerging the glass slide into a dish of clean water at an angle about 40° to the surface. Before the stripping, the foil on the glass slide was cut into 3 or 4 pieces about 1" x 1". The floating foils were then mounted on a metallic target frame with a hole in the center. This was done by slowly raising the mounting frame held with a

pair of forceps from under the water, picking up almost at right angle to the water surface. The excess water was then removed from the film by carefully blotting with a very soft filter paper. Another method which was used on several occasions was to float the carbon backing in water and mount it on a target frame. In this case, a prepared substrate consisting of several target frames mounted with carbon foils was placed directly above the crucible at the desired distance. It was found that to make a target of thickness 100 $\mu g/cm^2$, about 16 mg of molydenum oxide was required, if the distance between the substrate and the crucible was about 2 inches. It was also found that the physical strength of the target depends on its condensation conditions. Targets prepared at an approximately constant rate of condensation and high substrate temperature are more durable than others under the bombardment of particle beams.

The thickness of the targets was measured with two different techniques: the attenuation method using a calibrated alpha source, and the on-line elastic scattering method, comparing the differential cross sections with the values computed from the optical model. The latter method actually gives the measure of the product of target thickness and the solid angle subtended at the

target by the detector. Although most targets used are of thickness of the order of 100 $\mu g/cm^2$, they varied substantially from one to another. Details of the target thickness measurements are given in the section describing the experimental procedures in the next two chapters.

It should be pointed out that the carbon backings do not interfere with the present measurements on either the (d,p) or (^{3}He,d) reaction for the same reasons as those given above for the sodium and oxygen isotopes in the targets.

2.4 Charged Particle Identification

The study of nuclear reactions induced by charged particle beams often requires the identification of the nature of the product particle detected. For example, a beam of 18 MeV helium-3 particles bombarding a target of molybdenum can produce a variety of product particles from the inducing nuclear reaction, such as (^{3}He,^{3}He), (^{3}He,^{3}He'), (^{3}He,p), (^{3}He,d), (^{3}He,α) and others. To study a given reaction, it is necessary to identify and select the appropriate product particles.

There are several types of charged particle identification systems which are commonly used in nuclear reaction experiments. Most of them are based on one of

the following methods: (1) electromagnetic deflection, (2) time of flight and total energy measurements, (3) the rate of energy loss in traversing a thin slab of detecting material (the detector) and the total energy of the particle and (4) the range-energy relationship of the particle in the detecting material. The first one is equivalent to a measurement of either the charge to mass ratio of the particle in an electrostatic field or the magnetic rigidity of the particle in a magnetic field, while the second one is equivalent to a determination of the product of the particle kinetic energy and the square of the flight time over a fixed flight path. These two methods form the basis for part of the classical nuclear physics techniques.

The third method is based on the non-relativistic Bethe equation for the rate of energy loss, dE/dx, of a particle of energy 'E', mass 'M' and charge 'Z' passing through a slab of material of thickness x. This equation may be written as,

$$E(dE/dx) \propto Z^2 M \ln (CE/M) \qquad (2.4\text{-}1)$$

where C is a constant depending on the material. Since the factor ln (CE/M) is a slowly varying function of E, over a finite energy range it may be considered as a constant, whence $E\,(dE/dx) \propto Z^2 M$. This implies that if one detects the particles with a system consisting of a

thin detector of thickness Δx (transmission detector) in front of another detector which is sufficiently thick to stop the particle (total absorption detector), the sum of the energy signals from the two detectors will provide the total energy signal, which when multiplied by the energy signal from the transmission detector would generate a quantity proportional to Z^2M. To compensate for the energy dependence of the ln (CE/M) factor, a product function of the form $(dE/dx)(E+K(dE/dx)+E_o)$, where K and E_o are constants, has been commonly used in particle identifiers using this method. A study of this method for charged particle identification and the associated electronic circuits for the generation of the product function have been presented by several authors (Mark and Moore 1966, Legg 1963, Griffiths et al. 1962, Wahlin 1961, Deb and Sen 1961, Giannetic and Stranchi 1960, Stokes et al. 1958, Wolfe et al. 1955).

The above method has been found to work well for the identification of singly charged and doubly charged particles over a dynamic energy range of a factor of 5 (Mark and Moore 1966), provided that the thickness, Δx, of transmission detector (called ΔE detector) is properly chosen to simulate a differential quantity. But it is difficult to choose a thickness for the ΔE detector that suits both the simply and doubly charged particles because their stopping power, dE/dx, in matter differs

substantially (about one order of magnitude). This leads to the proposal of method 4 by Goulding et al. (1964). It is a well known fact that the range 'R' of a particle of total energy 'E_o' may be represented by the empirical relationship, $R = a E_o^n$ (Willamson and Boujot, 1962) over a finite energy region, where 'a' is a constant depending on the particle and 'n' is a constant depending on the material. For silicon (Goulding et al. 1964, Williamson et al. 1966):

$n = 1.73$

$a = 32.2 \times 10^3$ $(\mu g/cm^2)(MeV)^{-1.73}$ for proton

$= 19.1 \times 10^3$ for deuteron

$= 14.2 \times 10^3$ for triton

$= 3.54 \times 10^3$ for helium-3

$= 2.95 \times 10^3$ for alpha.

With these numerical values, the empirical range-energy relation fits the experimental data remarkably well over the energy region from about 10 MeV to 200 MeV for all singly and doubly charged particles.

This range-energy relationship has been exploited for the purpose of particle identification. Consider a two-detector telescope system -- a transmission followed by a total absorption detector, if the thickness of the transmission detector is Δx, it is easy to show that

$$\frac{\Delta x}{a} = (E + \Delta E)^n - E^n \qquad (2.4\text{-}2)$$

where ΔE and E are the energies deposited in the transmission and total absorption detectors. For a given Δx, the left hand side of the equation is a constant depending only on the particle. Therefore, generation of the function on the right hand side of the above equation based on the energy signals from the two detectors identifies the particle detected. An electronics circuit for the generation of this function has been designed and constructed by Goulding et al. (1964) using the logarithm current-voltage characteristics of the emitter-base junction of a transistor. In their design the power 'n' is adjustable so as to suit a variety of detectors. A circuit based on their design is now manufactured by Ortec Ltd., U.S.A. The method has been found to work very well (Goulding et al. 1964) for a variety of particles over a wide range of energy within the validity of the empirical relationship. Indeed, the limitation has been found to come more often from the electronics than from the basic method itself. In the Goulding et al. design, the electronics circuit is very complicated and difficult to adjust though it has flexibility. The transistors they used for the generation of the logarithmic and anti-logarithmic functions have to be carefully selected. The time required by the circuit to perform one computation is large -- 10 to 15 μs. For these reasons, a much simpler

circuit for the generation of equation (2.4 - 2) has been designed and constructed for the present work. This circuit is based on the idea of Mark and Standing (1965) and Fisher et al. (1967) using a field effect transistor (FET). It is only good for silicon detectors.

If one examines the drain current 'I_d' of an FET as a function of the gate voltage 'V_g' and drain voltage 'V_d' below the pinching point, one can represent I_d by the following equation (Lindmayer and Wrigley 1965)

$$I_d = A\,V_d - B\left[(V_g + V_d)^{1.5} - V_g^{1.5}\right] \qquad (2.4\text{-}3)$$

where A and B are constants of the FET. The term inside the square bracket is very similar to the right hand side of equation (2.4-2), except that the value for n is 1.73 for silicon detectors instead of 1.5. However, the difference between the two is very small over a dynamic energy range of, say, 7 if V_g and V_d are taken to be E and ΔE. Moreover, most FET's have a power law of about 1.6 rather than 1.5. Thus, a function which is a fairly good approximation to equation (2.4-2) can be readily generated if a circuit is designed around an FET such that the energy signal 'E' from the absorption detector (called E detector) is applied to the gate and the ΔE energy signal is applied to the drain, a current I_d will be induced in the FET. When a current proportional to ΔE (the term AV_d in equation 2.4-3) is subtracted from I_d, the resultant current is then approximately the

same as represented by the right hand side of equation (2.4-2). It has been found that the power law of 1.5 in an FET rather than the 1.73 as required can be partially compensated by varying the subtraction of the current proportional to ΔE, and by adding to I_d a component of current proportional to E. These compensations were found necessary if the generated function is to approximate equation (2.4-2) over a dynamic energy range of 10. The circuit used in this work which incorporated all these features is presented in figure 1.

The circuit is basically divided into two parts: the summing part which produces an output voltage signal proportional to the total energy ($E+\Delta E$) of the particle and the identification part which generates a voltage signal directly proportional to the right hand side of equation (2.4-2). The circuit takes two simultaneous positive, flat-top voltage pulses input derived from the two detectors ΔE and E, respectively. For convenience, these pulses are also called ΔE and E. The 100 Ω variable resistor, called ΔE gain, is used to control the voltage at point B so that the voltages at point A from the E input and point B from the ΔE input will have the same energy proportionality constants. The summing circuit, consisting of two operational amplifiers formed by transitors (T1, T2) and (T3,T4), derives its inputs from points A and B. The identification

circuit is centered around the field effect transistor, Q, whose terminals are labelled as S, G, D (S = source, G = gate, D = drain). The E input, after having past through a phase inverting operational amplifier (T5 and T6), is applied to Q at the gate G. The Δ E input is fed to a non-phase-inverting operational amplifier consisting of transistors T7, T8, T9 and T10 connected in a common mode configuration, and the output at the emitter of T9 is applied to the drain D of Q.

When the Δ E and E signals are applied to D and G of Q, the current I_d induced in Q will flow through T9 and amplified in the form of a voltage pulse across the collector load of T9. This pulse is then mixed with a quantity which is proportional to Δ E (derived from the emitters of T7 and T8 through a variable resistor "function") in the operational adder (T11 and T10) to obtain a pulse proportional to $I_d - A V_d$ in equation (2.4-3). To make this pulse approximate the function in the right-hand side of equation 2.4-2, a small component of current proportional to E is added to I_d by means of feeding a portion of the E signal into the base of T10 through a variable "compensation" (comp.) resistor. Transistors T13 and T14 constitute the output stage operational amplifier with a low output impedance. The circuit was designed to accept inputs of maximum amplitude 10 volts. The resistors R_1 R_2 and R_3 were chosen so that $5000/R_1 =$

$R_2/(R_2+R_3)$, depending on the dynamic range of the FET, Q. For the circuit used, $R_1 = 15\ k\Omega$, $R_2 = 5\ k\Omega$, and $R_3 = 10\ k\Omega$. This circuit has been tested both off-line and on-line and was found to perform satisfactorily for the present work.

In the off-line test, the particle energy signals from the two detectors were simulated by a pulser. The electronics used for this purpose is shown in figure 2. Apart from the particle identifier, all electronics units were commercially made and their suppliers and model numbers are listed in the figure caption. The output of the pulser was fed to the dual decade attenuator whose two outputs, called Δ E and E, were connected to the test inputs of the respective preamplifiers. The slow-decaying pulses from each preamplifier were fed to an amplifier, which gave unipolar and bipolar outputs. The unipolar pulses from the amplifiers were directed to the two linear gate / stretcher circuits, which supplied positive, flat-top pulses to the particle identifier, while the bipolar pulses were connected to the two timing single channel analysers (TSCA), whose outputs were fed to the fast coincidence circuit. The coincidence signals operated the two linear gate / stretcher units.

The voltage pulses at the E and Δ E inputs of the particle identifier (with " Δ E Gain" control set at maximum) were adjusted so that both inputs have a voltage-

energy equivalence of 10 volts = 30 MeV. The energy for E input and that for the ΔE input were computed from the range-energy table of Williamson and Boujot (1962) for all singly and doubly charged particles by assuming the thickness of the ΔE detector to be 100 μm and of E detector 2000 μm silicon and the maximum particle energy to be 30 MeV. The 'tuning' of the particle identifier circuit was especially simple. First set the "compensation" control to zero and vary the "function" control to obtain an optimum separation. Then increase the compensation control until a best separation is attained for the entire energy range. The result of this test is shown in figure 3. It can be seen that the particles are clearly separated.

An on-line test of the circuit was also conducted. The source of signals was two detectors ΔE and E; the ΔE detector was a 100 μm diffused junction silicon detector supplied by Simtec Ltd., and the E detector was a surface barrier silicon detector obtained from Ortec Inc. The electronics system used is given in figure 2. To match the energy scale in both the E and ΔE channels, an ^{241}Am alpha source was used. First the ΔE input to the particle identifier was disconnected, the amplifier in the E channel was adjusted to give approximately 10 volts = 30 MeV at the input of the identifier. The alpha particle pulses appearing at the sum energy

output of the identifier were recorded in a multi-channel pulse height analyser. After having done this, the Δ E channel was then connected and the E channel disconnected. The Δ E channel amplifier and the " Δ E Gain" control of the identifier were varied until the alpha particle peak in the analyser matched that of the E channel. It was found advisable to have the Δ E amplifier operate at maximum gain within its linear range so that the smallest signal (highest energy proton) could trigger the TSCA. The fast coincidence unit was set at a resolving time of 50 nanoseconds.

The particle beam used was the 18 MeV ^{3}He beam from the EN tandem accelerator at l'Université de Montréal. The mass output of the identifier was fed to a 512-channel Nuclear Data analyser. The 'tuning' procedure for the identifier was the same as that described above for the pulser. The charged particle mass spectra obtained for ^{9}Be and ^{94}Mo targets are displayed in figures 4 and 5, respectively. The spectrum for the ^{9}Be target exhibits a much better particle separation than that for the ^{94}Mo because the former was obtained at a count rate of about 4,000 per sec. in each detector and the latter was at about 15,000 per sec. in each detector, hence more pile-up pulses.

The performance of the particle identifier was remarkable. Three identifiers of this type have been

built and each one is housed in a single-width NIM module. Throughout the work described in this thesis, not a failure of these circuits was encountered. However, it must be pointed out that the FET is a temperature sensitive device, if the ambient temperature changes more than 5° C, its characteristics change significantly. Since those circuits were used in the superbly temperature regulated control room of the Nuclear Physics Laboratory at the University of Montreal, such a change was never observed during any measurement.

2.5 Electronics and Data Acquisition

The block diagram of the electronics system used in conjunction with each detector telescope is shown in figure 6. The electronics units were procured commercially, except the particle identifier, and their origins are specified in the figure caption. Aside from a few additions, the basic arrangement of the system and its adjustment were similar to those of the system used for testing the particle identifier. The particle identifying signals (mass output) were fed simultaneously to a series of timing single channel analysers (TSCA), one for each type of charged particle, and the sum energy signals were fed to a series of delayed amplifiers, each one being followed by a gated biased amplifier. Each

delayed amplifier - gated biased amplifier combination was operated by a TSCA whose "window" was set on the desired mass signals. Throughout this work, two types of charged particles were selected in each measurement although only the results of the (^{3}He,d) and (d,p) reactions are presented here.

The particle energy spectrum output from each gated biased amplifier was fed to a Northern Scientific Multiplexer (Model NS 414) which was interfaced with a 8 K-memory Northern Scientific Analyser (Model NS 624). The latter was operated in a 4 x 2048 channel mode with the output recorded by an Ampex Magnetic Tape Unit. The data were subsequently analysed in the CDC 6400 computer at the Centre de Calcul, de l'Université de Montréal.

The gated biased amplifiers were adjusted to give spectra with a gain of about 5 to 10 keV per channel and only those portions of the spectra of interest were allowed to register in the analyser. Since all logic electronics circuits have deadtimes, it is imperative to know what fraction of the events were detected and lost due to this cause. This loss of events due to electronics deadtimes in the various units is particularly severe if the beam intensity, hence the count rate in each detector fluctuates. To obtain information on this regard, a pulser was used to generate a signal to simulate a given type of particle. The pulser was triggered by a signal

derived from the output of the amplifier in the E channel and fed to a dual decade attenuator, whose ΔE and E outputs were connected to the test inputs of the preamplifiers. In this manner, the sampling pulse rate from the pulser is proportional to the count rate in the E detector, hence to the instantaneous beam intensity. By comparing the number of pulses in the pulser peak in the spectrum to the number of pulses from the pulser registered by the fast scaler, the fractional loss of the events registered in the spectrum was deduced.

The beam current of the unscattered beam was monitored by a Faraday cup connected at the exit port of the scattering chamber. The output of the Faraday cup was fed to an ORTEC Current Digitizer (Model 439), which in turn drove an ORTEC Scaler (Model 430).

The electronics system used for the $^{98}Mo(^{3}He,d)^{99}Tc$ measurements at McMaster University was very simple. Apart from the power supply and its NMR regulator for the spectrograph, there was only the electronics for the one monitor silicon detector. The detector output was connected to an ORTEC preamplifier (Model 109A), thence to an ORTEC amplifier (Model 451) and ORTEC single channel analyser (Model 420A). The events from the last unit were recorded in an ORTEC scaler (Model 430).

TABLE 1

Isotopic Composition of the Molybdenum and Bromine Isotopes in the Targets

The content values (in percentage) are taken from the data supplied by Oak Ridge Laboratories.

CONTENTS / TARGETS	^{92}Mo	^{94}Mo	^{95}Mo	^{96}Mo	^{97}Mo	^{98}Mo	^{100}Mo
^{94}Mo	0.83	<u>93.9</u>	2.85	1.04	0.40	0.75	0.22
^{96}Mo	0.18	0.18	0.94	<u>96.8</u>	0.96	0.82	0.10
^{98}Mo	0.10	0.07	0.16	0.23	0.33	<u>98.8</u>	0.33
^{100}Mo	0.60	0.23	0.40	0.81	0.36	1.69	<u>95.9</u>

CONTENTS / TARGETS	^{79}Br	^{81}Br
^{79}Br	<u>95.0</u>	5.0
^{81}Br	0.4	<u>99.6</u>

FIGURE 1

Charged Particle Identifier Circuit

Q: FET (p-channel) 2N3436

J: Diode IDQ10-500

Z: 6 Volt Silicon Zener Diode

R1: 15 kΩ

R2: 5 kΩ

R3: 10 kΩ

T1, T4, T5, T7, T9, T10, T11, T14:
NPN Transistor 2N3904

T2, T3, T6, T8, T12:
PNP Transistor 2N3906

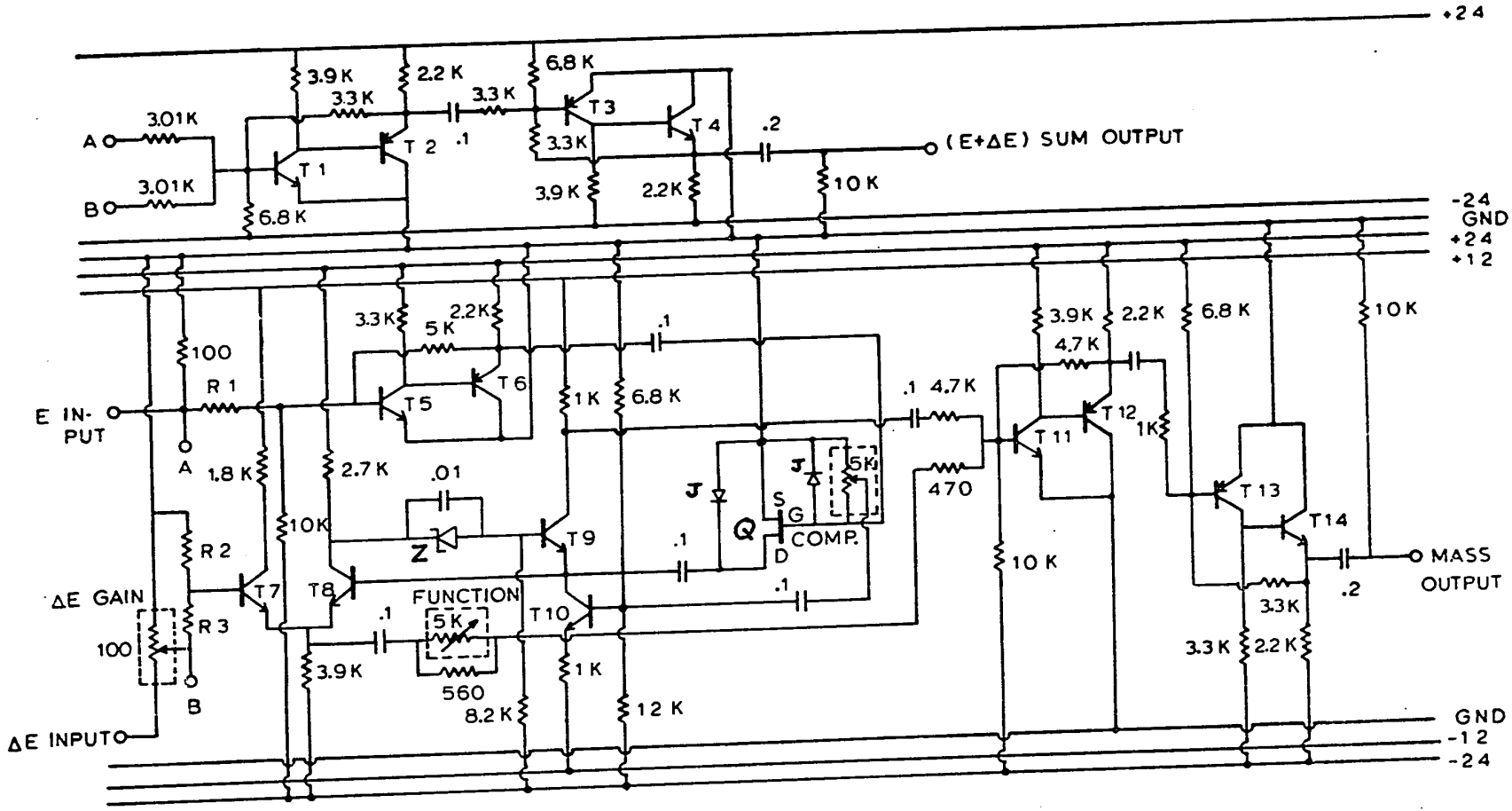
+24
3.9K
2.2K
6.8K
3.3K
3.3K
3.01K
A
T3
T4
.2
(E+ΔE) SUM OUTPUT
T2
.1
3.3K
T1
3.01K
B
3.9K
2.2K
10K
6.8K
-24
GND
+24
+12
3.3K
5K
2.2K
.1
3.9K
2.2K
6.8K
10K
100
4.7K
R1
T6
T5
1K
6.8K
.1 4.7K
T12
E IN-
PUT
A
1.8K
2.7K
.01
T11
1K
J
J
5K
S
G
470
T13
10K
Z
T9
Q
COMP.
T14
R2
.1
D
10K
MASS
OUTPUT
ΔE GAIN
T7
T8
FUNCTION
T10
.1
.2
3.3K
100
R3
5K
3.3K
2.2K
3.9K
1K
560
8.2K
12K
B
GND
ΔE INPUT
-12
-24

FIGURE 2

Electronics Block Diagram for Testing the Charged Particle Identifier

Electronics Units:-

Preamplifier	TC 136
Dual Decade Attenuator	ORTEC 422
Amplifier	ORTEC 451
TSCA	ORTEC 420A
Fast Coincidence	ORTEC 414A
Gate Stretcher	ORTEC 442
Pulser	ORTEC 448

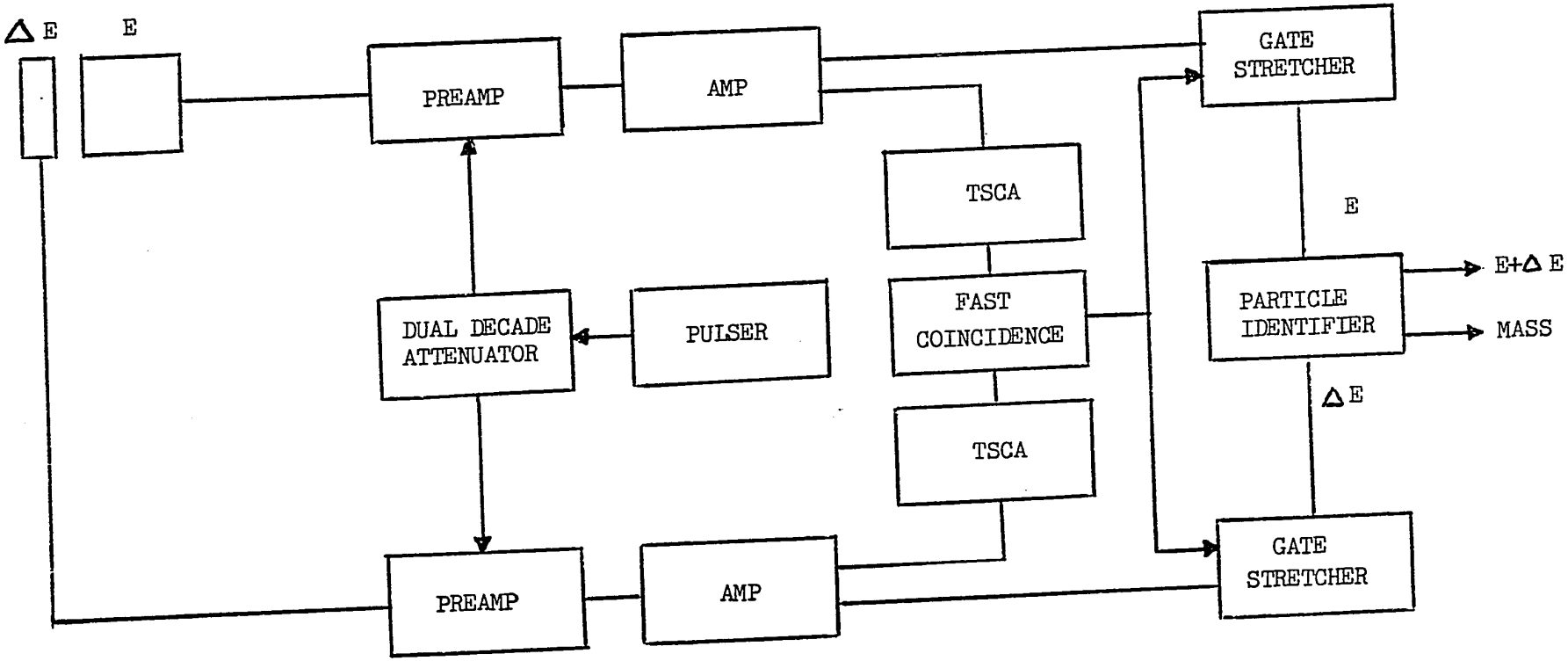
ΔE
E
PREAMP
AMP
GATE STRETCHER
TSCA
E
E+ΔE
DUAL DECADE ATTENUATOR
PULSER
FAST COINCIDENCE
PARTICLE IDENTIFIER
MASS
ΔE
TSCA
PREAMP
AMP
GATE STRETCHER

FIGURE 3

Simulated Mass Outputs of Charged Particle Identifier

Energy-voltage scale for each channel, 10 volt = 30 MeV

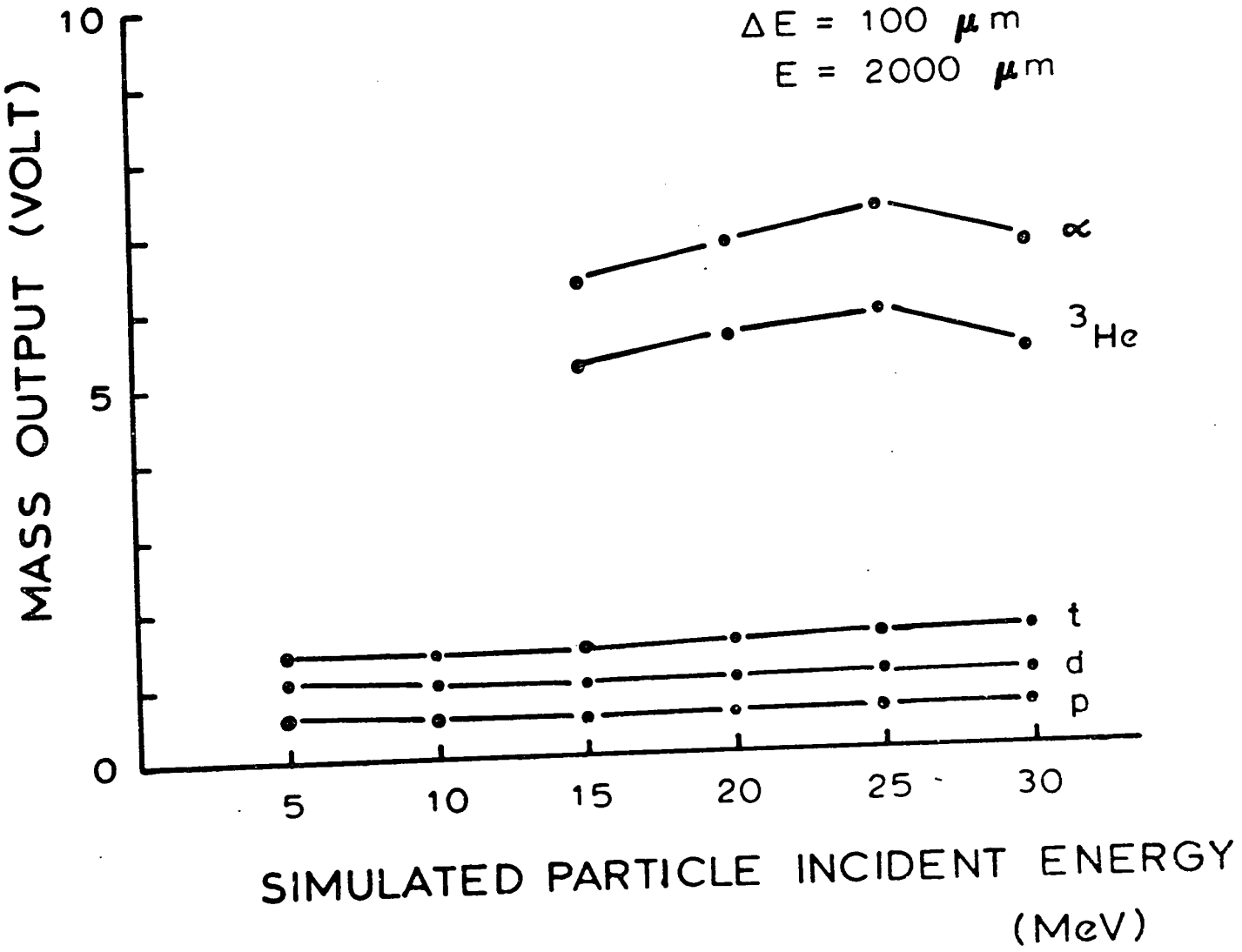
ΔE = 100 μm
E = 2000 μm
MASS OUTPUT (VOLT)
10
5
0
α
3He
t
d
p
5
10
15
20
25
30
SIMULATED PARTICLE INCIDENT ENERGY
(MeV)

FIGURE 4

Mass Spectrum from Charged Particle Identifier

Detectors: ΔE 100μm

E 2000μm

Particle Source: 18 MeV ^{3}He beam on ^{9}Be target, detected at 30^{o}

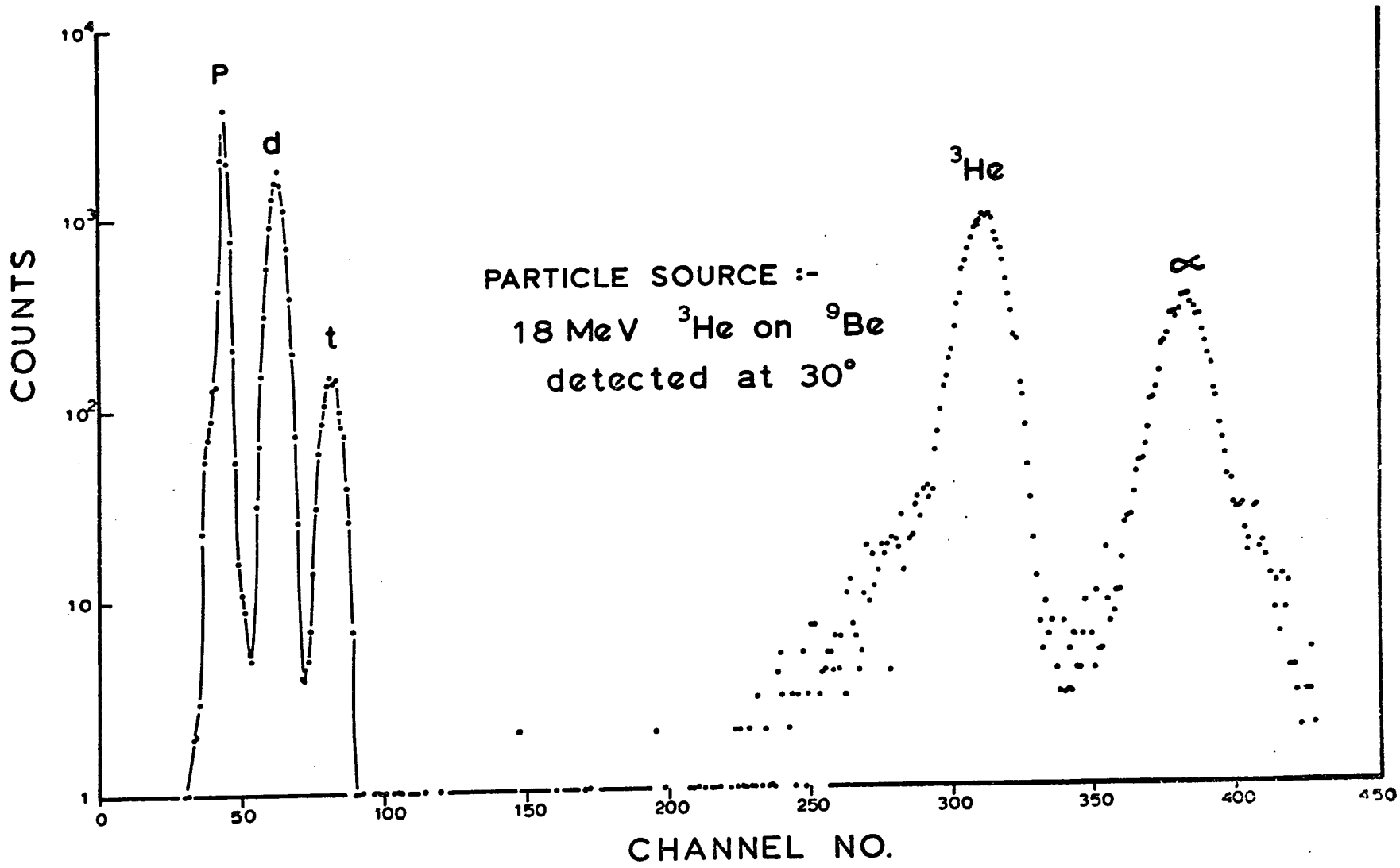
P
d
t
^{3}He
α
PARTICLE SOURCE :-
18 MeV ^{3}He on ^{9}Be
detected at 30°
COUNTS
10^4
10^3
10^2
10
1
0
50
100
150
200
250
300
350
400
450
CHANNEL NO.

FIGURE 5

Mass Spectrum from Charged Particle Identifier

Detectors: Δ E 100 μm

E 2000 μm

Particle Source: 18 MeV ^{3}He beam on ^{94}Mo target, detected at 80^{o}

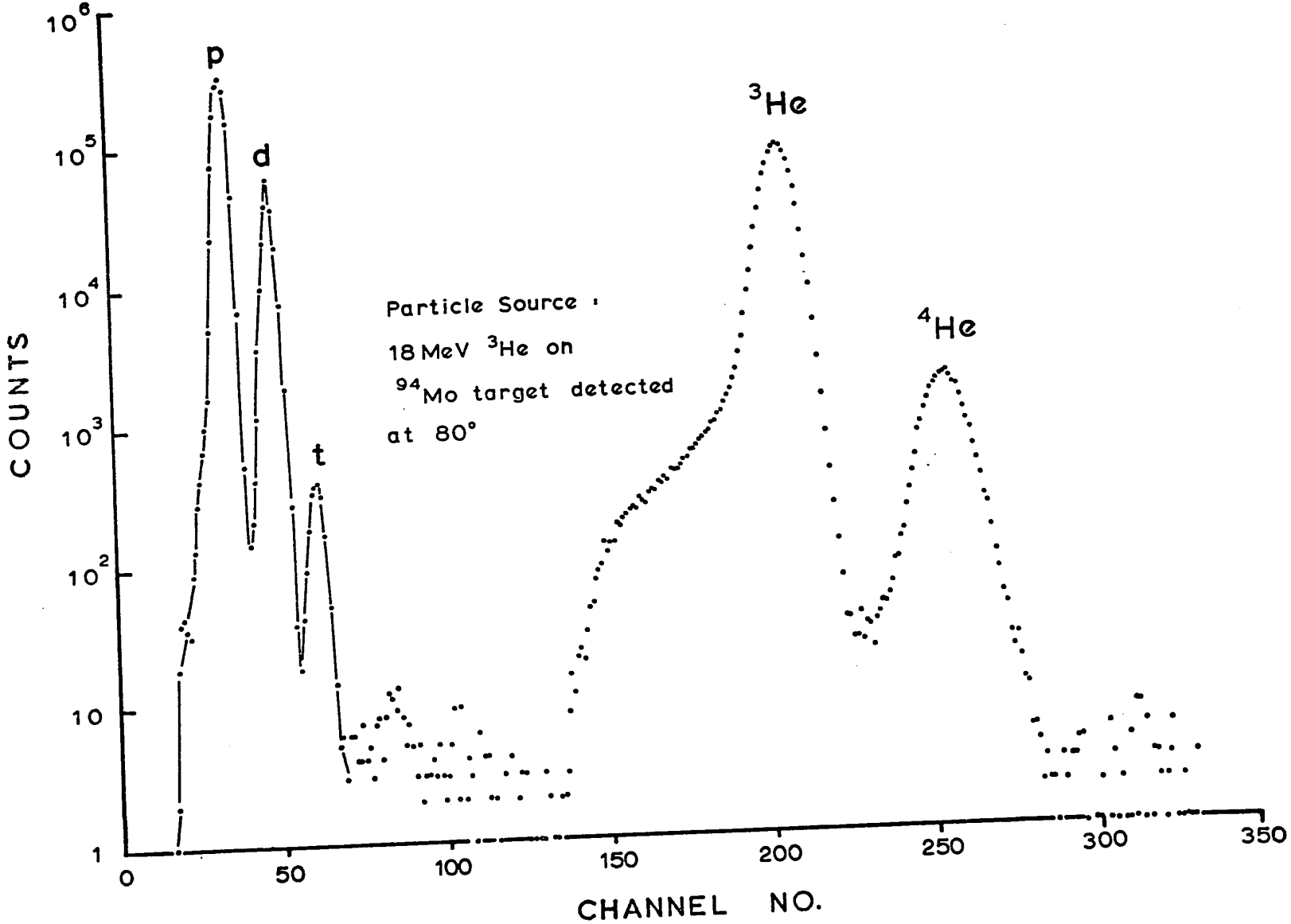
p
d
t
^{3}He
^{4}He
Particle Source :
18 MeV ^{3}He on
^{94}Mo target detected
at 80°
COUNTS
CHANNEL NO.
10^6
10^5
10^4
10^3
10^2
10
1
0
50
100
150
200
250
300
350

FIGURE 6

Block Diagram of the Electronics System Associated with each Detector Telescope

Electronics Units:

Preamp.	TC 136
Amp.	ORTEC 451
TSCA	ORTEC 420A
Fast Coinc.	ORTEC 414A
Linear Gate	ORTEC 442
Delay Amp.	ORTEC 427
Biased Amp.	ORTEC 444
SCA	ORTEC 406A
Pulser	BNC BH-1
Dual Attenuator	ORTEC 422
Fast Scaler	ORTEC 715

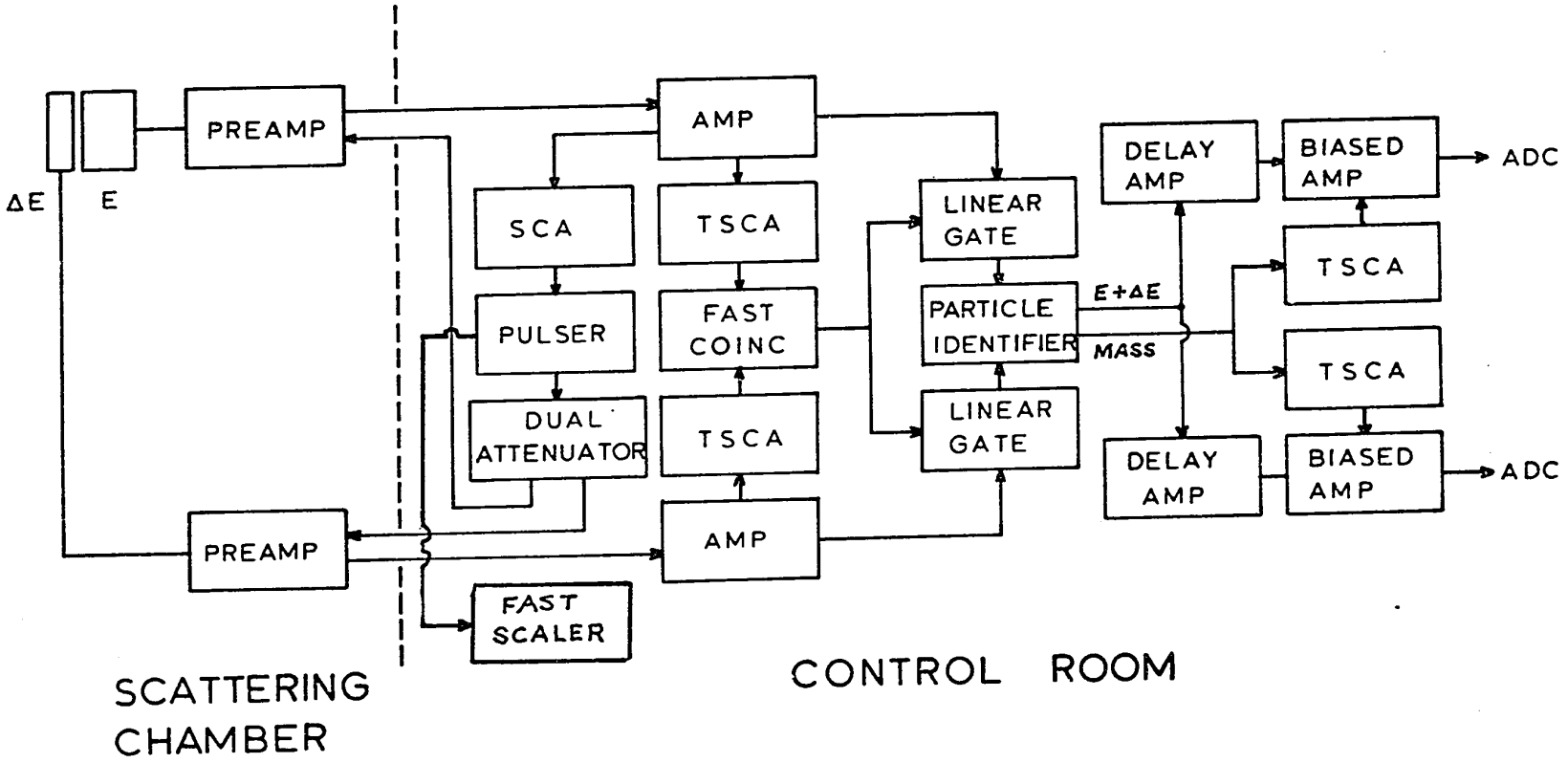
ΔE
E
PREAMP
PREAMP
AMP
AMP
SCA
TSCA
PULSER
FAST COINC
DUAL ATTENUATOR
TSCA
FAST SCALER
LINEAR GATE
PARTICLE IDENTIFIER
LINEAR GATE
E+ΔE
MASS
DELAY AMP
DELAY AMP
BIASED AMP
BIASED AMP
TSCA
TSCA
ADC
ADC
SCATTERING CHAMBER
CONTROL ROOM

CHAPTER III

THE (^{3}He,d) REACTIONS IN Mo-94,96,98 AND 100

3.1 Experimental Procedure

(i) The ^{94,96,100}Mo(^{3}He,d)^{95,97,101}Tc Reactions:

These reactions were studied using the 18 MeV ^{3}He beams from the University of Montreal tandem accelerator. Deuterons from these reactions were detected by two ΔE-E silicon solid state detector telescopes as described in the preceding chapter. Prior to data collection, the detectors and the electronics associated with each telescope were energy calibrated and adjusted so as to give a proper identification of differently charged particles and a correct energy range for each spectrum. An Ortec research pulser (Model 448) was used in conjunction with an ^{241}Am alpha particle source to calibrate the particle energy response of each set of detectors and preamplifiers. The detectors were placed inside the scattering chamber under vacuum (10^{-5} to 10^{-6} Torr). The output signals from each preamplifier induced by the alpha particles were then matched with the pulses generated by the Ortec

pulser, which were fed to the input of the preamplifier. The pulser output was normalized so that its dial scale provided a direct reading in energy. After having calibrated the detector-preamplifier sets and the energy scale in the Ortec pulser for each set, the energy resolution of each detector was examined by observing the line width of the alpha particles from the ^{241}Am source. It was found that all detectors used in this experiment have an energy resolution in the range from about 15 keV to 22 keV. This was acceptable for the present work.

Two detector telescopes were then assembled and mounted on the top rotatable plate of the scattering chamber with the axis of each telescope aligned to intercept the target at the point of incidence of the beam. Telescopes were placed 10^{o} apart. For the measurements of the reactions in ^{96}Mo and ^{100}Mo, the solid angles subtended by the two telescopes at the target were identical and equal to 0.225 m sr. However, it was found possible to use larger solid angles for the telescopes without decreasing the energy resolution, and also it was found more advantageous to make the solid angle larger for the telescope positioned at larger scattering angle than that for the telescope at smaller angle because of the difference in cross sections. It was, therefore, decided to use 0.548 m sr. for the

larger angle telescope for the measurements on the ^{94}Mo target.

The electronics system for each telescope was set up according to the diagram in figure 6 of the preceding chapter. Each charged particle identifier was first 'tuned up' using pulses from a pulser to simulate the different types of particles and according to the procedures described in section 2.4, chapter 2. After having obtained a satisfactory particle separation with the pulses, the energy calibrated Ortec pulser was used to calibrate the energy in the Δ E and E channel and match their 'gain' accurately. The biased amplifier, which feeds the sum energy (E+ΔE) to the ADC of the analyser, was adjusted so the deuterons with maximum possible energy were registered at about channel 2000 and the spectrum had an energy scale of about 5 to 10 keV/channel. The energy scale in the analyser was calibrated with the pulser.

The pulser used for deadtime correction (see figure 6) was adjusted to simulate a deuteron of an energy just a little higher than the highest energy possible for deuterons coming from the reaction under study. This provides a pulser pulse-peak near the end of the deuteron energy spectrum. The fast coincidence unit and the two TSCA units were also aligned and adjusted with the pulser. The time resolution of the

system used in this experiment was about 80 ns. Because of the difference in the charge collection times of the Δ E and E detectors, the coincidence alignment must be done in-beam and the pulses can only provide an approximate alignment.

After the alignment and calibration of the electronics system and data acquisition system were completed, the targets were then fastened onto their holder and inserted into the center of the scattering chamber, which was normally operated at a pressure of 10^{-6} Torr. Usually three targets plus a quartz were placed in the holder. The latter was for closed circuit TV viewing of the beam spot during beam alignment.

The helium-3 beam was sent through the beamline and focussed at the center of the scattering chamber with a beam spot about 2 mm in diameter. Several TV cameras were used to monitor the beam at different locations along the beamline. With a 2 mm-diameter collimator at the entrance port of the scattering chamber, a beam current transmission of 85% passing through the target and onto the Faraday cup at the exit port of the chamber was usually obtained. With the beam bombarding the target, the detector telescopes were counting real events and a final adjustment on the fast coincidence of each system was made. The "mass output" of the particle identifier was fed to a 512-channel analyser and some fine

adjustments on the "function" and "compensation" controls were made to obtain the best particle separation. The TSCA's, which were fed by the mass output of the identifier, were then carefully set to select the desired particles. In this experiment, both the deuterons and alpha particles were selected and their spectra were accumulated although only the results for the (^{3}He,d) reactions are presented here.

The deuteron spectra from the reactions were accumulated with the two telescope systems simultaneously. Each molydenum target was positioned with its normal at 30 degrees to the beam direction and remained unchanged during measurements at all scattering angles for the isotopes. Deuterons were detected only at angles in the forward hemisphere because of the low reaction differential cross sections at large angles. For each isotope, spectra were recorded for angles from 10 degrees to about 90 degrees in steps of 5 degrees. A low beam current was used for the measurements at small angles ($\leq 20^0$) to reduce pulse pile-up rates in the detectors and electronics to less than 5%. At angles larger than 20^o, these pile-up rates were negligibly small even if a beam of 500 na was used. In general, the beam current was adjusted to keep the count rates in all the detectors less than 15,000 counts per second. In most of the measurements, a stable He-3 beam current of about 500 na

on target was obtained.

Spectra were acquired at fourteen different angles for the $^{94}Mo(^{3}He,d)^{95}Tc$ reaction, each corresponding to an integrated incident beam of about 4000 Coulomb. Measurements at seventeen different angles were taken for the $^{96}Mo(^{3}He,d)^{97}Tc$ reaction at about 6000 μ Coulomb per angle. For the reaction of $^{100}Mo(^{3}He,d)^{101}Tc$, spectra for sixteen different angles were recorded, with an average bombarding charge of about 10,000 μ Coulomb per angle.

The thickness measurements for each target were performed on-line with the 18 MeV ^{3}He beam by recording the elastic scattering events at five different scattering angles ranging from 30 to 70 degrees. The results of these measurements will be presented in the next section of this chapter.

(ii) The $^{98}Mo(^{3}He,d)^{99}Tc$ Reaction:

Measurement of this reaction was performed at McMaster University using the 18 MeV ^{3}He beam from an FN tandem accelerator. Emerging deuterons from the reaction were detected on nuclear emulsion plates placed in the focal plane of an Enge split pole spectrograph with the magnet slits adjusted to provide an acceptance solid angle of 1.82 m sr. subtended to the center of the target.

The target was placed at the center of the scattering chamber making an angle of 9.58 degrees with the beam direction. The monitoring silicon surface barrier detector was placed at 30 degrees in the scattering chamber to measure the elastic scattering events. Prior to data accumulation, this detector was calibrated against a Faraday cup so that the relationship between the number of elastic events and the amount of integrated charge in the cup was established.

The thickness of the isotopically enriched ^{98}Mo target was measured off-line in a well-calibrated chamber (Burke and Tippett 1968), designed especially for this purpose. The apparatus consisted of a 2 mm ^{241}Am alpha particle source covered with collimator of that diameter. The elastically scattered (Rutherford scattering) alpha particles were measured by an annular silicon detector, which was located behind the target foil whose thickness was to be measured. The circuitry used to analyse the pulses from the detector consisted of a preamplifier, amplifier, single channel analyser and a scaler. The observed total elastic scattering cross section was then compared with the calculated Rutherford scattering cross section. This measurement yielded a thickness of 43 $\mu g/cm^2$ for the target used.

At each scattering angle, the magnet current and the NMR system of the spectrograph were set to select

deuterons of a particular momentum range, taking into consideration the kinematic shifts of the deuterons from the reaction. Thirteen deuteron spectra were recorded at scattering angles ranging from 8 degrees to 70 degrees. Each spectrum was exposed for an integrated incident beam of about 2000 μ Coulomb. The nuclear emulsion plates which recorded the deuteron events were subsequently developed and scanned in 1/4 mm swaths across the plates. One deuteron spectrum with high statistics was also acquired at bombarding energy 24 MeV. This spectrum was used for the determination of the precise energies of the various deuteron groups.

3.2 Data Reduction

(i) Reactions $^{94,96,100}Mo(^{3}He,d)^{95,97,101}Tc$:

The spectra obtained for these reactions were stored on magnetic tapes and were subsequently analysed with a CDC 6400 computer using a curve-fitting program GFITT (Zurstadt 1968). In this program, deuteron spectra in the form of multichannel data were analyzed by fitting the deuteron peaks with Gaussian curves. In each spectrum closely spaced (or unresolved) peaks up to a number of ten could be unfolded along with a polynomial or exponential type of background using the non-linear least squares

regression techniques. Centroid positions of all the peaks in one spectrum obtained from the fitting process were checked against those in the other spectra obtained at different angles for consistancy in kinematic shifts. Weak peaks appearing only in one spectrum and not in the others were discarded. Contaminant deuteron peaks resulting from reactions in the other isotopes in the target were recognized easily from their kinematic shifts and their reaction Q-values (Wapstra et al. 1971). They are mainly from reactions in ^{12}C, ^{13}C, ^{16}O and ^{18}O which were known to be present in the target. Contaminant peaks due to other molydenum isotopes in each target were not observed. However, since the Q-values of the (^{3}He,d) reactions in ^{13}C and ^{18}O are quite close to those of the molydenum isotopes, at some angles, the weak peaks in the region of interest in the spectra were partially or fully obscured by the contaminant peaks and were not resolvable. In those cases the obscured peaks in those measurements were ignored.

The areas of peaks in the spectra obtained at different angles were evaluated and converted into the experimental cross sections in the laboratory system, which may be expressed as

$$\frac{d\sigma}{d\Omega} = N \frac{e Z_2}{Q} \frac{M_2}{N_0 \rho t} \frac{\cos\theta_r}{\Delta\Omega} \qquad (3.3\text{-}1)$$

where N : number of events in a given peak leading to the final state in the residual nucleus,

Q : total integrated charge of the incident particles,

eZ_1 : number of electric charges carried by the incident particle,

N_o : Avogadro's number,

M_2 : mass of the target nuclei,

ρt : effective target thickness,

θ_T : the angle between the incident beam and the normal to the target, and

$\Delta\Omega$: solid angle subtended by the detector at the target center.

Since there were some real events lost due to the deadtimes in the electronics, the number of pulses in the pulser peak in each spectrum must be evaluated and compared with the number of pulser pulses fed into the electronics system in order to compute the fractional loss of events in the spectrum. The correction for this fractional loss must be applied to N in the calculation for the differential cross section.

The target thickness, ρt, was calculated from the results of elastic scattering measurements. At each elastic scattering, the number of events, N and

the corresponding incident charge Q were measured. The optical model was used to calculate the differential cross section, $d\sigma/d\Omega$, and then ρt was extracted from equation (3.2-1). If the experimental conditions used in the measurements of the elastic scattering were the same as those employed in the reaction experiment, as in the present case, the product of $\Delta\Omega$ and ρt for the reaction, could be directly deduced.

The optical model calculation was performed by the computer code DWUCK (Kunz 1969) and the optical potential parameters employed in this calculation are those used for the incident channel in the DWBA calculations for the (^{3}He,d) angular distributions. These parameters were taken from the work of Picard and Bassani (1969) in the study of (^{3}He,d) reactions on the isotopes of ^{88}Sr, ^{90}Zr and ^{92}Mo, at the same incident energy as used in the present work. They are given in section 3.4, this chapter.

It is interesting to see the variation of the elastic scattering cross sections with scattering angles and the quality of the agreement between the predictions of the optical model and the experiment. Fig. 7 shows the calculated elastic cross sections for

^{94}Mo expressed in terms of the Rutherford cross sections using the optical parameters mentioned above. It can be seen that nuclear potential plays a significant role in those events which are scattered through an angle larger than 20 degrees. The dots on the figure represent the experimental values, which have been normalized to the theoretical curve. While the fit between the optical model calculations and experiment is not excellent, it is believed that the elastic scattering differential cross sections computed from the model are accurate to $\pm$ 15%. This error will appear as a systematic error in absolute values of the (^{3}He,d) reaction differential cross sections. Using these theoretically calculated differential cross sections and the geometrical solid angle values the target thickness for the different molydenum targets were estimated. The values of 98 μg/cm^2, 103 μg/cm^2 and 51 μg/cm^2 were obtained for the Mo-94, 96 and 100 targets, respectively. The numerical computation for the (^{3}He,d) differential cross sections were performed using the computer code KINX (Zurstadt 1969).

The total error of the experimental differential cross sections can be considered as a sum of two parts: the uncertainties in the relative cross sections, which effect the shape of the angular distributions and the uncertainties in the absolute cross sections which

influence the absolute transition strengths. The major contribution to the relative errors comes mainly from the uncertainty of peak area extraction, which included the statistical fluctuation of the number of events in the peaks, the uncertainties in the unfolding of closely spaced peaks and the background subtractions. Other minor contributions to the relative errors were those coming from the uncertainties in the relative efficiency of the two detector telescopes and the electronics dead time corrections. However, the relative solid angles of the two telescopes were determined experimentally by repeating the elastic scattering measurements for each of the telescopes at the same angular position.

The ratio of number of elastic scattering events for the same amount of accumulated charge gave the relative values. In all cases, the experimentally measured values agreed with the values calculated from the geometry to within 2%.

For the systematic error, most of the contributions came from the uncertainty of the absolute target thickness and the solid angle determinations, as well as the accuracy of the beam current monitoring system. In the present case, the error in the product of the solid angle and target thickness dependent on the

accuracy of the theoretically calculated elastic scattering differential cross section mentioned above. Taking all these factors into account, the total systematic error in the absolute cross sections is estimated to be less than 20%. Finally, absolute accuracy for all angle measurements is believed to be better than 0.2 degree.

The precise energies of the deuteron peaks were determined using the known energies of the deuteron peaks arising from the (^{3}He,d) reaction in ^{16}O, which was present in the target. The Q-value for the (^{3}He,d) reaction in ^{16}O was taken from Wapstra and Gove (1971) and the energies of the various deuteron peaks observed in this reaction were taken from those compiled by Ajzenberg-Selove (1970). After compensating for the kinematic shifts in the various deuteron peaks, the energies of the states in the technetium isotopes observed in the (^{3}He,d) reactions were determined by a linear fitting to the centroid positions of the deuteron peaks.

The method for determining the energies of the states in the technetium nuclei come from the determination of the peak centroids and the uncertainties in the energies of the deuteron peaks from the (^{3}He,d) reaction in ^{16}O which included the errors in the corrections due to the kinematic shifts. It is believed that the overall

uncertainty in the technetium energy level determination was about 2.5 to 3 keV per 1 MeV excitation energy difference.

(ii) Reaction $^{98}Mo(^{3}He,d)^{99}Tc$:

The nuclear emulsion plates, which recorded all the deuteron events, were scanned with a microscope in 1/4 mm swaths across each plate for all plates. The resulting number of events in each swath was plotted as a function of position in each set of plates to obtain the deuteron spectrum for that particular scattering angle. The areas of the various deuteron peaks were evaluated and converted into differential cross sections according to equation (3.3-1).

In the measurements for this reaction, most of the relative errors arise from the uncertainties in the statistical fluctuation in the number of events registered in the deuteron peaks and in the photographic plate readings, which was about $\pm$ 5%.

The systematic errors for the measurements were mainly due to the inaccuracy in the target thickness measurement, current monitoring, detector calibration, and solid angle determinations. The target thickness was obtained from the measurement on the Rutherford scattering of alpha particles from a ^{241}Am source and the

accuracy of this measurement was estimated to be ± 20%. The beam current monitoring system is believed to be calibrated to accuracy of ± 3% and the solid angle measurement carried an accuracy of ± 2%. A combined systematic error of ± 25% has been estimated for all measurements on the differential cross sections of the (^{3}He,d) reaction on the ^{98}Mo target.

The energies of the various deuteron peaks leading to the excitation of the levels in ^{99}Tc were determined from the high statistics deuteron spectrum obtained with a 24 MeV ^{3}He beam. The position of some of the deuteron peaks was correlated with the corresponding known levels in ^{99}Tc observed in the beta decay of ^{99}Mo (Cook et al. 1969). A linear extrapolation of these peaks of known energies was made for all the other peaks. The level energy of ^{99}Tc determined this way is believed to be better than 2 keV per 1 MeV excitation energy.

3.3 Experimental Results

Fig. 8 presents the deuteron spectrum from the reaction of $^{94}Mo(^{3}He,d)^{95}Tc$ obtained at 60^{o} (lab.). The overall energy resolution is about 40 keV full width at half maximum (FWHM). The dead-time correction pulser peak has a FWHM of about 25 keV, which represents the energy resolution of the electronics system. This implies that the detector intrinsic energy resolution and the fluctuation in the energy degradation in the target accounted for the remaining energy spread observed. The peaks corresponding to the excitation of the various levels in ^{95}Tc and their associated differential cross sections have been analyzed up to an excitation energy of 4.709 MeV. A total of 38 levels in each of the spectra obtained at different angles have been studied. The density of levels populated in this reaction has been observed to increase rapidly with excitation energy and reliable analysis of levels at excitation energy higher than 4.7 MeV could not be obtained.

The results obtained for the excitation energies and the differential cross sections for the various levels in ^{95}Tc are listed in table 2. The differential cross sections and their associated relative errors, are given in the center of mass system. The total relative error in each differential cross section measurement and

the uncertainty in each level energy determination are also listed in the table. The listing format adopted was to give the error for each value directly under the value itself with the significance of its digits having a one to one correspondence with those in the mean value. It is understood that all errors carry a ± sign with them. The total systematic error in each differential cross section measurement, as discussed in the preceding section, was ± 20%. The blank entries in the table indicated that the deuteron peaks corresponding to the states were either unresolved from the neighboring peaks, or obscured by contaminant peaks, or poor statistics.

The doublets observed at 2.257, 2.308; 4.381, 4.428; 4.489 and 4.528 MeV could not be resolved reliably. Only their combined differential cross sections have been extracted. Graphs displaying the angular distributions for the excitation of the various states in ^{95}Tc will be presented in the next section together with the results of an analysis of the reaction.

A typical deuteron spectrum of the $^{96}Mo(^{3}He,d)$ ^{97}Tc reaction obtained at 50^{o} (lab.) is shown in fig. 9. The energy resolution of the experiment is the same as that stated above for the $^{94}Mo(^{3}He,d)^{95}Tc$ reaction. Deuteron peaks corresponding to the excitation of thirty-two states in ^{97}Tc have been analysed. The high level density above 3 MeV excitation energy rendered data

extraction on levels lying higher than this energy impossible. Table 3 presents the numerical results of the excitation energies and differential cross sections for the various levels in ^{97}Tc. The entry format for this table is the same as that used for table 2. As can be seen in figure 9, the peaks corresponding to states at 2.878 and 2.908 MeV were not well resolved in the present experiment, consequently, only their combined differential cross sections are given in table 3. A graphical display of the angular distributions for the various excited states will be presented together with the results of a theoretical analysis in the next section.

The total systematic error for the differential cross section measurements was $\pm$ 20%.

The measurements of the $^{98}Mo(^{3}He,d)^{99}Tc$ reaction were performed with the magnetic spectrograph. As a result, the overall experimental energy resolution is better than the other described in this thesis; a resolution of about 18 keV (FWHM) was obtained. A complete angular distribution for the outgoing deuterons was measured with an 18 MeV He-3 beam, and a typical deuteron spectrum obtain at 30^{o} (lab.) is shown in figure 10. One spectrum with much better statistics was accumulated at 50^{o} (lab.) using a 24 MeV He-3 beam and it is shown in figures 11 and 12 (two parts). To determine

the energies of the various deuteron peaks, the spectrum obtained at 24 MeV incident energy was used. In these spectra, the deuteron peaks are labelled by their corresponding level excitation energies in ^{99}Tc. As can be seen in figure 12, the density of levels populated in this reaction increases rapidly with excitation energy. Consequently, for the set of data obtained at 18 MeV incident energy, only deuteron peaks corresponding to excitation energy below about 2.7 MeV have been analysed. The excitation energies of the levels in ^{99}Tc and their associated differential cross sections in the C.M. system are listed in table 4, together with their total relative errors. The entry format for this table is the same as that used for tables 2 and 3. As discussed previously (section 3.2), the total systematic error for the differential cross section measurements in this experiment was $\pm$ 25%.

For the 'double' deuteron peaks corresponding to excitation energies 1.803, 1,825; 1.982, 2.000; 2.160, 2.176; 2.396, 2.414; 2.466, 2.486; 2.653, 2.675 MeV, only the combined differential cross sections for each pair are given in table 4. States in ^{99}Tc lying above excitation energy 2.7 MeV observed in the deuteron spectrum at 24 MeV incident energy are also listed in table 4, but no differential cross sections were extracted from the data obtained at 18 MeV incident

energy.

A graphical display of the angular distributions for the various states in ^{99}Tc will be presented in the next section together with the results of a theoretical calculation.

The experiment on the $^{100}Mo(^{3}He,d)^{101}Tc$ reaction was performed under a set of experimental conditions similar to that used for the study of $^{94}Mo(^{3}He,d)^{95}Tc$ and $^{96}Mo(^{3}He,d)^{97}Tc$ reactions. As a result, the experimental energy resolution and systematic error are the same as those given for the two reactions described previously. A typical deuteron energy spectrum obtained at 50^{o} (lab.) is shown in figure 13. In this spectrum it is seen that the level density in ^{101}Tc is relatively high, and only prominant deuteron peaks corresponding to excitation energy below about 1.7 MeV in ^{101}Tc could be studied in the present work. The excitation energies of these levels and the differential cross sections for their excitation are presented in table 5, together with the relative measurement errors. The entry format for the numerical values in this table is the same as the one employed for the other tables (2,3,4). The deuteron peaks corresponding to excitation energies at 1.280 and 1.319 MeV were not resolved in this experiment, consequently, only their combined differential cross sections are given in table 5.

From the deuteron energy spectra, it is apparent that the energy level density of the four odd-mass Tc isotopes is relatively high. Many deuteron peaks appeared to be multiplets. In such cases, although the computer program GFITT (Gaussian curve fitting) was used to effect the individual peak area separation, the differential cross sections for the excitation of the corresponding states involved always carried a relatively large error. Since some of the states in each Tc isotope studied were more strongly excited in the reaction than the others, it is conceivable that some of the weakly excited states were masked by the strongly excited neighboring states. This possibility is particularly likely in the measurements for the ^{95}Tc, ^{97}Tc and ^{101}Tc nuclei where the experimental energy resolution was relatively poor.

The present deuteron energy measurements can also yield the Q-values corresponding to ground state transitions obtained from this work. These values have been compared with the values given by Maples *et al.* (1966) and by Wapstra and Gove (1971), which are also given in table 6. In general, the agreement is fairly good.

3.4 Data Interpretation and Discussion

(i) Distorted Wave Born Approximation Calculations:

The (^{3}He,d) reactions at an incident energy higher than the Coulomb barrier of the incident particle take place primarily via the direct reaction mechanism (Austern 1969). That is, they proceed on a very short time scale, and involve only a few internal degrees of freedom of the colliding systems without the formation of compound nuclear systems (target nucleus plus projectile) as intermediate states. In such a reaction, the incident ^{3}He particle, which may be considered to be composed of a 'deuteron' and a 'proton', approaches a target nucleus, losing the proton to the latter and emerges as a deuteron. This reaction is a very useful spectroscopic tool because it can be viewed as the transfer of a proton into a definite single particle orbital in the target nucleus without the excitation of other degrees of freedom. In addition, the angular distribution of the outgoing deuterons reflects the properties of the single particle orbital and the wave functions of the initial and final nuclear states.

The direct reaction theory that is commonly used for the analysis of the (^{3}He,d) reaction is called the distorted wave Born approximation (DWBA) theory for single

nucleon transfer reactions. The formal derivation of the DWBA theory and the approximations involved in its calculations have been discussed in many review articles (Tobocman 1961, Satchler and Tobocman 1960, Satchler 1964 and 1965, Glendenning 1963, Bassel et al. 1962, Austern et al. 1964, Austern 1963 and 1969). In this theory, the ^{3}He incident particles are first elastically scattered by an absorptive optical potential of the target nucleus, distorting the otherwise plane waves of ^{3}He. These distorted ^{3}He waves then interact with the target so that a proton in the ^{3}He is captured by the target to form the final nuclear state, and the remaining n + p system of the ^{3}He emerges from the interaction as a deuteron. Thus, the interaction responsible for the transition from the initial nuclear state to the final nuclear state is primarily the interaction that binds the transferred proton to the deuteron to form the ^{3}He particle. Upon leaving the final nucleus the deuteron waves suffer a distorting elastic scattering in the absorptive optical potential of the latter. The transition in the stripping reaction, therefore, is one between the elastic scattering states.

From the DWBA theory, the differential cross section for the reaction A(^{3}He,d)B, for the unpolarized projectile and target nucleus, can be expressed in the form (Glendenning 1963),

$$\frac{d\sigma}{d\Omega}(\ell j)=\frac{3}{4}\frac{\mu_h\mu_d}{(2\pi\hbar^2)^2}\frac{k_d}{k_h}\frac{2J_f+1}{2J_i+1}\,C^2S(\ell j)\sum_{m_\ell}\left|B_\ell^{m_\ell}\right|^2 \tag{3.4-1}$$

$$B_\ell^{m_\ell}=i^{-\ell}(2\ell+1)^{-\frac{1}{2}}\int\psi_d^{(-)*}\left(\vec{k}_d,\vec{r}_{dp}+\frac{M_B}{M_B}\vec{r}_p\right)\phi_d^*(\xi_d)\,Y_\ell^{*m_\ell}(\hat{r}_p)\cdot$$
$$\cdot V_{dp}(r_{dp})\,\phi_h(\vec{r}_{dp},\xi_d)\,\psi_k^{(+)}\left(\vec{k}_h,\vec{r}_p+\frac{M_d}{M_h}\vec{r}_{dp}\right)d\vec{r}_{dp}\,d\vec{r}_p\,d\xi_d$$

$$S(\ell j)=(A+1)\left|\int\left[\Psi_{J_iT_i}(A)\times\phi_{\ell j}(r_p)\right]^*_{J_fT_f}\Psi_{J_fT_f}(A+1)\,d(A+1)\right|^2 \tag{3.4-2}$$

$$C=(T_iT_{3i}\cdot\tfrac{1}{2}\;-\tfrac{1}{2}\,|\,T_fT_{3f}) \tag{3.4-3}$$

(3.4-4)

where:

$\psi_h^{(+)}$ and $\psi_d^{(-)}$ are the incident and outgoing distorted waves of the ^{3}He (subscript h) and deuteron (subscript d), respectively, with wave number k_h and k_d and with reduced masses μ_h and μ_d; $\vec{r}_p$ and $\vec{r}_{dp}$ are the coordinated of the transferred proton relative to the C.M. of the initial nucleus A, and relative to the C.M. of the

deuteron; M_A, M_B M_h and M_d are the masses of the initial nucleus, final nucleus, ^{3}He particle and deuteron; $\phi_\ell^{m_\ell}(\vec{r}_p)$ is the orbital part of the single particle spin-orbit wave function $\phi_{\ell j}(\vec{r}_p)$ of the captured proton in the final nucleus characterized by the orbital quantum numbers $(n\ell j)$; $\phi_h(\vec{r}_{dp}, \xi_d)$ and $\phi_d(\xi_d)$ are the internal wave functions of the ^{3}He and deuteron, with ξ_d representing the relative coordinate of the n-p system forming a 'virtual deuteron' in the ^{3}He which eventually becomes the outgoing deuteron; $V_{dp}(r_{dp})$ is the interaction of the transferring proton with the 'virtual deuteron' forming the ^{3}He; $\Psi_{J_i T_i}(A)$ and $\Psi_{J_f T_f}(A+1)$ are the initial and final nuclear state wave functions, each characterized by the isospin T and total spin J. $S(\ell, j)$ is the spectroscopic factor defined by MacFarlane and French (1960) and is equal to (A+1) the nucleon numbers (or the equivalent nucleon numbers) of the final nucleus times the square of the corresponding fractional parentage coefficient; $C = (T_i\ T_{zi},\ 1/2\ -1/2 \mid T_f\ T_{zf})$ is the Clebsh-Gordan coefficient for the coupling of the initial state isospin to the captured proton to form the isospin of the final nuclear state.

To evaluate the amplitude $B_\ell^{m_\ell}$ (equation 3.4-2), several simplifying assumptions must be made as some of the

quantities involved are not very well known. The interaction V_{dp} and the internal wave function ϕ_h of ^3He are not well known although the deuteron internal wave function ϕ_d is better known (Bassel 1966). For the present calculation it has been assumed that the interaction has zero range. Hence, the factor in equation (3.4-2) may be written (Bassel et al. 1962),

$$\int \phi_d^*(\xi_d)\, V_{dp}(r_{dp})\, \phi_h(\vec{r}_{dp}, \xi_d)\, d\xi_d = D_o\, \delta(\vec{r}_{dp}) \qquad (3.4\text{-}5)$$

where D_o is a constant. The validity of the zero-range approximation has been discussed by Satchler (1964) and he concluded that it is a fairly good approximation for light ion ($A \leq 4$) induced nucleon transfer reactions at incident energies substantially higher than the Q-values of the reactions and that finite range effects are important when the momentum transfer in the reaction is large. The differential cross section of equation (3.4-1) can be reduced to

$$\frac{d\sigma}{d\Omega}(lj) = N\, \frac{2J_f+1}{2J_i+1}\, \frac{C^2 S(lj)}{2j+1}\, \sigma_{DWBA}(lj) \qquad (3.4\text{-}6)$$

where

$$\sigma_{DWBA}(lj) = \frac{\mu_h \mu_d}{(2\pi\hbar^2)^2}\, \frac{k_d}{k_h}\, \frac{2j+1}{2} \sum_{m_l} \left| F_l^{m_l} \right|^2 \qquad (3.4\text{-}7)$$

$$F_l^{m_l} = i^{-l}(2l+1)^{-\frac{1}{2}} \int \psi_d^{(-)*}(\vec{k}_d, \frac{m_A}{m_B}\vec{r}_p)\, \phi_l^{m_l}(\vec{r}_p)\, \psi_h^{(+)}(\vec{k}_h, \vec{r}_p)\, d\vec{r}_p \qquad (3.4\text{-}8)$$

and $N = (3/2)D_o^2 \times 10^{-4} = 4.42$ is the normalization constant for the (^{3}He,d) reaction taken from the work of Bassel (1966).

For even-even targets, as in the present study, the ground state spin $J_i = 0$, and therefore, the final state spin $J_f = j$. Thus, equation (3.4-6) reduces to

$$\frac{d\sigma}{d\Omega}(lj) = N C^2 S(lj)\, \sigma_{DWBA}(lj) \qquad (3.4\text{-}9)$$

To evaluate $S(lj)$ it requires a detailed knowledge of the initial and final state nuclear wavefunctions which is often not available. Moreover, in a proton stripping reaction, there are two possible values for the isospin T_f of the final state: $T_f = T_> = T_i + 1/2$ and $T_< = T_i - 1/2$. For $T_f = T_>$, $C_>^2 = 1/(N-Z+1)$, and for $T_f = T_<$, $C_<^2 = (N-Z)/(N-Z+1)$. It is customary to extract an experimental value for the $C^2\, S(l,j)$ by computing the quantity $\sigma_{DWBA}(l\,j)$ in equation 3.4-9 for each transition and comparing the result with the experimental $\frac{d\sigma}{d\Omega}$. For the low-lying states encountered in the present work, T_f is most properly equal to $T_<$.

In making the calculations for the present work

of (^{3}He,d) reaction on the even-even Mo isotopes, the distorted waves ψ_d and ψ_h were generated from the Schödinger equation

$$\left\{ \nabla^2 + k_s^2 - \frac{2\mu_s}{\hbar^2}\left[U(r) + U_c(r) \right] \right\} \psi_s(\vec{k}, \vec{r}) = 0 \qquad (3.4\text{-}10)$$

where 's' is for ^{3}He (h) or deuteron (d). The Coulomb potential U_c was assumed to be due to a uniform charged sphere of radius $R_c = r_c A^{1/3}$ and has the form

$$U_c = \frac{zZ}{r} e^2 \qquad \text{for } r \geq r_c \qquad (3.4\text{-}11)$$

$$= \frac{zZ}{2} \frac{e^2}{r_c} \left(3 - \frac{r^2}{r_c^2} \right) \qquad r < r_c$$

where z, Z denote the charge numbers of the pairs (^{3}He, Mo) or (d, Tc), r_c is called the Coulomb radius parameter and A refers to the atomic mass number of Mo or Tc. The optical potential U(r) was taken to be

$$U = -V f(r, r_r, a_r) - i W_V f(r, r_V, a_V) + i 4 W_D a_D \frac{d}{dr} f(r, r_D, a_D) + V_{so} \left(\frac{\hbar}{m_\pi c} \right)^2 \vec{\sigma} \cdot \vec{l} \frac{1}{r} \frac{d}{dr} f(r, r_{so}, a_{so}) \qquad (3.4\text{-}12)$$

The first term represents the real part of the Wood-Saxon potential, and its imaginary part includes both the volume (subscript V) and Surface potentials (subscript D) and the

last term is the spin-orbit potential. The function $f(r, r_x, a_x)$ is the Wood-Saxon form factor with 'x' standing for the various subscripts,

$$f(r, r_x, a_x) = \left[1 + \exp\left(\frac{r - r_x A^{\frac{1}{3}}}{a_x}\right)\right]^{-1} \quad (3.4\text{-}14)$$

The quantities, V, W_V, W_D and V_{so} are called the potential depths of the Wood-Saxon well and the r_x and a_x are the corresponding radius and diffuseness parameters. In the spin-orbit term, $\left(\frac{\hbar}{m_\pi c}\right)$ is the π meson compton wavelength, and $\vec{\sigma}\cdot\vec{\ell}$ is the usual spin-orbit interaction with $\vec{S} = \vec{\sigma}/2$. In the present analysis, however, only one imaginary potential, either the volume term or the surface term, was used.

In the evaluation of the distorted waves, appropriate optical parameters are needed. Since no detailed elastic scattering data are available, in the present work the values for the potential parameters were taken from those used in the other (^{3}He,d) reactions on the neighboring nuclei at the same incident energy. The parameters for both the He-3 and deuteron channels were taken from the work of Picard and Bassani (1969) in the study of (^{3}He,d) reactions on ^{88}Sr, ^{90}Zr and ^{90}Mo. The ^{3}He optical parameters were originally used by Conjeau et al. (1968) to analyse the He-3 elastic scattering on Sn

isotopes. The spin-orbit potential in the deuteron channel used by Picard and Bassani has been dropped in the present analysis. It has been shown in this work that the inclusion of this spin-orbit potential produced insignificant changes both in shape and in magnitude in the angular distribution in the forward hemisphere. The parameters used in this work are listed in table 7.

The stripped proton was assumed to be bound to the core (the target nucleus Mo) to form the final nucleus Tc. The bound state proton wavefunction was taken to be the eigenfunction of the Schrödinger equation

$$\left\{\nabla^2 + k_p^2 - \frac{2\mu_p}{\hbar^2}\left[U_p(r) + U_c(r)\right]\right\}\phi_p(\vec{r}) = 0 \qquad (3.4\text{-}14)$$

The Coulomb potential U_c is the same as that given by equation 3.4-11, and the average nuclear potential U_p is given by

$$U_p = -Vf(r, r_r, a_r) + \lambda_{so} V\left(\frac{\hbar}{2M_p c}\right)^2 \frac{\vec{\sigma}\cdot\vec{\ell}}{r}\frac{d}{dr} f(r, r_{so}, a_{so}) \qquad (3.4\text{-}15)$$

with the form factor $f(r, r_x, a_x)$ given by equation 3.4-13. The well depth V was adjusted to bind the proton to the orbital characterized by quantum numbers n, ℓ, j, with energy equal to its experimental separation energy for each final state. The separation energy is given by $Q(^3He,d) + 5.493$ MeV, the reaction Q-value for each final

state plus the binding energy difference between the ^{3}He particle and deuteron. In the spin-orbit term, $(\frac{\hbar}{m_p c})$ is the Compton wave length of the proton, and λ_{so} the spin orbit strength factor, which was set equal to 25 for all the calculations. This value is commonly used for single nucleon form factor calculations (Kunz 1969). Geometrical parameters r_{so}, a_{so} are taken as those in the central term, r_r, a_r. The proton parameters are given in table 7.

The computation of the quantity $\sigma_{DWBA}(\ell j)$ in equation (3.4-9) were carried out using the computer code DWUCK (Kunz 1969), with the zero range approximation and no lower-cutoff limit for the radial integral.

A computation has been performed for the theoretical prediction on the shape of the angular distribution for different orbital angular momentum ℓ transfer. The input data used for this computation were those pertaining to the ground state transition of the ^{100}Mo(^{3}He,d)^{101}Tc reaction, and the result is shown in figure 14. It should be noted that the angular positions of the first maximum of these distributions differ from each other by about 7° for each unity change in the ℓ-transfer value. The positions of the first maximum and minimum in each distribution are important as they have a strong bearing on the determination of the ℓ-transfer value for an observed transition.

Before proceeding to the analysis of the various experimentally observed angular distributions, it is useful to obtain a guideline from an elementary consideration of the structure of the molydenum isotopes. Each of these isotopes has 42 protons. In its ground state, the 14 valence protons beyond the Z = 28 presumably fill the orbitals $2p_{3/2}$, $1f_{5/2}$, $2p_{1/2}$ and $1g_{9/2}$, either fully or partially, and the orbitals $2d_{5/2}$, $1g_{7/2}$, $2d_{3/2}$, $3s_{1/2}$ and $1h_{11/2}$ in the major shell $50 < Z \leq 82$ are presumably vacant. In the proton stripping (^{3}He,d) reaction, the vacancies in these two sets of orbitals are available to the transferred proton. From the energy systematics of single particle orbitals, the excitation of low-lying states arises primarily from the $1g_{9/2}$ and $2p_{1/2}$ proton orbitals with $\ell = 4$ and 1 transfer, respectively. These states would be followed by those coming from orbitals $2p_{3/2}$, $2d_{5/2}$, $1f_{7/2}$, $1g_{7/2}$, $2d_{3/2}$ and $3s_{1/2}$ with $\ell = 1, 2, 3, 4, 2$, and 0 transfer.

All observed angular distributions of the ^{94,96,98,100}Mo(^{3}He,d)^{95,97,99,101}Tc reactions listed in tables 2, 3, 4 and 5 (section 3.3 of this chapter) have been analysed. For each transition, the orbital angular momentum ℓ transfer, the range of the most probable spin-parity J^π of the final state and the transition strength $C^2S(\ell, j)$ have been determined. The analysed angular distributions possessing definite ℓ-transfer

assignments are shown in figures 15, 16, 17 and 18 and the extracted spectroscopic information given in tables 8, 9, 10, and 11, for the four reactions. For the analysed distributions with no definite ℓ assignments either because of insufficient data due to poor statistics or because of interferences from deuteron peaks arising from impurities in the targets, no angular distributions are shown but the extracted spectroscopic information is listed in parentheses in tables 8, 9, 10 and 11. For each transition with a given ℓ value, there are two possible J_f values, i.e. $J_f = \ell \pm 1/2$, except for $\ell = 0$. Since the spectroscopic factor has a $(2j+1)$ dependence as well as the dependence of the proton wave function on the spin-orbit coupling potential, the values for $S(\ell, j)$ have been extracted for each possible j value.

In the analysis of some unresolved doublets, the angular distributions have been fitted with the following equation

$$\left(\frac{d\sigma}{d\Omega}\right)_{DOUBLET} = NC^2 S_1(\ell_1 j_1)\,\sigma_{DWBA}(\ell_1 j_1) + NC^2 S_2(\ell_2 j_2)\,\sigma_{DWBA}(\ell_2 j_2) \quad (3.4\text{-}16)$$

through least squares technique. In the fitting, all possible combinations of the shapes of ℓ_1 and ℓ_2 distributions were generated and a minimization of chi-square value was carried out. The spectroscopic factors $S_1(\ell_1 j_1)$ and $S_2(\ell_2 j_2)$ were then extracted from the chi-

square fitting results.

In tables 8, 9, 10 and 11, the values in the columns labelled as normalized C^2S were obtained from multiplying each corresponding observed C^2S by the ratio of the number of theoretical holes in the shells below the Z = 50 shell closure to the number of observed holes in these shells.

It should be pointed out that in the foregoing calculations, the spherical and local optical potentials have been used to generate the distorted waves and the d-p interaction has been assumed to have a zero range. The non-locality and finite-range effects can be corrected for in the DWBA calculations by the local energy approximation (Drisko and Satchler 1964, Perey and Saxon 1964, Li and Mark 1969). These corrections have the effect of damping the contributions from the nuclear interior to the transition amplitude $B_{\ell}^{m_\ell}$ (equation 4.2-2). While they have little effect on the shape of the angular distributions, their effect on the absolute magnitude of the differential cross sections is significant -- as much as 30%. However, the optical potential parameters used in the present calculations were obtained from fitting the elastic scattering data with the local potentials, hence they already absorbed some of the non-locality effects. Because of the lack of an appropriate set of optical potentials for the local energy approximation calculation, it is difficult

to know the exact contribution to the (^{3}He,d) reaction from the non-locality and finite-range effects.

In the present DWBA calculations, it has also been noted that the differential cross section is particularly sensitive to the radius parameter r_r of the bound state proton potential (table 7). For certain proton orbital (ℓ, j) the magnitude of the differential cross section changes by as much as 30% when r_r varied from 1.2 to 1.25 fm; however, the shape of the angular distributions remained practically unchanged for a small variation in r_r.

The spectroscopic information extracted from the present analysis as given in tables 8, 9, 10 and 11 for the various levels of the four odd mass Tc isotopes will be discussed with respect to the properties of the target states in the following sections.

(ii) Levels of ^{95}Tc:

The low-lying states of ^{95}Tc have been studied theoretically in different spherical nuclear models by Bhatt and Ball (1965), Vervier (1966), Kisslinger and Sorensen (1963) and Goswami and Sherwood (1967). In the shell model calculations of Bhatt and Ball (1965) and Vervier (1966), the nucleon-nucleon residual interactions were replaced by the effective interactions, and the

positive parity states in ^{95}Tc were generated by allowing the $1g_{9/2}$ shell protons to interact with the $2d_{5/2}$ shell neutrons. Their calculations reproduced the low-lying positive parity states observed in beta-decay. In the scheme of pairing-plus-quadrupole interaction coupling model, Kisslinger and Sorensen (1963) performed a series of systematic calculations for a wide range of spherical nuclei. A fair agreement with experiment for both the positive and negative parity low-lying states in ^{95}Tc was obtained. Sherwood and Goswami (1966) using the quasi-particle-phonon-coupling theory with the inclusion of correlation effects (so called extended-quasi-particle-phonon-coupling model) were able to obtain an improved agreement with experiment. However, when these calculations were performed, the amount of experimental data available on ^{95}Tc was very scanty, consequently, it was difficult to obtain a relative merit of these theories.

Experimental studies of the low-lying states of ^{95}Tc have been recently carried out by several workers. Riley et al. (1971) and Bommer et al. (1971) have investigated these levels using the (d,n) reaction at incident deuteron energy 12 MeV by the former group, and 6.25 and 7.0 MeV by the latter group. Measurements on the (p,n) reaction leading to levels in ^{95}Tc were performed by Kim et al. (1970, 1971), and the spin-parity assignments to

two levels were established from their studies of the neutron decay of analogue resonances. The data from the study of the beta decay of ^{95}Ru to ^{95}Tc have been reported recently by Tucker and Hein (1970). The results of these various studies have been summarized and given together with those obtained from the present work in table 8 for comparison.

The ground state and the 40 keV first excited state of ^{95}Tc have been well established as $9/2^+$ and $1/2^-$ states, respectively. Such assignments are consistent with the interpretation that these states are populated by the stripping of a proton into the $1g_{9/2}$ and $2p_{1/2}$ orbitals of the ^{94}Mo target nucleus in the (^{3}He,d) and (d,n) reactions. The 0.3364 MeV, $7/2^+$ state observed by Tucker and Hein (1970) in the beta-decay of ^{96}Ru and by Kim et al. (1970) in their (p,n) reaction work is not observed in the present (^{3}He,d) reaction study and in the two previous (d,n) reaction measurements. This state might be interpreted as primarily a seniority three state of $1g_{9/2}$ protons, and in which case it would not be populated in a one-step, single proton transfer reaction on a seniority zero ^{94}Mo target state.

The 0.629 MeV state, populated by an $\ell=1$ transfer transition in the present (^{3}He,d) reaction, has a spin-parity J^π assignment of $3/2^-$ or $1/2^-$, a result which is consistent with those obtained from the (d,n) reaction

by Riley et al. (1971) and from the (p,n) reaction by Kim et al. (1971), but disagrees with the results from the (d,n) reaction obtained by Bommer et al. (1971) and the beta-decay studied by Tucker and Hein (1970). According to the decay scheme proposed by Tucker and Hein (1970), the 0.628 MeV state in ^{95}Ru, with a log ft of 5.2, its J^{π} is most likely not $1/2^-$ or $3/2^-$. In view of this result it is probable that there are two closely spaced energy levels in the vicinity of 0.630 MeV, and one of which is a $3/2^-$ or $1/2^-$ state excited by the direct reactions, while the other is a $5/2^+$ state populated by the beta decay.

The $5/2^-$ 0.651 MeV state observed in (p,n) reaction is not populated in the present (^{3}He,d) reaction, indicating that the $1f_{5/2}$ orbital is full or nearly full in ^{94}Mo isotope. As can be seen in table 8, the level density in ^{95}Tc increases rapidly with the excitation energy. The set of levels above about 0.650 MeV observed in the stripping reactions may or may not have any similarity with those observed in the beta-decay and (p,n) reaction. For these higher lying levels, comparison of the present results can only be made with those obtained from the (d,n) reactions studies.

The 1.071 MeV state observed in the present experiment is presumably the same as the 1.10 MeV state observed in the (d,n) reaction by Riley et al. (1971).

Since this state is excited via an $\ell = 2$ transfer, it probably corresponds to the stripping of a proton into the $2d_{5/2}$ orbital of the ^{94}Mo target. And the state at 1.264 MeV observed here as due to an $\ell = 2$ transfer transition, which contradicts the assignment of $\ell = 4$ or $\ell = 1$ given by Riley et al. (1971). The ℓ values obtained for the 1.620 MeV state and 2.550 MeV state in the present work disagree with those given by Bommer et al. (1971) but are consistent with assignments made by Riley et al. (1971). The spectroscopic information obtained for those levels which have been observed in the present work as well as in the (d,n) reaction work ... in general, agree fairly well with each other. However, the present (^{3}He,d) reaction has been observed to populate many more states than those reported from the previous (d,n) reaction measurements.

All the other states observed in this work have either $\ell = 0$, 1 or 2 transfer characteristics, most probably they correspond to the stripping of a proton into the $3s_{1/2}$, $2p_{1/2}$, $2p_{3/2}$, $2d_{5/2}$ or $2d_{3/2}$, respectively. For most of the levels with an $\ell = 1$ transfer lying above the 0.040 MeV states, their excitation strengths most likely come from the $2p_{3/2}$ orbital because the 0.040 MeV state has almost exhausted all the strength of the $2p_{1/2}$ orbit. This will be shown in subsection (vi) of this section by the remarkable agreement between the deduced occupational

probabilities of the $2p_{1/2}$ and $2p_{3/2}$ orbitals from the present (^{3}He,d) work and from the (d,^{3}He) work (Ohnuma and Yntema 1968), and the consistency between the deduced experimental center of gravity energies of these two orbitals in the Tc isotopes and those in the Nb isotopes (Ohnuma and Yntema 1968, Cates et al. 1969).

In order to compare the spectroscopic factors deduced from the ^{94}Mo(^{3}He,d)^{95}Tc reaction systematically with those from the other Mo targets, the spectroscopic factors presently obtained have been renormalized and listed in the fifth column of table 8. The renormalization is based on the following assumptions: (A) no appreciable population of proton orbitals above Z = 50 shell closure in the even-mass molybdenum target ground state, (B) all the $2p_{1/2}$ strength is concentrated in the first $\ell = 1$ state (0.040 MeV state in ^{95}Tc) and the other $\ell = 1$ states are associated with the $2p_{3/2}$ orbital and (C) all the $1g_{9/2}$ strength is exhausted by the transition to the ground state of the residual nucleus. Thus, the spectroscopic factors were normalized with respect to the total number of 8 holes in the $1g_{9/2}$, $2p_{1/2}$, $2p_{3/2}$, and $1f_{5/2}$ orbitals. This renormalization amounts to a reduction of the original spectroscopic factors by about 17% for the ^{94}Mo(^{3}He,d)^{95}Tc reaction.

The spectroscopic factor obtained from this reaction will be further analysed together with those from the Mo targets in subsections (vi) and (vii).

(iii) Levels of ^{97}Tc:

Theoretical calculations for the low-lying states in ^{97}Tc have been performed by Vervier (1966), Kisslinger and Sorensen (1963), and Goswami and Sherwood (1967) using the same approaches as those described in the preceding subsection for the ^{95}Tc nucleus. The simple shell model calculation by Vervier (1966) did not enjoy the same success in this nucleus as it did in ^{95}Tc, probably due to the fact that ^{97}Tc is farther away from the N = 50 closed shell, and the effect of the valence neutrons other than those in the $2d_{5/2}$ orbital needed to be included in the calculation. The results obtained from the calculation of Kisslinger and Sorensen (1963) have the level order of the $9/2^+$ ground state and the $1/2^-$ first excited state inverted. The calculation in the extended quasi-particle-phonon-coupling model by Goswami and Sherwood (1967) seems to obtain a better prediction for the low-lying states of ^{97}Tc although it predicts a degenerated multiplet of $5/2^+$, $7/2^+$, $11/2^+$ and $13/2^+$ states at about 0.35 MeV whereas only a ($7/2^+$) 0.216 MeV and a ($5/2^+$) 0.324 MeV states have been observed experimentally (see

table 9).

The levels of ^{97}Tc have been studied by Riley et al. (1971) using the (d,n) reaction in connection with their study of the ^{93,95}Tc nuclei, by Kim et al. (1970, 1971) and Picone et al. (1972) with (p,n) reactions. The recent works on the decay of ^{97}Ru to ^{97}Tc have been reported by Phelps et al. (1971) and Cook et al. (1970). Earlier works on the level scheme of ^{97}Tc have been reviewed in the paper by Phelps et al. (1971). Table 9 summarizes the results of the previous works along with the spectroscopic information on the properties of the low-lying states of ^{97}Tc obtained from the present work for comparison.

As in the case of ^{95}Tc, the ground state and first excited state in ^{97}Tc are known to be $9/2^+$ and $1/2^-$ (Phelps et al. 1972, Cook et al. 1970), which are consistent with the present observation and the results of the (d,n) reaction of $\ell = 4$ and 1 transitions, respectively. These states probably correspond to the stripping of a proton into the $1g_{9/2}$ and $2p_{1/2}$ orbits of the ^{96}Mo target. The weakly excited 0.216 MeV state with an angular pattern approximating an $\ell = 4$ transition falls in line with the $7/2^+$ assignment obtained from the decay of ^{97}Ru. Since this state is so low in energy it is not favorable for a $1g_{7/2}$ shell transfer transition.

An $\ell = 2$ assignment to the 0.326 MeV state is

consistent with the established spin-parity of $5/2^+$ by Phelps et al. It appears to correspond to a $2d_{5/2}$ shell stripping. The $3/2^-$ assignment to the 0.575 MeV state established in the (p,n) reaction work by Kim et al. (1971) may serve to exclude the possibility of $1/2^-$ since it has been found to correspond to an $\ell = 1$ transfer in both the (^{3}He,d) and (d,n) reaction. This state most probably corresponds to a $2p_{3/2}$ orbital stripping. The $\ell = 3$ transfer observed here for the 0.655 MeV state is confirmed by the spin-parity $5/2^-$ assignment from the (p,n) reaction measurement. This state is believed from the stripping of a proton into the $1f_{5/2}$ orbit, indicating the incompleteness of the $1f_{5/2}$ shell in ^{97}Tc. This is to be contrasted with the ^{93}Tc (Picard and Bassani 1969) and ^{95}Tc (preceeding subsection) nuclei, in which cases the $1f_{5/2}$ shell appears to be fully occupied.

The $\ell = 2$ assignment to the 0.783 MeV state is consistent with most of the other experimental results given in table 9, except the tentative assignment given by Cook et al. This state may be attributed to the $2d_{5/2}$ shell proton stripping. The tentative $\ell = 2$ assignment to the weakly excited 0.852 MeV state made on the basis of the present work is consistent with the tentative ($5/2^+$, $7/2^+$) assignment made by Phelps et al. but contradicts the suggestion of ($7/2^-$) by Cook et al. Probably,

this state is a $5/2^+$ state resulting from a transfer of a proton into the $2d_{5/2}$ orbital in ^{96}Mo. The $\ell = 1$ excitation character of the 0.947 MeV state agrees with the results from (d,n) reaction, leading to a $J^\pi = 1/2^-$ or $3/2^-$ for the state. This state probably corresponds to the 0.940 MeV state observed by Picone et al. in their (p,n) measurements. The 1.053 MeV state, characterized by an $\ell = 1$ angular distribution is not observed in the (d,n) experiment, but observed both by Kim et al. and Picone et al. in the (p,n) reactions. The $\ell = 4$, 1.316 MeV state and the $\ell = 2$, 1.374 MeV state observed in the present experiment are probably related to the doublet at 1.32 MeV state observed by Riley et al. (1971). Among the higher-lying states, the ℓ assignments at the 1.951 MeV state and the 2.264 MeV state are found different to the (d,n) results.

As in the case of ^{95}Tc, the (^{3}He,d) reaction populates a great many more states in ^{97}Tc than the (d,n) reaction. In subsection (vi) it will be shown that the transitions to the $9/2^+$ ground state and the $1/2^-$ first excited state almost exhaust all spectroscopic strengths associated with the $1g_{9/2}$ and $2p_{1/2}$ shells of ^{96}Mo, respectively. Therefore, it might be assumed that all the other transitions with an $\ell = 1$ are associated with the $2p_{3/2}$ shell. The spectroscopic factor for each transition given in table 9 has been renormalized by the same

procedure as outlined for the case of ^{95}Tc (preceding subsection). This renormalization has the effect of reducing the observed values by about 11%.

(iv) Levels of ^{99}Tc:

The nature of low-lying states in ^{99}Tc has been studied theoretically by many workers: Vervier (1966), Kisslinger and Sorensen (1963), Goswami and Sherwood (1967). The approaches used in their calculations were more or less the same as those employed by them in the interpretation of the ^{95,97}Tc described in the preceding subsections. However, the agreement between their predictions and the experiment data for ^{99}Tc is not as successful as in the case of ^{95}Tc.

The low-lying states of ^{99}Tc populated in the beta decay of ^{99}Mo have recently been investigated by Cook et al. (1969) and several states of this nucleus have also been observed in the Coulomb excitation of ^{99}Tc with ^{35}Cl ions by Bond et al. (1972). Their results are shown in table 10, along with the results obtained from the present (^{3}He,d) reaction.

There are several $\ell = 4$ transitions observed in this study. The transition leading to the ground state with a large transition strength is consistent with the established $9/2^{+}$ value (Cook et al. 1969), corresponding

to a $1g_{9/2}$ orbital stripping. For the transition of the 0.142 MeV state, the angular distribution exhibits mainly an $\ell=1$ character possibly with a small amount of $\ell=4$ admixture. This observation is consistent with the results of Cook et al. (1969) that this state is a doublet made up of a $7/2^+$ 0.14051 MeV state and a $1/2^-$ 0.14263 MeV state. The other $\ell=4$ transitions are the 0.625 MeV state and the 0.720 MeV state. The 0.720 MeV state is probably equivalent to the 0.7263 MeV state observed in the Coulomb excitation measurements by Bond et al. (1972), who suggested a $J^\pi = 9/2^+$ or $7/2^+$ for the state. The 0.625 MeV state was not observed in the beta decay study by Cook et al. and was not established by Bond et al. However, in the gamma ray spectrum measured by Bond et al. following the Coulomb excitation, a broad peak at about 621 keV region was noted, but its assignment to ^{99}Tc was not determined. It is interesting to note that the number of low-lying states associated with the $\ell=4$ transitions in the Tc isotopes increase with mass: One in ^{95}Tc, three in ^{97}Tc, four in ^{99}Tc. Since the $1g_{7/2}$ shell presumably lies much higher in excitation energy, the observed $\ell=4$ transitions probably arise from the $1g_{9/2}$ shell. The transition strength for the $9/2^+$ ground states of these nuclei is an order of magnitude larger than that for the other states associated with the $\ell=4$ transitions. It is reasonable to assume that the former are basically single

proton states of the $1g_{9/2}$ shell and the latter are either multi-particle states containing small components of $1g_{9/2}$ or $1g_{7/2}$ single proton configuration or associated with two-step processes.

From the transition strength, the 0.142 MeV state appears to arise primarily from the $2p_{1/2}$ orbital stripping, agreeing with the $J^{\pi} = 1/2^-$ assignment deduced by Cook et al. from beta decay. The 0.509 MeV state with an $\ell = 1$ transfer has been assigned a $J^{\pi} = 3/2^-$, in accordance with the observation of Cook et al. It is arisen from a $2p_{3/2}$ proton transfer. The other states at 1.203 MeV and 2.321 MeV with an $\ell=1$ transfer are probably the result of small fragments of the $2p_{3/2}$ orbit coupled with the other higher-lying configurations

The $\ell = 3$ transfer leading to the 0.672 MeV state is consistent with the $5/2^-$ assignment to the 0.6715 MeV state observed by Cook et al. As in the case of ^{97}Tc, the $1f_{5/2}$ shell in ^{98}Mo appears to be partially vacant. The large number of states associated with the $\ell = 2$ and $\ell = 0$ transfers observed in ^{99}Tc resembles the observations for ^{95}Tc and ^{99}Tc. These ℓ values for those states lying below 1 MeV excitation are consistent with the spin-parity assignments of Cook et al. In particular, the value $\ell = 0$ for the 0.919 MeV state may be used to eliminate the possibility of a $J^{\pi} = 3/2^+$, leaving a $J^{\pi} = 1/2^+$ for the state (see table 10). Moreover, the $\ell = 2$

character for the excitation of the 0.762 MeV state supports the $5/2^+$ assignment for the state deduced from beta decay but disagrees with the suggestion of ($7/2^+$, $9/2^+$) by Bond *et al*.

The transitions between the low-lying states, the $5/2^+$ state at 181.1 keV, the $7/2^+$ state at 140.5 keV and the $9/2^+$ ground state, have been recently studied by McDonald and Bäcklin (1971). From their measurements, the $5/2^+ \rightarrow 9/2^+$ transition has a multipolarity of E2 and a rate which is enhanced more than 50 times the Weisskopf estimate (Wilkinson 1960); and the $7/2^+ \rightarrow 9/2^+$ transition is an M1 with a rate which is only weakly retarded (Normal M1 retardation in this mass region is about several hundred) by a factor of 23. Based on the shell model, if the $5/2^+$, $7/2^+$ and $9/2^+$ states are considered to be the members of a pure $1g_{9/2}^3$ multiplet in ^{99}Tc, the E2 transitions among them would have normal rates and the M1 transitions would be forbidden (deShalit and Talmi 1963). Because of their observation, McDonald and Bäcklin (1971) suggested a deformed nuclear structure for ^{99}Tc and deduced the wavefunctions for the low-lying states using Nilsson model. The $9/2^+$ ground state wavefunction as suggested by them is made of $\sim$ 65% $9/2[404]$, $\sim$ 25% $7/2[413]$ and $\sim$ 10% $5/2[422]$ (Nilsson orbits labelled by $K[N\ n_z\ \Lambda]$). However, this ground state wavefunction can not explain the strong transition of the

$\ell = 4$ with a strength of $C^2S \sim 0.57$ observed in the present (^{3}He,d) reaction measurement. Also, the recent experiment of Coulomb excitation by Bond et al. (1972) indicated that this nucleus is not as deformed as suggested by McDonald and Bäcklin (1971).

Again, the transition strengths for the various states deduced from the present (^{3}He,d) reaction and listed in table 10 have also been renormalized. The renormalization factor for this nucleus has been found, in contrast with the two previous cases, to increase the absolute spectroscopic factor by about 17%. The spectroscopic strength of the individual single particle orbital will be analysed further in subsection (vi) and (vii).

(v) Levels of ^{101}Tc:

The beta decay of ^{101}Mo to ^{101}Tc has recently been studied by Cook and Johns (1972). The results of present (^{3}He,d) reaction work and the results of the beta decay study up to the 1.7753 MeV state are tabulated in table 11. In the internal conversion measurements, Cook et al. (1972) observed several low energy transitions and from which they were able to establish closely spaced levels at 9.317 and 15.601 keV with $J^\pi = 7/2^+$ and $5/2^+$, respectively, lying above the $9/2^+$ ground state. In the present measurement only one deuteron peak with an angular

distribution corresponding to an $\ell = 4$ pattern were observed. This peak was largely the result of the excitation of the $9/2^+$, because excitation of the $7/2^+$ and $5/2^+$ states is an order of magnitude weaker than that of the ground state, as has been the case for $^{95,97,99}Tc$.

The $\ell = 1$ transfer for the transition to the 0.207 MeV state is consistent with the $J^\pi = 1/2^-$ assignment deduced in beta decay. The 0.288 MeV state with an $\ell = 1$ transfer concurs with the results of Cook and Johns (1972) that its $J^\pi = 3/2^-$ with a possibility of $1/2^-$. Most probably its excitation is the result of a $2p_{3/2}$ orbital transfer. If this indeed is the case, it would be interesting to note the excitation energy of the low-lying $3/2^-$ states in the Tc isotopes. In ^{95}Tc such a state occurs at 0.629 MeV, in ^{97}Tc at 0.576 MeV, in ^{99}Tc at 0.509 MeV and in ^{101}Tc at 0.288 MeV. Also, apart from the one in ^{99}Tc, the excitation strength of such a state increases with the mass.

The $\ell = 3$ transfer for the excitation of the 0.394 MeV and 0.670 MeV states agrees with the $J^\pi = 5/2^-$ assignment to both states by Cook and Johns (1972). Of the four Tc isotopes studied in this work, this nucleus is the only one with two $\ell = 3$ transitions. From the strength with which these states are being excited, it appears that the $1f_{5/2}$ shell becomes more accessible to stripping.

The 0.515 MeV state with an $\ell = 2$ limits the spin-parity of this state to $5/2^+$ when the range of J^π deduced by Cook and Johns (1972) is taken into consideration. The $\ell = 1$ transfer for the 0.620 MeV state may be correlated to the 0.62215 MeV state from beta decay, eliminating the possibility of $5/2^-$ assignment given by Cook and Johns, and limiting its J^π to $1/2^-$ or $3/2^-$. The 0.890 MeV state does not have a unique confident fitting to its angular distribution in the present analysis. The possibilities of $\ell = 4$ and $\ell = 2$ have been proposed, both fittings have been shown for comparison in fig. 18. From the ℓ values obtained in this work for the 1.197 MeV state and 1.319 MeV state they may be used to rule out the possibilities of $5/2^-$ and $1/2^+$ J^π assignments to the states, respectively, deduced from the beta decay work.

As in the cases of the Tc isotopes, several $\ell = 2$ transitions have been observed, but only one $\ell = 0$ transition observed in ^{101}Tc. In all four Tc isotopes studied here, the $2d_{5/2}$ and/or $2d_{3/2}$ orbits appear to be severally fragmented; and in ^{97,99,101}Tc, there is no single strong $\ell = 2$ transition being observed.

The structure of ^{101}Tc has been studied theoretically by Kisslinger and Sorensen (1963) and Goswami and Sherwood (1967) using the similar methods they employed for the other Tc isotopes described previously. The agreement

between their calculations and the experiments in energy spectra appears to deteriorate more and more from ^{95}Tc to ^{101}Tc. This seems to confirm the suspicion expressed above that the complexity in the structure of the Tc nuclei increases with the number of neutrons beyond the N = 50 closed shell.

The transition strengths for the various levels observed in this work have been renormalized according to the procedure outlined previously for the other Tc isotopes. These renormalized strengths are also given in table 11, and they will analysed further in the next two subsections. The renormalization has the effect of reducing the observed values by about 36%.

(vi) Spectroscopic Analysis of Proton Orbitals in $28 < Z \leq 50$ Shell:

The spectroscopic factors obtained from the present study of proton stripping reactions may be used to extract information about the distribution of proton holes in the ground state of the even mass Mo nuclei. In a stripping reaction, the number of holes, $n_h(\ell, j)$ in orbit (ℓ, j) of an even-even target, is given by the summation of all the transition strengths, $(2j+1)C^2S(\ell, j)$, corresponding to the same ℓ, j(Riley et al. 1971):

$$n_h(lj) = \sum_f (2j+1)\, C^2 S_f(lj)_{\text{STRIPPING}} \qquad (3.4\text{-}17)$$

and the fractional emptiness (unoccupation probability) $U^2_{\ell,j}$ is related to $n_h(\ell,j)$ by

$$U^2_{lj} = \frac{n_h(lj)}{2j+1} = \sum_f C^2 S_f(lj)_{\text{STRIPPING}} \qquad (3.4\text{-}18)$$

In a pick-up reaction, the number of particles, $n_p(\ell,j)$, in orbit (ℓ,j) of an even-even target, is given by the summation of all the spectroscopic strengths, $C^2S(\ell,j)$, corresponding to the same ℓ,j:

$$n_p(lj) = \sum_f C^2 S_f(lj)_{\text{PICK-UP}} \qquad (3.4\text{-}19)$$

and the occupation probability $V^2_{\ell,j}$ is related to $n_p(\ell,j)$ by

$$V^2_{lj} = \frac{n_p(lj)}{2j+1} = \frac{1}{2j+1} \sum_f C^2 S_f(lj) \qquad (3.4\text{-}20)$$

For a consistent analysis, the sum of $U^2_{\ell,j}$ determined from stripping reaction and $V^2_{\ell,j}$ from pick-up reaction for a given ℓ,j in the same target should be unity.

The proton configurations of the molydenum isotopes, as discussed previously, may be considered as composing an inert core (^{56}Ni) plus 14 valence protons

distributed among the $1g_{9/2}$, $2p_{1/2}$, $2p_{3/2}$ and $1f_{5/2}$ orbits. The fractional emptinesses U^2 corresponding to these four orbits determined from the (^{3}He,d) reactions and the occupation probabilities V^2 determined from the (d,^{3}He) reactions, and the sums, $U^2 + V^2$, for the five stable even-even Mo isotopes are summarized in table 12. The data used for the (^{3}He,d) in Mo-92 were taken from Picard and Bassani (1969) and those of the Mo-94, 96, 98 and 100 were from the present work (tables 8 - 11). The (d,^{3}He) data on Mo-92, 94, 96 and 98 were taken from the work of Ohnuma and Yntema (1968). As can be seen in this table the sums, $U^2 + V^2$, for the $1f_{5/2}$ orbital do not give as consistent a value as the other orbitals in these nuclei This may be attributed to the severe fragmentation of the $1f_{5/2}$ single proton state, and only a portion of its strength have been exhausted in the pick-up reaction measurements (Ohnuma and Yntema 1968).

In spite of the inconsistency of the observed results for the $1f_{5/2}$ orbit, the sums, $U^2 + V^2$ for the other three orbits are generally fairly consistent, although in the case of Mo-96, the sum for $1g_{9/2}$ orbit is about 25% below those for the 2p shells. However, this may be due to the statistical variation in experimental data and the fluctuations in the DWBA treatments. Since the occupation number V^2 from (d,^{3}He) reactions has not been renormalized, the value of the sum, $U^2 + V^2$,

for each orbit, is not necessary equal to one.

It can be seen in table 12, the observed fractional emptinesses U^2 for the four orbitals exhibit some remarkable systematic characteristics in the Mo nuclei; the $1g_{9/2}$ proton orbitals in these nuclei are about 60-70% empty and have a slightly larger occupation probability in the higher mass nuclei (more neutrons). Conversely, the number of proton holes in the $2p_{1/2}$, $2p_{3/2}$ and $1f_{5/2}$ orbits have an increasing tendency as the number of neutrons in these nuclei increases from 50 to 58. In the ^{98}Mo isotope, there are six valence neutrons outside the N = 50 shell closure and they may form a $(2d_{5/2})^6$ closed subshell. This nucleus exhibits a proton hole distribution among the four orbits similar to that of the single closed shell nucleus ^{92}Mo.

The major proton configurations for the ground state of each even-even molybdenum isotope may be written in the form

$$C_1\left[(2p_{\frac{1}{2}})_0^2(1g_{\frac{9}{2}})_0^2\right] + C_2\left[(2p_{\frac{1}{2}})_0^0(1g_{\frac{9}{2}})_0^4\right] + C_3\left[(2p_{\frac{3}{2}})_0^{-2}(1g_{\frac{9}{2}})_0^4\right] + C_4\left[(1f_{\frac{5}{2}})_0^{-2}(1g_{\frac{9}{2}})_0^4\right] \qquad (3.4\text{-}21)$$

which consists of proton particle and/or hole pairs in the orbital $1g_{9/2}$, $2p_{1/2}$, $2p_{3/2}$ and $1f_{5/2}$ as expected intuitively. The first term of this proton wave function

describes the ground state configuration of two $1g_{9/2}$ protons while the other orbits are all filled. The other three terms of the wavefunction are the configurations for two $1g_{9/2}$ protons coupled to a pair of proton holes arising from each of the $2p_{1/2}$, $2p_{3/2}$ and $1f_{5/2}$ shells. The coefficients of this wave function for each target can be deduced from the experimental fractional emptinesses $U^2_{\ell,j}$ (table 12). They are related by (Kozub and Youngblood 1971)

$$C_i^2 = \frac{(2j+1)\ U^2_{\ell j}}{n_h^i(\ell j)} \qquad (3.4\text{-}22)$$

where $n_h^i(\ell, j)$ is the number of proton holes in the orbit ℓ, j in the i^{th} term of the wave function. In the present analysis, the coefficients C_2^2, C_3^2, and C_4^2 are calculated directly from the observed spectroscopic information for the $2p_{1/2}$, $2p_{3/2}$ and $1f_{5/2}$ orbits, and C_1^2 is obtained from the normalization $\sum_i C_i^2 = 1$ relationship.

Table 13 lists the deduced C_i^2 coefficients of the target proton wavefunctions. The fractional emptiness values for the calculations are those listed in table 12. From the table 13, it can be seen that the $(1g_{9/2})^2$ component is slightly less than 50% in ^{92}Mo and drops drastically as the number of neutrons increases. Since all the five odd-even Tc isotopes have a $9/2^+$ ground state that is associated with an $\ell=4$ transfer, the wave functions for

their ground states are primarily comprising a $1g_{9/2}$ proton coupled to the corresponding even mass Mo isotopes. Allowing certain amount of fluctuations in the results shown in table 13, due to errors in both the experimental and theoretical (DWBA) uncertainties, the results of the present analysis may be taken to imply that the ground states of ^{93,95,97,99,101}Tc contain an appreciable component of $(1g_{9/2})^5_{9/2}$ proton configuration in their wave functions, and in the case of ^{101}Tc such a configuration dominates the ground state wave function.

From the results of (^{3}He,d) reactions measurements, the center of gravity energy of each single proton orbital in the final nucleus can be determined from the relation

$$\overline{E}(\ell j) = \frac{\sum_f C^2 S_f(\ell j)\, E_f}{\sum_f C^2 S_f(\ell j)} \qquad (3.4\text{-}23)$$

where E_f is the excitation energy in the final nucleus and the summation is carried over all the final states arising from the same transferring orbit ℓ, j. In nuclear pairing theory (Yoshida 1961) the observed center of gravity energies from the (^{3}He,d) reactions on even-even Mo isotopes, are the energies of the single proton quasi-particle states relative to the ground state in the odd mass Tc isotopes. These single proton quasi-particle energies are related to the single proton occupation probabilities in the corresponding target nucleus. Table

14 presents the observed center of gravity energies in ^{93,95,97,99,101}Tc from the (^{3}He,d) reactions at 18 MeV incident energy, comparing them with the theoretical values. The experimental values for ^{93}Tc were deduced from the work of Picard and Bassani (1969) and for ^{95,97,99,101}Tc were from the present work. The theoretical values are the calculated single proton quasi-particle energies relative to the $1g_{9/2}$ state, obtained by Kisslinger and Sorensen (1960, 1963). The agreement between the theory and experiment is in general poor except, perhaps for ^{93}Tc.

The experimentally determined $\bar{E}(1g_{5/2})$ may be less certain because of the relatively low cross sections for the states associated with the $1f_{5/2}$ orbital. The experimental values show a relatively small energy spacing between the $\bar{E}(2p_{1/2})$ and $\bar{E}(1g_{9/2})$, while the experimental values for $\bar{E}(2p_{3/2})$ in these nuclei decrease drastically as neutron number increases from 50 to 58, while the theoretical values vary only by a small amount.

In the foregoing analyses in this subsection, it has been assumed that the transition strength in the (^{3}He,d) reactions for the $2p_{1/2}$ orbit in all the Mo targets is completely concentrated in the transition leading to the lowest-lying state in the Tc nuclei with an $\ell = 1$ transfer. The strengths for the other transitions with an $\ell = 1$

transfer have been attributed to the $2p_{3/2}$ orbit. This assumption is supported by the consistency in their respective $U^2 + V^2$ sums of the two orbits in comparing with the values deduced from the (d,^{3}He) reactions as shown in table 12. It is also substantiated by the consistent values of $\bar{E}(2p_{3/2}) - \bar{E}(2p_{1/2})$ observed in the adjacent Nb isotopes. In the odd mass ^{91,93,95,97}Nb (with neutron numbers 50, 52, 54 and 56), the observed $\bar{E}(2p_{3/2}) - \bar{E}(2p_{1/2})$ are 1.42, 1.04, 0.80 and 0.50 from the (d,^{3}He) reactions (Ohnuma and Yntema 1968), and are 1.49, 0.95, 0.60 and 0.55 from the (^{3}He,d) measurements (Gates et al. 1969), respectively. In the five odd-mass Tc isootpes, Tc-93,95,97,99 and 101, the observed values (table 14) are: 1.22, 1.06, 0.65, 0.50 and 0.26, respectively.

Figure 19 shows the distributions of $\ell = 1$ transfer transition strengths in ^{93,95,97,99,101}Tc as a function of excitation energy, obtained from the (^{3}He,d) reactions. In the figure, the first $1/2^-$ state in each nucleus is denoted by a dotted line; and the other states associated with the $\ell = 1$ transitions are denoted by solid lines, and of these states only a few of the stronger excited levels are known to have a $J^\pi = 3/2^-$ (see tables 8 to 11). The center of gravity energy of the $2p_{3/2}$ orbit in each nucleus and its corresponding width of the

distribution is denoted in the figure by a crossed circle with a horizontal bar, by taking all the solid lines into account. All these odd-mass Tc nuclei are characterized by a strong $\ell = 4$ transition to their ground states in the (^{3}He,d) reactions. And in the excited state, no other strong transition corresponding to $\ell = 3$ transfer was observed. It is obvious that these nuclei exhibit no evidence for a well developed rotation-like, deformed shape structure in their low-lying states. However, there are remarkable changes in their nuclear systematics and the degree of fragmentation of the single particle orbitals, indicating a substantial configuration mixing in the ground state wave functions of the Mo nuclei as the number of neutrons increased from N = 50. These probably are due to the effects of the correlations between the protons and neutrons in these nuclei, as their neutron number deviates from the N = 50 neutron closed shell.

(vii) Spectroscopic Analysis of Proton Orbitals in $50 < Z \leq 82$ Shell:

Proton orbits in the $50 < Z \leq 82$ major shell comprise the $2d_{5/2}$, $1g_{7/2}$, $3s_{1/2}$, $2d_{3/2}$ and $1h_{11/2}$. In contrast with the orbitals in $28 < Z \leq 50$ shell, these

orbits are most likely completely vacant in the ground state of the even-mass molydenum targets, therefore, a large amount of transition strength from these orbits is expected. As discussed in the part (i) of this section, the excited states resulting from the (^{3}He,d) reactions may have two different final isospins, $T_>$ and $T_<$. Since the valence neutrons in even-mass molydenum isotopes are also in this major shell, $50 < N \leq 82$, the $T_>$ states populated from the proton stripping reactions are the isobaric analogue states of the odd-mass Mo isotopes. Such unbound isobaric analogue states have been studied recently by McGrath et al. (1970) in (^{3}He,d) reaction and are not remeasured in the present work. Most of the transition strengths observed in the present experiment will then be concentrated in the $T_<$ states and they distribute over a wide range of excitation energies in the odd-mass Tc nuclei.

Figure 20 shows the observed transitions strengths $(2J+1)C^2S$ for the low-lying excited levels in Tc-93,95, 97,99 and 101, corresponding to the transitions with an $\ell = 2$ transfer. The data for ^{93}Tc are taken from Riley et al. (1971) and the others are from the present work. In ^{93}Tc, nine $\ell = 2$ levels have been located apparently separated into two groups with a distance of about 2 MeV between their centroids. The lower energy group comprises

two weak transitions leading to states at excitation energies 2.59 and 3.17 MeV and a strong transition to a state at 3.36 MeV. Based on the predictions of the shell model, these states have most probably arisen from the $2d_{5/2}$ orbital transfer, hence have $J^{\pi} = 5/2^{+}$. The upper energy group has six rather weak $\ell = 2$ transitions to levels lying between 4.76 and 5.78 MeV. Their excitation may be attributed to the transitions to the $2d_{3/2}$ orbit, giving a $J^{\pi} = 3/2^{+}$ for these states. In ^{95}Tc, 15 levels have been identified with $\ell = 2$ transitions (those of tentative ℓ assignments are shown in parentheses in fig. 20). Although a strong transition appears at 2.816 MeV, but no obvious grouping occurs in the distribution of these states. No definite spin assignments for these states can be made in general, however, the 2.816 MeV state and most of the other states lying below it with an $\ell = 2$ probably are associated with the $2d_{5/2}$ orbital. In Tc-97,99 and 101, excited states with $\ell = 2$ transition occur even below 1 MeV excitation energy. There are 16, 17 and 9 such levels below 3.1, 2.6 and 1.8 MeV excitation energies in Tc-97,99 and 101, respectively. No single strong $\ell = 2$ transition was observed deviating from the observations in ^{93}Tc and ^{95}Tc. In fig. 15, the transition strengths for the $\ell = 2$ states in ^{95,97,99,101}Tc are shown by those values associated with the $2d_{5/2}$ orbit.

The present measurements on the four even-mass Mo isotopes, did not exhaust the theoretically possible transition strength associated with the $2d_{5/2}$ or the $2d_{3/2}$ orbit. The total observed transition strengths for $\ell = 2$ orbit in ^{95,97,99,101}Tc are only 3.36 (Tc-95), 2.52 (Tc-97), 2.82 (Tc-99) and 2.34 (Tc-101), if all the observed $\ell = 2$ states arise from the $2d_{5/2}$ orbital. From the sum rules for $T_<$ states (Schiffer 1969), the total transition strength for a given shell model orbit ℓ, j is given by

$$\sum_f (2j+1) C^2 S_f(\ell j) = N_{\ell j}(p) - \frac{1}{2T_0+1} N_{\ell j}(n) \qquad (3.4\text{-}24)$$

where $N_{\ell,j}(p)$ and $N_{\ell,j}(n)$ are the numbers of proton holes and neutron holes in orbit ℓ, j in the corresponding even-even target nucleus, whose isospin equals T_0. For the Mo nuclei, the number of proton holes is $2j+1$, and the number of neutron holes can be obtained from the neutron stripping and pick-up measurements by Hjorth et al. (1964) and Diehl et al. (1970). Using their results, the maximum theoretical spectroscopic strengths for the $2d_{5/2}$ orbit in these nuclei are about: 5.58 (Tc-95), 5.76 (Tc-97), 5.88 (Tc-99) and 5.88 (Tc-101) for the $2d_{5/2}$ orbit, and about 3.68 (Tc-95), 3.72 (Tc-97), 3.80 (Tc-99) and 3.84 (Tc-101). These values are substantially higher than the experimental values quoted above.

Figure 21 shows the $\ell = 0$ transition strength distribution as a function of excitation energy in ^{93,95,97,99,101}Tc. Similar to the case of figure 20, the data for ^{93}Tc are taken from Riley et al. (1971) and the others are from present measurements. Since in ^{101}Tc only angular distributions for states up to 1.703 MeV excitation energy were analysed, a lone state with an $\ell = 0$ transfer in this energy region has been observed. The total spectroscopic strength $(2j+1)C^2S$ observed in the present measurements are 0.38 (Tc-95), 0.45 (Tc-97), 0.30 (Tc-99) and 0.06 (Tc-101) while the expected full strength (equation 3.4-24) for the $T_<$ states should be about 0.92 (Tc-95), 0.94 (Tc-97), 0.94 (Tc-99) and 0.97 (Tc-101).

Besides the strong $\ell = 4$ transitions to the ground states of the odd mass Tc nuclei, there are only three $\ell = 4$ transitions observed in the present measurements, namely the 1.316 MeV state in Tc-97 and the 0.625 and 0.720 MeV states in ^{99}Tc. Since the J^π assignments for these states are not uniquely defined, it is not certain whether these states are due to proton stripping to the $1g_{7/2}$ orbit or to the $1g_{9/2}$ orbit. The odd-mass Tc isotopes are also characterized by a low-lying $7/2^+$ state, above their $9/2^+$ ground states (Cook et al. 1972). The excitation of most of them are too weak to be observed in the present measurements, except the weakly excited state at 0.216 MeV

in ^{97}Tc. The present results lend strong support to the contention that they are belonging to the $1g_{9/2}$ shell higher seniority states. A weak transition to these states implies that they may contain a small component of the single particle configuration in their wave functions, or their excitations are due to a two-step process in the (^{3}He,d) reactions. For instance, this transition may proceed via core excitation to a one phonon state, followed by stripping a proton to the orbit of $1g_{9/2}$.

No $\ell = 5$ transition has been identified in the present work. A detailed study on the $\ell = 4$ and 5 transfer to the excited states of these nuclei may be accomplished by the use of the reactions such as (α,t), (^{16}O,^{15}N) in which high values of ℓ -transfer are more favorable.

The high degree of fragmentation of the strengths associated with the $\ell = 2$ and $\ell = 0$ transitions may be attributed to the spreading of the antianalogue states due to the core polarization mixing (French 1964). This phenomenon has been recently discussed by Vourvopoulos et al. (1969) in conjunction with the reaction of ^{89}Y (^{3}He,d)^{90}Zr, and they obtained a fairly good prediction for the number of observed $T_<$ states. From the present work and those of Hjorth et al. (1964) and Diehl et al. (1970), it is known that the even-mass Mo isotopes have a significant mixed configurational structure for both the

protons and the neutrons. The $J_o \neq 0$ core polarization states (Vourvopoulos et al. 1969) may arise from a large number of different orbits and cause an extremely complicated mixture of different configurations to the anti-analogue states. In addition, according to the core polarization mixing, states with larger spin values are more fragmented. This property, plus the unfavored cross sections for high ℓ transitions in the (^{3}He,d) reactions, perhaps, explains the scanty information about the distribution of the $1g_{7/2}$ strength in the present measurements.

FIGURE 7

Comparison of the Experimental Elastic Cross Section with Optical Model Calculations for 18 MeV ^{3}He on a ^{94}Mo Target.

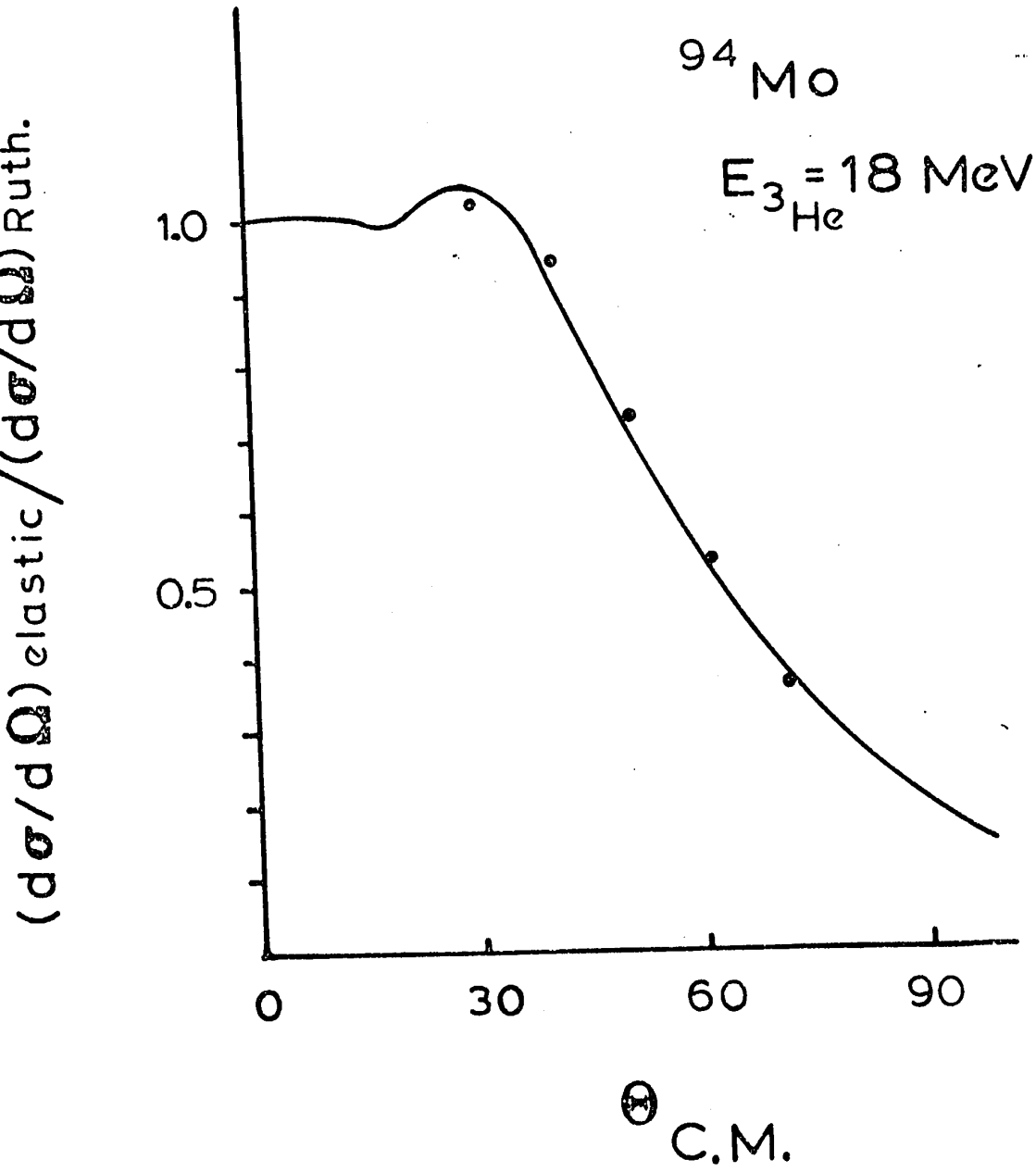
^{94}Mo
$E_{^3He}$ = 18 MeV
1.0
0.5
0
30
60
90
$(d\sigma/d\Omega)_{elastic}/(d\sigma/d\Omega)_{Ruth.}$
$\Theta_{C.M.}$

FIGURE 8

Deuteron Spectrum Obtained from $^{94}Mo(^{3}He,d)^{95}Tc$ Reaction

Deuteron peaks are labelled by their corresponding level excitation energies (in MeV) in ^{95}Tc.

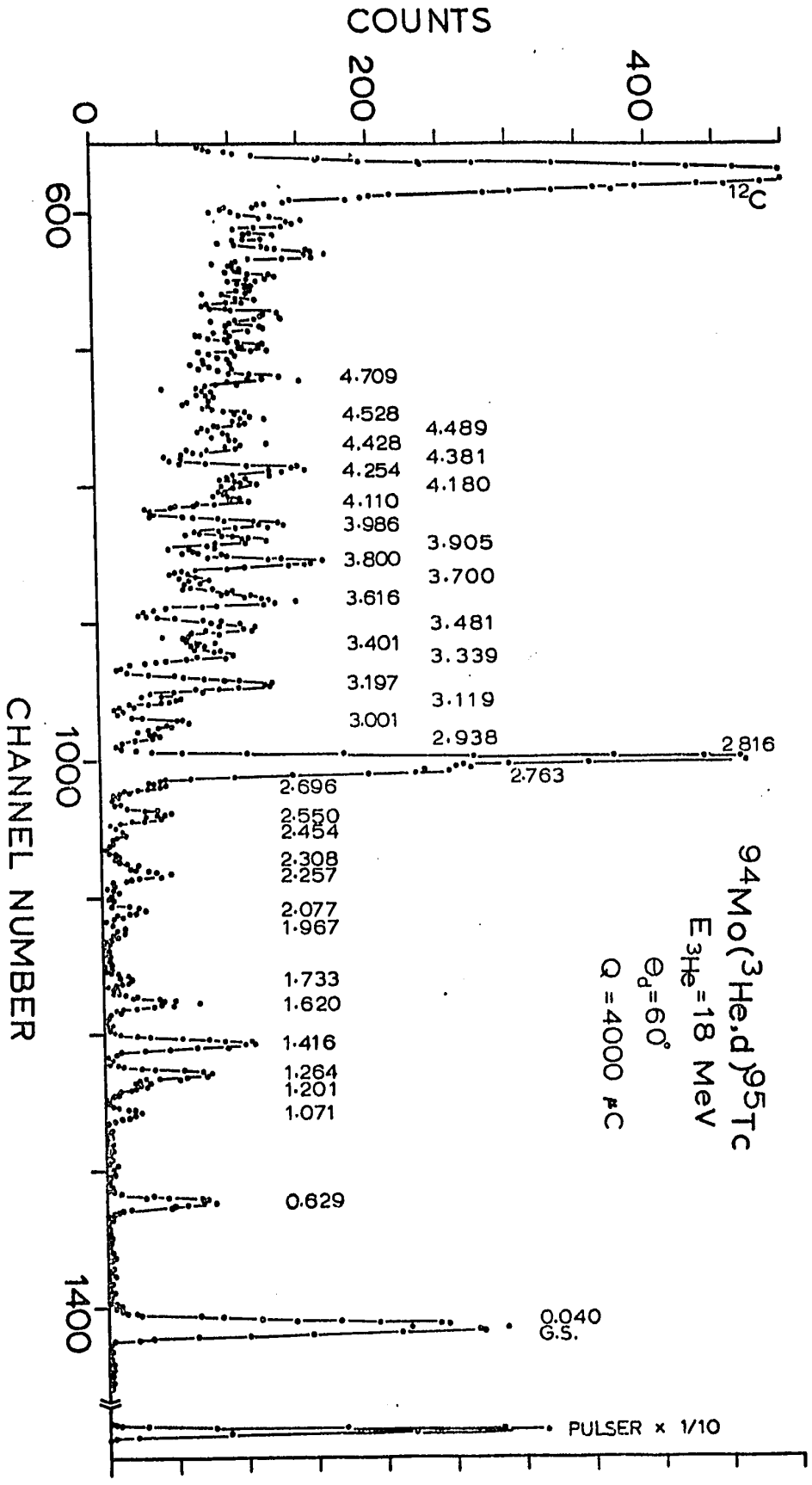
COUNTS
0
200
400
600
1000
1400
CHANNEL NUMBER
12C
4.709
4.528
4.489
4.428
4.381
4.254
4.180
4.110
3.986
3.905
3.800
3.700
3.616
3.481
3.401
3.339
3.197
3.119
3.001
2.938
2.816
2.763
2.696
2.550
2.454
2.308
2.257
2.077
1.967
1.733
1.620
1.416
1.264
1.201
1.071
0.629
0.040
G.S.
PULSER x 1/10
94Mo(3He,d)95Tc
E3He=18 MeV
θd=60°
Q=4000 μC

TABLE 2

Excitation Energies and Differential Cross Sections of the Various Levels in ^{95}Tc Obtained from the ^{94}Mo(^{3}He,d) ^{95}Tc Reaction.

The differential cross sections are given in the C.M. system. The total relative errors for all measurements are given directly under their respective mean values with the significance of their digits having a one-to-one correspondence with those in the mean values. The total systematic error of all differential cross section measurements was ± 20% (see section 3.2 for details). Blank entries indicate that no reliable data could be extracted (see text).

Excitation energy (MeV)	Differential Cross-Sections (μb/sr)												
	15°	20°	25°	30°	35°	40°	45°	50°	55°	60°	65°	70°	80°
Ground state			169.1 9.2	371.4 29.2	263.1 26.7	248.4 25.0	237.3 12.8	256.8 15.9	219.3 46.0	210.7 11.8	158.6 7.4	110.9 7.8	118.9 5.4
0.040 2	140.0 33.4	113.0 16.4	107.9 8.0	135.8 25.5	157.1 23.7	114.0 23.8	108.7 11.3	93.7 13.8	76.5 19.9	102.5 10.6	55.5 6.0	58.1 6.6	24.7 4.2
0.629 2	127.4 19.6	94.6 12.5	65.4 6.8	32.0 3.9	117.5 7.2	101.3 3.9	87.1 3.9	66.6 5.8	56.4 3.9	65.5 2.8	41.9 3.0	37.9 2.4	22.6 1.3
1.071 3	30.0 4.5	34.6 5.7	27.9 4.6	16.8 3.9	65.6 4.4	35.6 2.7	25.5 2.2	28.0 3.5	15.8 1.9	20.5 1.6	15.0 2.0	11.1 1.7	6.0 0.9
1.201 4	23.1 4.0	16.8 4.6	13.8 4.6	102.2 6.4	18.5 2.9	14.1 3.6	10.2 2.0	14.0 2.9	19.7 2.5	20.4 1.8	10.2 2.3	8.5 2.5	4.9 0.9
1.264 4	77.2 16.0	80.2 8.9	62.9 7.1	135.8 6.5	112.4 5.6	91.6 4.9	79.5 3.6	66.0 5.2	61.2 3.8	58.7 2.6	34.9 3.4	31.6 3.2	19.6 1.5
1.416 4	77.0 15.0	118.0 12.2	112.6 7.1	99.1 6.5	144.8 6.2	140.8 4.0	114.8 3.9	105.7 6.0	77.9 4.4	94.1 3.2	59.1 3.9	46.3 3.4	32.2 2.0
1.620 5	102.6 10.0	83.1 8.9	82.2 6.5	21.1 3.6	72.5 11.4	98.4 3.7	80.6 3.5	86.1 8.6	44.6 3.1	46.9 2.3	36.6 3.8	19.1 6.0	16.8 1.5
1.733 5	44.4 4.0		33.7 4.9	15.7 2.2	21.7 3.8	23.4 2.2	17.4 2.3	21.0 7.0	17.9 2.3	12.5 1.5	11.2 1.8	4.9 2.0	4.2 0.9
1.967 5	8.6 5.0	17.6 7.0			9.6 2.2	5.8 1.8	10.0 2.9	4.7 2.1	2.6 1.2	6.7 1.5	4.8 2.0	4.1 1.8	2.6 1.0

Excitation energy (MeV)	Differential Cross Sections (μb/sr)												
	15°	20°	25°	30°	35°	40°	45°	50°	55°	60°	65°	70°	80°
2.077	28.8	30.0	21.4		32.9	32.6	25.7	22.2	10.6	18.2	15.0	9.7	6.5
5	5.5	6.4	3.7		3.5	2.6	3.4	3.3	2.0	2.4	2.0	3.5	1.9
2.257 6 – 2.308 6	58.0	59.8	35.5	55.0	49.8	59.2	43.5	40.8	27.6	36.9	21.0	19.2	10.5
	10.0	7.1	11.0	8.0	3.4	5.1	6.4	4.9	2.5	4.1	2.7	2.5	1.9
2.454	14.4	25.6	24.2	34.5	19.7	14.1	5.4	4.1	2.6	6.8	3.7	3.8	
6	4.9	5.0	4.6	4.0	3.9	77.2	3.1	3.0	1.2	1.8	2.2	1.6	
2.550	53.0	52.3	45.9	60.5	38.2	39.4	44.6	36.6	22.0	33.5	23.3	25.6	9.7
7	14.0	6.8	5.2	5.1	4.1	8.5	4.7	3.3	3.4	2.9	3.7	13.5	1.8
2.696	21.0	41.2		18.7	24.0	29.7	17.9	19.1	12.7	25.9	13.8	11.5	3.2
7	7.2	14.3		8.9	9.1	4.9	10.3	5.4	3.2	2.0	4.3	5.6	1.9
2.763	94.4	362.5	261.7	289.8	247.3	223.7	253.8	244.9	154.6	189.8	114.2	88.3	53.9
7	15.0	32.2	19.1	16.2	13.9	18.1	13.1	11.8	8.7	4.8	7.5	7.4	4.1
2.816	361.0	544.2	473.5	5.3.9	505.6	576.8	540.8	429.4	315.2	356.2	267.9	209.9	144.1
8	140.3	39.3	22.4	21.2	19.7	21.8	23.0	14.9	12.7	5.8	11.6	12.4	6.4
2.938		117.4	89.1	63.6	33.4	34.2	64.3	24.9	40.1	22.0	36.0	18.4	18.9
8		22.2	9.5	8.9	7.3	4.7	7.3	5.0	8.3	2.3	4.4	3.4	2.3
3.001		279.8	78.0	49.8	71.4	56.8	66.5	43.8	26.4	42.3	40.2	18.5	18.5
9		26.4	9.2	10.2	9.3	6.0	7.3	6.6	4.5	2.8	5.7	3.6	2.7

Excitation energy (MeV)	Differential Cross-Sections (μb/sr)												
	15°	20°	25°	30°	35°	40°	45°	50°	55°	60°	65°	70°	80°
3.119	12.0	34.5	103.4	62.1	49.3	34.9	34.3	37.0	30.6	36.0	29.5	13.0	9.5
9	5.8	14.4	11.1	18.6	7.7	6.3	5.2	6.6	9.3	4.4	6.6	3.7	2.5
3.197	39.2	123.3	197.6	155.8	142.4	148.1	134.0	163.4	109.7	110.6	73.4	43.6	37.4
9	10.0	21.4	13.8	24.9	11.4	9.5	7.9	11.8	13.9	6.6	7.1	8.8	4.7
3.339	34.6	83.5	74.6	140.4	120.6	63.4	100.4	85.9	57.3	70.1		24.8	21.1
9	14.6	18.9	15.1	24.9	14.1	11.6	13.0	8.7	9.1	6.3		5.4	4.4
3.401	44.4	35.7	76.7	57.9	85.2	51.7	80.9	63.1	53.4	51.6		23.8	15.5
10	8.1	12.0	15.5	18.8	16.8	10.8	15.4	12.6	9.9	6.1		5.7	5.7
3.481	75.5		109.1	164.4	165.9	84.1	151.4	114.2	73.9	91.0	63.6	42.7	35.4
10	16.0		19.5	31.8	19.2	12.8	19.6	7.8	12.1	8.1	15.3	7.7	6.0
3.616				164.2	229.6	175.2	157.4	90.8	118.5	118.9	91.1	70.1	43.7
10				31.0	21.4	18.2	39.2	7.8	13.5	10.2	17.8	13.9	6.0
3.700				121.2	110.6	76.5	136.8	41.7	56.6	53.9		45.7	25.5
11				18.4	17.9	13.7	38.8	11.8	10.0	7.8		12.0	5.9
3.800				199.4	216.6	196.5	183.4	115.6	102.6	119.7	69.7	66.5	37.0
11				28.7	25.6	21.9	24.7	9.5	13.4	7.7	16.4	15.0	9.3
3.905					135.4	114.1	114.2	57.7	53.5	74.8	34.5	48.0	25.3
11					25.3	21.6	22.4	8.7	12.7	6.9	13.3	15.3	7.9
3.986					190.5	121.3	155.8	79.7	86.1	89.5	55.2	64.5	32.4
12					30.6	23.2	27.0	12.6	14.0	7.9	16.3	18.5	9.1

Excitation energy (MeV)	Differential Cross-Sections (μb/sr)												
	15°	20°	25°	30°	35°	40°	45°	50°	55°	60°	65°	70°	80°
4.110		35.7				68.6	61.8	52.8	43.2	66.6	28.2	18.3	15.6
12		12.5				26.5	6.4	12.6	11.9	8.2	9.8	4.5	4.0
4.180	57.6	60.7		97.7		85.0	91.3	66.7	41.1	69.7	30.8	27.5	17.6
12	24.6	12.0		18.0		31.4	6.9	13.0	9.1	8.6	8.8	4.8	3.8
4.254	115.6	107.2		130.3		122.3	92.8	91.3	62.8	104.3	56.4	37.4	22.1
12	30.5	30.8		25.0		45.2	6.9	16.5	10.1	12.2	11.0	6.0	4.2
4.381													
12 }	46.1	62.5		52.1			46.2	36.5	27.5	58.2	19.6	8.8	9.5
4.428 }	10.0	7.5		7.4			6.8	11.1	7.3	9.3	7.1	3.9	4.3
12													
4.489													
13 }	92.2	71.5		104.2			36.7	33.0	30.4	58.5	23.3	24.9	13.1
4.528 }	40.0	31.5		30.4			6.8	9.5	7.0	9.4	6.5	4.4	5.4
13													
4.709	69.2			143.3				53.9	42.6	31.2	25.0	11.6	12.8
13	30.1			35.4				10.1	8.7	7.5	10.8	4.1	2.8

FIGURE 9

Deuteron Spectrum Obtained from $^{96}Mo(^{3}He,d)^{97}Tc$ Reaction

Deuteron peaks are labelled by their corresponding level excitation energies (in MeV) in ^{97}Tc.

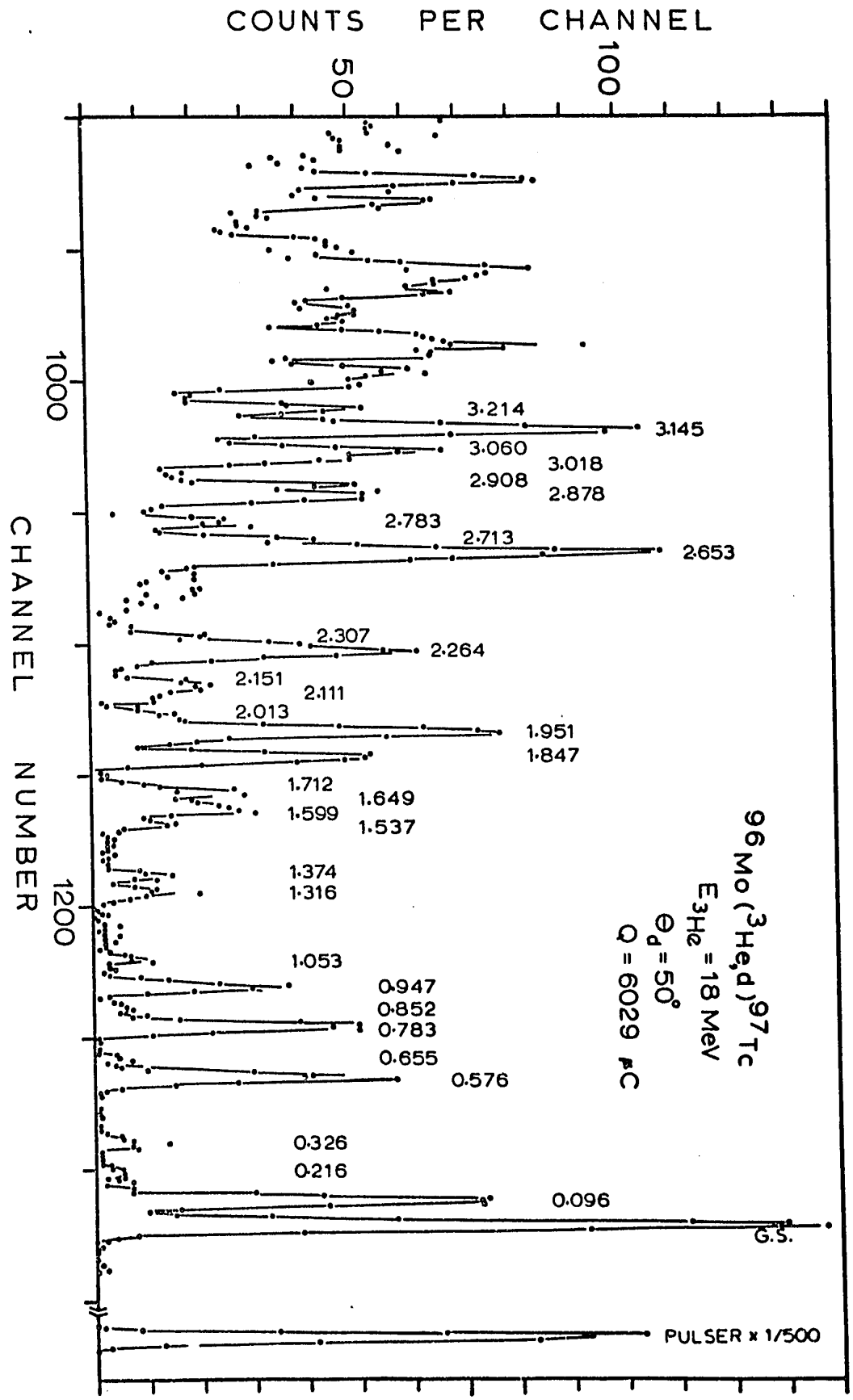
COUNTS PER CHANNEL
50
100
CHANNEL NUMBER
1000
1200
3.214
3.145
3.060
3.018
2.908
2.878
2.783
2.713
2.653
2.307
2.264
2.151
2.111
2.013
1.951
1.847
1.712
1.649
1.599
1.537
1.374
1.316
1.053
0.947
0.852
0.783
0.655
0.576
0.326
0.216
0.096
G.S.
PULSER x 1/500
96Mo (3He,d)97Tc
E3He = 18 MeV
θd = 50°
Q = 6029 keV

TABLE 3

Excitation Energies and Different Cross sections of the Various Levels in ^{97}Tc Obtained from the $^{96}Mo(^{3}He,d)$ ^{97}Tc Reaction

The differential cross sections are given in the C.M. system. The total relative errors for all measurements are given directly under their respective mean values with the significance of their digits having a one-to-one correspondence with those in the mean values. The total systematic error of all differential cross section measurements was $\pm$ 20% (see section 3.2 for details). Blank entries indicate that no reliable data could be extracted.

Excitation energy (MeV)	Differential Cross-Sections (μb/sr)															
	15°	20°	25°	30°	35°	40°	45°	50°	55°	60°	65°	70°	75°	80°	85°	90°
Ground state	29.3 7.7	83.9 8.6	157.3 15.3	200.4 8.0	206.2 8.5	184.0 6.4	196.8 9.3	192.9 8.5	174.1 6.0	144.2 6.2	125.2 6.0	122.7 6.2	113.5 6.0	103.5 10.8	77.5 3.0	65.9 12.1
0.096 2	166.0 14.5	89.6 8.6	120.2 12.7	168.7 8.4	167.7 8.0	136.1 5.7	123.2 7.8	110.4 6.6	88.3 4.5	84.7 4.9	75.1 4.9	56.2 4.3	40.5 3.5	37.0 6.0	30.0 2.1	25.3 15.0
0.216 6			4.6 1.9	6.4 3.8	5.6 2.4	6.0 3.0	5.5 3.0	4.5 2.0	3.0 1.7			2.5 0.6				
0.326 3	19.5 5.0	24.8 5.5	19.2 4.6	15.0 3.1	23.0 5.5	16.4 4.4	12.0 4.0	13.5 5.0	10.0 2.5	11.0 2.5	9.5 2.7	5.2 1.2	5.4 1.5		3.7 1.3	3.4 1.5
0.576 2	100.8 20.0	51.5 7.3	63.9 13.0	92.4 9.3	90.7 6.0	88.5 4.8	82.8 6.9	69.2 4.8	60.4 4.3	51.4 5.0	38.6 3.5	32.9 2.7	25.5 2.4	19.0 2.5	19.5 3.4	14.0 7.7
0.655 6	6.0 2.4	8.7 2.1	6.2 3.0	8.6 3.4	8.3 3.0	6.5 1.6	6.0 2.3	4.7 1.5	4.0 1.5	2.7 1.6	2.9 1.5	3.4 1.3	4.6 1.9	2.8 1.2	2.5 1.2	
0.783 3		136.2 8.3	73.6 14.0	94.0 10.0	107.0 10.6	95.4 11.0	85.9 9.2	74.4 6.5	66.7 5.5	55.1 5.0	49.2 4.9	31.4 3.9	27.1 3.0	24.1 3.2	24.1 4.0	20.0 9.2
0.852 6		19.4 10.0	16.5 8.0	5.2 2.2	8.2 4.0	3.9 1.9	9.3 4.2	9.3 4.2	4.8 3.0	5.5 2.5						
0.947 3	60.8 6.0		75.5 8.0	80.7 17.8	57.7 7.6	60.0 19.3	58.1 6.0	44.6 4.0	43.5 3.5	43.0 4.1	25.4 3.0	25.6 3.5	17.1 3.5		10.0 3.4	9.5 3.0
1.053 4	13.5 4.0		17.0 4.3	17.8 5.0	12.4 2.6	8.6 4.5	8.4 3.4	9.7 1.2	10.2 2.3	10.5 2.3	9.1 1.8	5.8 1.2	5.7 1.8		3.2 1.7	3.2 1.7

Excitation energy (MeV)	Differential Cross-Sections (μb/sr)															
	15°	20°	25°	30°	35°	40°	45°	50°	55°	60°	65°	70°	75°	80°	85°	90°
1.316	10.6	15.8	33.0	20.3	28.7	19.0	26.6	23.4	22.0	15.2	20.2	9.2	14.4		10.7	7.2
4	3.5	2.8	6.0	3.5	5.0	5.0	3.5	3.5	4.5	2.2	2.8	2.6	4.6		1.8	2.0
1.374	19.0	37.0	16.7	20.2	18.5	15.1	14.3	19.5	13.4	15.0	11.0	12.0	4.7		5.2	5.2
4	4.4	4.3	5.0	7.5	3.5	2.3	2.2	3.0	3.0	4.1	2.0	2.2	2.1		1.1	2,4
1.537	10.6	24.5	14.4	18.3	16.2		8.0	15.2	4.8	4.3	5.4	4.0			2.4	
4	4.5	10.0	6.0	7.0	4.0		4.5	5.0	2.1	1.7	2.5	2.4			0.9	
1.599	38.0	50.4	30.4	33.5	37.0	30.6	21.2	4.4	27.0	25.5	16.0	22.0	12.6		6.9	
4	6.2	5.3	10.0	7.5	4.0	10.0	8.5	0.6	2.5	2.5	3.4	5.4	3.0		1.1	
1.649	44.2	51.1	76.2	50.1	52.0	47.8	40.0	34.3	23.5	16.4	11.2	20.0	9.3		9.5	
7	6.6	8.0	14.5	10.0	9.0	7.0	8.0	4.5	4.1	4.5	4.3	5.0	4.7		2.0	
1.712	24.3	43.9	76.8	30.0	56.9	35.6	36.6	23.3	21.4	21.4	14.8	12.4	7.7		7.2	
5	4.8	4.7	14.0	6.2	6.5	15.1	7.1	5.1	4.5	4.1	4.7	4.1	4.2		1.7	
1.847	49.7	99.3	118.8	82.9	115.1	122.7	124.9	100.3	69.0	64.3	39.3	43.5	34.1	26.0	25.2	
5	7.1	7.1	18.0	10.0	10.1	9.5	20.0	10.5	9.2	6.5	4.0	8.4	3.0	4.5	5.0	
1.951	105.3	138.5	77.2	79.6	162.2	138.2	104.3	111.6	113.3	97.5	65.0	57.1	43.9	27.1	29.3	21.3
5	10.3	8.5	10.7	20.0	10.5	15.0	6.5	5.9	7.9	7.5	4.2	4.0	4.0	7.0	4.5	6.5
2.013	36.5	45.4	38.3	35.5	41.7	34.0	25.2	17.6	8.8	16.0	13.7	11.6	8.5		5.5	
7	6.0	4.8	6.6	5.0	4.5	6.0	4.9	3.0	3.0	4.3	2.6	1.5	2.0		2.4	
2.111	25.4	22.3	20.6	19.0	19.0	24.5	20.5	14.4	16.3	14.5	9.6	8.5	8.3			
9	5.8	3.5	5.1	4.3	4.2	5.4	6.8	4.5	4.1	4.2	4.6	2.2	4.0			
2.151	10.3	15.0	19.5	24.3	24.5	28.8	25.5	27.1	17.0	12.5	8.0	7.1	6.0	6.0		
9	3.5	3.3	5.0	4.0	4.5	4.6	8.0	7.3	6.0	6.7	4.1	2.0	2.5	2.5		

Excitation energy (MeV)	Differential Cross-Sections (μb/sr)															
	15°	20°	25°	30°	35°	40°	45°	50°	55°	60°	65°	70°	75°	80°	85°	90°
2.264	57.0	105.8	130.1	112.5	110.5	104.1	108.1	92.6	72.2	69.6	44.7	37.7	27.4		22.0	13.5
7	7.5	7.3	38.5	12.0	12.7	11.0	10.3	8.5	8.0	15.0	6.5	5.0	4.0		8.3	9.3
2.307	38.1	55.0	47.0	40.0	52.0	59.3	30.4	23.4	30.8	22.3	34.2	15.7	14.4			11.5
8	6.2	10.0	8.5	10.8	10.0	8.1	6.0	5.0	10.0	10.0	7.0	3.5	3.7			7.2
2.653	87.6	174.3	247.5	162.2	162.5	184.6	183.6	136.7	107.1	74.5	81.8	68.9	60.0	43.7	27.1	
8	9.4	20.0	53.0	24.0	20.9	25.0	20.0	20.0	10.0	8.3	11.0	88.0	20.0	26.0	6.5	
2.713	48.5	45.1	61.0	64.4	65.0	70.4	40.7	38.2	26.9	22.6	24.7	30.9	23.2	11.3		
8	6.9	9.3	20.8	16.7	12.0	22.3	8.4	10.0	6.8	3.9	8.4	9.5	5.3	4.0		
2.783		40.0	40.8	20.9	37.4	29.5	21.4	23.5	16.8	22.6	15.3	18.9	19.3		9.0	
8		10.5	13.4	9.5	12.9	9.3	4.8	8.8	5.5	9.5	5.5	5.0	10.4		2.6	
2.878 9 / 2.908 9	93.4	102.0	103.5	99.5	104.3	101.2	100.4	101.5	74.5	93.4	55.3	43.0	45.0		27.5	
	9.6	7.3	18.0	10.3	10.0	8.1	7.8	8.3	6.9	7.5	6.1	4.3	4.5		3.2	
3.018	49.0	70.0	48.1	46.3	31.5	35.2	35.6	34.5	46.0	24.0	18.0		12.5		9.8	
9	27.5	30.0	13.7	23.0	13.4	8.9	6.7	9.1	11.0	5.5	8.2		3.8		16.3	
3.060	77.3	75.6	94.2	70.2	78.1	73.8	62.2	60.2	75.9	49.7	45.6	32.8	29.8		18.9	
9	30.0	35.2	33.2	30.5	17.5	11.0	8.2	11.0	25.0	7.3	11.0	4.9	5.4		5.4	
3.145	106.2	145.8	214.9	180.7	141.9	150.3	121.8	130.8	105.0	97.5	76.2	52.0	48.8		38.9	
9	26.3	35.3	33.3	25.0	14.8	9.9	7.8	8.5	14.3	8.4	9.4	5.7	5.8		4.1	
3.214	45.8	43.5	101.0	107.5	81.4	55.7	54.4	45.9	39.6	40.7	29.9	10.3	15.0		19.2	
9	16.6	20.0	42.4	25.0	11.3	7.9	6.2	7.8	10.8	6.9	6.3	3.6	3.6		3.3	

FIGURE 10

Deuteron Spectrum Obtained from $^{98}Mo(^{3}He,d)^{99}Tc$ Reaction at 18 MeV Incident Energy

Deuteron peaks are labelled by their corresponding level excitation energies in ^{99}Tc.

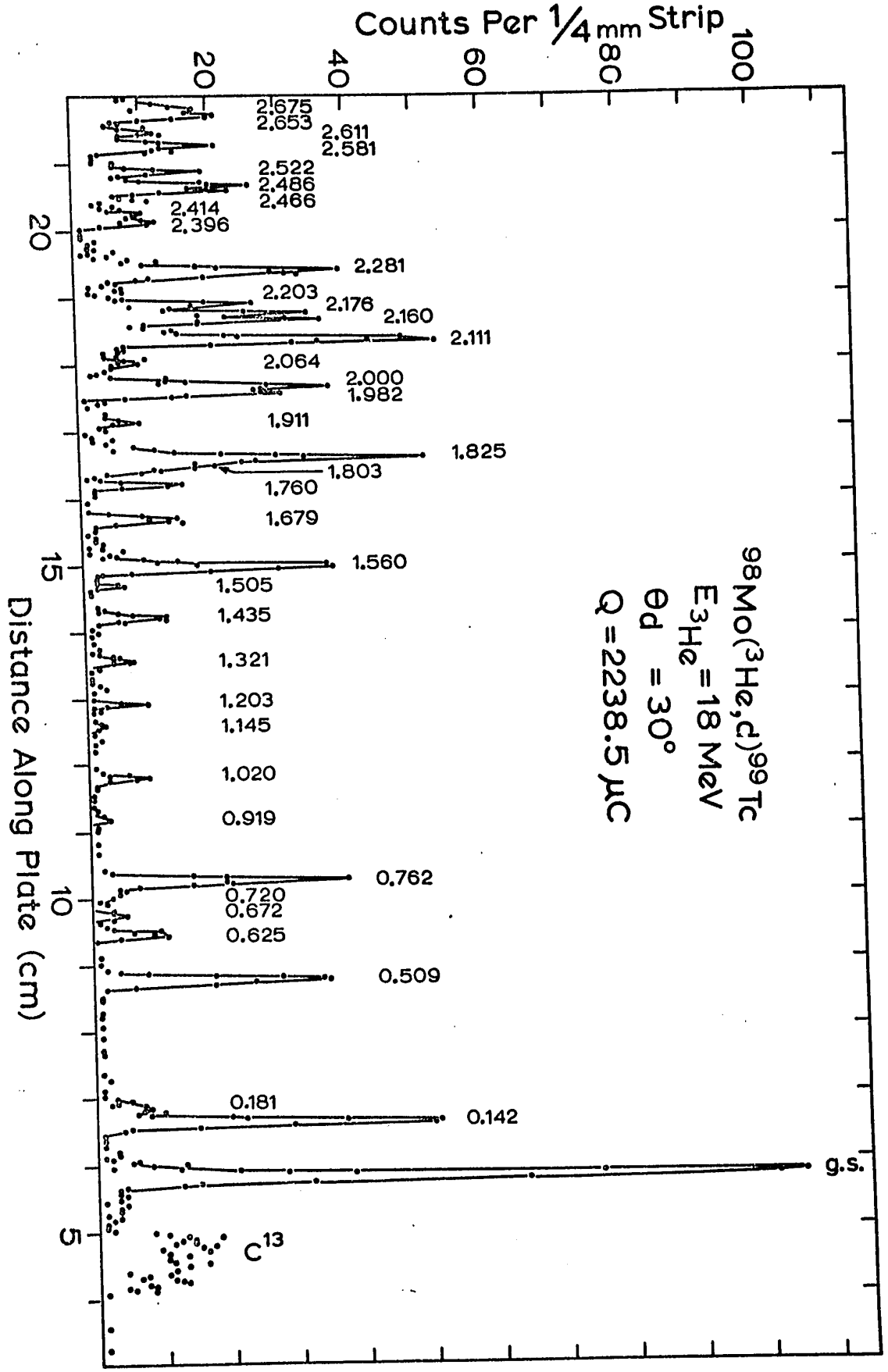
Counts Per 1/4 mm Strip
20
40
60
80
100
Distance Along Plate (cm)
20
15
10
5
2.675
2.653
2.611
2.581
2.522
2.486
2.466
2.414
2.396
2.281
2.203
2.176
2.160
2.111
2.064
2.000
1.982
1.911
1.825
1.803
1.760
1.679
1.560
1.505
1.435
1.321
1.203
1.145
1.020
0.919
0.762
0.720
0.672
0.625
0.509
0.181
0.142
g.s.
C13
98Mo(3He,d)99Tc
E3He = 18 MeV
θd = 30°
Q = 2238.5 μC

FIGURE 11

Deuteron Spectrum Obtained from $^{98}Mo(^{3}He,d)^{99}Tc$ Reaction at 24 MeV Incident Energy (Part I)

Spectrum covers the excitation energy region below about 1.6 MeV. All deuteron peaks are labelled by their corresponding excitation energies in ^{99}Tc.

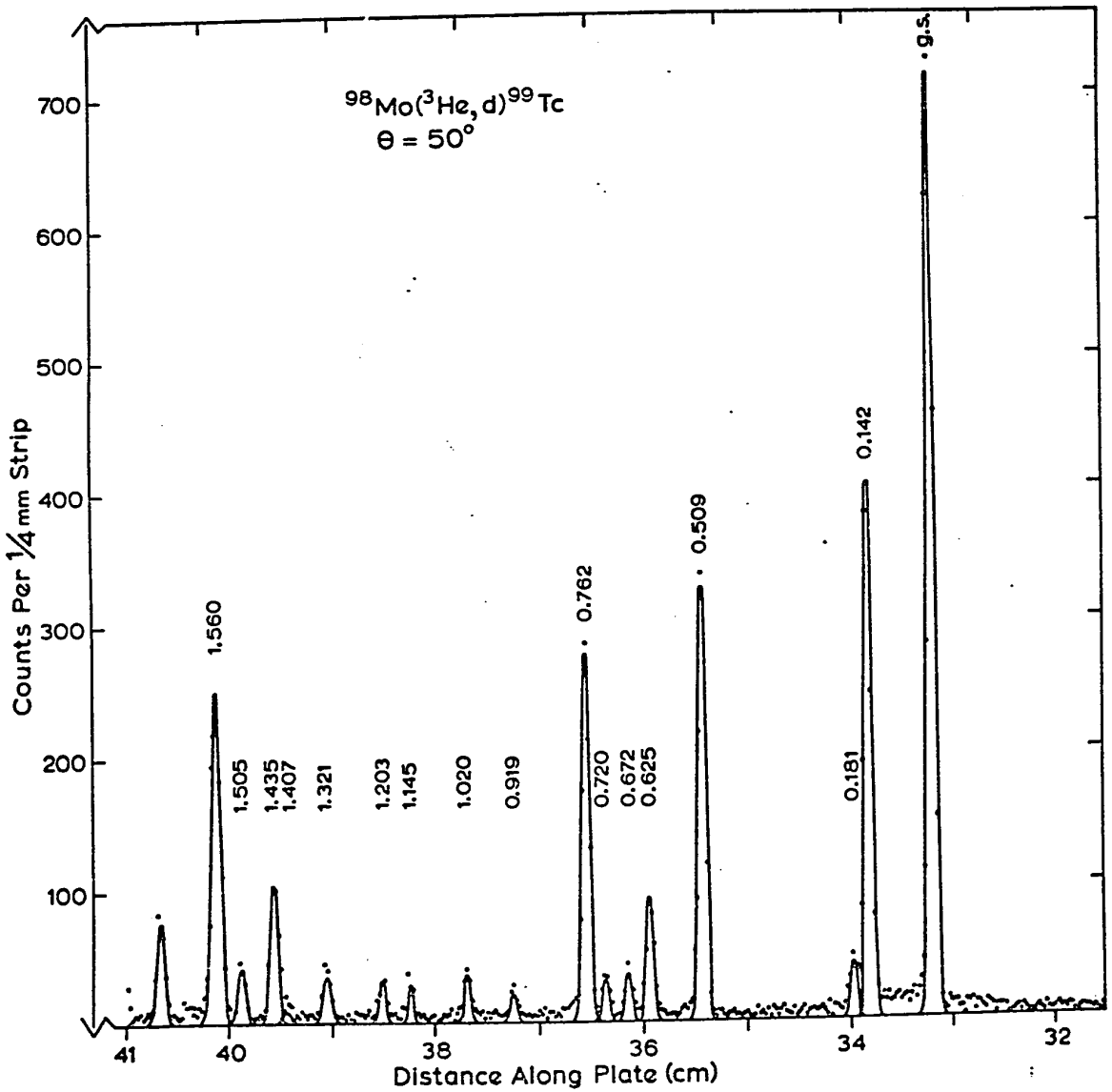
$^{98}Mo(^{3}He,d)^{99}Tc$
θ = 50°
Counts Per 1/4 mm Strip
Distance Along Plate (cm)
700
600
500
400
300
200
100
41
40
38
36
34
32
g.s.
0.142
0.509
0.762
1.560
0.181
0.720
0.672
0.625
1.505
1.435
1.407
1.321
1.203
1.145
1.020
0.919

FIGURE 12

Deuteron Spectrum Obtained from $^{98}Mo(^{3}He,d)^{99}Tc$ Reaction at 24 MeV Incident Energy (Part II)

Spectrum covers the excitation energy region from about 1.6 MeV to 2.5 MeV. All peaks are labelled by their corresponding excitation energies in ^{99}Tc.

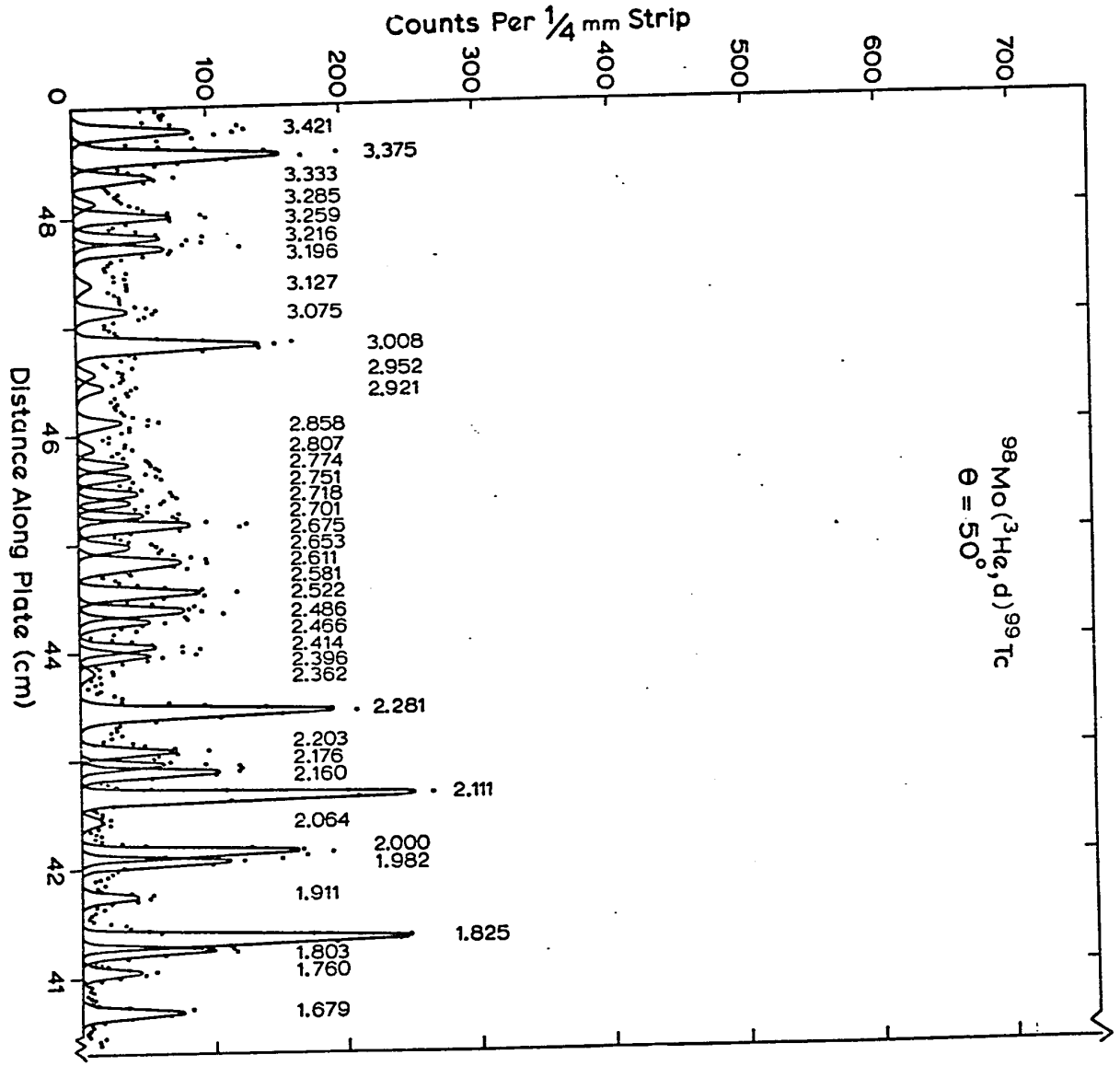
Counts Per 1/4 mm Strip
0
100
200
300
400
500
600
700
Distance Along Plate (cm)
48
46
44
42
41
3.421
3.375
3.333
3.285
3.259
3.216
3.196
3.127
3.075
3.008
2.952
2.921
2.858
2.807
2.774
2.751
2.718
2.701
2.675
2.653
2.611
2.581
2.522
2.486
2.466
2.414
2.396
2.362
2.281
2.203
2.176
2.160
2.111
2.064
2.000
1.982
1.911
1.825
1.803
1.760
1.679
98Mo(3He,d)99Tc
θ = 50°

TABLE 4

Level Excitation Energy in ^{99}Tc and Differential Cross Sections for the $^{98}Mo(^{3}He,d)^{99}Tc$ Reaction

Excitation energies were determined from the spectrum obtained at 24 MeV incident energy, and the differential cross sections are for the 18 MeV incident energy. The total relative errors are listed directly under their respective mean values with the significance of their digits having a one-to-one correspondence with those in the mean values. The systematic error for the differential cross sections is $\pm$ 25%. No differential cross sections were extracted for the states above 2.7 MeV. The differential cross sections are given in the C.M. system.

Excitation energy (MeV)	Differential Cross-Sections (μb/s.r.)												
	8°	12°	16°	20°	25°	30°	35°	40°	45°	50°	55°	60°	70°
Ground state	22.8 2.6	30.0 3.1	48.7 3.9	72.0 4.7	125.9 6.0	157.7 6.6	146.8 5.8	119.4 6.0	134.3 6.5	130.4 6.0	118.3 6.0	88.0 5.2	77.7 4.9
0.142 1	86.8 5.2	95.2 5.5	54.0 4.1	56.7 4.2	55.9 4.1	77.3 4.6	58.3 6.0	50.6 4.2	58.1 4.3	43.2 3.6	44.6 3.7	38.7 3.4	19.4 2.4
0.181 2	1.9 1.0	4.2 1.2	7.1 1.5	7.0 1.5	4.8 1.2	4.9 1.2	4.0 1.1	4.5 1.2	5.2 1.3	3.3 1.0	1.8 0.7	2.3 0.8	
0.509 1	72.1 4.7	82.7 5.1	57.7 4.2	34.4 3.3	40.8 3.6	55.9 4.0	52.5 4.0	46.2 3.8	43.3 4.7	39.0 3.5	35.7 3.3	21.4 2.6	21.6 2.5
0.625 1	6.3 1.4	6.4 1.4	4.7 1.3	9.1 1.7	11.3 1.9	16.3 2.3	11.9 1.9	12.9 2.0	17.3 2.4	14.2 2.1	14.3 2.1	6.7 1.5	5.2 1.3
0.672 1	3.1 1.0	5.6 1.2	4.7 1.3	4.7 1.2	6.6 1.4	5.6 1.3	6.6 1.4	3.2 1.0	6.8 1.5	6.0 1.4	5.1 1.3	3.5 1.1	1.6 1.1
0.720 1	1.0 0.6	1.6 0.6		1.3 0.6	6.0 1.4	4.8 1.3	5.7 1.4	4.4 1.2	6.3 1.4	5.4 1.3	4.8 1.3	4.2 1.2	1.3 0.7
0.762 1	39.6 3.6	46.5 4.0	56.2 4.3	59.1 4.4	43.6 3.7	48.6 4.0	52.8 4.3	44.0 3.8	37.6 3.5	34.6 3.4	31.2 3.2	23.7 2.8	17.7 2.4
0.919 2	8.1 1.6	1.6 0.6	4.4 1.2	6.9 1.5	5.0 1.3	3.1 1.0	7.9 1.6	5.0 1.3	4.4 1.2	2.8 0.9	1.6 0.7	1.6 0.8	
1.020 2	4.0 1.2	5.4 1.3	6.0 1.8	10.2 2.0	4.7 1.2	10.1 1.8	8.2 1.6	6.6 1.4	6.6 1.4	5.0 1.3	4.1 1.2	2.6 1.0	2.9 1.0

Excitation energy (MeV)	Differential Cross-Sections (μb/s.r.)												
	8°	12°	16°	20°	25°	30°	35°	40°	45°	50°	55°	60°	70°
1.145	3.4	5.0	33.7	5.9	3.1	2.0	2.5	3.8	4.7	2.8	2.5	4.2	1.3
2	1.1	1.3	1.1	1.4	1.0	0.8	1.0	1.1	1.2	1.0	1.0	1.2	0.6
1.203	2.8	5.9	6.2	2.2	3.0	6.7	4.7	4.1	4.7	4.4	4.4	1.3	1.0
2	1.0	1.4	1.4	1.0	1.0	1.4	1.3	1.2	1.2	1.2	1.2	0.6	0.7
1.321	10.6	10.6	15.6	4.1	8.5	8.7	9.1	4.7	8.1	3.5	3.8	3.8	3.2
2	1.8	1.8	2.2	1.2	1.6	1.6	1.7	1.2	1.6	1.1	1.1	1.1	1.1
1.407										1.0			
4										0.4			
1.435		15.3	18.1	19.1	24.1	18.8	23.5	17.6	20.4	18.9	16.9	12.2	6.4
2		2.2	2.4	2.4	2.8	2.4	2.7	2.3	2.5	2.4	2.3	3.0	1.4
1.505			11.2	7.5	7.5	5.6	56.5	10.0	9.1	6.3	5.1	1.2	1.9
2			1.9	1.5	1.5	1.3	1.4	1.8	1.7	1.4	1.3	0.6	0.8
1.560	78.3	34.2	24.0	75.6	74.6	66.5	69.0	82.8	70.8	43.1	46.1	33.9	29.3
3	5.0	2.8	2.7	4.9	4.9	4.6	4.7	5.2	4.9	3.7	3.9	3.3	3.1
1.679	9.4	24.4	20.9		14.2	21.6	16.9	11.3	14.7	15.7	12.7	11.2	8.7
2	1.7	2.8	2.6		2.1	2.6	2.3	1.8	2.1	2.2	2.0	1.9	1.6
1.760	8.4	9.7	14.0		16.9	14.6	11.3	9.1	10.0	8.2	8.3	8.0	5.2
2	1.6	1.7	2.1		2.3	2.1	1.9	1.6	1.8	1.6	1.6	1.6	1.3
1.803													
2	71.7	81.3	92.5	94.6	104.6	90.9	90.0	92.5	82.7	69.8	64.2	59.8	31.6
1.825	4.8	5.1	5.5	5.5	6.0	5.4	5.4	5.4	5.1	4.8	4.7	4.4	3.5
2													

Excitation energy (MeV)	Differential Cross-Sections (μb/s.r.)												
	8°	12°	16°	20°	25°	30°	35°	40°	45°	50°	55°	60°	70°
1.911 3		19.9 2.5	13.8 1.9	22.2 2.6	19.7 2.5	10.7 1.8	14.7 2.1	13.2 2.0	8.5 1.6	8.4 1.6	5.7 1.4	7.7 1.5	3.2 1.0
1.982 3 / 2.000 3	76.7 4.9	68.2 4.7	90.3 5.4	101.8 6.2	62.0 4.5	76.3 4.9	87.2 5.3	84.4 5.2	68.0 4.9	66.4 4.6	66.1 4.6	55.9 4.3	30.9 3.2
2.064 5													
2.111 5	33.6 3.3	54.2 4.2	65.1 4.6	62.1 4.5	55.7 4.2	83.3 5.1	63.7 4.5	66.8 4.6	47.0 3.9	54.4 4.2	53.7 4.2	33.6 3.3	32.5 3.2
2.160 3 / 2.176 4	54.8 4.2	28.0 3.0	46.7 3.9	59.9 4.4	51.7 4.1	67.0 4.6	55.5 4.2	50.8 4.0	50.1 4.0	44.0 3.8	36.6 3.5	32.3 3.2	20.0 2.5
2.203 3	3.1 1.0	8.1 1.4	26.2 2.9	31.5 3.2	31.0 3.2	28.6 3.0	34.8 3.4	29.8 3.1	26.9 2.9	24.6 2.8	20.4 2.5	15.3 2.2	48.3 3.9
2.281 3	87.2 5.3	57.9 4.3	52.9 4.1	67.1 4.6	78.3 5.0	71.5 4.8	67.1 4.6	60.8 4.4	58.2 4.4	48.1 4.0	47.7 3.9	37.4 3.9	21.6 2.6
2.362 5													

Excitation energy (MeV)	Differential Cross-Sections (μb/sr)												
	8°	12°	16°	20°	25°	30°	35°	40°	45°	50°	55°	60°	70°
2.396 4 2.414 4	33.6 3.3	25.8 2.9	30.0 3.1	39.9 3.6	32.6 3.3	25.2 2.8	37.9 3.5	36.1 3.4	33.2 3.3	25.8 2.9	21.3 2.6	15.7 2.2	6.4 1.4
2.466 5 2.486 5	81.9 5.1	42.3 3.7	44.8 3.8	72.1 4.8	58.2 4.4	46.0 3.9	43.9 3.8	45.1 3.8	43.2 3.7	37.7 3.5	34.0 3.3	24.6 2.8	19.0 2.4
2.522 5	31.1 3.2	36.7 3.3	23.7 2.8	32.8 3.2	30.0 3.1	47.2 3.9	26.6 2.9	34.5 3.4	27.9 3.0	23.6 2.7	20.0 2.5	15.7 2.2	13.9 2.1
2.581 5	17.4 2.3	39.5 3.6	37.3 3.5	39.9 3.6	30.4 3.1	33.6 3.3	44.8 3.8	50.8 4.1	39.8 3.6	26.7 2.9	25.4 2.9	24.6 2.8	13.2 2.0
2.611 6													
2.653 5 2.675 5	52.9 4.2	56.3 4.3	35.5 3.4	49.9 4.0	54.4 4.2	44.0 3.8	38.9 3.6	49.5 4.0	37.6 3.5	24.8 2.8	19.7 2.5	20.8 2.6	
2.701 5													
2.718 5													

Excitation energy (MeV)	Excitation energy (MeV)
2.751 5	3.127 7
2.774 5	3.196 7
2.807 6	3.216 7
2.858 5	3.259 7
2.921 6	3.285 8
2.953 6	3.333 8
3.008 6	3.375 8
3.075 7	3.421 8

FIGURE 13

Deuteron Spectrum Obtained from $^{100}Mo(^{3}He,d)^{101}Tc$ Reaction

Deuteron peaks are labelled by their corresponding level excitation energies (in MeV) in ^{101}Tc.

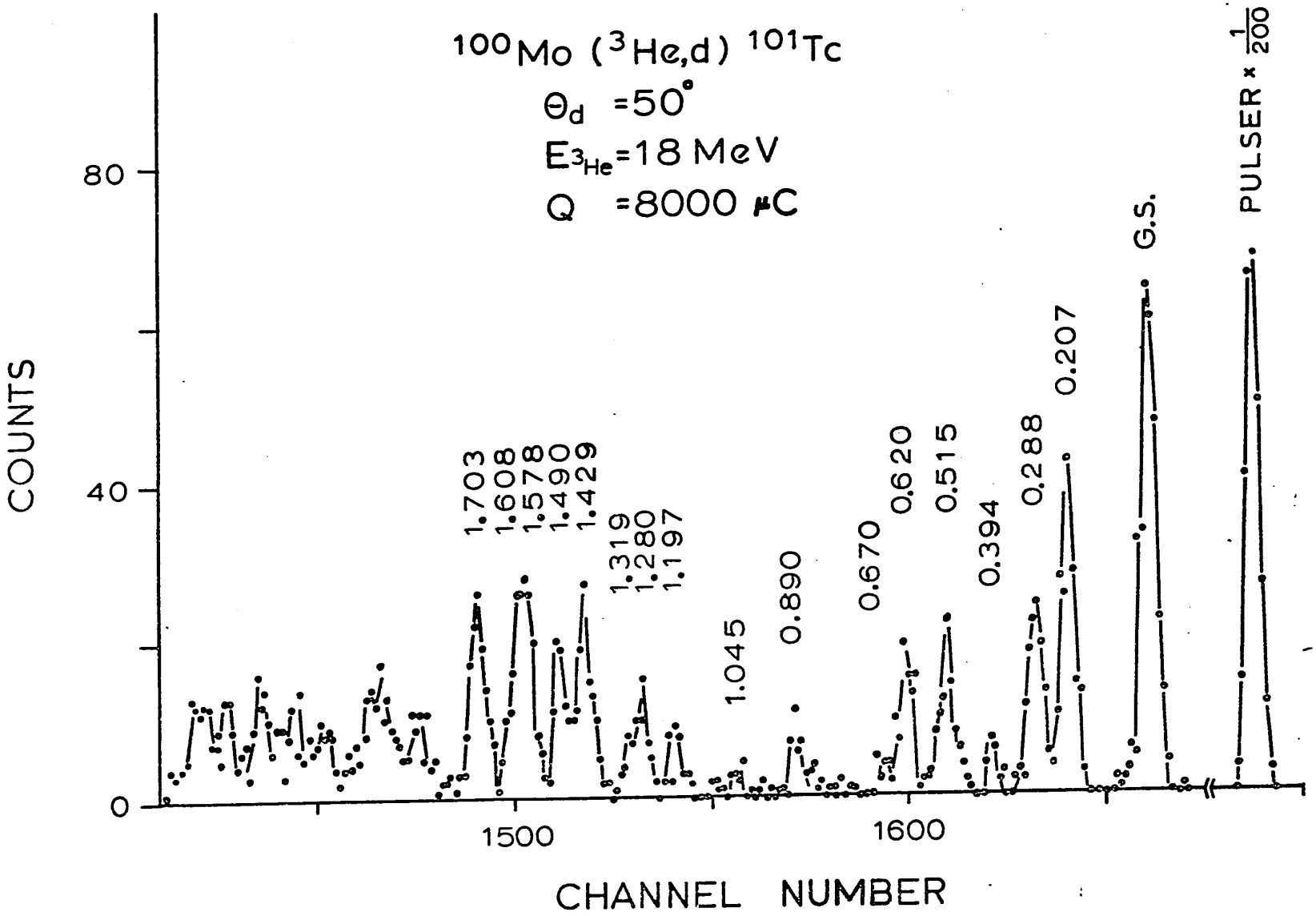
$^{100}Mo\ (^{3}He,d)\ ^{101}Tc$
$\Theta_d = 50°$
$E_{^3He} = 18\ MeV$
$Q = 8000\ \mu C$
COUNTS
80
40
0
1500
1600
CHANNEL NUMBER
PULSER × 1/200
G.S.
0.207
0.288
0.394
0.515
0.620
0.670
0.890
1.045
1.197
1.280
1.319
1.429
1.490
1.578
1.608
1.703

TABLE 5

Excitation Energies and Differential Cross Sections of the Various Levels in ^{101}Tc Obtained from the ^{100}Mo $(^{3}He,d)^{101}Tc$ Reaction

The differential cross sections are given in the C.M. system. The total relative errors for all measurements are given directly under their respective mean values with the significance of their digits having a one-to-one correspondence with those in the mean values. The total systematic error of all differential cross section measurements was $\pm$ 20%. Blank entries indicate that no reliable data could be extracted.

Excitation energy (MeV)	Differential Cross-Sections (μb/sr)															
	10°	15°	20°	25°	30°	35°	40°	45°	50°	55°	60°	65°	70°	75°	80°	85°
Ground state		44.9 12.7	72.7 6.9	166.7 11.0	172.2 8.9	156.1 13.2	150.2 17.0	162.5 13.5	148.4 10.0	108.9 10.0	102.7 7.0	89.4 8.1	103.3 9.5	73.0 5.1	86.4 7.7	63.6 7.5
0.207 2	177.2 27.0	145.7 12.7		97.2 9.1	138.5 8.2	100.6 10.8	104.3 10.5	103.5 12.4	85.8 8.1	66.6 11.2	60.5 5.5	44.3 6.0	42.9 6.4	26.2 3.2	32.0 5.4	25.3 2.6
0.288 3	141.0 30.0	107.5 18.3		64.3 7.3	77.8 6.4	88.3 10.8	75.8 9.0	67.5 9.8	59.2 6.5	47.2 9.3	41.2 4.5	34.1 5.5	35.3 5.8	19.0 3.0	17.0 3.5	16.0 1.9
0.394 5	8.2 4.1	16.1 4.0	10.6 3.3	21.4 6.4	8.9 2.8	20.6 5.9	15.5 4.5	5.5 4.0	8.4 3.0	4.8 3.0	4.1 2.0	4.7 2.6	7.6 2.9	1.6 1.0	4.2 2.3	1.9 1.0
0.515 4	40.0 12.5	55.4 13.8	108.7 32.0	64.0 14.0	68.2 6.0	73.1 9.8	74.3 9.0	43.0 7.5	44.9 5.5	38.4 8.3	35.1 4.0	29.8 4.7	28.5 5.5	12.1 2.7	19.7 3.9	9.1 2.6
0.620 4	72.3 20.0	50.9 14.4	51.1 3.3	39.2 8.7	54.3 8.9	49.5 10.3	59.4 10.0	60.0 9.3	37.5 6.4	36.1 10.0	34.1 5.0	34.5 7.3	16.7 4.7	19.1 3.2	20.8 5.0	15.3 1.9
0.670 7		6.6 3.4	15.3 3.3	15.1 7.8		8.3 4.4	15.0 5.5		6.0 3.0	9.7 6.0	8.6 3.0	11.5 5.1	2.9 2.0		3.1 2.0	
0.890 5		16.6 8.9	20.8 2.9	17.3 5.0	39.0 6.7	26.0 15.2	31.9 6.5	13.5 6.2	15.3 4.3	18.5 6.6	13.7 3.5	8.5 3.4	8.4 2.5		6.2 2.7	7.8 2.6
1.045 5		11.6 4.0	6.2 2.2	99.1 3.7	9.2 3.5	3.9 2.0	7.2 2.2	5.0 2.0	7.0 3.0		2.5 1.5	2.3 1.4	2.2 1.0			2.0 1.0
1.197 5		25.0 6.6	11.3 2.9	18.2 5.5	16.0 3.2	22.6 8.0	33.4 6.6	24.0 5.7	14.8 4.2	18.1 7.8	9.1 3.4	8.1 3.4	9.1 3.7	4.7 1.6	9.3 3.5	9.7 2.6

Excitation energy (MeV)	Differential Cross-Sections (μb/sr)															
	10°	15°	20°	25°	30°	35°	40°	45°	50°	55°	60°	65°	70°	75°	80°	85°
1.280 6 } 1.319 7		38.7 7.8	49.9 5.5	28.7 7.8	31.5 6.7	36.3 4.8		40.0 4.5	37.0 13.1	29.0 4.8	22.3 3.0	17.4 4.3	16.0 2.5		12.0 4.1	9.7 4.0
1.429 6		73.0 13.0	113.0 7.3	97.5 15.1	80.1 6.7	101.9 14.3	102.2 10.0	78.4 6.5	54.2 7.0	49.3 5.3	40.6 6.0	39.6 6.8	38.9 5.8	25.2 3.2	24.7 5.4	20.8 3.6
1.490 6		100.7 10.5	57.2 5.8	50.1 11.9	48.6 5.7	51.9 10.8	45.9 10.0	49.9 5.5	39.4 6.0	30.4 4.4	27.9 5.0	20.0 4.7	24.0 4.7	18.0 3.0	15.0 4.6	9.4 2.6
1.578 7		73.0 16.1	102.4 9.4	70.6 19.6	57.4 14.2	72.0 20.1		118.3 7.5	60.1 23.5	38.8 9.3	34.0 10.2	14.9 10.2	40.4 13.8	20.7 4.6	14.3 8.1	19.1 7.5
1.608 7	20.5 8.2	14.4 8.0	43.4 9.1	54.7 16.9	56.0 14.0	66.1 20.1	84.2 28.5		34.5 21.5	24.7 8.8	16.3 9.5	23.0 9.8	20.7 12.7	9.3 3.8	19.7 8.1	
1.703 7	62.1 16.0	63.0 9.4	63.4 6.2	74.7 16.4	75.7 7.8	91.6 13.2	70.8 8.0	61.4 6.5	62.5 7.0	56.4 5.7	49.8 6.5	33.6 8.5	45.4 6.2	16.9 3.2	20.8 5.0	22.0 3.6

TABLE 6

Q-Values for $^{94,96,98,100}Mo(^{3}He,d)^{95,97,99,101}Tc$ Reactions

(Energies in MeV)

REACTION	Maples et al. (1966)	Wapstra and Gove (1971)	Present Work
$^{94}Mo(^{3}He,d)^{95}Tc$	-0.561 ± 0.021	-0.602 ± 0.011	-0.55 ± 0.02
$^{96}Mo(^{3}He,d)^{97}Tc$	0.241 ± 1.000	0.194 ± 0.009	0.25 ± 0.02
$^{98}Mo(^{3}He,d)^{99}Tc$	1.013 ± 0.006	1.012 ± 0.005	1.01 ± 0.02
$^{100}Mo(^{3}He,d)^{101}Tc$	1.934 ± 0.025	1.935 ± 0.025	1.93 ± 0.02

TABLE 7

Optical Potential and Bound State Potential Parameters Used in the (^{3}He,d) Reaction Analysis

PARTICLE	r_c (fm)	V (MeV)	r_r (fm)	a_r (fm)	W_V (MeV)	W_D (MeV)	r_i [b] (fm)	a_i [b] (fm)	λ_{so}
He-3	1.4	170	1.14	0.75	20		1.6	0.8	
Deuteron	1.3	98	1.1	0.85		18	1.4	0.7	
Proton [a]	1.2	V	1.2	0.65					25

a) The V was adjusted to reproduce the proton separation energy for each final state, and $r_{so}=r_r$, $a_{so}=a_r$.

b) $r_i = r_V$ or r_D and $a_x = a_V$ or a_D.

FIGURE 14

DWBA Predictions for the Angular Distributions of the (^{3}He,d) Reaction for Different ℓ-Transfer Values.

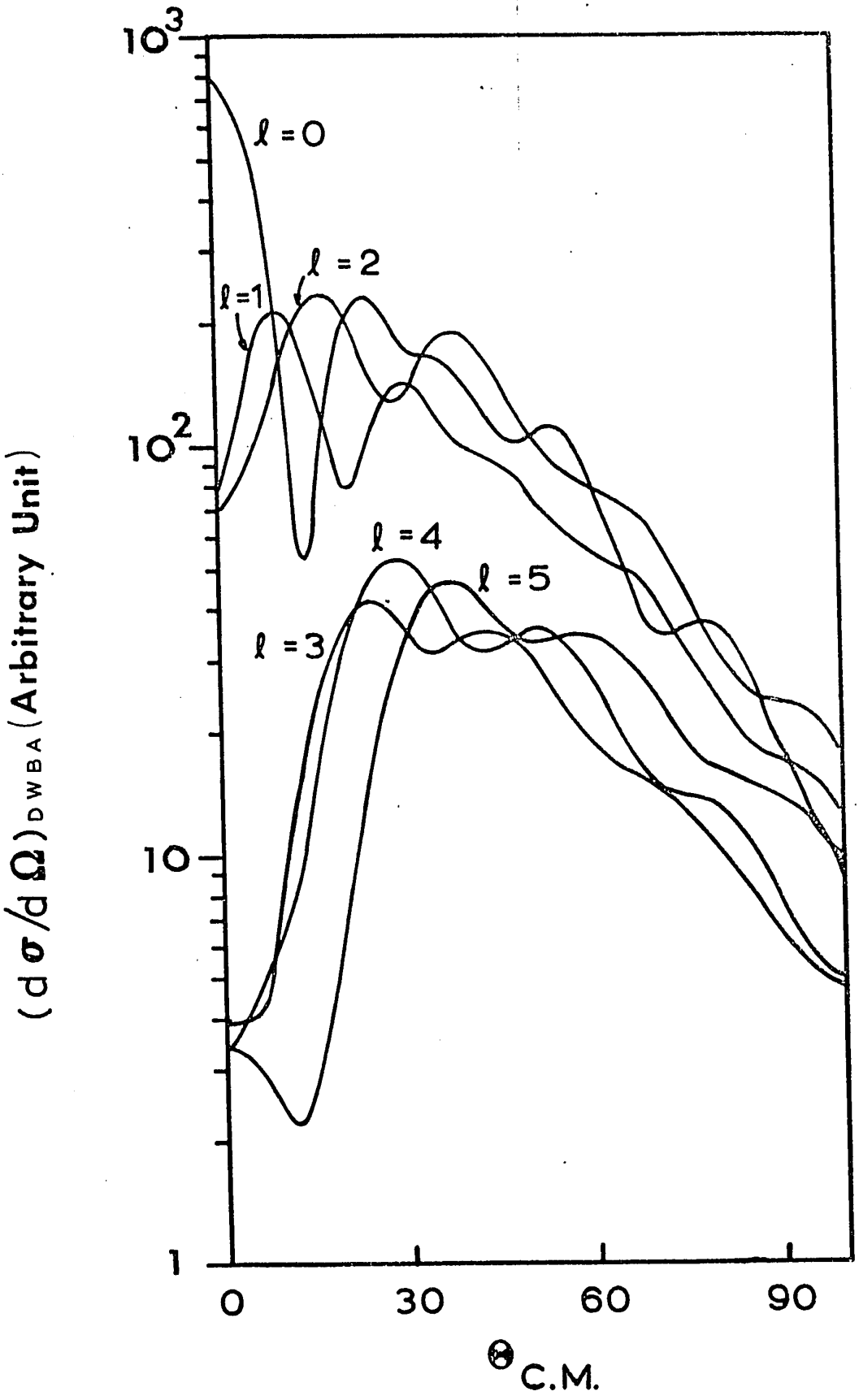
10^3
10^2
10
1
$\ell = 0$
$\ell = 1$
$\ell = 2$
$\ell = 3$
$\ell = 4$
$\ell = 5$
$(d\sigma/d\Omega)_{DWBA}$ (Arbitrary Unit)
0
30
60
90
$\Theta_{C.M.}$

FIGURE 15

DWBA Analysis of Angular Distributions of the $^{94}Mo(^{3}He,d)$ ^{95}Tc Reaction

Experimental numerical values are given in table 2. Angular distributions are identified by the excitation energies of the corresponding states in ^{95}Tc.

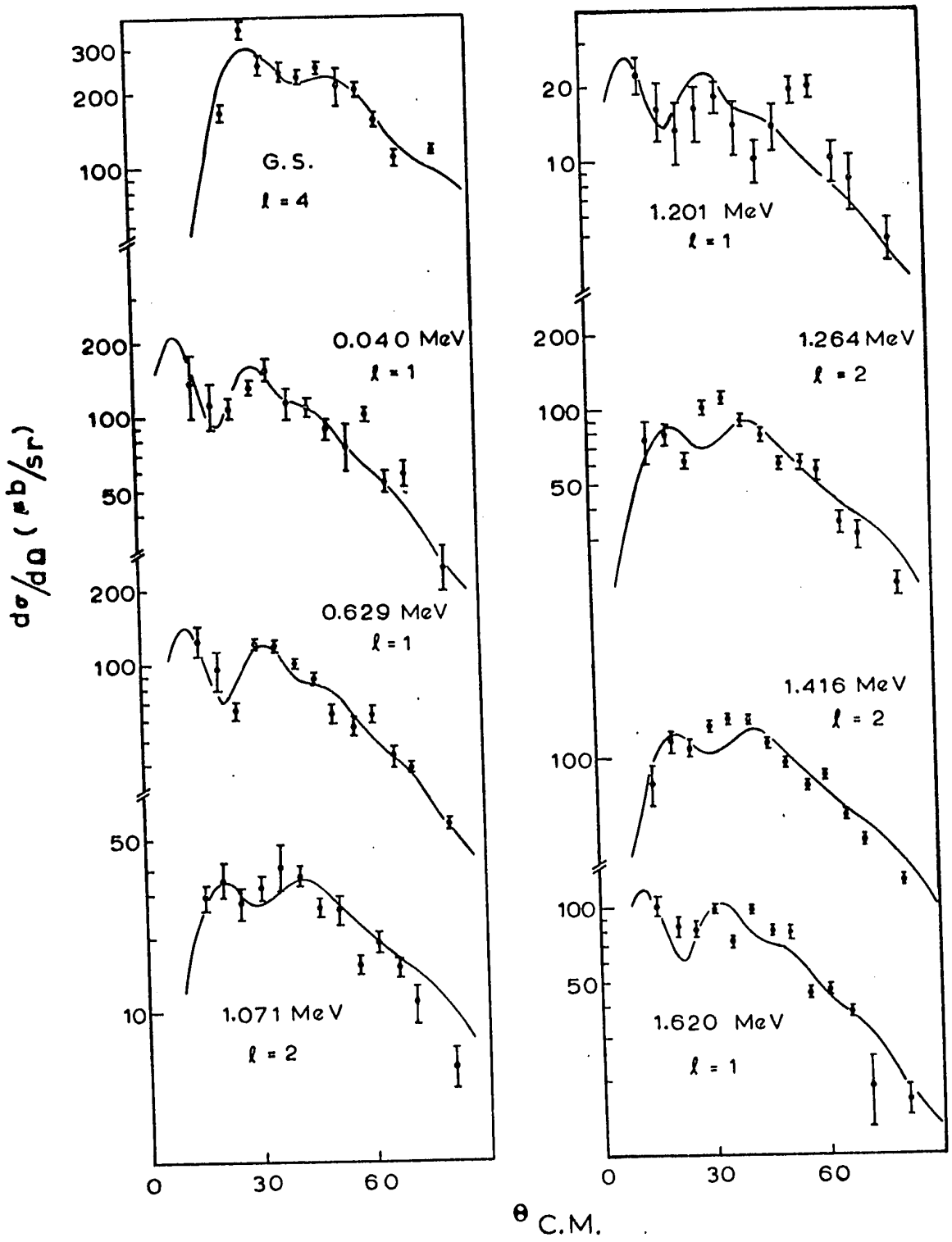
G.S.
ℓ = 4
0.040 MeV
ℓ = 1
0.629 MeV
ℓ = 1
1.071 MeV
ℓ = 2
1.201 MeV
ℓ = 1
1.264 MeV
ℓ = 2
1.416 MeV
ℓ = 2
1.620 MeV
ℓ = 1
dσ/dΩ (μb/sr)
θ C.M.
0
30
60

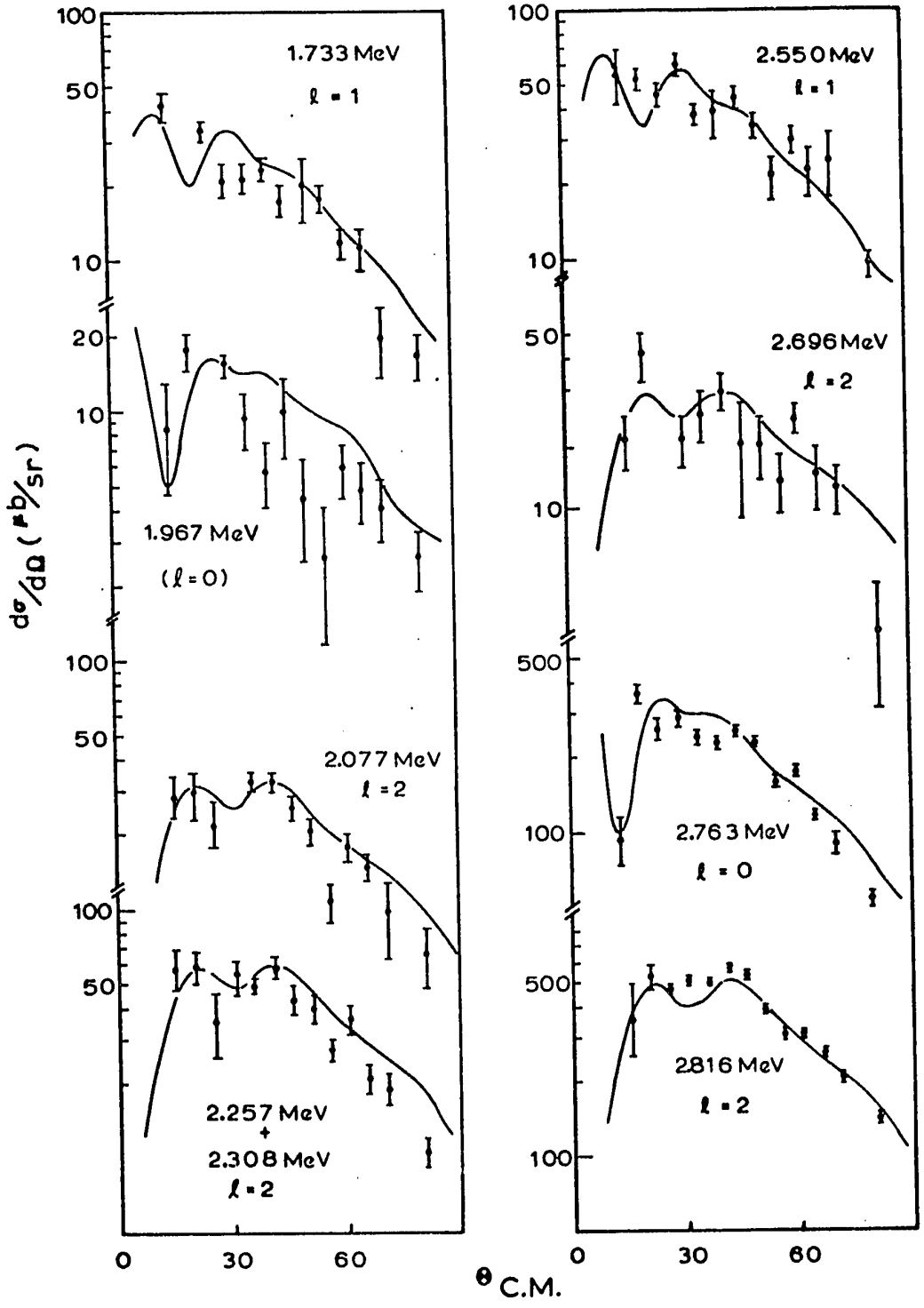
1.733 MeV
ℓ = 1
1.967 MeV
(ℓ = 0)
2.077 MeV
ℓ = 2
2.257 MeV
+
2.308 MeV
ℓ = 2
2.550 MeV
ℓ = 1
2.696 MeV
ℓ = 2
2.763 MeV
ℓ = 0
2.816 MeV
ℓ = 2
dσ/dΩ (μb/sr)
θ C.M.
0
30
60
100
50
20
10
500

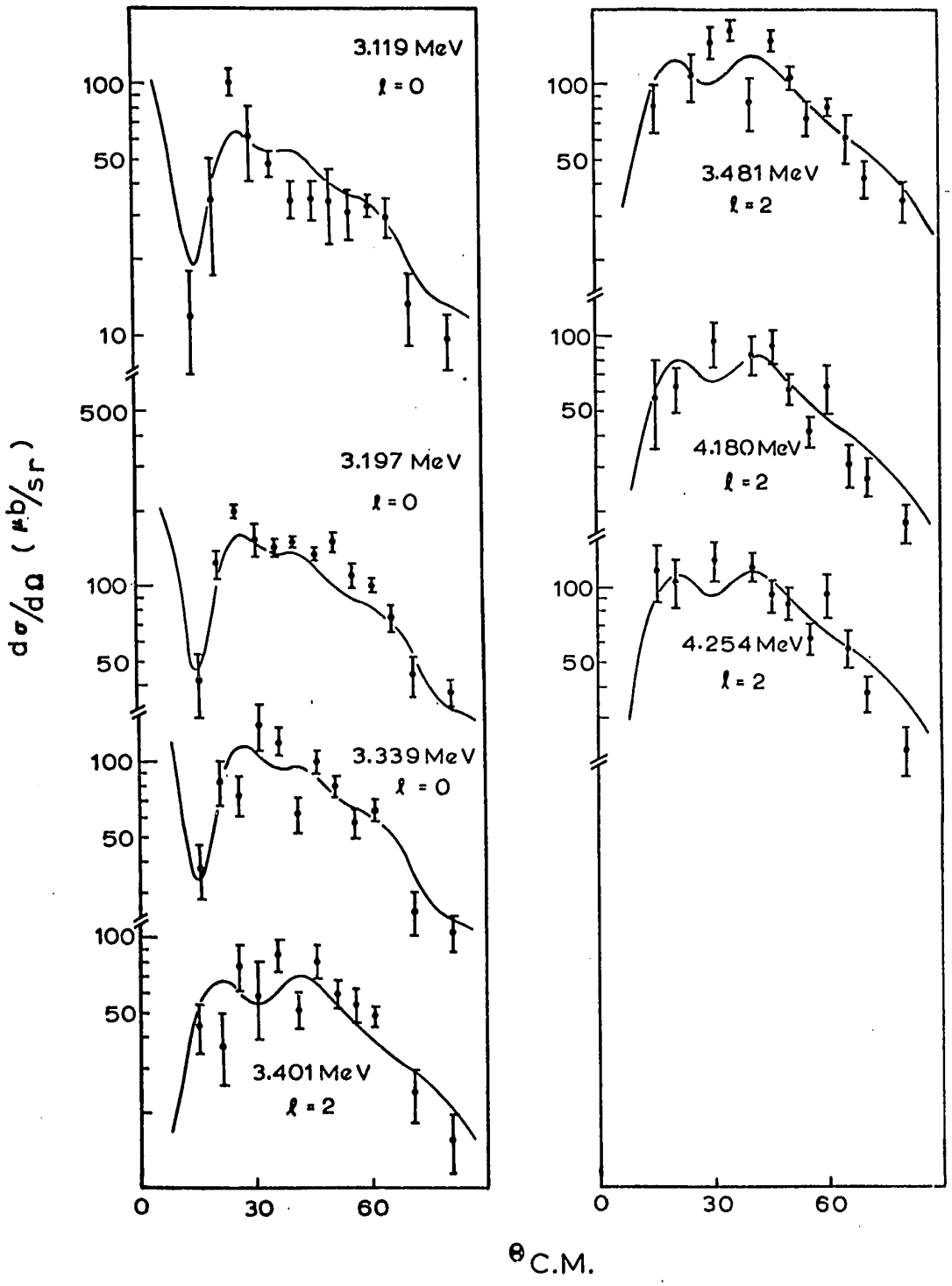
3.119 MeV
ℓ = 0
3.197 MeV
ℓ = 0
3.339 MeV
ℓ = 0
3.401 MeV
ℓ = 2
3.481 MeV
ℓ = 2
4.180 MeV
ℓ = 2
4.254 MeV
ℓ = 2
100
50
10
500
0
30
60
dσ/dΩ (μb/sr)
θ C.M.

FIGURE 16

DWBA Analysis of Angular Distributions of the $^{96}Mo(^{3}He,d)$ ^{97}Tc Reaction

Experimental numberical values are given in table 3. Angular distributions are identified by the excitation energies of the corresponding states in ^{97}Tc.

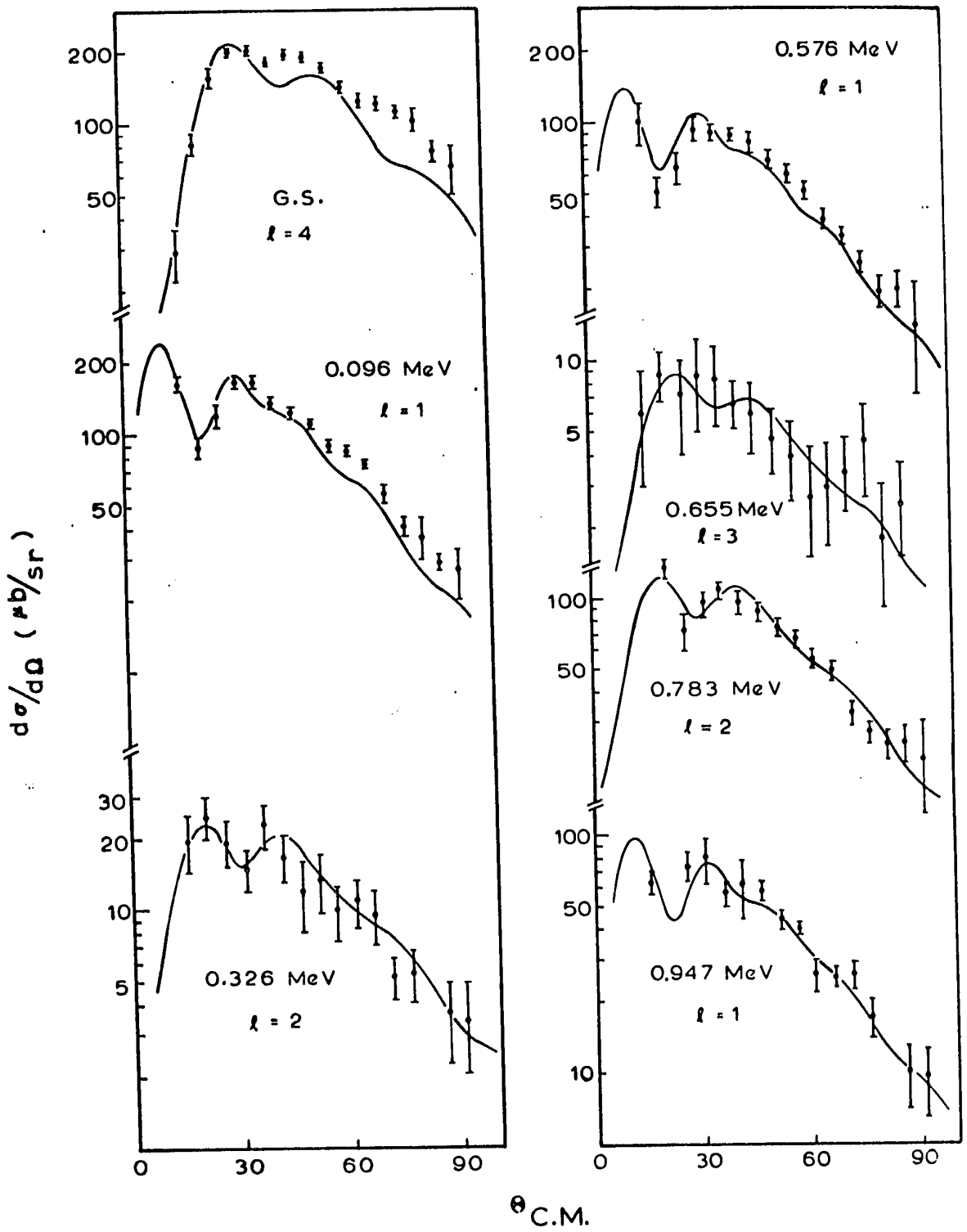
G.S.
ℓ = 4
0.096 MeV
ℓ = 1
0.326 MeV
ℓ = 2
0.576 MeV
ℓ = 1
0.655 MeV
ℓ = 3
0.783 MeV
ℓ = 2
0.947 MeV
ℓ = 1
dσ/dΩ (μb/sr)
θ C.M.
0
30
60
90

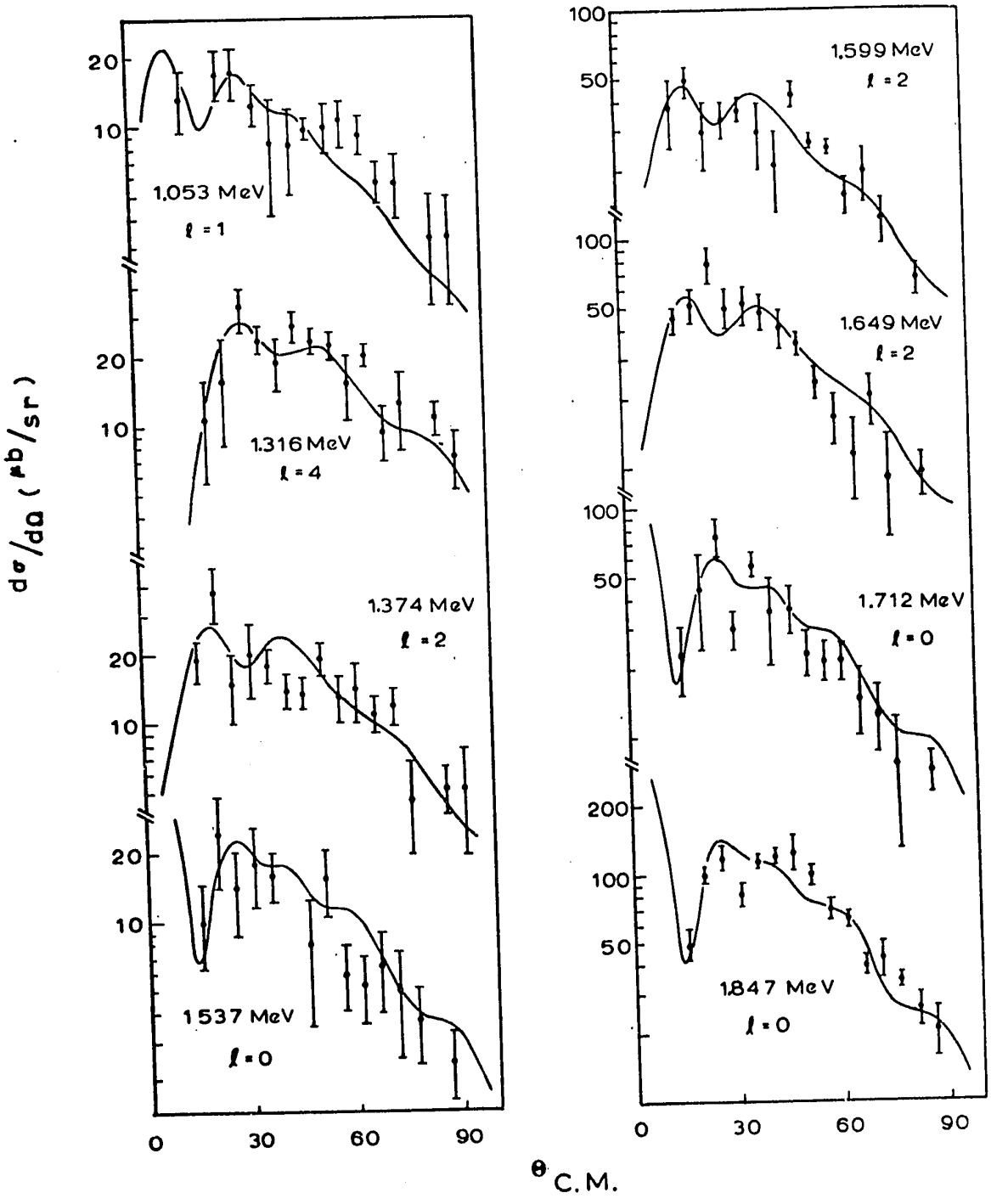
dσ/dΩ (μb/sr)
1.053 MeV
ℓ = 1
1.316 MeV
ℓ = 4
1.374 MeV
ℓ = 2
1.537 MeV
ℓ = 0
1.599 MeV
ℓ = 2
1.649 MeV
ℓ = 2
1.712 MeV
ℓ = 0
1.847 MeV
ℓ = 0
θ C.M.

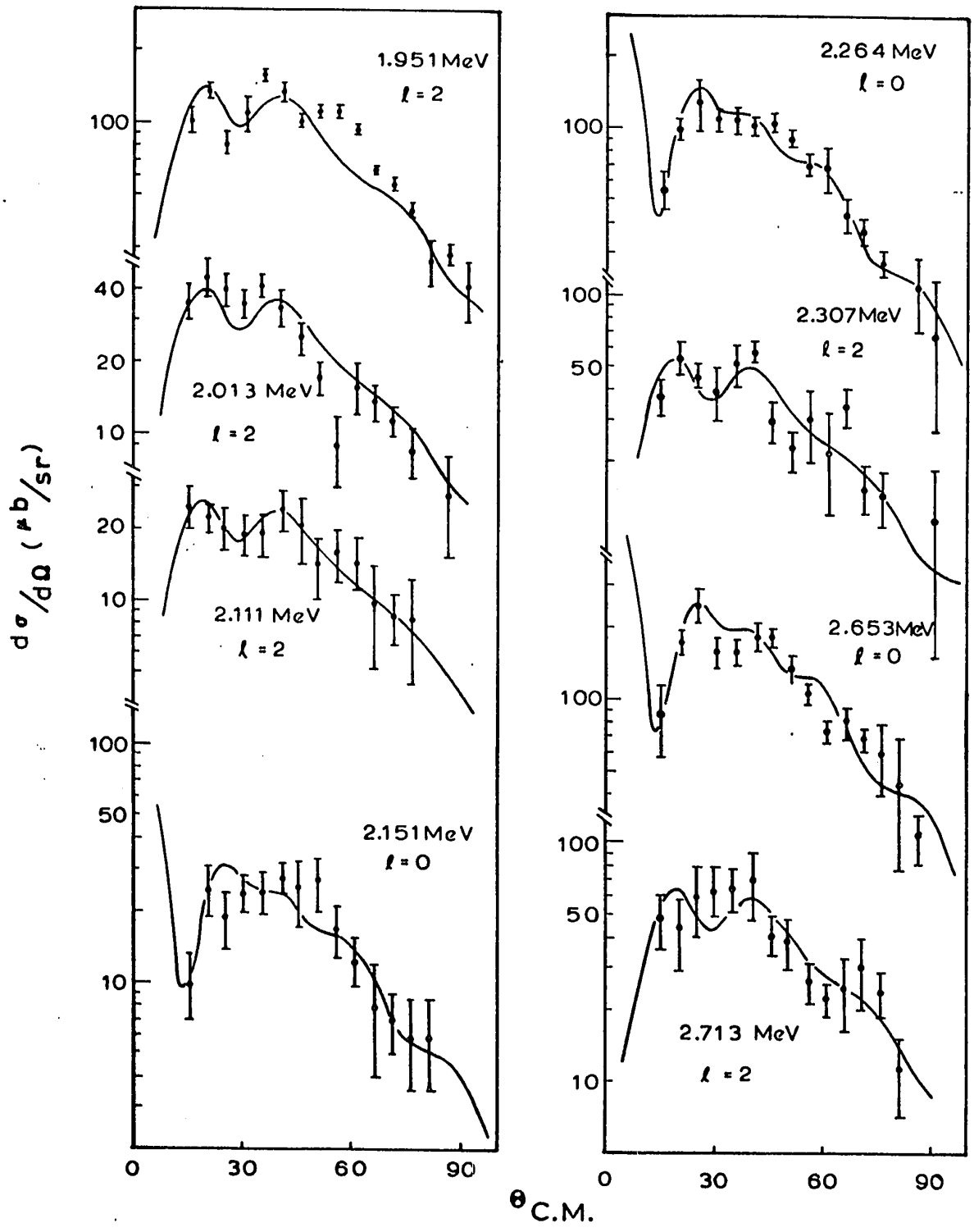
1.951 MeV
ℓ = 2
2.013 MeV
ℓ = 2
2.111 MeV
ℓ = 2
2.151 MeV
ℓ = 0
2.264 MeV
ℓ = 0
2.307 MeV
ℓ = 2
2.653 MeV
ℓ = 0
2.713 MeV
ℓ = 2
dσ/dΩ (μb/sr)
θ C.M.
0
30
60
90
100
40
20
10
50

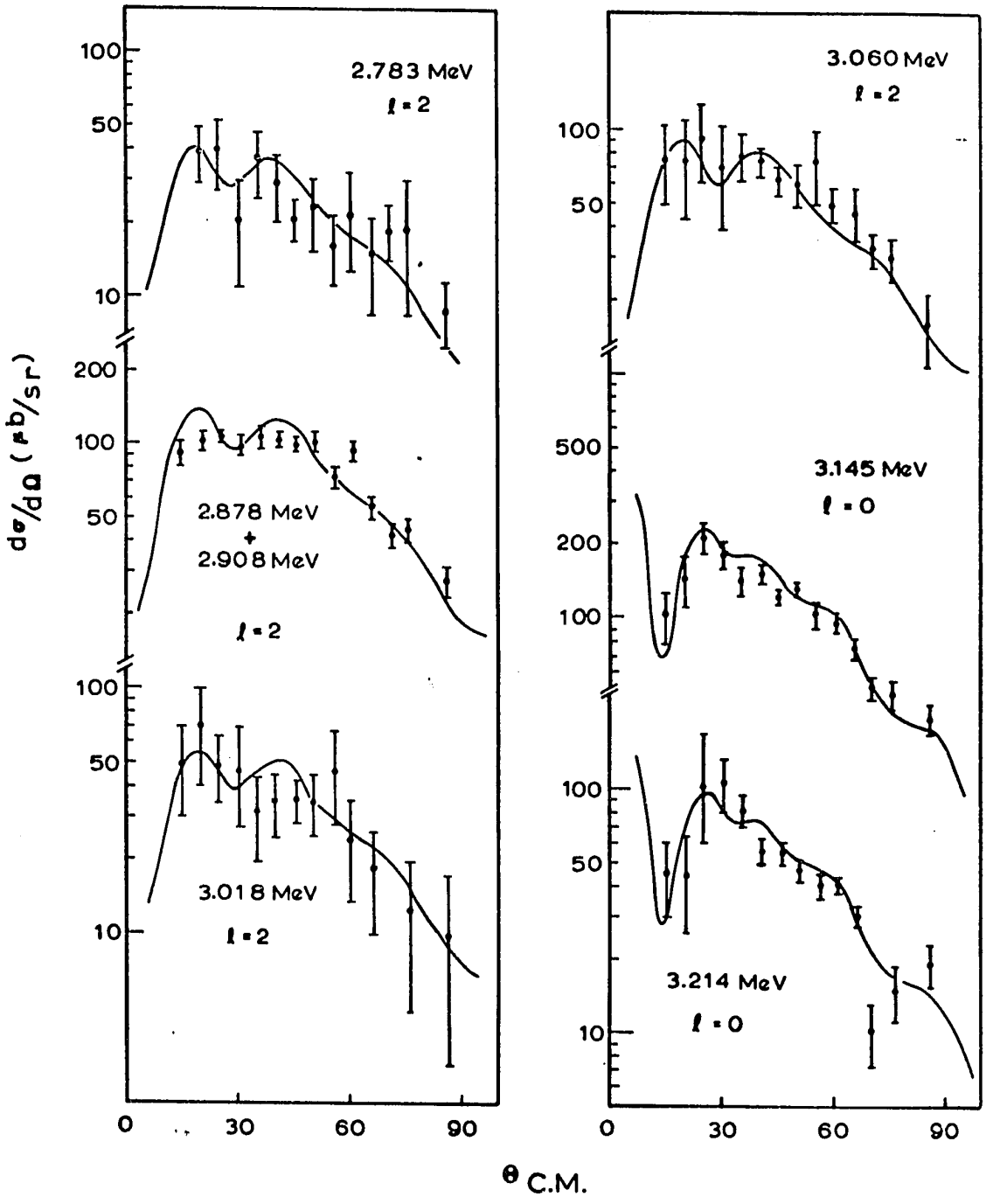
2.783 MeV
l = 2
2.878 MeV
+
2.908 MeV
l = 2
3.018 MeV
l = 2
3.060 MeV
l = 2
3.145 MeV
l = 0
3.214 MeV
l = 0
dσ/dΩ (μb/sr)
θ C.M.
0
30
60
90
10
50
100
200
500

FIGURE 17

DWBA Analysis of Angular Distributions of the ^{98}Mo $(^{3}He,d)^{99}Tc$ Reaction

Experimental numerical values are given in table 4. Angular distributions are identified by the excitation energies of the corresponding states in ^{99}Tc.

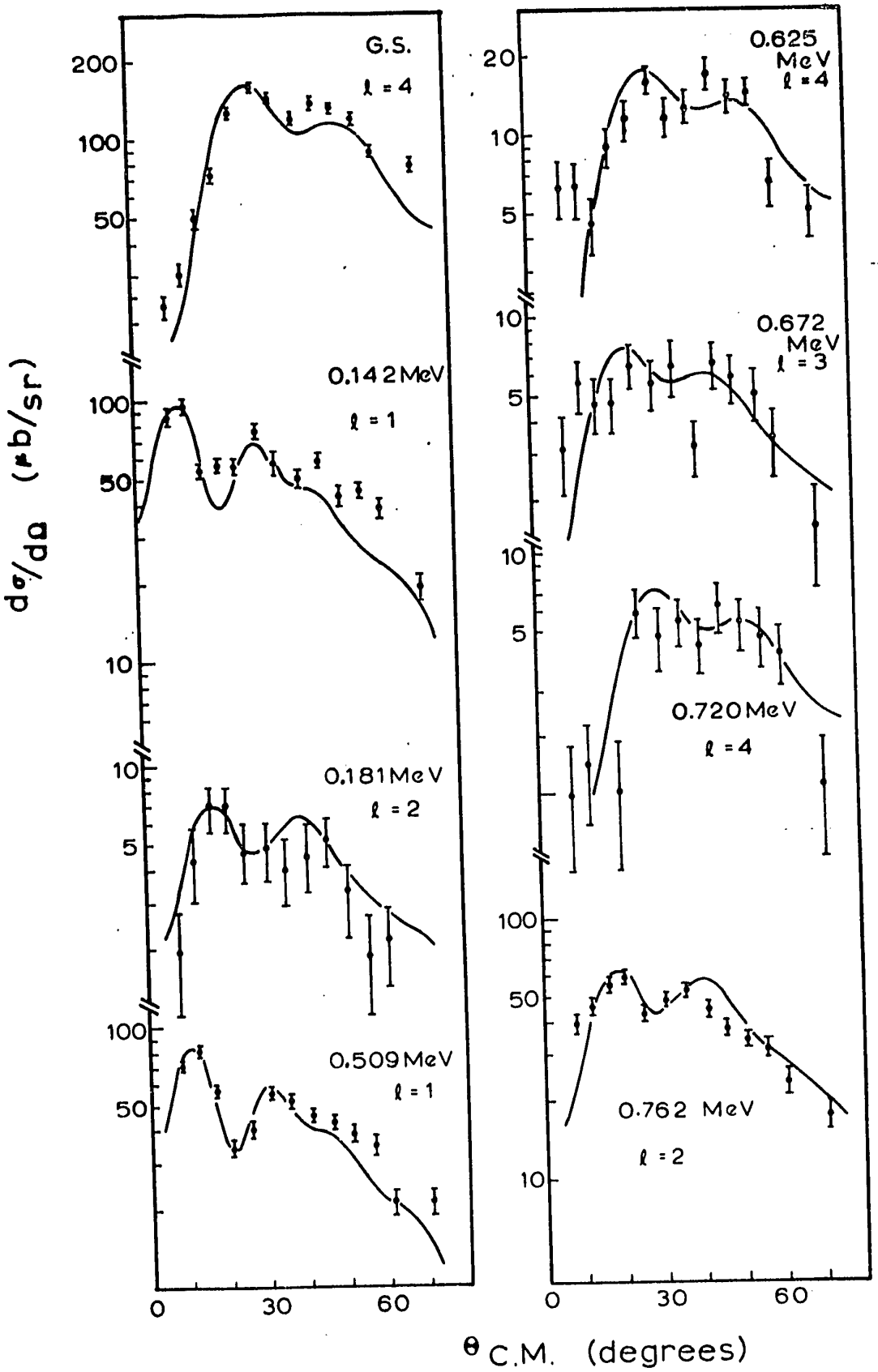
G.S.
ℓ = 4
0.142 MeV
ℓ = 1
0.181 MeV
ℓ = 2
0.509 MeV
ℓ = 1
0.625 MeV
ℓ = 4
0.672 MeV
ℓ = 3
0.720 MeV
ℓ = 4
0.762 MeV
ℓ = 2
dσ/dΩ (μb/sr)
θ C.M. (degrees)
0
30
60

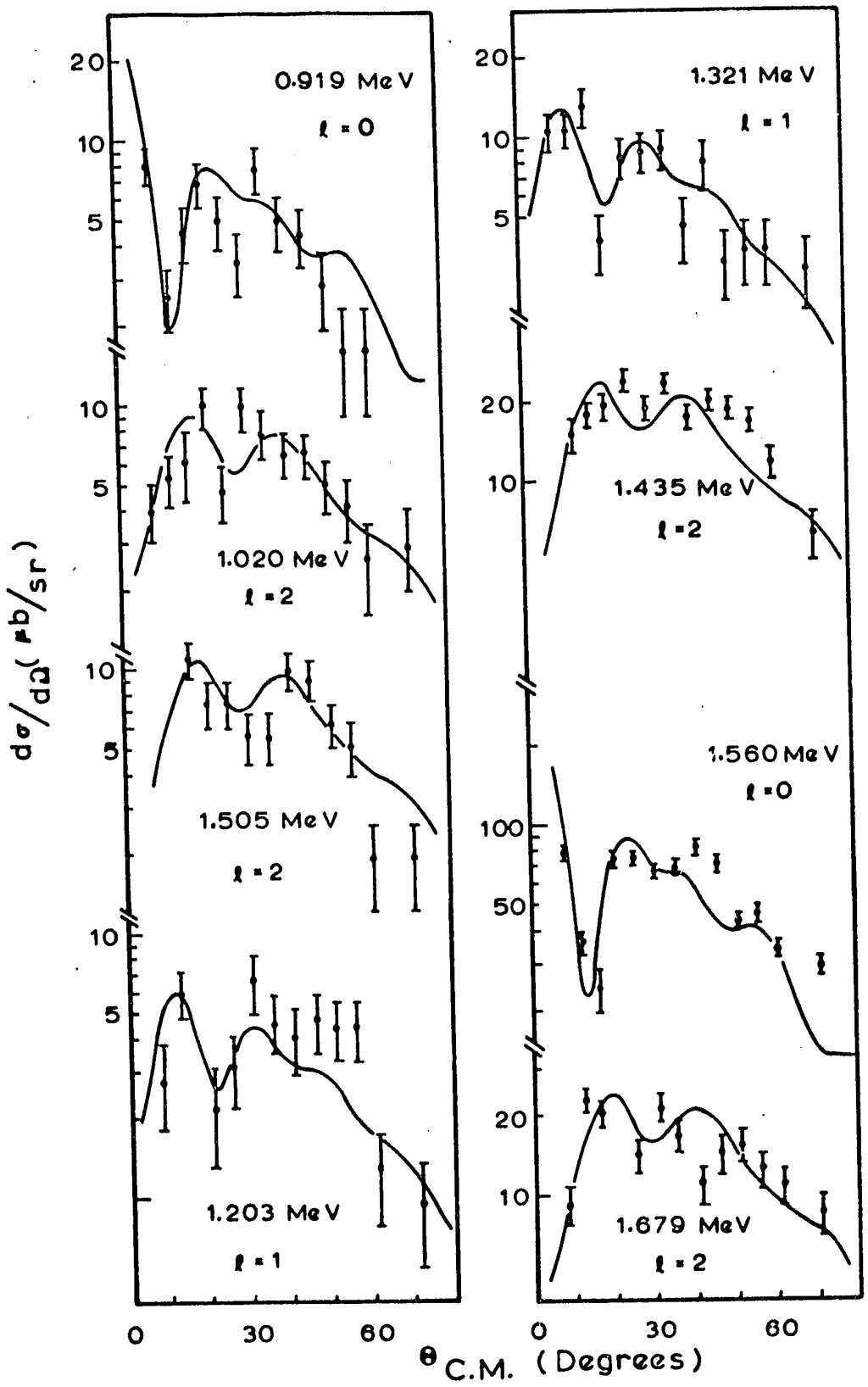
0.919 MeV
ℓ = 0
1.020 MeV
ℓ = 2
1.505 MeV
ℓ = 2
1.203 MeV
ℓ = 1
1.321 MeV
ℓ = 1
1.435 MeV
ℓ = 2
1.560 MeV
ℓ = 0
1.679 MeV
ℓ = 2
dσ/dΩ (μb/sr)
θ C.M. (Degrees)
0
30
60

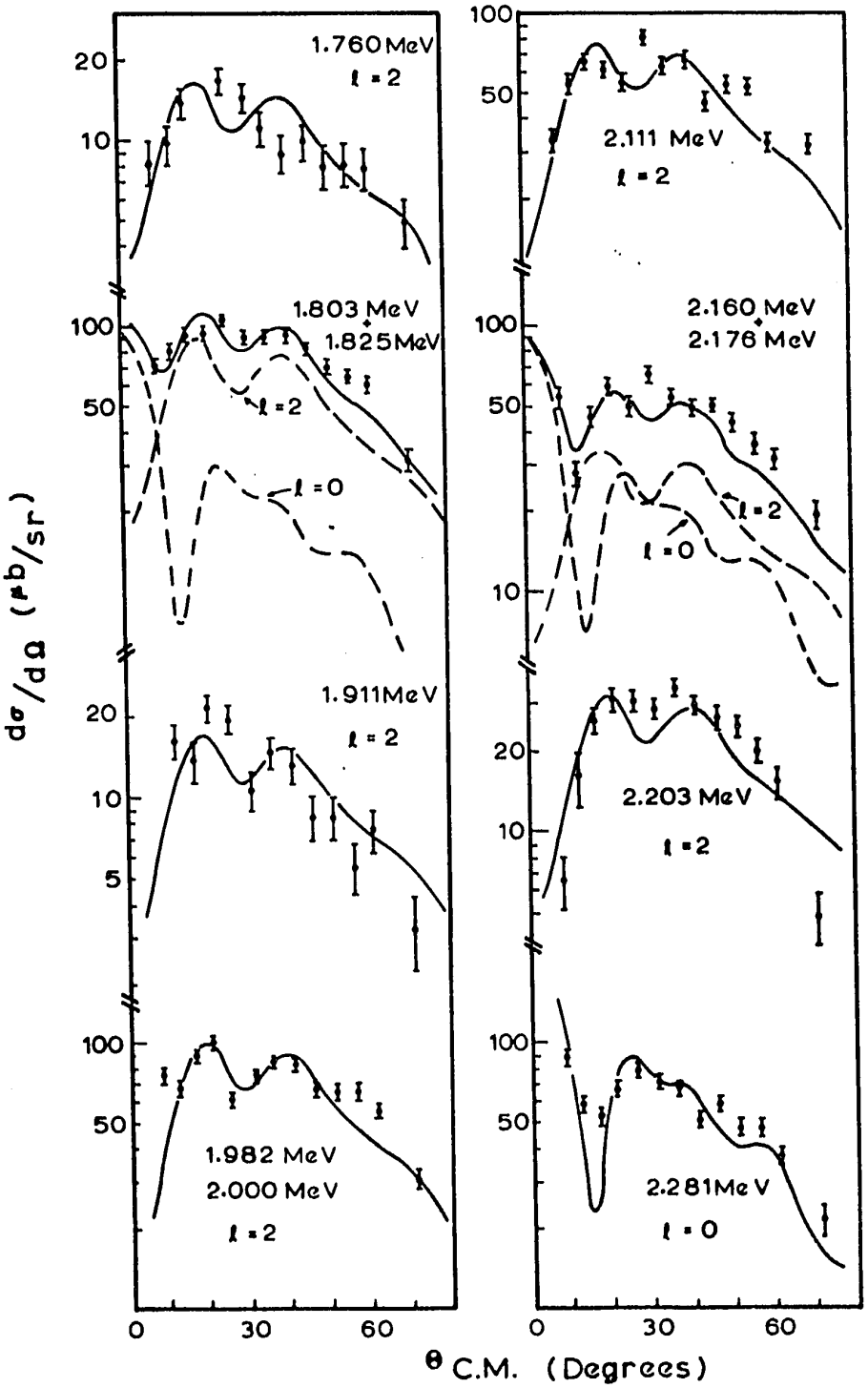
1.760 MeV
ℓ = 2
1.803 MeV
1.825 MeV
ℓ = 2
ℓ = 0
1.911 MeV
ℓ = 2
1.982 MeV
2.000 MeV
ℓ = 2
2.111 MeV
ℓ = 2
2.160 MeV
2.176 MeV
ℓ = 2
ℓ = 0
2.203 MeV
ℓ = 2
2.281 MeV
ℓ = 0
dσ/dΩ (μb/sr)
θ C.M. (Degrees)

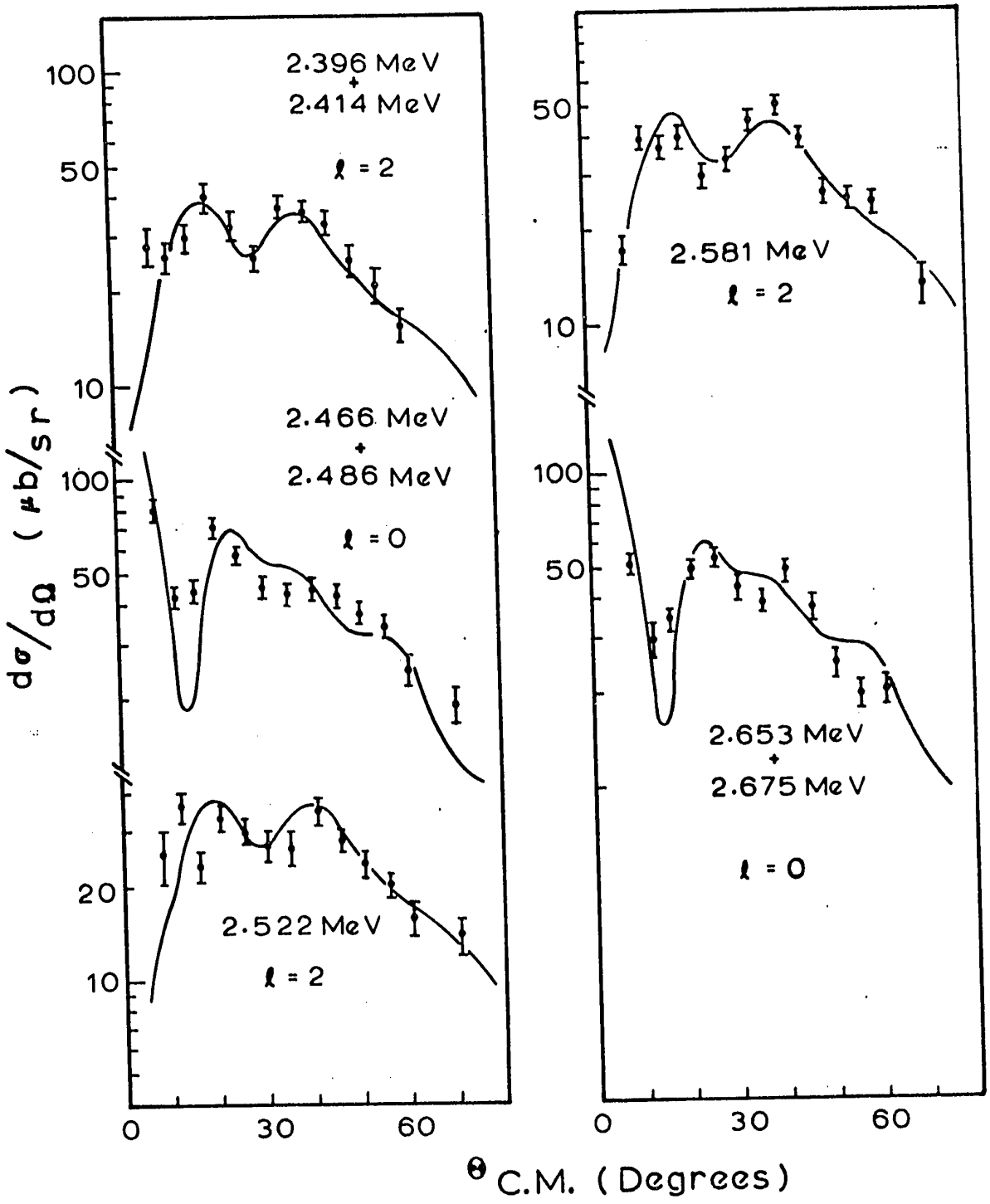
2.396 MeV
+
2.414 MeV
ℓ = 2
2.466 MeV
+
2.486 MeV
ℓ = 0
2.522 MeV
ℓ = 2
2.581 MeV
ℓ = 2
2.653 MeV
+
2.675 MeV
ℓ = 0
dσ/dΩ (μb/sr)
θ C.M. (Degrees)
100
50
10
20
0
30
60

FIGURE 18

DWBA Analysis of Angular Distributions of the ^{100}Mo $(^{3}He,d)^{101}Tc$ Reaction

Experimental numerical values are given in table 5. Angular distributions are identified by the excitation energies of the corresponding states in ^{101}Tc.

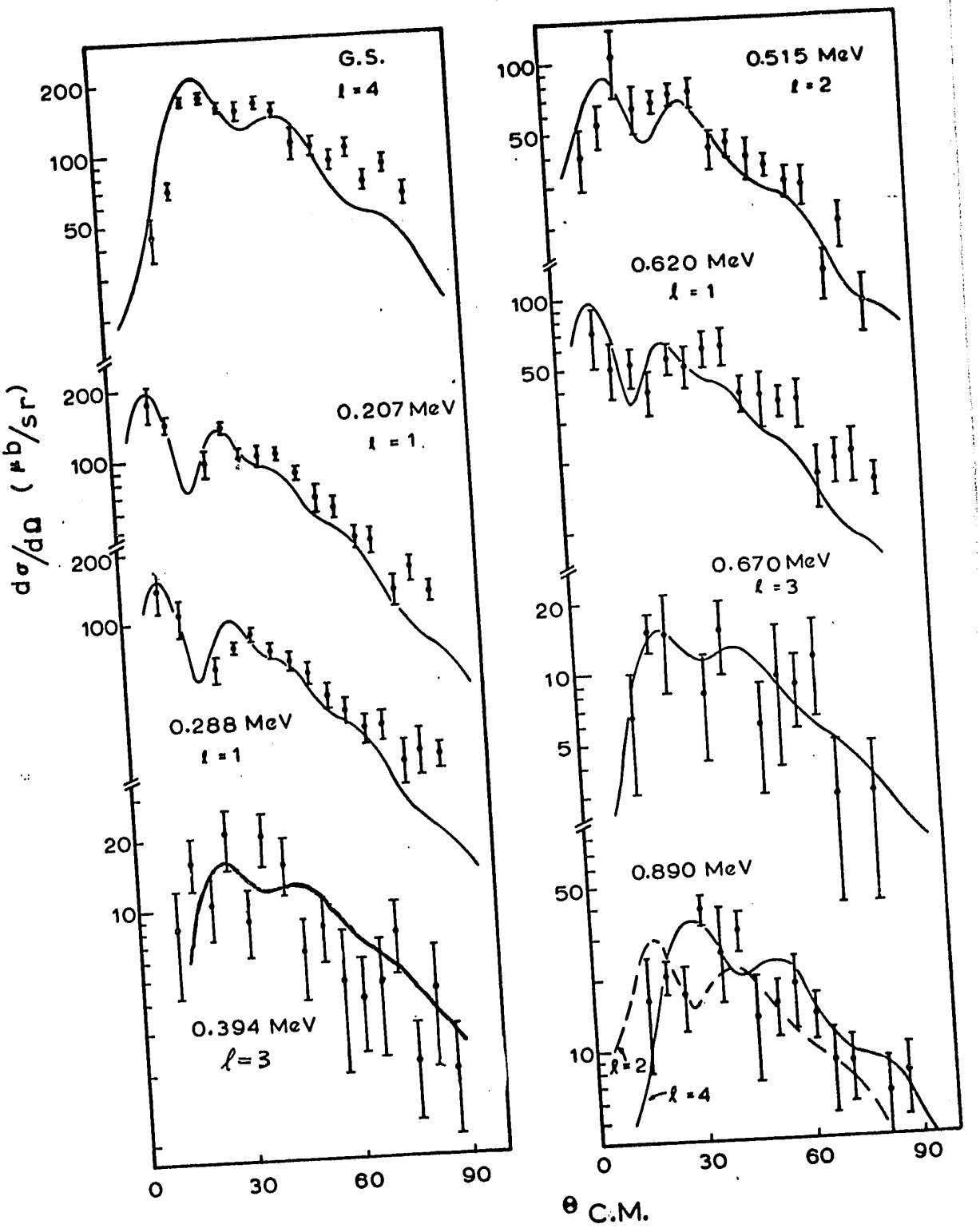
G.S.
l = 4
0.207 MeV
l = 1
0.288 MeV
l = 1
0.394 MeV
l = 3
0.515 MeV
l = 2
0.620 MeV
l = 1
0.670 MeV
l = 3
0.890 MeV
l = 2
l = 4
dσ/dΩ (μb/sr)
θ C.M.
0
30
60
90

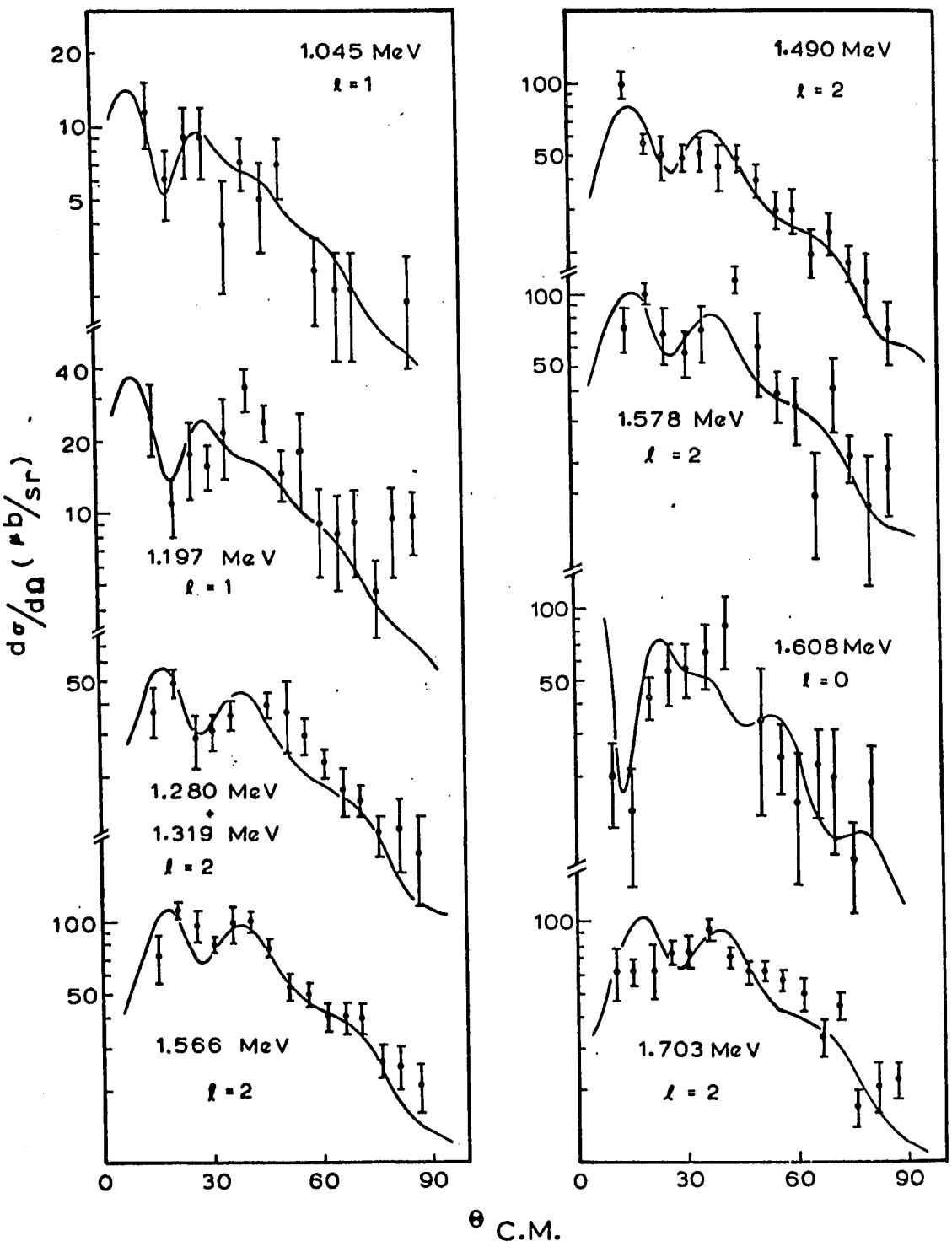
1.045 MeV
ℓ = 1
1.490 MeV
ℓ = 2
1.578 MeV
ℓ = 2
1.197 MeV
ℓ = 1
1.608 MeV
ℓ = 0
1.280 MeV
+
1.319 MeV
ℓ = 2
1.566 MeV
ℓ = 2
1.703 MeV
ℓ = 2
dσ/dΩ (μb/sr)
θ C.M.
0
30
60
90

TABLE 8

Summary of Spectroscopic Properties of the Low-Lying States of ^{95}Tc from the Present Work and Previous Measurements

Present Work $^{94}Mo(^3He,d)^{95}Tc$					Riley et al. (1971) $^{94}Mo(d,n)^{95}Tc$				Bonner et al. (1971) $^{94}Mo(d,n)^{95}Tc$				Tucker et al. (1970) β-γ		Kim et al. (1970) (1971) $^{95}Mo(p,n)^{95}Tc$	
Ex (MeV)	ℓ	J^π	C^2S	C^2S (Norm.)	Ex (MeV)	ℓ	J^π	C^2S	Ex (MeV)	ℓ	J^π	C^2S	Ex (MeV)	J^π	Ex (MeV)	J^π
0.	4	$9/2^+$	0.824	0.683	0.	4	$9/2^+$	0.77	0.	4	$9/2^+$	0.49	0.	$9/2^+$	0.	
0.040	1	$1/2^-$	0.324	0.269	0.04	1	$1/2^-$	0.32	0.04	1	$1/2^-$	0.35	0.0389	$1/2^-$	0.046	
													0.3364	$7/2^+$	0.34	
0.629	1	$3/2^-$	0.087	0.072	0.64	1	$3/2^-$	0.11	0.648	2	$5/2^+$	0.02	0.6268	$(5/2^+)$	0.631	$3/2^-$
		$1/2^-$	0.200	0.166			$1/2^-$	0.24							0.651	$5/2^-$
															0.67	
													0.9278	$(5/2^-,3/2^+)$	0.932	
													0.9901	$(7/2^+,5/2^+)$	0.960	
									0.98	-			1.0494	$(3/2^+)$	1.087	
1.071	2	$5/2^+$	0.021	0.017	1.10	2	$5/2^+$	0.003					1.1786	$(7/2^+,5/2^+)$	1.178	
		$3/2^+$	0.041	0.034											1.213	
1.201	1	$3/2^-$	0.014	0.012											1.281	
		$1/2^-$	0.032	0.027											1.332	
1.264	2	$5/2^+$	0.049	0.041	1.27	4	$9/2^+$	0.054	1.30	-						
		$3/2^+$	0.097	0.080		1	$3/2^-$	0.040								
							$1/2^-$	0.080								
1.416	2	$5/2^+$	0.072	0.060	1.45	2	$5/2^+$	0.028	1.45	2	$5/2^+$	0.03	1.4332	$(5/2^+,7/2^+)$	1.415	
		$3/2^+$	0.134	0.111											1.435	
1.620	1	$3/2^-$	0.055	0.046	1.63	0	$1/2^+$	0.011	1.66	0	$1/2^+$	0.02	1.6763	$(5/2^+,7/2^+)$	1.618	
		$1/2^-$	0.127	0.105		1	$3/2^-$	0.011					1.6913	$(5/2^+,7/2^+)$	1.636	
							$1/2^-$	0.023								
1.733	1	$3/2^-$	0.017	0.014	1.75	1	$3/2^-$	0.018					1.7470	$(5/2^+,7/2^+)$		
		$1/2^-$	0.032	0.032			$1/2^-$	0.035					1.7852	$(5/2^+,7/2^+)$		
1.967	(0)	$(1/2^+)$	(0.009)	(0.007)					1.93	0	$1/2^+$	0.02	1.9785	$(5/2^+,7/2^+)$		
2.077	2	$5/2^+$	0.015	0.012									2.0860	$(3/2^+)$		
		$3/2^+$	0.029	0.024												
2.257	2	$5/2^+$	0.019	0.016									2.2519	$(7/2^+,5/2^+)$		
		$3/2^+$	0.038	0.032												
2.308	2	$5/2^+$	0.007	0.006	2.29	2	$5/2^+$	0.019					2.3245	$(7/2^+,5/2^+)$		
		$3/2^+$	0.013	0.011												
2.454	weak															
2.550	1	$3/2^-$	0.022	0.018	2.57	1	$3/2^-$	0.036	2.56	0	$1/2^+$	0.01				
		$1/2^-$	0.050	0.041			$1/2^-$	0.081								
2.696	2	$5/2^+$	0.011	0.009												
		$3/2^+$	0.022	0.018					2.78	0	$1/2^+$	0.04				
2.763	0	$1/2^+$	0.107	0.089												
2.816	2	$5/2^+$	0.184	0.153	2.83	2	$5/2^+$	0.21	2.83	2	$5/2^+$	0.13				
		$3/2^+$	0.375	0.311							$3/2^+$	0.22				
2.938	(0)	$(1/2^+)$	(0.027)	(0.022)												
3.001	(2)	$(5/2^+)$	(0.022)	(0.018)												
		$(3/2^+)$	(0.045)	(0.037)												
3.119	0	$1/2^+$	0.024	0.020	3.21	0	$1/2^+$	0.016								
3.197	0	$1/2^+$	0.058	0.048												
3.339	0	$1/2^+$	0.041	0.034												
3.401	2	$5/2^+$	0.020	0.017												
		$3/2^+$	0.042	0.035												
3.481	2	$5/2^+$	0.036	0.030												
		$3/2^+$	0.077	0.064												
3.616	(2)	$(5/2^+)$	(0.050)	(0.041)	3.63	2	$5/2^+$	0.021	3.65	2	$5/2^+$	0.04				
		$(3/2^+)$	(0.105)	(0.086)							$3/2^+$	0.06				
3.700	weak								3.81	0	$1/2^+$	0.02				
3.800	(0)	$(1/2^+)$	(0.069)	(0.057)	3.81	0	$1/2^+$	0.029								
3.905	(0)	$(1/2^+)$	(0.042)	(0.035)	3.92	0	$1/2^+$	0.006								
3.986	(2)	$(5/2^+)$	(0.045)	(0.037)	3.99	2	$5/2^+$	0.009								
		$(3/2^+)$	(0.093)	(0.077)			$3/2^+$	0.015								
4.110	(0)	$(1/2^+)$	(0.020)	(0.017)					4.04	0	$1/2^+$	0.04				
4.180	2	$5/2^+$	0.020	0.017												
		$3/2^+$	0.040	0.033												
4.254	2	$5/2^+$	0.027	0.022												
		$3/2^+$	0.055	0.046												

TABLE 9

Summary of Spectroscopic Properties of the Low-Lying States of ^{97}Tc from the Present Work and Previous Measurements

Present Work $^{96}Mo(^3He,d)^{97}Tc$					Riley et al. (1971) $^{96}Mo(d,n)^{97}Tc$				Kim et al. (1970) $^{97}Mo(p,n)^{97}Tc$		Phelps et al. (1971) β-γ		Cook et al. (1970) β-γ		Picone et al. (1972) $^{97}Mo(p,n\gamma)^{97}Tc$	
Ex (MeV)	ℓ	J^π	C^2S	C^2S (Norm.)	Ex (MeV)	ℓ	J^π	C^2S	Ex (MeV)	J^π	Ex (MeV)	J^π	Ex (MeV)	J^π	Ex (MeV)	J^π
0.	4	$9/2^+$	0.691	0.626	0.	4	$9/2^+$	0.415	0.		0.	$9/2^+$	0.	$9/2^+$	0.0	$(9/2)^+$
0.096	1	$1/2^-$	0.471	0.426	0.097	1	$1/2^-$	0.231	0.101		0.0965	$1/2^-$	0.0964	$1/2^-$	0.0965	$(1/2)^-$
0.216	(4)	$(7/2^+)$	(0.051)	(0.046)					0.213		0.21571	$7/2^+$	0.2158	$(7/2^+)$	0.216	$(7/2)^+$
0.326	2	$5/2^-$	0.018	0.016					0.328		0.32449	$5/2^+$	0.3244	$(5/2^+)$	0.324	$(5/2)^+$
0.576	1	$3/2^-$	0.105	0.095	0.57	1	$3/2^-$	0.056	0.575	$3/2^-$	0.5742	$(3/2^-)$			0.574	$(3/2)^-$
		$1/2^-$	0.259	0.234			$1/2^-$	0.138								
0.655	3	$5/2^+$	0.040	0.036					0.662	$5/2^-$	0.65682	$(5/2^-)$	(0.6567)	-	0.657	$(5/2)^-$
0.783	2	$5/2^+$	0.085	0.077	0.77	2	$5/2^+$	0.017	0.785		0.78505	$5/2^+$	0.7851	$(5/2^-,7/2^-)$	0.785	$(5/2)^+$
		$3/2^+$	0.164	0.148											0.807	
0.852	(2)	$(5/2^-)$	(0.008)	(0.007)					0.854		0.85545	$(7/2,5/2)^+$	0.8554	$(7/2^-)$	(0.833)	
		$(3/2^-)$	(0.016)	(0.014)											(0.850)	
0.947	1	$3/2^-$	0.066	0.060	0.93	1	$3/2^-$	0.031	0.941		0.9465	-			0.855	$(7/2,5/2)^+$
		$1/2^-$	0.167	0.151					0.962		0.96979	$(5/2,7/2)^+$	0.9697	-	0.896	
1.053	1	$3/2^-$	0.015	0.014					0.987		0.99469	$3/2^+$	0.9944	-	0.940	$(3/2,1/2)^-$
		$1/2^-$	0.037	0.033					1.050						0.969	$(5/2,7/2)^+$
1.316	4	$9/2^+$	0.075	0.068	1.32	4	$9/2^+$	0.031	1.134						0.994	$(3/2)^+$
		$7/2^+$	0.195	0.177		2	$5/2^+$	0.005	1.202						1.049	
1.374	2	$5/2^+$	0.016	0.014					1.234						1.127	
		$3/2^+$	0.031	0.028					1.268						1.141	
1.537	0	$1/2^+$	0.016	0.014					1.376						1.173	
1.599	2	$5/2^+$	0.026	0.024					1.407						1.200	
		$3/2^+$	0.054	0.049					1.517						1.220	
1.649	2	$5/2^+$	0.030	0.027	1.67	2	$5/2^+$	0.019	1.580						(1.240)	
		$3/2^+$	0.059	0.053											1.277	
1.712	0	$1/2^+$	0.039	0.035											1.311	$(9/2,5/2)^+$
1.847	0	$1/2^+$	0.088	0.080	1.84	-									1.380	
1.951	2	$5/2^+$	0.073	0.066	1.94	1	$3/2^-$	0.061							(1.410)	
		$3/2^+$	0.142	0.129			$1/2^-$	0.138							(1.513)	
2.013	2	$5/2^+$	0.019	0.017											1.523	
		$3/2^+$	0.037	0.033											1.580	
2.111	2	$5/2^+$	0.012	0.011												
		$3/2^+$	0.024	0.022												
2.151	0	$1/2^+$	0.018	0.016												
2.264	0	$1/2^+$	0.078	0.071	2.26	2	$5/2^+$	0.023								
2.307	2	$5/2^+$	0.025	0.023												
		$3/2^+$	0.048	0.043	2.48	-										
2.653	0	$1/2^+$	0.121	0.110	2.64	0	$1/2^+$	0.050								
2.713	2	$5/2^+$	0.025	0.023	2.73	-										
		$3/2^+$	0.049	0.043												
2.783	2	$5/2^+$	0.016	0.015												
		$3/2^+$	0.032	0.029												
2.878	2	$5/2^+$	0.028	0.025	2.89	-										
		$3/2^+$	0.056	0.051												
2.908	2	$5/2^+$	0.024	0.022												
		$3/2^+$	0.048	0.043												
3.018	2	$5/2^+$	0.021	0.019												
		$3/2^+$	0.041	0.037												
3.060	2	$5/2^+$	0.032	0.029	3.05	2	$5/2^+$	0.009								
		$3/2^+$	0.064	0.058												
3.145	0	$1/2^+$	0.096	0.087												
3.214	0	$1/2^+$	0.039	0.035												

TABLE 10

Summary of Spectroscopic Properties of the Low-Lying States of ^{99}Tc from the Present Work and Previous Measurements

Present Work $^{98}Mo(^{3}He,d)^{99}Tc$					Cook et al. (1969) β-γ		Bond et al.(1972) $^{99}Tc(^{35}Cl,^{35}Cl'\gamma)^{99}Tc$	
Ex (MeV)	ℓ	J^π	C^2S	C^2S (Norm.)	Ex (MeV)	J^π	Ex (MeV)	J^π
0.	4	$9/2^+$	0.572	0.668	0.	$9/2^+$	0.	$9/2^+$
0.142	(4)	$(7/2^+)$	(<0.046)	(<0.054)	0.14051	$7/2^+$	0.1404	$7/2^+$
	1	$1/2^-$	0.248	0.290	0.14263	$1/2^-$		
0.181	2	$5/2^+$	0.006	0.007	0.18107	$5/2^+$	0.1817	$5/2^+$
0.509	1	$3/2^-$	0.076	0.089	0.5091	$3/2^-$		
0.625	4	$9/2^+$	0.057	0.067	0.5343	-		
		$7/2^+$	0.152	0.178				
0.672	3	$5/2^-$	0.045	0.053	0.6715	$5/2^-$		
0.720	4	$9/2^+$	0.023	0.027			0.7263	$(7/2^+,9/2^+)$
		$7/2^+$	0.062	0.072				
0.762	2	$5/2^+$	0.048	0.056	0.7616	$5/2^+$	0.7618	$(7/2^+,9/2^+)$
0.919	0	$1/2^+$	0.008	0.009	0.9205	$(3/2^+,1/2^+)$		
					1.004	$3/2^-$		
1.020	2	$5/2^+$	0.007	0.008				
		$3/2^+$	0.013	0.015				
					1.0729	$5/2^-$		
					1.1293	$(1/2^-,3/2^-)$		
1.145	weak				1.142	$3/2^-$		
1.203	1	$3/2^-$	0.005	0.006	1.199	$(1/2^-,3/2^-)$		
		$1/2^-$	0.012	0.014				
1.321	1	$3/2^-$	0.010	0.012				
		$1/2^-$	0.026	0.030				
1.407	weak							
1.435	2	$5/2^+$	0.018	0.021				
		$3/2^+$	0.033	0.039				
1.505	weak							
1.560	0	$1/2^+$	0.071	0.083				
1.679	2	$5/2^+$	0.017	0.020				
		$3/2^+$	0.032	0.037				
1.760	2	$5/2^+$	0.011	0.013				
		$3/2^+$	0.021	0.025				
1.803	0	$1/2^+$	0.023	0.027				
1.825	2	$5/2^+$	0.055	0.064				
		$3/2^+$	0.105	0.123				
1.911	2	$5/2^+$	0.011	0.013				
		$3/2^+$	0.021	0.025				
1.982	2	$5/2^+$	0.038	0.044				
		$3/2^+$	0.072	0.084				
2.000	2	$5/2^+$	0.026	0.030				
		$3/2^+$	0.050	0.058				
2.064	weak							
2.111	2	$5/2^+$	0.047	0.055				
		$3/2^+$	0.090	0.105				
2.160	2	$5/2^+$	0.019	0.023				
		$3/2^+$	0.037	0.043				
2.176	0	$1/2^+$	0.022	0.026				
2.203	2	$5/2^+$	0.019	0.022				
		$3/2^+$	0.037	0.043				
2.281	0	$1/2^+$	0.058	0.068				
2.362	weak							
2.396	2	$5/2^+$	0.010	0.012				
		$3/2^+$	0.020	0.023				
2.414	2	$5/2^+$	0.011	0.013				
		$3/2^+$	0.022	0.026				
2.466	0	$1/2^+$	0.017	0.020				
2.486	0	$1/2^+$	0.026	0.030				
2.522	2	$5/2^+$	0.022	0.026				
		$3/2^+$	0.042	0.049				
2.581	2	$5/2^+$	0.026	0.030				
		$3/2^+$	0.050	0.058				
2.611	weak							
2.653	0	$1/2^+$	0.024	0.028				
2.675	0	$1/2^+$	0.011	0.013				

TABLE 11

Summary of Spectroscopic Properties of the Low-Lying States of ^{101}Tc from the Present Work and Previous Measurement

Present Work $^{100}Mo(^{3}He,d)^{101}Tc$					Cook and Johns (1972) β-γ	
Ex (MeV)	ℓ	J^{π}	C^2S	C^2S (Norm.)	Ex (MeV)	J^{π}
0.	4	$9/2^+$	0.860	0.553	0.	$9/2^+$
					0.009317	$7/2^+$
					0.015601	$5/2^+$
0.207	1	$1/2^-$	0.637	0.410	0.20753	$1/2^-$
0.288	1	$3/2^-$	0.195	0.126	0.28845	$3/2^-(1/2^-)$
		$1/2^-$	0.477	0.308		
0.394	3	$5/2^-$	0.138	0.089	0.39440	$5/2^-$
					0.50045	$(1/2^-, 3/2^-, 5/2^{\pm})$
0.515	2	$5/2^+$	0.073	0.047	0.51519	$(5/2^+, 7/2^+)$
		$3/2^+$	0.183	0.118		
					0.53355	$(5/2^+, 7/2^+)$
					0.60641	$(1/2^+, 3/2^+)$
					0.61620	$(1/2^-, 3/2^-$
0.620	1	$3/2^-$	0.011	0.007	0.62215	$(1/2^-, 3/2^-, 5/2^-)$
		$1/2^-$	0.026	0.017		
0.670	3	$5/2^-$	0.118	0.076	0.66945	$5/2^-$
					0.71112	$(3/2^+$
					0.74222	$(5/2^-)$
0.890	(2,4)	$(5/2)^+$	(0.030)	(0.019)	0.88665	$(5/2^{\pm}, 7/2^+)$
		$(3/2)^+$	(0.057)	(0.037)	1.02559	$(1/2^+, 3/2^{\pm})$
		$(9/2)^+$	(0.127)	(0.082)		
		$(7/2)^+$	(0.333)	(0.214)		
1.045	1	$3/2^-$	0.014	0.009	1.0279	$3/2^+$
		$1/2^-$	0.034	0.022	1.1035	$(1/2^-, 3/2^-, 5/2^-)$
					1.1415	$(1/2^-, 3/2^-, 5/2^-)$
					1.18804	$(1/2^-, 3/2^-, 5/2^-)$
1.197	1	$3/2^-$	0.035	0.023	1.1973	$(1/2^-, 3/2^-, 5/2^-)$
		$1/2^-$	0.084	0.054		
1.280	2	$5/2^+$	0.022	0.014	1.2313	$(1/2^-, 3/2^-, 5/2^-)$
		$3/2^+$	0.042	0.027		
1.319	2	$5/2^+$	0.021	0.014	1.31946	$(1/2^+, 3/2^+)$
		$3/2^+$	0.041	0.026		
1.429	2	$5/2^+$	0.104	0.067	1.449	$(1/2^+, 3/2^{\pm})$
		$3/2^+$	0.203	0.131	1.56509	$(1/2^+, 3/2^{\pm})$
1.490	2	$5/2^+$	0.068	0.044	1.59439	$(1/2^+, 3/2^+)$
		$3/2^+$	0.132	0.085	1.59894	$(5/2^{\pm}, 7/2^+)$
1.578	2	$5/2^+$	0.087	0.056	1.61466	$(1/2^+, 3/2^+)$
		$3/2^+$	0.167	0.107	1.6778	$(1/2^+, 3/2^{\pm})$
1.608	0	$1/2^+$	0.083	0.053	1.7753	$(1/2^+, 3/2^+)$
1.703	2	$5/2^+$	0.092	0.059		
		$3/2^+$	0.179	0.115		

TABLE 12

Occupation Probability of Proton Orbitals Below the Z = 50 Shell Closure

The experimental (^{3}He,d) data for the calculation of U^{2} were taken from the present work, except those for ^{92}Mo which were taken from Picard and Bassani (1969). The (d,^{3}He) data for the calculation of V^{2} were taken from Ohnuma and Yntema (1968).

NUCLEUS	SUBSHELL	$U^2_{\ell j}$ (^{3}He,d)	$V^2_{\ell j}$ (d,^{3}He)	$U^2 + V^2$
Mo-92	$1g_{9/2}$	0.67	0.27	0.94
	$2p_{1/2}$	0.30	0.70	1.00
	$2p_{3/2}$	0.10	0.85	0.95
	$1f_{5/2}$	-	0.82	0.82
Mo-94	$1g_{9/2}$	0.68	0.29	0.97
	$2p_{1/2}$	0.27	0.80	1.07
	$2p_{3/2}$	0.14	0.78	0.92
	$1f_{5/2}$	-	0.58	0.58
Mo-96	$1g_{9/2}$	0.63	0.29	0.92
	$2p_{1/2}$	0.43	0.80	1.23
	$2p_{3/2}$	0.17	1.05	1.22
	$1f_{5/2}$	0.04	0.35	0.39
Mo-98	$1g_{9/2}$	0.67	0.22	0.89
	$2p_{1/2}$	0.29	0.55	0.84
	$2p_{3/2}$	0.11	0.63	0.74
	$1f_{5/2}$	0.05	0.42	0.47
Mo-100	$1g_{9/2}$	0.55		
	$2p_{1/2}$	0.41		
	$2p_{3/2}$	0.16		
	$1f_{5/2}$	0.16		

TABLE 13

Coefficients of the Ground State Proton Wave Function of ^{92,94,96,98,100}Mo deduced from (^{3}He,d) Reactions

Values deduced from equations (3.4-21) and (3.4-22).

Mo	c_1^2	c_2^2	c_3^2	c_4^2
92	0.48	0.31	0.21	-
94	0.44	0.27	0.29	-
96	0.16	0.43	0.34	0.07
98	0.34	0.29	0.21	0.16
100[a)]	0.	0.33	0.27	0.40

a) Coefficients normalized by $\sum_{i=2}^{4} c_i^2 = 1.$

TABLE 14

Quasi-Particle Energies of ^{93,95,97,99,101}Tc deduced from (^{3}He,d) Reactions

NUCLEUS	SUBSHELL	$\bar{E}(\ell,j)$ (exp.)	$\bar{E}(\ell,j)$ (theor.)
Tc-93	$1g_{9/2}$	0.	0.
	$2p_{1/2}$	0.39	0.56
	$2p_{3/2}$	1.61	1.60
	$1f_{5/2}$	-	2.16
Tc-95	$1g_{9/2}$	0.	0.
	$2p_{1/2}$	0.04	0.47
	$2p_{3/2}$	1.10	1.47
	$1f_{5/2}$	-	2.05
Tc-97	$1g_{9/2}$	0.	0.
	$2p_{1/2}$	0.10	0.45
	$2p_{3/2}$	0.75	1.42
	$1f_{5/2}$	0.66	2.01
Tc-99	$1g_{9/2}$	0.	0.
	$2p_{1/2}$	0.14	0.37
	$2p_{3/2}$	0.64	1.31
	$1f_{5/2}$	0.67	1.90
Tc-101	$1g_{9/2}$	0.	0.
	$2p_{1/2}$	0.21	0.00
	$2p_{3/2}$	0.47	1.23
	$1f_{5/2}$	0.51	1.82

FIGURE 19

Distribution of Transition Strengths as a Function of Excitation Energy for Transitions with $\ell = 1$ Transfer in Mo(^{3}He,d)Tc Reactions

The circle indicates the position of the center of gravity energy of the $2p_{3/2}$ orbit.

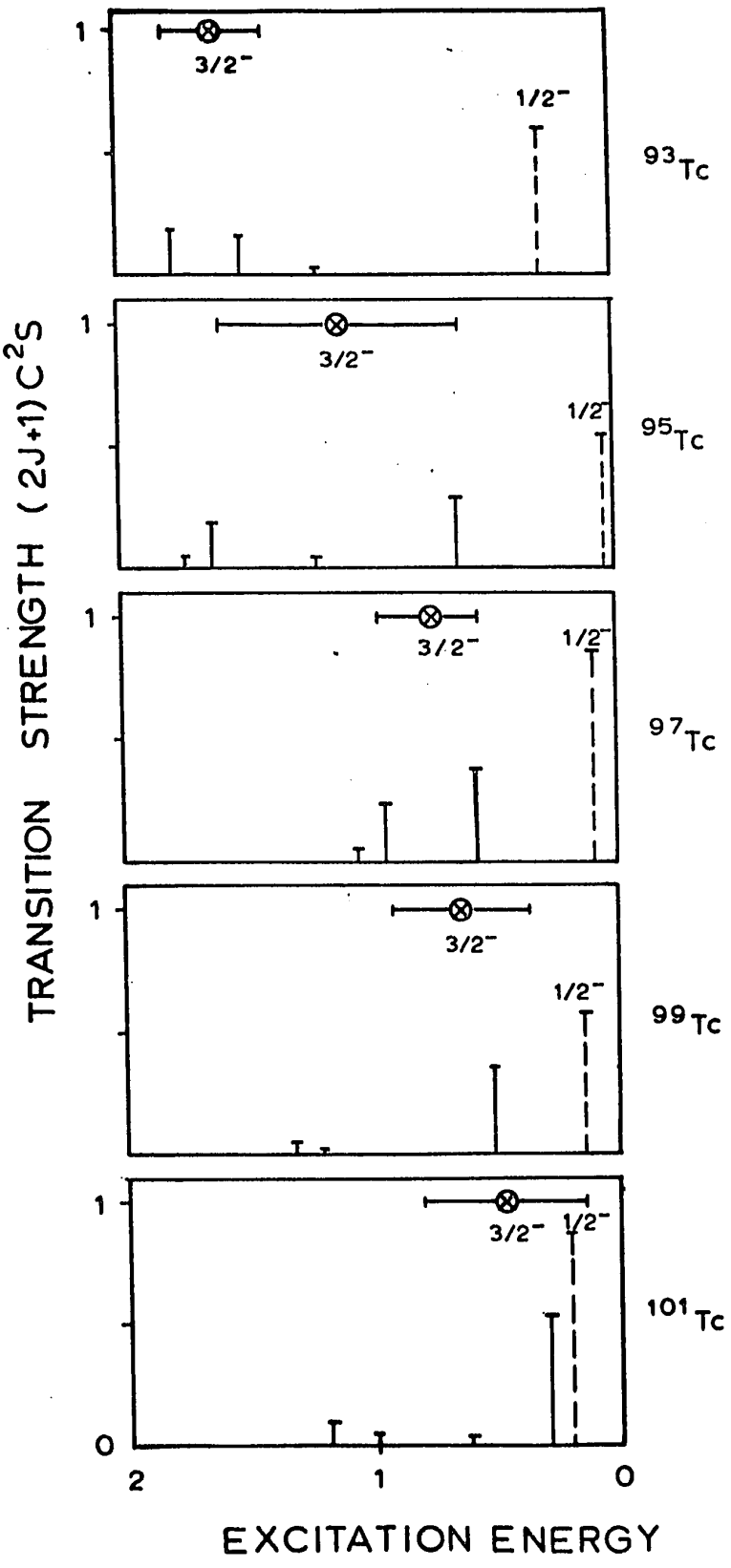
1
3/2⁻
1/2⁻
93Tc
1
3/2⁻
1/2⁻
95Tc
1
3/2⁻
1/2⁻
97Tc
1
3/2⁻
1/2⁻
99Tc
1
3/2⁻
1/2⁻
101Tc
0
2
1
0
TRANSITION STRENGTH (2J+1)C²S
EXCITATION ENERGY

FIGURE 20

Distribution of $\ell = 2$ Transition Strengths as a Function of Excitation Energy from Proton Stripping Reactions on Mo Isotopes

See text for details.

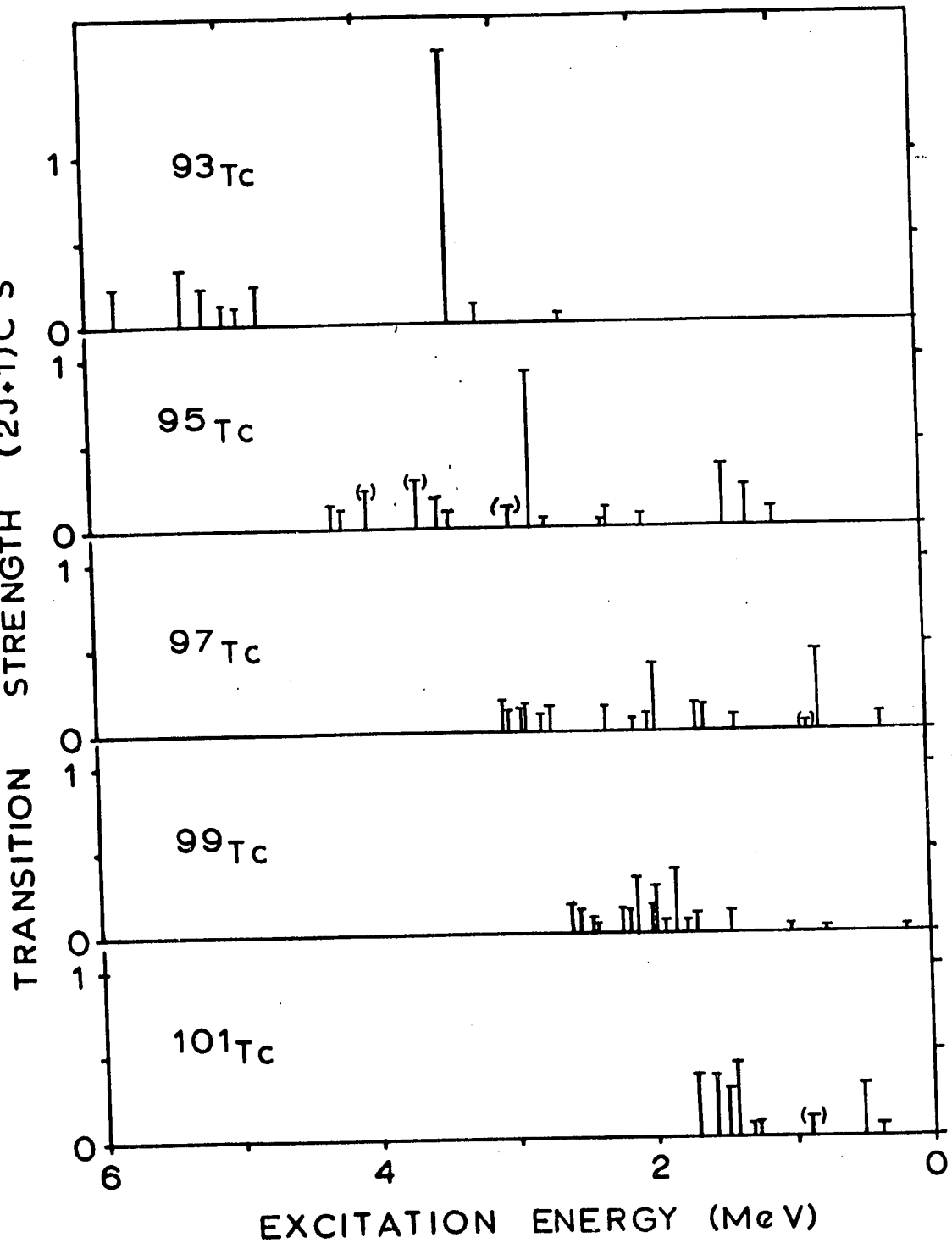
93Tc
95Tc
97Tc
99Tc
101Tc
TRANSITION STRENGTH (2J+1)C²S
EXCITATION ENERGY (MeV)
0
1
6
4
2
0

FIGURE 21

Distributions of $\ell = 0$ Transition Strengths as a Function of Excitation Energy from Proton Stripping Reactions on Mo Isotopes

See text for details.

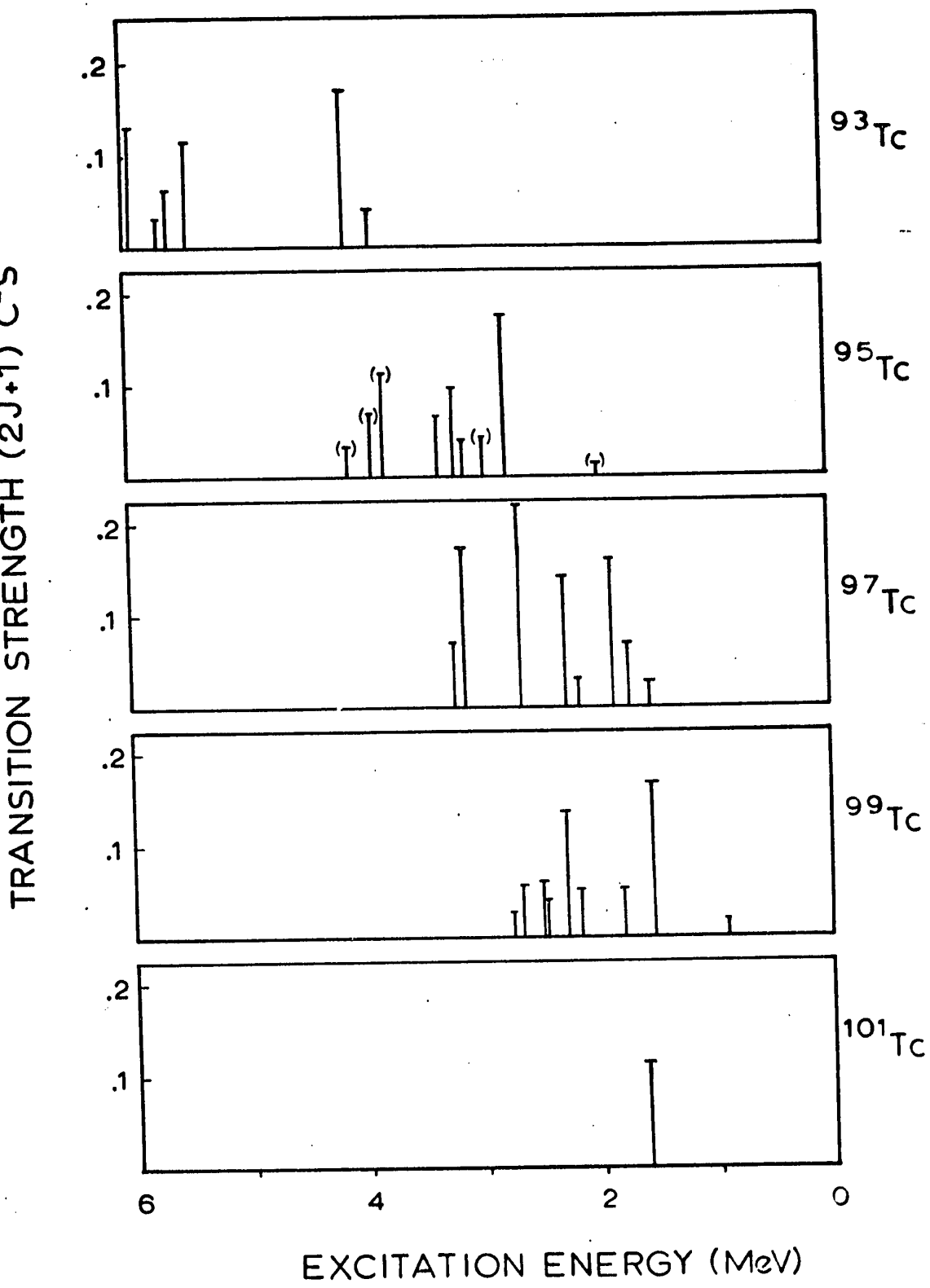
TRANSITION STRENGTH (2J+1) C²S
.2
.1
93Tc
95Tc
97Tc
99Tc
101Tc
6
4
2
0
EXCITATION ENERGY (MeV)

CHAPTER IV

THE (d,p) REACTIONS IN Br-79 AND 81

4.1 Experimental Procedure and Data Reduction

Measurements of the reactions ^{79,81}Br(d,p) ^{80,82}Br were performed using the 12 MeV deuteron beam from the EN tandem Van de Graaff accelerator at the University of Montreal. The preparation of the isotopically enriched Br targets and the experimental techniques and apparatus for these measurements have been described in Chapter II. The experimental procedures followed were generally along the same lines as those already described in the preceding chapter for the ^{94,96,100}Mo (^{3}He,d) ^{95,97,101}Tc reactions. Two detector telescopes separated by 10^{o} were used; the solid angle of the telescope positioned at smaller scattering angle was chosen to be 0.156 m sr. subtended at the center of the bromine target, while the solid angle of the other one at a larger scattering angle was chosen to be 0.324 m sr. The angular acceptance of each detection system was sufficiently small to minimize the kinematic broadening in the proton peaks arising from induced reactions in the lighter elements, Na and C, in the targets. As already described in section 2.2, the ΔE and E detectors used for this experiment were silicon detectors of thickness 200 μm and 2000 μm, respectively.

The method used for incident particle beam alignment, detector and electronics systems alignments and calibration, and beam current monitoring were similar to those described in section 3.2.

The charged particle identifiers were 'tuned' to provide an optimum separation for protons. However, because of the difference in the incident beam energy and the reaction Q-values for the present experiments as compared to those for the (^{3}He,d) reaction experiments, the energy-voltage relation at the charged-particle identifier inputs were adjusted to about 20 MeV = 10 volts. Apart from using the calibrated pulser for energy calibration, the energies of the proton groups in the spectrum were determined by using the known energies of the proton peaks from the (d,p) reactions in ^{23}Na and ^{12}C (Schiffer et al. 1967; Maples et al. 1966 and Daum 1963).

Proton spectra from the reactions were measured over an angular range from about 10° to 90°, and angular distributions for the various proton groups were evaluated according to equation (3.2-1). As in the analysis of the (^{3}He,d) reaction, for closely spaced proton peaks in the spectra, a computer program, called GFITT (Zurstadt 1968), which performs Gaussian curve fitting, was used to effect their separation.

The target thickness measurements for the ^{79}Br

and ^{81}Br targets were made by means of 'on-line' deuteron elastic scattering techniques. The energy of the deuteron beam from the tandem was reduced to 4 MeV, which is just below the deuteron Coulomb barrier heights of the bromine nuclei (about 4.5 MeV, for a nuclear radius parameter $R_o = 1.2$ fm). The forward angle elastic scattering events were, therefore, the results of Coulomb scatterings. The product of target thickness and solid angle of each detector telescope was thus obtained by comparing the experimental elastic scattering differential cross section, measured at four scattering angles from 25 to 40 degrees, with the calculated Rutherford scattering cross sections (Marion and Young 1968). The target thicknesses thus obtained, using the measured a solid angle values, were 90 μ g/cm^2, and 82 μ g/cm^2 for the ^{79}Br and ^{81}Br targets, respectively.

As discussed in section 3.2 of the preceeding chapters, there were two types of errors involved in the differential cross section measurements: those of a systematic nature and those of a random nature. The systematic errors arise primarily from the uncertainty in the target thickness and solid angle measurements and the accuracy of the beam current monitoring device. In the measurement of elastic scattering of 4 MeV deuterons, it was the product, $(\rho t)\cdot(\Delta\Omega)$, of target thickness and solid angle which had been evaluated. It is believed

that the quantity $\rho t \Delta\Omega$ was measured to better than ± 8% accuracy for both targets. The current monitoring system is believed to be calibrated to better than ± 4%. This gives a total systematic error of ± 12%. The random errors arose mainly from the statistical fluctuation in the number of events in the peaks, the uncertainties in the peak area evaluation, back ground subtraction and electronics deadtime corrections. These various random errors will be added quadratically to obtain a total relative error to be given together with the results.

4.2 Experimental Results

Fourteen proton spectra were accumulated at scattering angles ranging from 10° to 90° for the $^{79}Br(d,p)^{80}Br$ reaction and nineteen spectra from 12.5° to 95° for the $^{81}Br(d,p)^{82}Br$ reaction. Proton groups from the bromine nuclei were distinguished from those originating in the Na and C nuclei by means of their kinematic shifts at different angles. Figures 22 and 23 show the proton spectra of the $^{79}Br(d,p)^{80}Br$ reaction at a scattering angle of 15°, and of the $^{81}Br(d,p)^{82}Br$ reaction at 50°. The energy resolution for this experiment was about 40 keV at FWHM. During the measurements of the $^{81}Br(d,p)^{82}Br$ reaction, a maximum beam current of 500 na was available from the tandem, therefore, each

spectrum for this reaction was accumulated for a total incident charge of about 2000 μC to yield sufficiently good statistics. But in the runs for the $^{79}Br(d,p)^{80}Br$ reaction, only 30 na beam current was available from the tandem because the ion source was not working properly, consequently, each spectrum for this reaction was collected for about 500 μC of incident charge, giving relatively poor statistics.

Proton groups corresponding to thirty-two levels of ^{80}Br lying below an excitation energy of 2.0 MeV, and twenty-one levels of ^{82}Br lying below 2.2 MeV of excitation energy have been identified and analysed. Above these excitation energies, strong proton groups from the carbon and sodium contaminants in the targets rendered the identification and data extraction of proton groups from the two bromine isotopes impossibly difficult. Also, weak proton groups from the bromine nuclei above 1 MeV excitation energy could have escaped observation because they may have been obscured by the contaminant proton groups in the forward angles and may have been too weak to be identified at the larger angles. It is evident from figures 22 and 23 that the proton groups from ^{23}Na are much stronger than those from the bromine nuclei.

The excitation energies for the various levels of ^{80}Br and ^{82}Br and their excitation differential cross

sections in the laboratory system are tabulated in table 15 and 16 respectively. The uncertainties in the level energy determination and the total relative error in each differential cross section measurement are also given in these tables. The uncertainties associated with the excitation energies arise from the peak position determination and energy calibration. The relative errors associated with the differential cross sections are those from peak extraction in each spectrum as discussed in the preceding session. The entry format adopted for these two tables is the same as that used for table 2. Graphs displaying the angular distributions for the various levels in ^{80}Br and ^{82}Br will be shown together with the results of the theoretical analysis in the next section.

As can be seen from figures 22 and 23 and tables 15 and 16 the present measurements provide a set of reasonably good quality data for transitions leading to the low-lying states ($\leq$ 1 MeV) in ^{80}Br and ^{82}Br. However, because of the relatively high level density in these nuclei, much better energy resolution is required for the study of levels lying above 1 MeV excitation energy by means of (d,p) reaction. Ideally, the targets should also be free from contaminants which might interfere with the measurements.

The Q-values for the (d,p) reactions in ^{79}Br and ^{81}Br have been determined to be 5.64 $\pm$ 0.02 MeV and

5.40 ± 0.02 MeV, respectively. These values are in good agreement with the 5.6544 ± 0.0046 MeV and 5.3719 ± 0.0071 MeV given by Maples et al. (1966) and the 5.658 ± 0.004 MeV and 5.376 ± 0.008 MeV given by Wapstra and Gove (1971).

4.3 DWBA Analysis

The (d,p) reaction belongs to the same class of nuclear reactions, called the single-nucleon transfer reaction, as the (^{3}He,d) reaction; a neutron instead of a proton is transferred from the incident projectile to the target nucleus. Historically, the (d,p) reaction was the first kind of nucleon-transfer reaction to be studied, thoroughly, experimentally and theoretically. As early as two decades ago Burrow et al. (1950) and Hott et al. (1950) observed that in such reactions with an incident energy above a few MeV, the outgoing protons exhibited a pronounced diffractive pattern in their angular distributions which were generally peaked in the forward direction. These observations led Butler (1950,1951) to the interpretation of this reaction in terms of single-step processes in which the neutron in the incident projectile is captured by the target nucleus into one of its vacant orbitals without forming any intermediate state between the incident and outgoing reaction channels.

This concept of nuclear reactions was subsequently evolved into a general theory of direct reactions with nucleon(s)-transfer reactions forming a subclass (Tobocman 1961, Austern 1963).

The distorted wave Born approximation (DWBA) of the direct reaction theory for nucleon(s)-transfer reactions, as noted in the preceding chapter, will not be repeated here. In terms of physics, the nuclear spectroscopic information that is obtainable from a (d,p) reaction is similar to that from a (^{3}He,d) reaction; the former studies the neutron single-particle states in the target nucleus whereas the latter probes the proton single-particle states.

Apart from the structural differences in the incident and outgoing projectiles the DWBA formalism for the (d,p) reaction should have very similar appearance to that given in section 3.4 of Chapter III for the (^{3}He,d) reaction. Following the formalism given by Glendenning (1963), the differential cross section for the A(d,p)B reaction may be written as,

$$\frac{d\sigma}{d\Omega}(lj) = \frac{1}{2}\frac{\mu_d \mu_p}{(2\pi\hbar^2)^2}\frac{k_p}{k_d}\frac{2I_f+1}{2I_i+1} C^2 S(lj) \sum_{m_l} |B_l^{m}|^2 \qquad (4.3\text{-}1)$$

$$B_l^{m_l} = i^{-l}\cdot(2l+1)^{-\frac{1}{2}}\cdot \int \psi_p^{(-)*}\left(\vec{k}_p, \vec{r}_p + \frac{m_n}{M_B}\vec{r}_n\right) \phi_{l m_l}^{*}(\vec{r}_n)\cdot \qquad (4.3\text{-}2)$$

$$\cdot V_{np}(r_p)\, \phi_d(\vec{r}_p)\, \psi_d^{(+)}\left(\vec{k}_d, \vec{r}_n + \frac{m_p}{m_d}\vec{r}_p\right) d\vec{r}_n\, d\vec{r}_p$$

$$S(\ell j)=(A+1)\left|\int[\Psi^{T}_{J_i T_i}(A)\times\phi_{j\ell}]_{J_f T_f}\Psi^{T}_{J_f T_f}(A+1)\,d(A+1)\right|^2 \qquad (4.3\text{-}3)$$

$$C = C(T_i\, T_{3i}, \tfrac{1}{2}\,\tfrac{1}{2} \mid T_f\, T_{3f}) \qquad (4.3\text{-}4)$$

where:

$\Psi_{J_i T_i}$ and $\Psi_{J_f T_f}$ are initial and final nuclear state wavefunctions characterized by total spin J_i, J_f and the isospin T_i, T_f, $\phi_{\ell m_\ell}$ is the orbital part of the spin-orbit wave function $\phi_{j\ell}$ of the captured neutron in the potential field of the target nucleus, $\psi^{(+)}_d$ and $\psi^{(-)}_p$ are the distorted waves of the incident and outgoing particles with momenta $\vec{k}_d$ and $\vec{k}_p$ and with coordinates relative to the C.M. of the target nucleus and to that of the final nucleus, ϕ_d is the internal wave function of the deuteron, V_{np} is the n-p interaction in the process, $S(\ell\, j)$ is the spectroscopic factor as defined in section 3.4 and gives the strength for the stripping of a neutron into the orbit ℓ, j of the target nucleus.

As in the case of the (^{3}He,d) reaction, to evaluate the angular distribution it is necessary to compute the transition amplitude $B^{m_\ell}_{\ell}$ explicitly. This requires a detailed knowledge of the incoming and outgoing distorted waves, and the bound state wave function of the

captured neutron, the internal wave function of the deuteron and the n-p interaction. In this calculation the deuteron internal wave function ϕ_d was taken to be the Hulthén function, as usually the case (Glendenning, 1963), and the n-p interaction V_{np} was assumed to be a zero-range interaction:

$$\phi_d(r) = K \frac{e^{-\alpha r} - e^{-\beta r}}{r} \qquad (4.3\text{-}5)$$

$$V_{np}(r) = V_o \delta(r) \qquad (4.3\text{-}6)$$

where $K = \sqrt{\frac{\alpha\beta(\alpha+\beta)}{2\pi(\alpha-\beta)^2}}$, $\beta = 7\alpha$ and $\alpha = 0.2317$ fm^{-1}. The square of the integral $\int V_{np}(r_p)\phi_d(\vec{r}_p)d\vec{r}_p$ has a value $\sim 1.5 \times 10^4$ fm^2 MeV^3 (Bassel et al. 1962)which is equivalent to the quantity D_o^2 introduced in the equation (3.4-5) of the preceding chapter.

The deuteron and proton channel distorted waves were obtained by iterating the Schrödinger equation given as equation (3.4-10) in the preceding chapter with the optical potentials having the same form as that given by equation (3.4-12). Again, no spin-orbit potential was used for either the deuteron or the proton channel as it has been shown that this potential affects the angular distribution in the forward hemisphere only slightly for (d,p) reactions in the energy range of the present experiments. The optical parameters were listed in

table 17. Two sets of parameters were used: one with a volume absorption imaginary potential, called set I, and the other with a surface absorption imaginary potential, called set II, for both the deuteron and proton potentials. Set I was taken from Morton et al. (1971) who use the same potential to study the ^{84,86}Sr (d,p)^{85,87}Sr reactions at 12 MeV and set II was originally taken from Forster et al. (1967) in their study of the ^{90}Zr(d,p)^{91}Zr reaction at 12 MeV. In both parameter sets, the Coulomb potential radius parameter was assumed to be equal to that of the real potential.

The bound state neutron wave function was obtained by computing the Schrödinger equation given in equation (3.4-14) with a potential similar in form to that given by equation (3.4-15), except that the spin-orbit term was defined slightly differently as follows:

$$\left(\frac{\hbar}{m_\pi c}\right)^2 V_{so} \frac{\vec{l}\cdot\vec{\sigma}}{r} \frac{d}{dr} f(r, r_{so}, a_{so}) \qquad (4.3\text{-}7)$$

The spin-orbit geometrical parameters, r_{so} and a_{so}, were assumed to be the same as those, r_r and a_r, of the real central neutron potential. The values for r_r, a_r and V_{so} were taken from the work of Scharpey-Schafer (1968), and the potential depth V_o was adjusted to give the transferred neutron a binding energy of Q(d,p)+ 2.23 MeV

(conventional separation energy method). All neutron potential parameters are also given in table .

The spectroscopic factor $S(\ell, j)$ contains the nuclear structure information of the initial and final states. As in the case of the (^{3}He,d) reaction, it is convenient to extract an experimental value for $S(\ell, j)$ by computing all the other quantities in equation (4.3-1) and then normalizing the calculated value to the experimental differential cross section $(d\sigma/d\Omega)_{exp}$. Therefore, equation (4.3-1) may be written

$$\left(\frac{d\sigma}{d\Omega}\right)_{exp} = \frac{2J_f+1}{2J_i+1} C^2 S(\ell j)\, \sigma_{DWBA}(\ell j) \qquad (4.3\text{-}8)$$

The computer program used to calculate the quantity $\sigma_{DWBA}(\ell j)$, was written by Smith (1967) specifically for the analysis of (d,p) reaction. Since most of the final states in both ^{80}Br and ^{82}Br have unknown spins J_f, it was more convenient to extract experimental values for the quantity, $\frac{2J_f+1}{2J_i+1} \cdot C^2 \cdot S(\ell j)$, called the transition strength. Since $T_i = T_{zi}$, the isospin Clebsh-Gordan coefficient squared, is unity, i.e. $C^2 = 1$, for neutron stripping reaction. Thus, in all subsequent discussion on the transition strength the C^2 is dropped from the expression.

Figure 24 shows the predicted angular distributions from the DWBA calculations for different orbital

angular momentum, ℓ-transfer values, of the transferred neutron using the optical potential parameter set I. The positions of the first maxima of these angular distribution patterns differ by approximately 10^{o} as the transferred angular momentum values changed by one. This is an important feature to be used in the identification of different ℓ-values for the various observed angular distributions. Both potentials defined by parameter set I and set II gave similar angular distributions, except in the region of small scattering angles ($\leq 15^{o}$). However, the absolute differential cross section, predicted by the two potentials and thus the deduced spectroscopic strength, may differ by as much as 20%.

The angular distributions of the various observed proton groups together with the results of their DWBA analysis are presented in fig. 25 and 26 for the reactions $^{79}Br(d,p)^{80}Br$ and $^{81}Br(d,p)^{82}Br$, respectively. Both sets of potential parameters gave good fits to the experimental angular distributions. The solid curves in the figures refer to the set I parameters and the dashed curves refer to the set II parameters. The deduced spectroscopic information and the spin parity (J^{π}) assignments from the DWBA analysis are listed in table 18 and 19 for the two reactions studied.

As can be seen from figures 25 and 26 , the angular distributions for states with excitation energies

below 1 MeV in both nuclei have a unique fitting with respect to the ℓ-transfer values in the DWBA predictions; four states in ^{80}Br and five states in ^{82}Br have been identified to be the result of an $\ell=4$ transfer, and eight levels in ^{80}Br and three levels in ^{82}Br have been identified to be due to an $\ell=1$ transfer. Only the distributions corresponding to the 314 keV and 547 keV states in ^{80}Br and the 377 keV state in ^{82}Br have been fitted with combined DWBA predictions of an $\ell=1$ and $\ell=4$ transfer. It is likely that the proton groups corresponding to these excitation energies contained contributions from more than one state. As will be seen later, more than one state at these energies in the two nuclei have been observed. This could very well explain the multiple ℓ-value fittings to the distributions of these proton groups.

As shown in tables 15 and 16, most of the proton groups corresponding to excitation energy higher than 1 MeV in both ^{80}Br and ^{82}Br were obscured by the strong proton peaks from the Na contaminant, particularly in the small scattering angles region where the ℓ-value identification is very crucial in the DWBA analysis. In addition, the high level density in these odd-odd bromine isotopes made the peak extraction from the present results difficult and highly uncertain. As a result, only the 1.201 MeV and 1.748 MeV states in ^{80}Br and the 1.650 MeV and 1.807 MeV

states in ^{82}Br have been analysed and their angular distributions have been fitted with $\ell = 2$ patterns.

As listed in tables 18 and 19 , there are other states in ^{80}Br and ^{82}Br which have been observed in the two reactions but have not been analysed or have been only partially analysed for reasons of weakness in transition strength and/or interferences from the Na contaminant in the targets. The partially analysed transitions have each been assigned a tentative most probable ℓ-value, based on the position of the maximum differential cross section in its angular distribution. All tentative values are shown in parentheses in the tables.

Because of the use of a spin-orbit potential for the bound state neutron wave function, it is necessary to know the total angular momentum j of the orbital into which the neutron is being captured. Therefore, in the above analyses, the following assumptions have been made: for angular distributions with an $\ell = 4$ transfer, the neutron orbit used was $1g_{9/2}$ and for $\ell = 3$ and 2 transfer, the neutron orbit used were $1f_{5/2}$ and $2d_{5/2}$, respectively. For $\ell = 1$ transfers, the states at 0, 266 and 314 keV in ^{80}Br and at 78 and 377 keV in ^{82}Br were assumed to be of the $2p_{1/2}$ type, and the other states were taken to be formed from the $2p_{3/2}$ orbit. The reasons for these assumptions will be given in the next section.

It is interesting to note that most of the angular distributions corresponding to states below 1 MeV in both nuclei exhibited either an $\ell = 1$ or an $\ell = 4$ pattern. This can be understood easily in terms of the simple shell model. The ^{79}Br and ^{81}Br with their 44 and 46 neutrons have six holes and four holes in the shells immediately below the N = 50 closed shell. In a (d,p) reaction, when the neutron is captured into one of these holes it will generate a series of low-lying states in the residual nucleus. Therefore it is expected that the low-lying states of ^{80}Br and ^{82}Br are the results of the coupling of a $1g_{9/2}$ or a $2p_{1/2}$ neutron with a $2p_{3/2}$ proton. The information obtained from this analysis will be discussed in relation to the structure of the states in the Br isotopes involved in the following section.

4.4 Discussion

(i) The $^{79}Br(d,p)^{80}$Reaction:

The results of the DWBA analysis of the angular distributions of this reaction have been presented in table 18 ; the last four columns in the table summarized the orbital angular momentum transfer, the transition strengths obtained with two different sets of optical potential parameters and the deduced most probable J^{π}

values. The ^{79}Br nucleus has 35 protons and 44 neutrons. The spin-parity of its ground state is $3/2^-$, which was determined from atomic beam and magnetic moment measurements (Artna 1966), indicating that this is a $\pi(2p_{3/2})$ state (π = proton, ν = neutron). Assuming that the ground state of this target nucleus has six neutron holes in the N = 50 major closed shell and the valence neutrons (N > 28) occupy primarily the orbitals lying in the region N = 28-50. The set of low-lying states populated by an $\ell = 4$ transfer in the (d,p) reaction can be attributed to the results of the coupling of a $2p_{3/2}$ proton to a $1g_{9/2}$ neutron. This coupling yields a multiplet of four states with $J^{\pi} = 3^-, 4^-, 5^-$ and 6^-. The 84 keV metastable state in ^{80}Br is known to be 5^- (Artna 1966) and is presumably the 5^- member of this multiplet. The other members of this multiplet may be tentatively identified from the present results as the states lying at 368 keV $(6)^-$, 314 keV $(4)^-$, and 547 keV $(3)^-$ by virtue of the (2J+1) dependence of their differential cross sections. Although some deviations from the 2J+1 dependence are observed, these may be attributed to configuration mixing. Configurations such as $\left[\nu(d_{5/2}) \times {}^{79}Br_{g.s.}\right]_{3^-,4^-}$ and coupling of a neutron to the low-lying excited states of ^{79}Br might be admixed with the configuration $\left[\nu(g_{9/2}) \times {}^{79}Br_{g.s.}\right]_{3^-,4^-,5^-,6^-}$. These states presumably

arise from the coupling of a $2p_{1/2}$ or a $2p_{3/2}$ neutron with a $2p_{3/2}$ proton. From the filling sequence of the shell model orbitals as observed in neighbouring nuclei, the $2p_{1/2}$ neutron orbit is expected to be lowest. Thus the three low-lying states (the ground state, 266 keV and 314 keV states) would be expected to be associated with the coupling of the $2p_{1/2}$ neutrons while other states of $\ell = 1$ transfer would be associated with the coupling of a $2p_{3/2}$ neutron. As stated in the preceding section the spectroscopic strengths shown in table 18 were calculated according to these j-transfer values. The states resulting from the configurations of $\left[\nu(2p_{1/2}) \times {}^{79}Br_{g.s.}\right]$ and $\left[\nu(2p_{3/2}) \times {}^{79}Br_{g.s.}\right]$ will carry a range of $J^{\pi} = (1,2)^{+}$ and $(0,1,2,3)^{+}$, respectively, except the ground state, which is known to be 1^{+}.

The total neutron transition strength of each orbit (ℓ, j) in the target nucleus, observed in the (d,p) reaction, gives information about its unoccupation probability (fractional emptiness) $U^2_{\ell j}$. This is given by the sum rule (Schiffer 1968), that

$$U^2_{\ell j} = \frac{1}{2j+1} \sum_{J_f} \frac{2J_f+1}{2J_i+1} S(\ell j) \qquad 4.4\text{-}1$$

and the average number of neutron holes in a given orbital ℓ, j in the target is given by

$$n_{lj} = (2j+1)\, U_{lj}^2 = \sum_{J_f} \frac{2J_f+1}{2J_i+1} S(lj) \qquad 4.4\text{-}2$$

A sum rule analysis for some N = 44 nuclei is shown in table 20 . The average number of neutron holes in $1g_{9/2}$ and $2p_{1/2}$ orbits obtained from the present results are compared with those from the reaction of $^{78}Se(d,p)^{79}Se$ (Lin 1965). It is seen that a reasonable agreement is obtained. The values obtained from the optical potential parameter set I seem to give a better agreement than those from set II.

Transitions to the higher-lying states in ^{80}Br may be ascribed to the stripping of a neutron into the N = 50-82 shells as well as in the N = 28-50 shells. In these states strong admixture of the various configurations resulting from the coupling these available neutron orbitals to the ground state or to the low-lying states of ^{79}Br can be expected. Two angular distributions have been fitted to the patterns of an $l = 2$ transfer in figure 25. Consequently, the states associated with these distributions most probably contain a fragmented $2d_{5/2}$ neutron state.

The results of the present work together with those obtained in (p,n) reaction studies (Finckh et al. 1970) and from the gamma decay studies (Artna 1966) are

shown in table 21. The measurements of the (p,n) reaction obtained at incident proton energy about 4 MeV, is predominated by compound nucleus reaction. This reaction has produced many more loy-lying states and some of them overlap with the results of the present more selective direct reaction measurements. The 37 keV state of spin parity 2^-, observed in both gamma decay and (p,n) reaction studies, is not observed in the present (d,p) reaction. This observation is consistent with the assumption that the neutron component of the wave function for this state is a seniority three configuration of $\nu(1g_{9/2})^5$. This is deduced from the fact that the N = 45 isotones, the ground states of both the Kr-81 and Se-79, have $J^\pi = 7/2^+$, which is unexpected from simple shell model considerations. Moreover, in the work of Lin (Lin 1965), the ground state of ^{79}Se was not populated in the ^{78}Se(d,p)^{79}Se reaction and he attributed a configuration of $\nu(1g_{9/2})^5_{7/2}$ to this state. Similarly, the $7/2^+$ state at 0.231 MeV excitation in ^{85}Sr was not populated in the ^{84}Sr(d,p)^{85}Sr reaction (Morton et al. 1971), and the $7/2^+$ state at 0.103 MeV excitation in ^{81}Se was only weakly excited by $\ell = 4$ transfer in the ^{80}Se(d,p)^{81}Se reaction (Lin 1966). On the basis of the above observations, that the seniority three states occur at relative low energy, it is, therefore, likely that the low-lying 2^- state in ^{80}Br is a result of the coupling of the $2p_{3/2}$

proton to the $\nu(1g_{9/2})^5_{7/2}$ state. Although the remaining members of the $\left[\pi(2p_{3/2}) \times \nu(1g_{9/2})^5_{7/2}\right]_J$ multiplet of $J^\pi = 5^-, 4^-, 3^-$ are not identified from the results shown in table 21. Some of the states observed in the (p,n) reaction but not in the (d,p) reaction may belong to this multiplet. It should be noted that the low-lying 5^- state at 85 keV observed in the (d,p) reaction is not associated with this multiplet for the reasons given above. Furthermore, this 5^- state was not observed in $^{80}Se(d,p)^{81}Br$ reaction. This might be due to the hinderance on high ℓ-partial waves in the formation of this compound nuclear reaction (Finch et al. 1970).

(ii) The $^{81}Br(d,p)^{82}Br$ Reaction

As tabulated in table 19, the results of the DWBA analysis of the angular distributions of the proton groups in this reaction reveal that, of the states populated in ^{82}Br, five of them are populated by $\ell = 4$ transfer and three by $\ell = 1$ transfer transitions. The target, ^{81}Br has 35 protons and 46 neutrons. Based on the same arguments used in ^{79}Br, the low-lying states in ^{82}Br associated with $\ell = 4$ transfer transitions may arise from the coupling of $2p_{3/2}$ proton to $1g_{9/2}$ neutron. However, only a multiplet of four states can be generated by this configuration $\left[\pi(2p_{3/2}) \times \nu(1g_{9/2})\right]$

$J = 3^-, 4^-, 5^-, 6^-$. Consequently, a slight fragmentation has occured. A sum rule analysis shows that the available strength for transitions to these states is equivalent to that of other N = 46 nuclei (Morton et al. 1971, Lin 1965, Bercaw and Warner 1970). The results of this analysis are listed in table 22.

The two low-lying levels, 78 keV and 377 keV, populated by $\ell = 1$ transfers are probably associated with the configuration $[\pi(2p_{3/2}) \times \nu(2p_{1/2})]$. This is supported by the results of the sum rule analysis (table 22). The other states in ^{82}Br populated via $\ell = 1$ transitions are most likely the results of coupling of a $2p_{3/2}$ proton to the $2p_{3/2}$ transferred neutron.

Finally as in the case in ^{80}Br, the two states lying above 1 MeV populated by $\ell = 2$ transitions probably belong to a $2d_{5/2}$ neutron configuration.

Except for the ground state of ^{82}Br, which is obviously known to be a 5^- state (Artna 1966), no definite J^π assignments for most of the observed states can be made. It is possible to deduce a range of most probable J^π for these states and it has been summarized in table 19. The range of J^π arising from the various configurations are given below: $J^\pi = (1,2)^+$ for the configuration of $[\pi(2p_{3/2}) \times \nu(2p_{1/2})]$, $(0,1,2,3)^+$ for the configuration $[\pi(2p_{3/2}) \times \nu(1g_{9/2})]$ and $(1,2,3,4)^-$

for the configuration $\left[\pi(2p_{3/2}) \times \nu(2d_{5/2})\right]$.

A comparison of the available information concerning the level structure of ^{82}Br is presented in table 23, which contains the results from the (p,n) reaction (Finckh et al. 1970), the present (d,p) reaction and the gamma decay studies (Artna 1966). In contrast to the results observed for ^{80}Br, the density of levels in ^{82}Br populated by the (d,p) reaction is lower, and the data deduced from the (d,p) reaction overlap with those from the (p,n) reaction to a greater degree.

The (p,n) reaction does not populate the ground state, which has a $J^{\pi} = 5^-$, most probably because of high spin value. A broad neutron group corresponding to 70 keV excitation energy has been observed in the (p,n) reaction. This group probably contains contributions from transitions to the 2^- excited state at 46 keV as well as to another level at 78 keV observed in the present work. Since the low-lying 2^- state is not populated in the present (d,p) reaction, it has probably the same origin as the 2^- state at 37 keV in ^{80}Br and, therefore, it may be assigned a configuration of $\left[\pi(2p_{3/2}) \times \nu(1g_{9/2})^{-3}_{7/2}\right]$ 2^-.

(iii) Systematics:

Figure 27 shows the fractional emptiness (U^2_{lj}) of

the $1g_{9/2}$ neutron orbit in ^{79}Br and ^{81}Br (from the present measurements) as well as in the neighboring nuclei (obtained from neutron stripping or pick-up measurements). See the figure caption for references. In the preparation of this figure, the following procedure has been adopted. The valence neutrons ($N > 28$) in each case were assumed to occupy the orbitals $2p_{3/2}$, $1f_{5/2}$, $2p_{1/2}$, and $1g_{9/2}$. The experimental values $n_{\ell j}$ (average number of holes in the ℓj orbit) are first added up to obtain the total number of observed neutron holes in these orbits. Then the 'average fraction of observed holes' is obtained by dividing this sum by the theoretical total number of holes in these orbits. The normalized $U^2_{\ell j}$ for the $1g_{9/2}$ orbit is then obtained by multiplying the experimental value by the 'average fraction of observed holes'. This procedure has the advantage of minimizing the systematic errors in the various experiments. However, because of the lack of complete experimental information on the $\bar{n}_{\ell j}$ values for the ^{79}Br and ^{81}Br, the unnormalized experimental $U_{\ell j}$ values have been used (potential parameter set I).

It is seen that the fractional emptiness values (unoccupation probabilities) of the $1g_{9/2}$ neutron orbit decrease gradually as the number of neutrons in the nucleus increases from 30 to 50. The $1g_{9/2}$ neutron orbit is almost empty at $N = 30$ and 32 and becomes slightly

filled in the region from N = 34 to 40, indicating the $1f_{5/2}$ and 2p subshells are being filled preferentially. For N > 40, the $1g_{9/2}$ shell is being filled rapidly, and is completely full at N = 50.

From the present results, the center of gravity of the excitations corresponding to the $2p_{1/2}$ neutron orbit is lower than that of the $1g_{9/2}$ orbit in both ^{80}Br and ^{82}Br. The energy differences, $\bar{E}(1g_{9/2}) - \bar{E}(2p_{1/2})$, are about 0.14 and 0.10 MeV for ^{80}Br and ^{82}Br. The $2p_{1/2}$ neutron orbit has been shown (table 20 and 22) to be almost half empty in ^{79}Br and about 70% full in ^{81}Br. These results are consistent with the values obtained for the neighboring nuclei.

Finally, the systematics of the low-lying states of the odd-odd bromine isotopes in this region is shown in fig. 28 . The data for the other Br isotopes are taken from Houdayer (1972), Lederer et al. (1967), Artna (1966) and Auble (1971). From the present measurements, the low-lying 2^- state in both the ^{80}Br and ^{82}Br nuclei is being tentatively assigned with a neutron configuration of seniority three in the $1g_{9/2}$ shell. By systematics, this character may be extended to the other 2^- states which appear as the ground state in ^{84}Br and probably the 32 keV state in ^{78}Br and the 45 keV state in ^{76}Br. Similarly, the 1^+ low-lying states of these nuclei may belong to the same dominant configuration $[\pi(2p_{3/2})$ x

$\nu(2p_{1/2})]$, as discussed in the two preceding subsections. However, the 5^- states assigned to the $[\pi(2p_{3/2})$ x $\nu(1g_{9/2})]$ configuration in ^{80}Br and ^{82}Br have no observed counterpart in the other Br isotopes.

A paper based on the present work of the (d,p) reaction in ^{79}Br and ^{81}Br has been published in the Nuclear Physics Journal and a reprint of the article is given in Appendix.

FIGURE 22

The Proton Spectrum from the $^{79}Br(d,p)^{80}Br$ Reaction Obtained at $\theta_{lab} = 15^{o}$

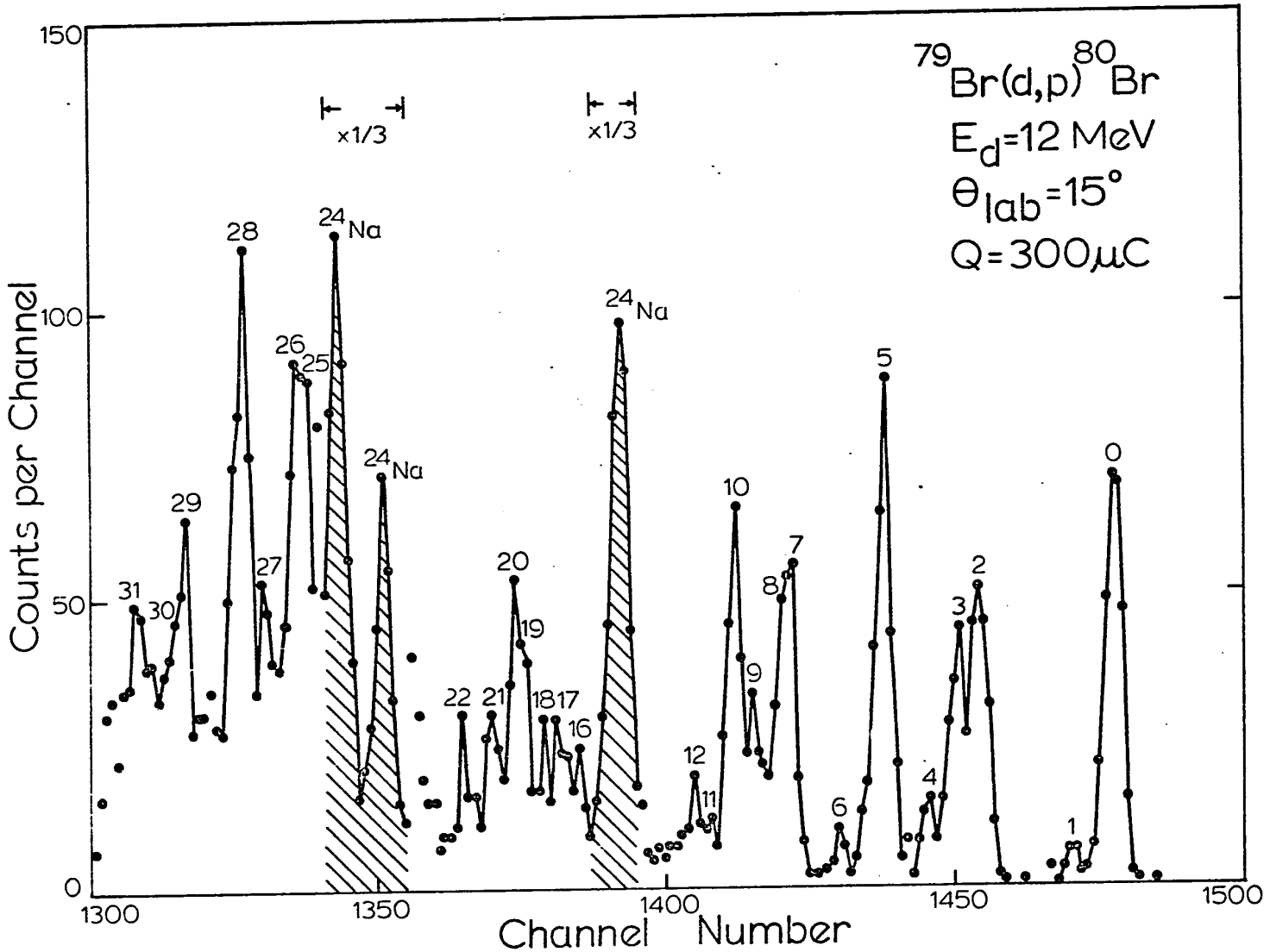
150
100
50
0
Counts per Channel
1300
1350
1400
1450
1500
Channel Number
79Br(d,p)80Br
Ed=12 MeV
θlab=15°
Q=300μC
x1/3
x1/3
24Na
24Na
24Na
31
30
29
28
27
26
25
22
21
20
19
18
17
16
12
11
10
9
8
7
6
5
4
3
2
1
0

FIGURE 23

The Proton Spectrum from the $^{81}Br(d,p)^{82}Br$ Reaction Obtained at $\theta_{lab} = 50^{o}$

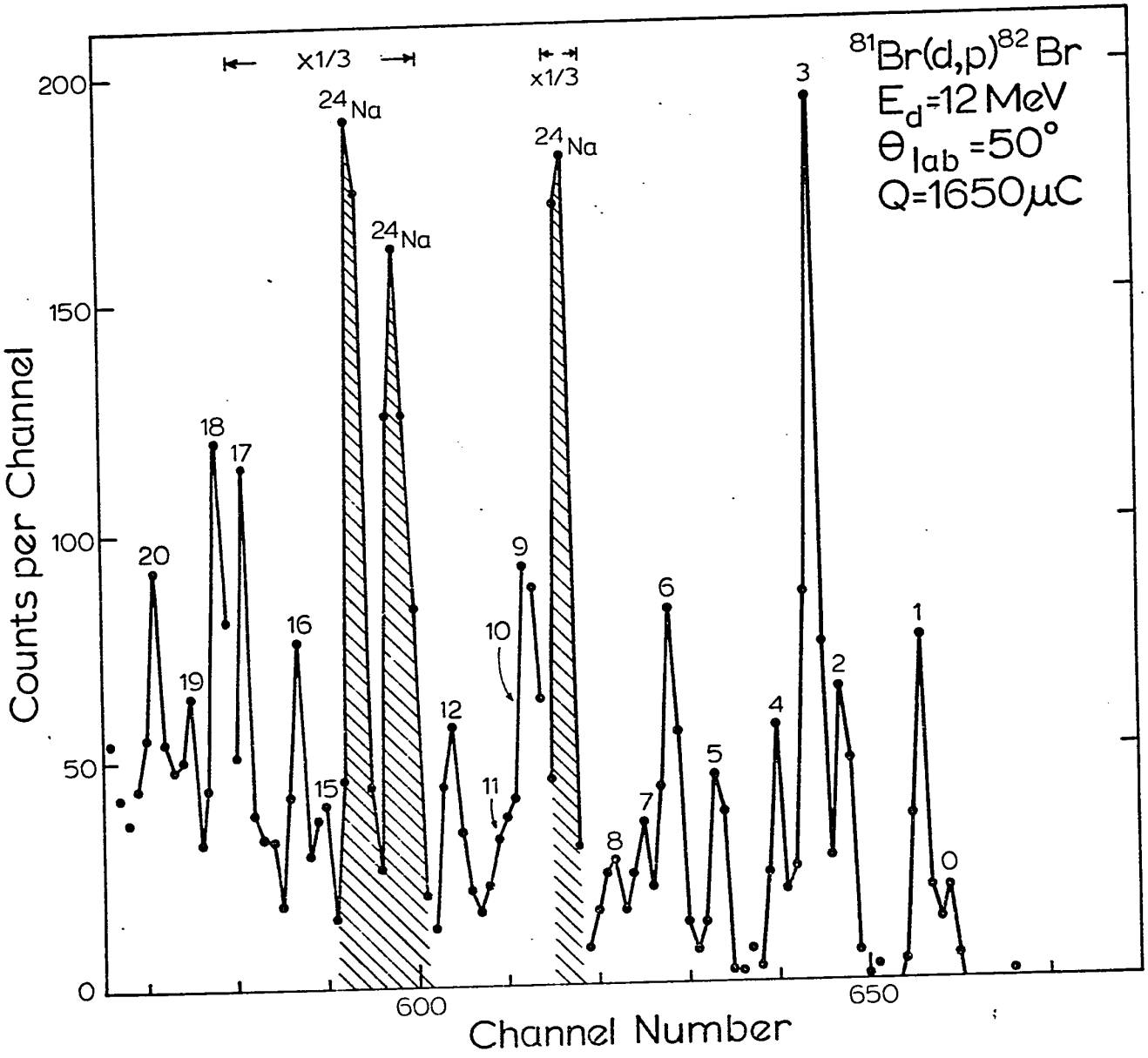
$^{81}Br(d,p)^{82}Br$
E_d=12 MeV
θ_{lab}=50°
Q=1650μC
x1/3
x1/3
^{24}Na
^{24}Na
^{24}Na
Counts per Channel
Channel Number
0
50
100
150
200
600
650
0
1
2
3
4
5
6
7
8
9
10
11
12
15
16
17
18
19
20

TABLE 15

Excitation Energies of Levels in ^{80}Br and their Excitation Differential Cross Sections Observed in the $^{79}Br(d,p)^{80}Br$ Reaction at 12 MeV.

Differential cross sections are given in the laboratory system. The total relative error of each differential cross section value and the uncertainty in each level energy are also given in this table and are being placed directly under their respective mean values with the significance of their digits having a one-to-one correspondence with those in the mean values. The total systematic error in the differential cross sections is ± 12%. Blank entries or 'Na' entries means data could not be extracted reliably or data were obscured by proton groups from the Na contaminant.

Group No.	Excitation energy (keV)	Differential cross section (μb/sr)													
		10°	15°	20°	25°	30°	35°	40°	45°	50°	55°	60°	70°	80°	90°
0	g.s.	490 55	776 44	572 35	306 32	132 23	117 22	158 30	206 23	135 16	80 10	33 9	63 12	35 6	34 5
1	84 4	35 14	48 13	60 12	54 12	75 15	83 12	63 12	80 12	51 9	15 5	20 5	37 12	25 6	13 3
2	266 2	443 58	514 22	405 51	254 35	199 25	209 21	167 28	168 7	114 19	70 16	76 18	30 10	53 10	25 8
3	314 2	308 40	366 37	312 45	228 33	119 24	209 24	202 32	172 34	103 21	84 17	64 21	30 10	40 10	32 8
4	368 4	90 17	110 18	160 27	191 23	215 27	278 21	359 36	342 34	216 22	147 18	113 19	119 24	107 17	79 9
5	461 3	556 72	744 47	683 41	569 41	379 38	249 36	285 40	245 29	244 22	188 7	126 25	75 15	66 9	36 6
6	547 4	35 10	55 14	59 16	35 10	48 21	67 13	69 17	23 10	33 11	15 17	13 7	27 10	13 7	6 4
7	653 4	405 53	544 50	369 45	223 30	62 22	123 20	127 21	110 17	82 20	72 11	45 15	15 10	21 7	8 5
8	691 4		204 24	200 24	148 22	122 18	96 15	89 16	44 10	67 14	74 11	59 10			
9	722 4		295 29	195 23	148 21	117 18	117 17	137 18	108 16	114 15	40 8	33 7		22 6	
10	759 4	466 50	598 57	401 45	302 33	55 20	97 16	135 24	134 25	97 15	93 14	45 7	26 7	21 7	28 10

Group No.	Excitation energy (keV)	Differential cross section (μb/sr)													
		10°	15°	20°	25°	30°	35°	40°	45°	50°	55°	60°	70°	80°	90°
11	810 5	24 13	28 10	22 7	27 9	20 8	22 8	17 7	29 8	25 7	26 66	13 5	6 4	7 4	11 5
12	835 5	80 22	110 18	82 15	63 13	23 8	19 7	29 8	15 7	26 7	15 5	111 4	6 4	3 2	3 2
13	974 6		Na	Na	Na	36 10	27 8	30 9	50 12	47 9	30 7	30 7	20 6		
14	1024 6		Na	Na	Na	180 25	99 15	80 14	63 13	55 10	70 11	53 9	50 9		
15	1048 6		Na	Na	Na	450 38	340 29	324 28	230 29	200 19	180 17	140 15	64 9		
16	1070 6		240 26	Na	Na	Na	50 11	42 10	70 14	41 9	62 18	35 7	41 8		
17	1116 6		231 25	240 26	Na	Na	110 16	63 13	53 10	83 12	44 8	30 7	24 6		
18	1139 7		233 27	147 20	Na	Na	Na	Na	122 17	68 11	70 11	30 7	24 6		
19	1174 7						Na	Na		90 13	68 10	70 11	30 7		
20	1201 7	535 60	549 68	640 65	494 55	378 44	Na	Na	84 10	210 18	150 14	107 12	94 8	20 4	18 4
21	1244 7	250 29	120 18	110 17	94 16	93 15	Na	Na	71 13	82 12	59 10	30 7	44 9		

Group No.	Excitation Energy (keV)	Differential Cross Section (μb/sr)													
		10°	15°	20°	25°	30°	35°	40°	45°	50°	55°	60°	70°	80°	90°
22	1301		250	190	230	150	130	Na	Na	54	48	35	70		
	7		26	23	25	21	18			10	9	8	10		
23	1401		Na	273	400	543	677	270	156	Na	Na	77	59		
	8			30	38	38	40	29	25			11	9		
24	1594		Na	Na	Na	Na	300	278	140	211	255	Na	Na		
	8						47	37	19	27	34				
25	1637		350	Na	Na	Na	Na	Na	200	183	Na	Na	Na		
	8		441						27	23					
26	1665		358	Na	Na	Na	Na	Na	215	167	Na	Na	Na		
	8		50						29	24					
27	1702		200	200	258	Na	Na	Na	Na	70	82	Na	Na	20	
	8		24	23	26					11	14			5	
28	1746	405	718	822	765	425	Na	Na	Na	278	283	152	Na	32	41
	8	51	70	80	85	43				30	35	19		10	12
29	1857		400	378	450	251									
	8		133	132	135	106									
30	1880		132	150	150	135									
	8		39	40	36	24									
31	1953		250	253	300	310									
	8		136	102	128	113									

TABLE 16

Excitation Energies of Levels in ^{82}Br and Their Excitation Differential Cross Sections Observed in the ^{81}Br(d,p)^{82}Br Reaction at 12 MeV.

Differential cross sections are given in the laboratory system. The total relative error of each differential cross section value and the uncertainty in each level energy are also given in this table and are being placed directly under their respective mean values with the significance of their digits having a one-to-one correspondence with those in the mean values. The total systematic error in the differential cross sections is ±12%. Blank entries or 'Na' entries means data could not be extracted reliably or data were obscured by proton groups from the Na contaminant.

Group No.	Excitation energy (keV)	Cross section (μb/sr)																	
		12.5°	15°	17.5°	22.5°	25°	27.5°	30°	35°	40°	45°	50°	55°	60°	65°	70°	75°	80°	85°	95°
0	g.s.	13 10	38 12	29 13	26 12	20 10	40 13	29 5	48 8	53 11	31 10	30 5	5 3	7 3	6 3	18 4	22 3	10 2	10 3	4 1
1	78 4	538 50	518 25	430 35	266 50	217 20	57 17	102 8	110 11	125 20	146 20	102 10	37 10	35 10	44 6	20 4	25 4	20 3	23 4	14 2
2	293 4	77 5	52 12	29 14	71 28	48 12	58 15	80 15	91 15	110 20	103 20	87 10	41 7	31 5	34 7	40 6	39 4	28 5	37 4	18 3
3	377 4	586 60	575 55	415 35	373 30	302 30	138 23	232 30	264 30	299 30	346 30	281 30	157 12	116 16	110 10	103 10	119 7	92 20	97 6	50 4
4	476 4	45 20	34 15	108 20	67 21	49 13	51 20	61 12	72 15	81 17	75 17	63 20	28 8	27 6	27 5	27 6	39 4	34 4	30 4	17 3
5	638 4	Na	Na	Na	Na	80 15	60 15	54 25	60 25	75 12	82 10	80 8	38 7	50 10	25 6	21 4	24 4	15 5	10 5	7 5
6	771 4	377 60	463 100	447 43	Na	Na	Na	Na	57 30	84 30	113 12	116 10	84 10	37 8	76 10	38 4	19 4	27 5	43 6	10 6
7	845 5	53 22	89 30	91 30	Na	Na	Na	Na	Na	80 27	36 9	32 5	30 10	20 7	26 7	6 4	21 7	17 7	14 5	11 5
8	959 7	Na	Na	44 22	Na	70 17	Na	Na	Na	Na	Na	26 5	21 5	16 7	26 7	29 10	12 5	9 3	13 4	8 3
9	1138 7	Na	Na	Na	Na	Na	Na	Na	60 36	78 40	116 50	Na	Na	Na	56 30	38 19	46 22	19 10	33 17	16 8
10	1180 8	Na	Na	Na	Na	Na	Na	Na	86 40	40 30	92 40	Na	Na	Na	Na	17 8	27 10	30 10	24 10	11 6

Group No.	Excitation energy (keV)	Cross section (μb/sr)																	
		12.5°	15°	17.5°	22.5°	25°	27.5°	30°	35°	40°	45°	50°	55°	60°	65°	70°	75°	80°	85°	95°
11	1246 8	Na	Na	Na	Na	Na	Na	Na	Na	39 19	55 27	Na	Na	Na	Na	Na	Na	16 8	15 7	6 3
12	1386 7	154 25	164 29	150 22	Na	Na	Na	Na	Na	Na	44 14	64 15	20 7	22 5	31 15	Na	Na	21 10	26 12	6 3
13	1497 8	1628 213	1581 188	1180 225	1387 149	1502 150	830 104	1622 210	1140 213	Na	Na	Na	317 55	269 55	361 55	216 25	Na	Na	141 19	54 11
14	1650 8	1342 94	1428 145	1324 227	1582 162	1595 133		1396 251	901 100	392 66	483 49	Na	Na	Na	376 47	186 41	Na	Na	116 38	83 39
15	1743 8	515 85	376 60	58 15	58 15	223 38		346 171			99 30	147 40	Na	Na	Na	40 22	Na	Na	Na	Na
16	1807 8	374 71	413 69	469 73	432 68	528 70		551 154	292 71	219 64	207 35	260 38	Na	Na	Na	92 30	Na	55 21	36 10	41 13
17	1955 8	660 138	763 110	611 157	655 146	1227 250		1168 230	486 128	276 60	403 39	440 45	240 29	151 32	320 45	Na	Na	110 37	128 33	55 30
18	2026 9					344 97		235 85			103 25	118 35		89 30	95 32					
19	2112 9							95 31			66 24	50 21		18 10	10 5					
20	2212 9							254 103			104 48	85 39		26 13	42 20					

TABLE 17

Potential Parameters Used in the DWBA Calculations for the $^{79,81}Br(d,p)^{80,82}Br$ Reactions

Particle	V (MeV)	r_r (fm)	a_r (fm)	W_V (MeV)	W_D (MeV)	r_i [b] (fm)	a_i [b] (fm)	V_{so} (MeV)
Deuteron (Set I)	83.9	1.35	0.57	12.7		1.30	1.0	
(Set II)	89.95	1.23	0.73		14.65	1.25	0.79	
Proton (Set I)	47.7	1.27	0.55	10.0		1.27	0.55	
(Set II)	51.72	1.17	0.63		8.035	1.31	0.65	
Neutron (Bound State) [a]	V	1.20	0.682					7.0

a) The potential depth V of the bound state was adjusted to reproduce the separation energy for each final state. $r_{so} = r_r$, $a_{so} = a_r$.

b) $r_i = r_V$, $a_i = a_V$ in Set I, and $r_i = r_D$, $a_i = a_D$ in Set II.

FIGURE 24

Predicted Angular Distributions in the (d,p) Reactions Given by the DWBA for Different ℓ-Transfer Values

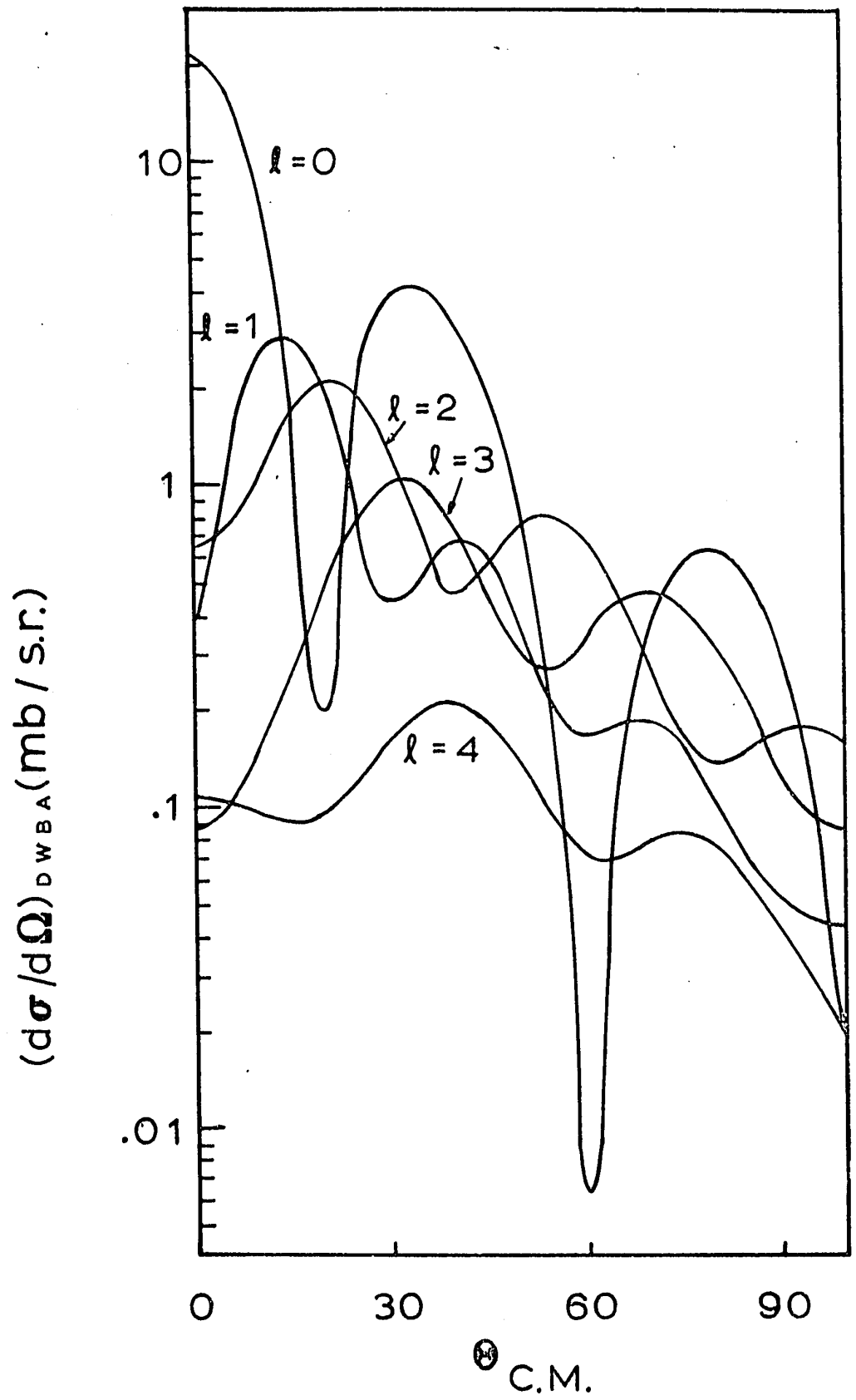
10
1
.1
.01
ℓ = 0
ℓ = 1
ℓ = 2
ℓ = 3
ℓ = 4
0
30
60
90
Θ C.M.
(dσ/dΩ)DWBA(mb/s.r.)

FIGURE 25

Proton Angular Distributions Observed in the ^{79}Br $(d,p)^{81}Br$ Reaction and Their DWBA Analysis

The solid curves refer to potential parameter set I and the dashed curves refer to set II of table 17 . The numbers in the upper right corner represent the level number, ℓ -transfer values and excitation energies in ^{80}Br.

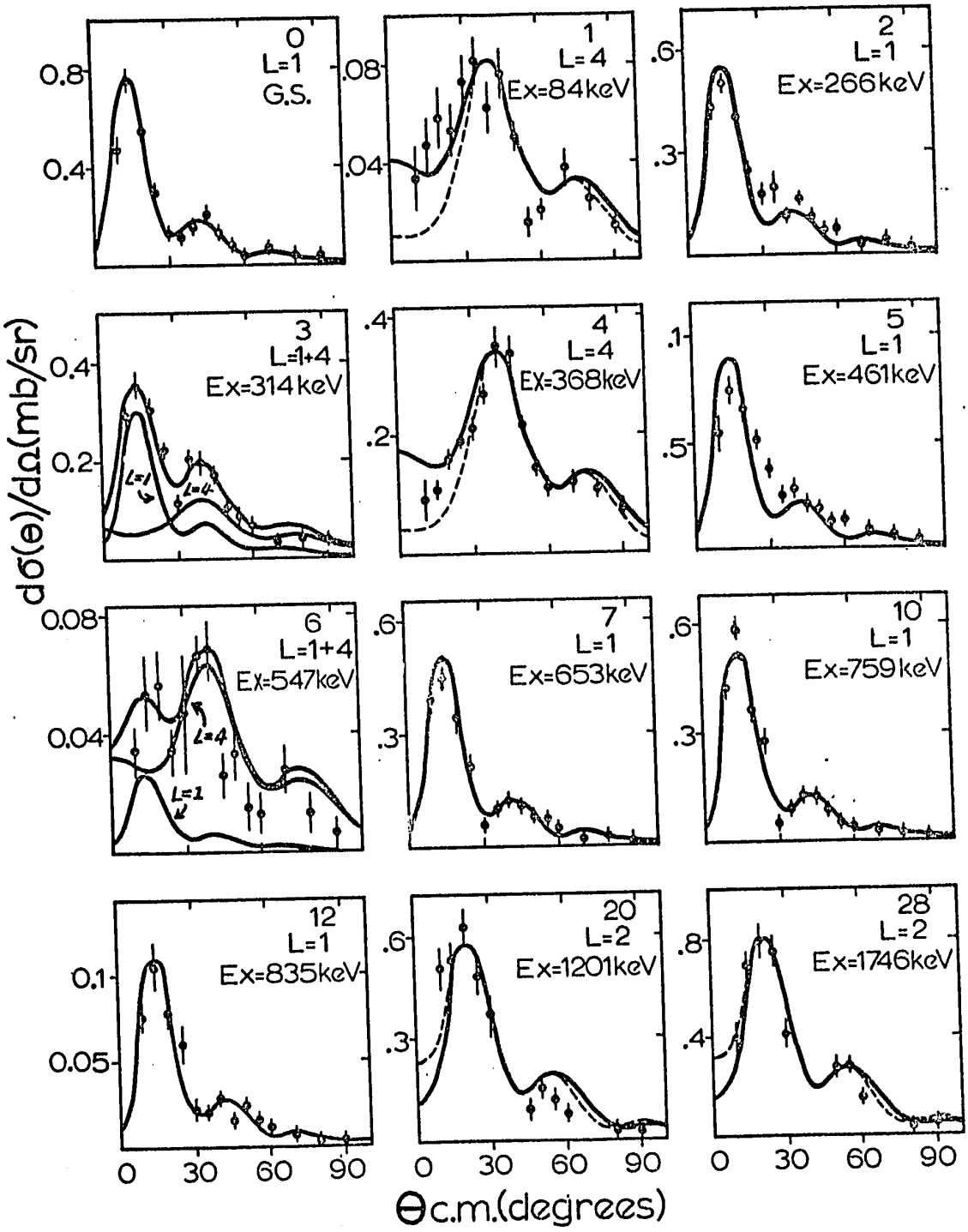
0
L=1
G.S.
1
L=4
Ex=84keV
2
L=1
Ex=266keV
3
L=1+4
Ex=314keV
L=1
L=4
4
L=4
Ex=368keV
5
L=1
Ex=461keV
6
L=1+4
Ex=547keV
L=4
L=1
7
L=1
Ex=653keV
10
L=1
Ex=759keV
12
L=1
Ex=835keV
20
L=2
Ex=1201keV
28
L=2
Ex=1746keV
dσ(θ)/dΩ(mb/sr)
θc.m.(degrees)
0
30
60
90

FIGURE 26

Proton Angular Distributions Observed in the ^{81}Br $(d,p)^{82}Br$ Reaction and Their DWBA Analysis

The solid curves refer to potential parameter set I and the dashed curves refer to set II of table 17. The numbers in the upper right corners represent the level number, ℓ-transfer values and excitation energies in ^{82}Br.

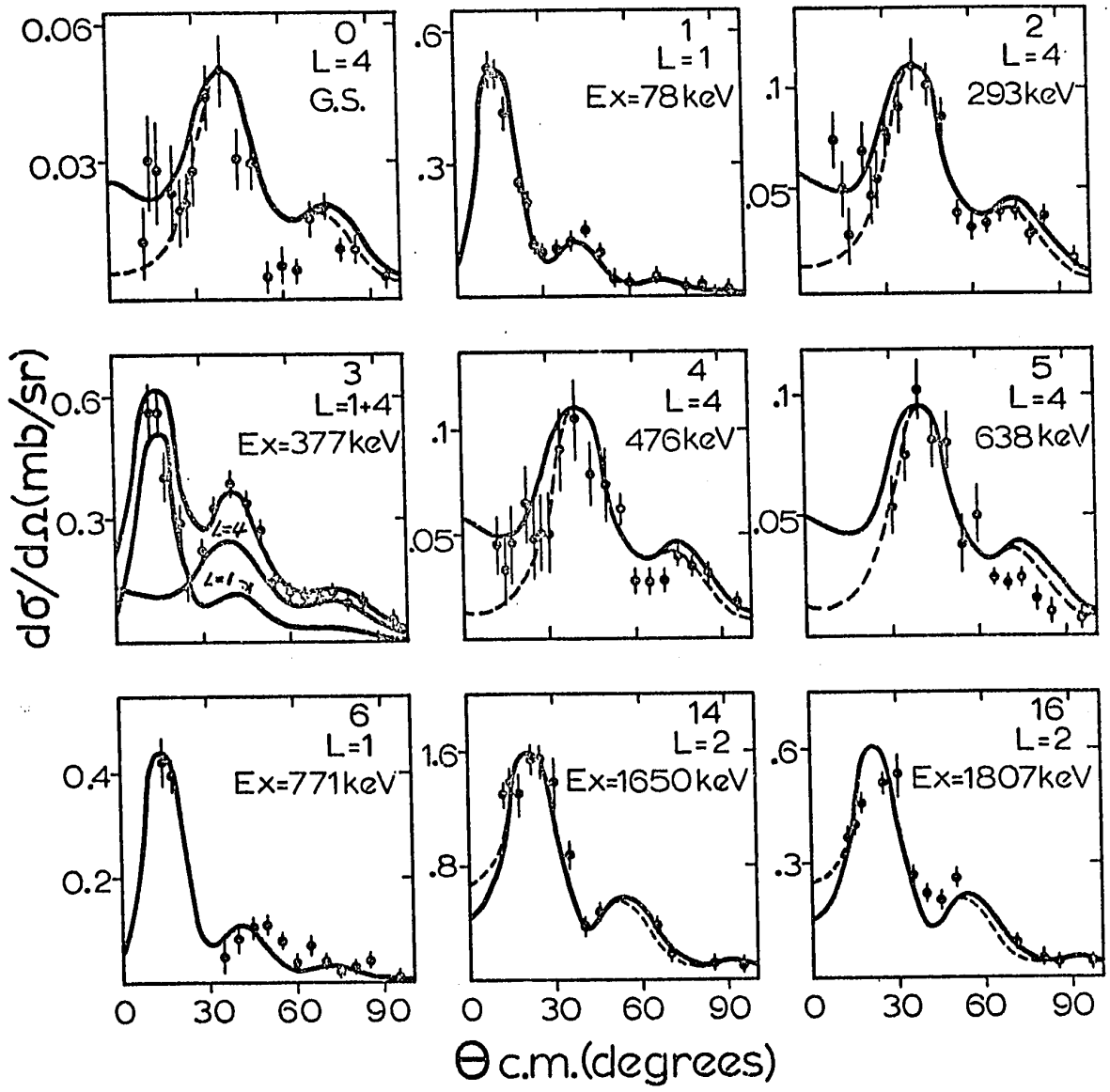
0
L=4
G.S.
1
L=1
Ex=78keV
2
L=4
293keV
3
L=1+4
Ex=377keV
L=4
L=1
4
L=4
476keV
5
L=4
638keV
6
L=1
Ex=771keV
14
L=2
Ex=1650keV
16
L=2
Ex=1807keV
dσ/dΩ(mb/sr)
Θ c.m.(degrees)

TABLE 18

Spectroscopic Information Obtained from the DWBA Analysis of the $^{79}Br(d,p)^{80}Br$ Reaction

LEVEL	EXCITATION ENERGY (keV)	ℓ	$\frac{2J_f + 1}{2J_i + 1} S$ SET I	SET II	J^π
0	0	1	0.26	0.32	1^+
1	84	4	0.49	0.39	5^-
2	266	1	0.16	0.20	$(1,2)^+$
3	314	1	0.40	0.49	$(1,2)^+$
		4	0.75	0.60	$(4)^-$
4	368	4	1.98	1.59	$(6)^-$
5	461	1	0.25	0.30	$(0,1,2,3)^+$
6	547	1	0.01	0.01	$(0,1,2,3)^+$
		4	0.36	0.29	$(3)^-$
7	653	1	0.14	0.17	$(0,1,2,3)^+$
8	691	(2)	(0.10)	(0.09)	
9	722	(1)	(0.09)	(0.11)	
10	759	1	0.15	0.18	$(0,1,2,3)^+$
11	810	-			
12	835	1	0.03	0.04	$(0,1,2,3)^+$
13	974	-			
14	1024	-			
15	1048	-			
16	1070	-			
17	1116	(1,2)			
18	1139	(1)	(0.07)	(0.09)	
19	1174	-			
20	1201	2	0.30	0.28	$(1,2,3,4)^-$
21	1244	(1,2)			
22	1301	(1,2)			
23	1401	-			
24	1594	-			
25	1637	-			
26	1665	-			
27	1702	(2)	(0.11)	(0.09)	
28	1746	2	0.39	0.33	$(1,2,3,4)^-$
29	1857	(1,2)			
30	1880	(2)	(0.13)	(0.13)	
31	1953	-			

TABLE 19

Spectroscopic Information Obtained from the DWBA Analysis of the $^{81}Br(d,p)^{82}Br$ Reaction

LEVEL	EXCITATION ENERGY (keV)	ℓ	$\frac{2J_f + 1}{2J_i + 1} S$ SET I	SET II	J^π
0	0	4	0.30	0.24	5^-
1	78	1	0.16	0.20	$(1.2)^+$
2	293	4	0.63	0.52	$(3,4,5,6)^-$
3	377	1	0.40	0.50	$(1,2)^+$
		4	0.22	0.18	$(3,4,5,6)^-$
4	476	4	0.59	0.49	$(3,4,5,6)^-$
5	638	4	0.55	0.46	$(3,4,5,6)^-$
6	771	1	0.13	0.16	$(0,1,2,3)^+$
7	845	(1.2)			
8	959	(3,4)			
9	1138	-			
10	1180	-			
11	1246	-			
12	1386	(1)	(0.05)	(0.06)	
13	1497	(2)	(0.71)	(0.68)	
14	1650	2	0.69	0.66	$(1,2,3,4)^-$
15	1743	(0)	(0.09)	(0.09)	$(1,2)^-$
16	1807	2	0.25	0.24	$(1,2,3,4)^-$
17	1955	(2)	(0.53)	(0.51)	
18	2026	-			
19	2112	-			
20	2212	-			

TABLE 20

Sum Rule Analysis for Some N = 44 Nuclei

NUMBER OF NEUTRON HOLES IN / REACTION	$1\,g_{9/2}$	$2\,p_{1/2}$
$^{78}Se(d,p)^{79}Se$ a)	4.10	0.82
$^{79}Br(d,p)^{80}Br$ b)	3.58 i)	0.82 i)
	2.87 ii)	1.10 ii)
Maximum number of holes	6	2

i) Set I optical parameters

ii) Set II optical parameters

a) Taken from Lin (1965)

b) Present work

TABLE 21

A Comparison of States in ^{80}Br below 2 MeV of Excitation Observed in Different Works

References:- a) Finckh *et al.* 1970

b) present work

c) Artna 1966

$^{80}Se(p,n)^{80}Br$ a)	$^{79}Br(d,p)^{80}Br$ b)		NUCLEAR DATA c)	
Ex (keV)	Ex (keV)	J^π	Ex (keV)	J^π
0	0	1^+	0	1^+
			37	2^-
35	84	5^-	85	5^-
			250	
253				
269	266	$(1,2)^+$		
310	314	$(4)^-,(1,2)^+$		
326				
366	368	$(6)^-$		
381				
465	461	$(1,2,3)^+$		
490				
546	547	$(3)^-,(0,1,2,3)^+$		
582				
610				
655	653	$(0,1,2,3)^+$		
684	691			
722	722			
733				
760	759	$(0,1,2,3)^+$		
808	810			
824				
849	835	$(0,1,2,3)^+$	840	
878				
907				
	974			
	1024			
	1048			
	1070			
	1116			
	1139			
	1174			
	1201	$(1,2,3,4)^-$	1210	
	1244			
	1301			
	1401			
	1594			
	1637			
	1665			
	1702			
	1746	$(1,2,3,4)^-$		
	1857			
	1880			
	1953		1930	

TABLE 22

Sum Rule Analysis for Some N = 46 Nuclei

NUMBER OF NEUTRON HOLES IN / REACTION	$1g_{9/2}$	$2p_{1/2}$
$^{80}Se(d,p)^{81}Se$ a)	2.83	0.60
$^{84}Sr(d,p)^{85}Sr$ b)	3.06 i)	0.40 i)
	2.23 ii)	0.49 ii)
$^{84}Sr(d,p)^{85}Sr$ c)	2.09	0.54
$^{81}Br(d,p)^{82}Br$ d)	2.27 i)	0.56 i)
	1.70 ii)	0.70 ii)
Maximum number of holes	4	2

i) Set I optical parameters

ii) Set II optical parameters

Ref.:- a) Lin (1965)

b) Morton et al. (1971)

c) Bercaw and Warner (1970)

d) Present work.

TABLE 23

A Comparison of States in ^{82}Br Below 2 MeV Excitation Energy Observed in Different Works

References:- a) Finckh *et al.* (1970)
b) present work
c) Artna (1966)

$^{82}Se(p,n)^{82}Br$ a)	$^{81}Br(d,p)^{82}Br$ b)		NUCLEAR DATA c)	
Ex (keV)	Ex (keV)	J^π	Ex (keV)	J^π
	0	5^-	0	5^-
			46	2^-
	78	$(1,2)^+$		
70	293	$(3,4,5,6)^-$	300	
295	377	$(1,2),(3,4,5,6)^-$		
368				
425	476	$(3,4,5,6)^-$		
477				
548	638	$(3,4,5,6)^-$		
646				
692	771	$(0,1,2,3)^+$		
772				
830	845			
856				
934	959		950	
975				
993				
1027				
1062				
1082				
1116	1138			
1159	1180			
1190	1246			
1243				
1284	1386			
1374				
1391				
1440				
1486	1497		1540	
1497				
1543				
1556	1650	$(1,2,3,4)^-$		
1637				
1686	1743			
1729				
1758				
1782	1807	$(1,2,3,4)^-$		
1815				
1838				
1874				
1905				
1924				
1950	1955			

FIGURE 27

Fractional Emptiness of the $1g_{9/2}$ Neutron Orbit in Nuclei with $30 \leq N \leq 50$

References:- a) Cosman et al. (1966,1967)

b) Turiewicz et al. (1970)

c) Von Ehrenstein and Schiffer (1970)

d) Goldman (1968)

e) Fournier et al. (1972)

f) Lin (1965)

g) present work

h) Bercaw and Warner (1970)

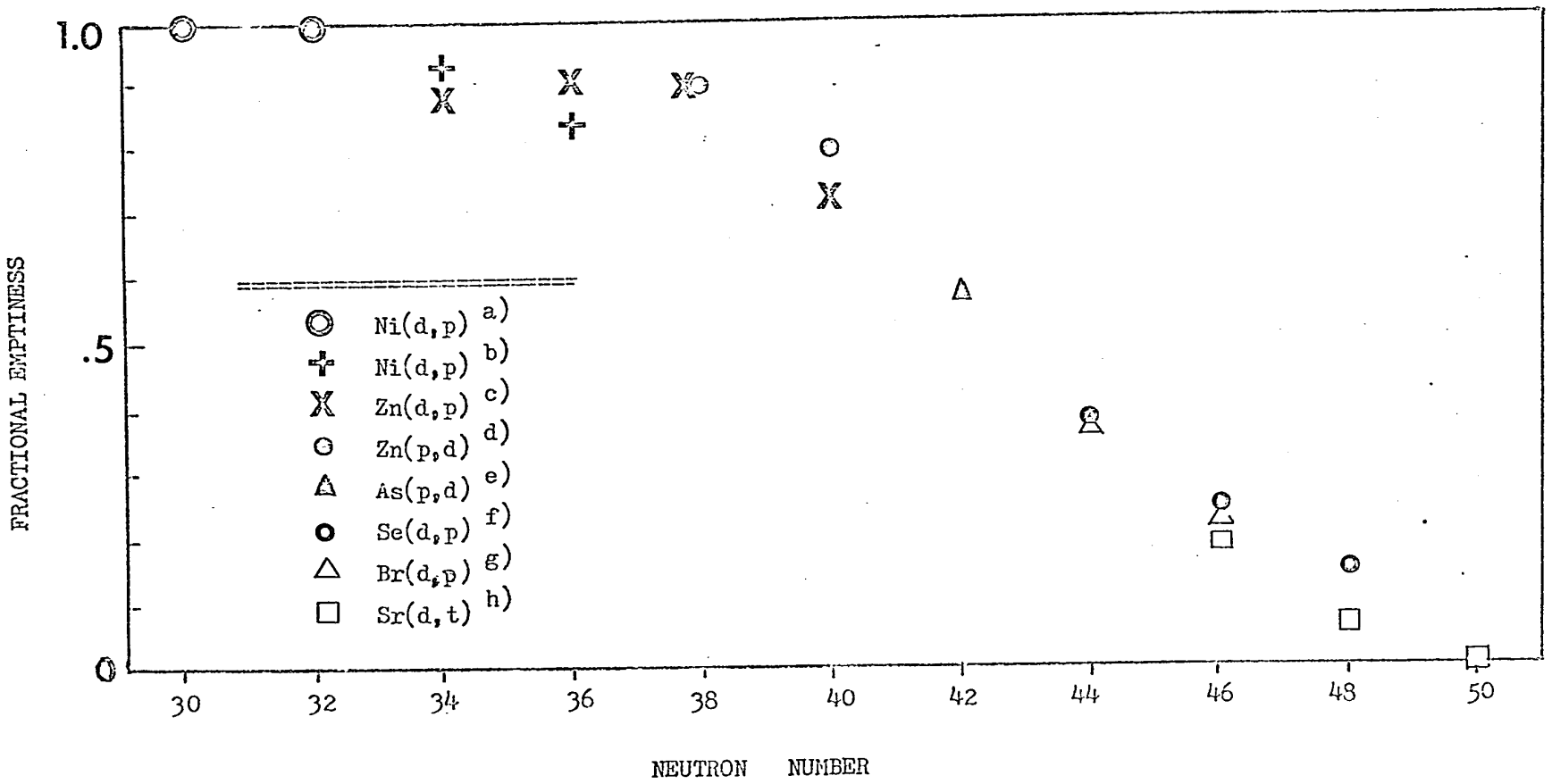
1.0
.5
0
FRACTIONAL EMPTINESS
30
32
34
36
38
40
42
44
46
48
50
NEUTRON NUMBER
Ni(d,p) a)
Ni(d,p) b)
Zn(d,p) c)
Zn(p,d) d)
As(p,d) e)
Se(d,p) f)
Br(d,p) g)
Sr(d,t) h)

FIGURE 28

Systematics of Low-lying States in the Odd-Odd Br Isotopes

References:- a) Houdayer (1972)
b) Lederer et al. (1967)
c) Artna (1966); present work
d) Auble (1971)

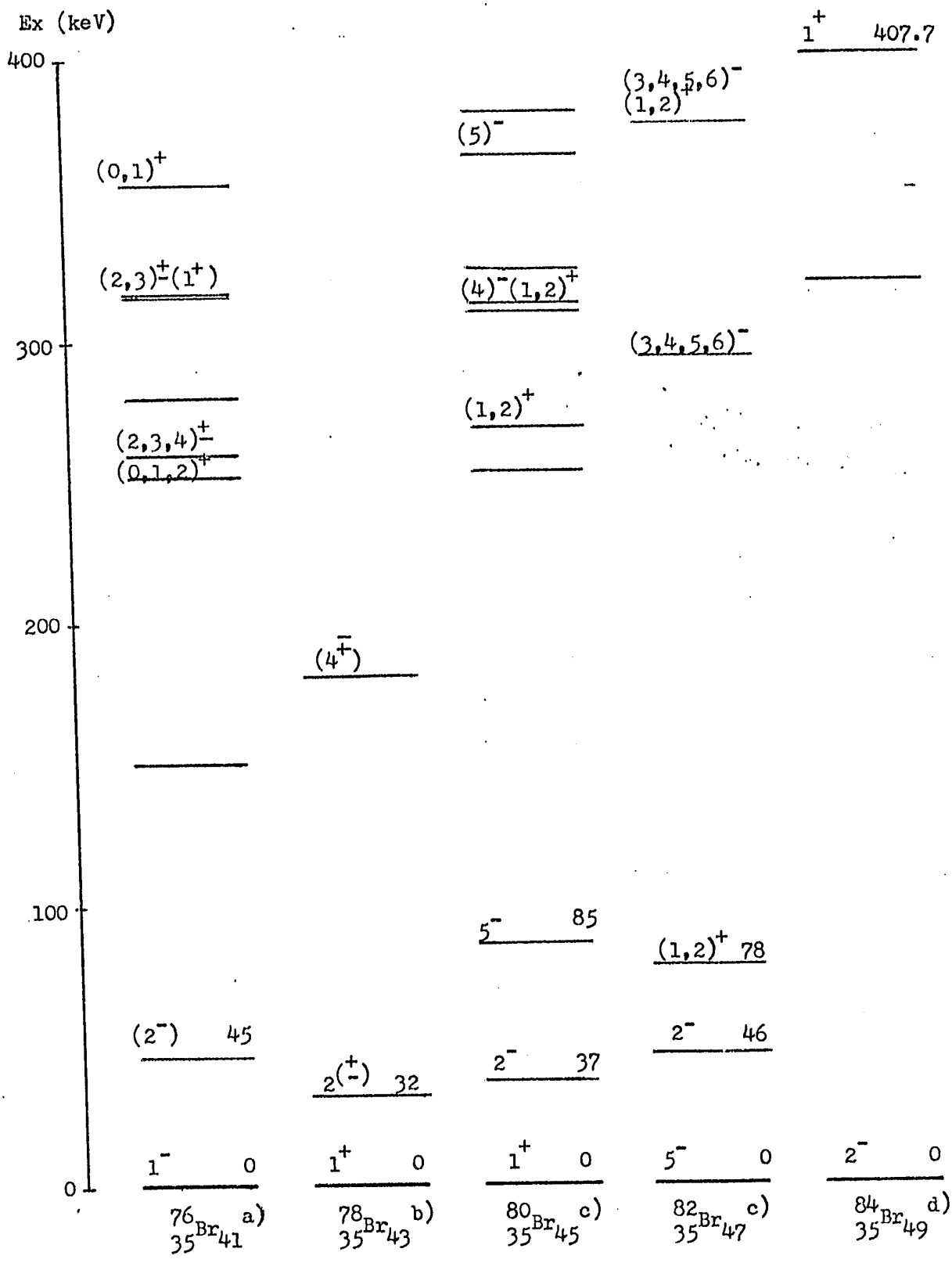
Ex (keV)
400
300
200
100
0
(0,1)+
(2,3)±(1+)
(2,3,4)±
(0,1,2)+
(2−) 45
1− 0
76Br41 a)
(4±)
2(±) 32
1+ 0
78Br43 b)
(5)−
(4)−(1,2)+
(1,2)+
5− 85
2− 37
1+ 0
80Br45 c)
(3,4,5,6)−
(1,2)+
(3,4,5,6)−
(1,2)+ 78
2− 46
5− 0
82Br47 c)
1+ 407.7
2− 0
84Br49 d)

CHAPTER V

SUMMARY AND CONCLUSIONS

The (^{3}He,d) proton stripping reactions on Mo-94,96,98 and 100 and the (d,p) neutron stripping reactions on Br-79 and 81 have been studied. The measurements on the ^{94,96,100}Mo(^{3}He,d)^{95,97,101}Tc reactions and ^{79,81}Br (d,p)^{80,82}Br reactions were performed with the 18 MeV helium-3 beam and the 12 MeV deuteron beam, respectively, from the EN tandem Van de Graaff accelerator at the University of Montreal; the measurements on the ^{98}Mo (^{3}He,d)^{99}Tc reaction were carried out using the helium-3 beam from the FN tandem Van de Graaff accelerator at McMaster University at an incident energy of 18 MeV. In the set up for the measurements conducted at the University of Montreal, two silicon detector ΔE-E telescopes were employed simultaneously in the detection of the outgoing deuterons and protons from these two types of reactions. Each telescope was coupled to a complete electronics system for charged particle identification and data accumulation. Two 'range-energy' type electronic charged particle identifiers have been constructed and found to perform very well in differentiating signals from various kinds of charged particles.

In the measurements performed at McMaster University the outgoing deuterons were analysed by an Enge split-pole broad range magnetic spectrograph and recorded in nuclear emulsion plates. The isotopically enriched molybdenum and bromine targets of thickness of about 100 $\mu g/cm^2$ each, used in the experiments were fabricated using techniques of high vacuum evaporation on thin carbon foil backings.

Spectra for each of these six reaction experiments were taken at different scattering angles in the forward hemisphere, and the peaks corresponding to different particle groups in the spectra were extracted using a Gaussian-curve-fitting computer program. In total, 198 states in $^{95,97,99,101}Tc$ and $^{80,82}Br$ have been identified, and most of them are observed for the first time. Angular distributions of the transitions to these states were analysed with the theoretical calculations using the distorted wave Born approximation, which led to a determination of 127 orbital angular momentum transfer values, and in many cases led to unique spin-parity J^{π} assignments for the levels.

The properties of low-lying states in the odd-mass Tc isotopes have been studied systematically using the (^{3}He,d) reactions. From the present work, thirty-eight levels below 4.8 MeV excitation energy in ^{95}Tc, thirty-two levels below 3.3 MeV excitation energy in ^{97}Tc,

fifty-eight levels below 3.5 MeV excitation energy in ^{99}Tc and seventeen levels below 1.8 MeV excitation energy in ^{101}Tc have been identified. The transferred proton orbital angular momenta and spectroscopic factors for these transitions have been obtained from the DWBA analysis of the deuteron angular distributions. It has been found that in each case the stripped proton occupies one of the following single particle orbital: $1g_{9/2}$, $2p_{1/2}$, $2p_{3/2}$ and $1f_{5/2}$ in the major shell $28 < Z \leq 50$; $2d_{5/2}$, $1g_{7/2}$, $2d_{3/2}$ and $3s_{1/2}$ in the major shell $50 < Z \leq 82$. The deduced spin-parity and other spectroscopic information on each level have been compared with other previously obtained experimental results from the studies of beta-gamma spectroscopy, Coulomb excitation, (p,n), (p,nγ) and (d,n) reactions (Riley et al. 1971, Bommer et al. 1971, Tucker et al. 1970, Kim et al. 1970 and 1971, Phelps et al. 1971, Cook et al. 1969, 1970 and 1972, Picone et al. 1972, Bond et al. 1972) in these nuclei.

In ^{95}Tc, the transitions to the ground state and the 0.04 MeV state characterized by $\ell = 4$ and 1, are consistent with the previously determined spin-parity values $9/2^+$ and $1/2^-$, respectively. For the higher lying levels, the spin-parity values established from the present work, are: $(\underline{3/2}, 1/2)^-$ for the states at 0.629, 1.201, 1.620, 1.733 and 2.550 MeV excitation energies. The underlined value represents the most probable spin.

$(5/2, 3/2)^+$ for the states at 1.071, 1.264, 1.416, 2.077, 2.257, 2.308, 2.696, 2.816, 3.401, 3.481, 4.180 and 4.254 MeV excitation energies; and, $1/2^+$ for the states at 2.763, 3.119, 3.197 and 3.339 excitation energies. Among them, some strongly excited states were found in good agreement with the results obtained from the previous work using (d,n) reactions. Levels with questionable assignments are given in praentheses in table 8.

In Tc-97, the ℓ -transfer values for the ground state, 0.096, 0.326, 0.576, 0.655 and 0.783 MeV excited states from the present work, are consistent with previously determined J^π values of $9/2^+$, $1/2^-$, $5/2^+$, $3/2^-$, $5/2^-$ and $5/2^+$ for these levels. For the other states, the J^π values established, are:

$(3/2, 1/2)^-$ for the 0.947, 1.053 MeV states;

$(5/2, 3/2)^+$ for the 1.374, 1.599, 1.649, 1.951, 2.013, 2.111, 2.307, 2.713, 2.783, 2.878, 2.908, 3.018, 3.060 MeV states;

$(7/2, 9/2)^+$ for the 1.316 MeV state;

$1/2^+$ for the 1.537, 1.712, 1.847, 2.151, 2.264, 2.653, 3.145 and 3.214 MeV states.

The spin-parity assignments for the strongly excited levels agree well with the results from the corresponding (d,n) reaction. Levels with doubtful assignments are given in parentheses in table 9.

In Tc-99, the ℓ -transfer values for the ground

state, 0.142, 0.181, 0.509, 0.672, 0.762 MeV states are consistent with the previously determined J^{π} values of $9/2^+$, $1/2^-$, $5/2^+$, $3/2^-$, $5/2^-$ and $5/2^+$ for these levels. For the other states, the spin-parity values established from the present reaction are:

$(\underline{3/2}, 1/2)^-$ for the states at 1.203 and 1.321 MeV excitation energies;

$(7/2, 9/2)^+$ for the states at 0.625 and 0.720 MeV excitation energies;

$(\underline{5/2}, 3/2)^+$ for the states at 1.020, 1.435, 1.679, 1.760, 1.825, 1.911, 1.982, 2.000, 2.111, 2.160, 2.176, 2.203, 2.396, 2.414, 2.522 and 2.581 MeV excitation energies;

$1/2^+$ for the states at 0.919, 1.560, 1.803, 2.176, 2.281, 2.466, 2.486, 2.653 and 2.675 MeV excitation energies.

Other levels with doubtful assignments are given in parentheses in table 10.

In Tc-101, the transitions to the ground state, 0.207, 0.394 and 0.670 MeV states characterized by $\ell = 4$, 1, 3 and 3 transfers, are consistent with the previously determined spin-parity values of $9/2^+$, $1/2^-$, $5/2^-$ and $5/2^-$ for these levels. The $\ell = 2$ transitions for the 0.515 MeV and 1.319 MeV states restricted the J^{π} values for these levels to $5/2^+$ and $3/2^+$, respectively, by taking into consideration the tentative J^{π} assignments of $(5/2^+, 7/2^+)$ and $(1/2^+, 3/2^+)$ to these levels by Cook

and Johns (1972). For the other states, the J^{π} values established from the present work are:

$(5/2, 3/2)^{+}$ for 1.280, 1.429, 1.490, 1.578, 1.703 MeV states;

$1/2^{+}$ for the 1.608 MeV state;

$(3/2, 1/2)^{-}$ for the 0.288, 0.620 and 1.045 MeV states. Other levels with doubtful assignments are given in parentheses in table 11.

These four reactions, ^{94,96,98,100}Mo(^{3}He,d) ^{95,97,99,101}Tc are characterized by a strong $\ell = 4$ and a strong $\ell = 1$ transitions to the ground state and the lowest-lying $1/2^{-}$ excited state of the odd-mass Tc isotopes, and by a large number of excited states resulting from varying degree of fragmentation of the single proton $2p_{3/2}$, 2d and 3s orbitals. No obvious evidence pointing to a deformed equilibrium shape for these odd-mass Tc isotopes has been observed, although their structural properties may be strongly influenced by the collective effects. The low-lying $7/2^{+}$ and $5/2^{+}$ states in these nuclei were not populated, or were only weakly excited in the (^{3}He,d) reactions, which is consistent with the contention that they are associated with phonon states or three quasi-particle states (for example, Cook et al. 1972). The distributions of proton holes in the target nuclei Mo-92,94,96,98 and 100 were deduced, the results were found to be in good agreement

with the results obtained from proton pick-up (d,^{3}He) reactions. The systematics of the major proton configurations in the ^{92,94,96,98,100}Mo ground states were obtained in the form of A $(g_{9/2})^2$ + B $(g_{9/2})^4(p_{1/2})^0$ + C$(g_{9/2})^4(p_{3/2})^{-2}$ + D$(g_{9/2})^4(f_{5/2})^{-2}$ from the spectroscopic results of the present measurements and those of Picard and Bassain (1969) for ^{92}Mo. The proton configuration thus deduced for the $9/2^+$ ground states of the odd-mass Tc nuclei was shown to be dominated by the $(g_{9/2})^5$ component.

It has been found from these reactions that as the number of neutrons in the target increases from 50 to 58, the transition strengths corresponding to the 2p and 1f shells are generally enhanced, and the spacing between the center of gravity energies of the $1g_{9/2}$ and the 2p proton orbits decreases rapidly. These properties appear to be characteristic of nuclei whose neutron number deviates more and more from a magic number.

No single strong transition has been observed for either $\ell = 2$ or 0 transfer in the reactions studied, except for the ^{94}Mo(^{3}He,d)^{95}Tc reaction in which a strong $\ell = 2$ transition seems to be evident. Such high fragmentation in these single particle orbits may arise from the spreading of the antianalogue states due to the effects of core-polarizations - as seen in the study of ^{90}Zr(^{3}He,d)^{89}Y (Vourvopoulos et al. 1969).

The low-lying states in ^{80}Br and ^{82}Br have been studied via the reactions ^{79,81}Br(d,p)^{80,82}Br at incident energy 12 MeV. Thirty-two levels below 2.0 MeV excitation energy have been identified in ^{80}Br and twenty-one levels below 2.2 MeV excitation energy have been identified in ^{82}Br. The results have been compared with those obtained from gamma decay (Artna 1966) and (p,n) reactions (Finckh et al. 1971). The orbital angular momenta transferred and the other spectroscopic information have been deduced from the DWBA analysis of the observed proton angular distributions. Four $\ell = 4$, eight $\ell = 1$ and two $\ell = 2$ transitions in the ^{79}Br(d,p)^{80}Br, reaction and five $\ell = 4$, three $\ell = 1$ and two $\ell = 2$ transitions in the ^{81}Br(d,p)^{82}Br reaction have been identified. Besides the J^{π} values of the ground state and 84 keV excited state in ^{80}Br and the ground state in ^{82}Br which were previously determined (Artna 1966), the other states whose J^{π} values are identified in this work are given below: ^{80}Br: $(1,2)^+$, 266 keV; $(1^+,2^+;4^-)$, 314 keV; $(6)^-$, 368 keV; $(0,1,2,3)^+$, 461 keV; $(0^+,1^+,2^+,3^+;3^-)$, 547 keV; $(0,1,2,3)^+$, 653 keV; $(0,1,2,3)^+$, 759 keV; $(0,1.2.3)^+$ 835 keV; $(1,2,3,4)^-$, 1201 keV; $(1,2,3,4)^-$, 1746 keV; and,

^{82}Br: $(1,2)^+$, 78 keV; $(3,4,5,6)^-$, 293 keV; $(1^+,2^+;3^-,4^-,5^-,6^-)$, 377 keV; $(3,4,5,6)^-$, 476 keV $(3,4,5,6)^-$, 638 keV; $(0,1,2,3)^+$, 771 keV; $(1,2,3,4)^-$,

1650 keV; $(1,2,3,4)^-$, 1807 keV.

From the present results, it is suggested that the low-lying states in ^{80}Br and ^{82}Br may arise from the coupling of a $2p_{3/2}$ proton with the stripped neutron captured in either the $1g_{9/2}$ or the $2p_{1/2}$ orbit. From the $2J+1$ dependence of the cross sections, the ordering of the states from the coupling of the $\left[\pi(2p_{3/2}) \times \nu(1g_{9/2})\right]_J$ in ^{80}Br was found, in the order of increasing excitation, $J^\pi = 5^-, 4^-, 6^-$ and 3^-. For both nuclei, the first excited state of $J^\pi = 2^-$, was not excited in the present reaction, which is consistent with the contention that they are associated with seniority three $1g_{9/2}$ neutrons coupled to a $2p_{3/2}$ proton. The existence of such states was observed in other nuclei in this mass region. From a sum rule analysis, the average numbers of neutron holes of the $1g_{9/2}$ and $2p_{1/2}$ orbits in the target nuclei Br-79 and 81 have been deduced, and agree very well with the previous experimental results obtained for the other $N = 44$ and 46 isotones.

REFERENCES

Ajzenberg-Selove, F. 1970. Nucl. Phys. A166 1.

Arnison, G.T.J. 1967. Atomic Weapons Research Establishment Report No. O-32/67.

Arseniev, D.A., Sobiczewski, A. and Soloviev, V.G. 1969. Nucl. Phys. A139 269.

Arima, A. 1966. Nucl. Data B, vol. 1, No. 4.

Auble, R.L. 1971. Nuclear Data Sheets vol. 5, no. 2.

Auerbach, N. and Talmi, I. 1965. Nucl. Phys. 64, 458.

Auerbach, T. and French, J.B. 1955. Phys. Rev. 98 1276.

Austern N. 1963. In Fast Neutron Physics II, edited by J.B. Marion and J.L. Fowler. (Interscience, New York) p. 1113.

Austern, N. 1969. Direct Nuclear Reaction Theories (Wiley-Interscience, New York).

Austern N., Drisko, R.M., Halbert, E.C. and Satchler, G.R. 1964. Phys. Rev. 133 B3.

Bassel, R.H. 1966. Phys. Rev. 149 791.

Bassel, R.H., Drisko, R.M. and Satchler, G.R. 1962. Oak Ridge National Laboratory Report No. ORNL - 3240.

Bercaw, R.W. and Warner, R.E. 1970. Phys. Rev. C2 297.

Bhatt, K.H. and Ball, J.B. 1965. Nucl. Phys. 63 286.

Brien, M. 1970. M.Sc. Thesis, McGill University, Montreal (Unpublished).

Bommer, J., Fuchs, H., Grabisch, K., Kluge, H. and Roschert, G. 1971. Nucl. Phys. A173 383.

Bond, P.D., May, E.C., Jha, S. 1972. Nucl. Phys. A179 389.

Burke, D.G. and Tippett, J.C. 1968. Nucl. Instr. and Meth. 63 353.

Burrows, H.B., Gibson, W.H. and Rotblat, J. 1950. Phys. Rev. 80 1095.

Butler, S.T. 1950. Phys. Rev. 80 1095.

Butler, S.T 1951. Proc. Roy. Soc. A208 559.

Castern, R.F., Flynn, E.R., Hansen, O. and Mulligan, T.J. 1972. Nucl. Phys. A184 357.

Cates, M.R., Ball, J.B. and Newman, E. 1969. Phys. Rev. 187 1682.

Cheifetz, E., Jared, R.C., Thompson, S.G. and Wilhelmy, J.B. 1970. Phys. Rev. Letts. 25 38.

Cohen, S., Lawson, R.D., MacFarlane, M.H. and Soga, M. 1964. Phys. Letts. 10 195.

Conjeaud, M., Hara, S. and Cassagnou, Y. 1968. Nucl. Phys. A117 449.

Cook, W.B. and Johns, M.W. 1972. Can. J. Phys. 50 1957.

Cook, W.B., Johns, M.W., Geiger, J.S. and Graham, R.L. 1972. Can. J. Phys. 50 1511.

Cook, W.B., Schellenberg, L. and Johns, M.W. 1969. Nucl. Phys. A139 277.

Cook, W.B., Schellenber, L. and Johns, M.W. 1970. Can. J. Phys. 48 217.

Cosman, E.R. 1966. Phys. Rev. 142 673.

Cosman, E.R., Schramm, D.N., Enge, H.A., Sperduto, A. and Paris, C.H. 1967. Phys. Rev. 163 1134.

Daum, C. 1963. Nucl. Phys. 45 273.

Deb, S. and Sen, J.K. 1961. Rev. Sci. Instr. 32 189.

De-Shalit, A. and Talmi, I. 1963. Nuclear Shell Theory (Academic Press, New York).

Diehl, R.C., Cohen, B.L., Moyer, R.A. and Goldman, L. H. 1970. Phys. Rev. C1 2132.

Drisko, R.M. and Satchler, G.R. 1964. Phys. Letts. 9 342.

Enge, H.A. and Smith, D.L. 1966. Massachusetts Institute of Technology Report No. 2098-276.

Finckh, E., Jahnke, U., Schreiber, B. and Weidinger, A. 1970. Nucl. Phys. A144 199.

Fisher, P.S. and Scott, D.K. 1967. Nucl. Instr. and Meth. 49 301.

Forster, J.S., Green, L.L., Henderson, N.W., Hutton,

J.L., Jones, G.D., Sharpey-Schafer, J.F., Graig, A.G. and Stephens, G.A. 1967. Nucl. Phys. A101 113.

Fournier, R., Hsu, T.H., Kroon, J., Hird, B. and Ball, G.C. 1972. Nucl. Phys. A188 632.

French, J.B. 1964. Argonne National Laboratory Report No. 6878, p. 181.

French, J.B. and Raz, B.J. 1956. Phys. Rev. 104 1411.

Giannetic, G. and Stranchi, L. 1960. Nucl. Instr. and Meth. 8 79.

Glendenning, N.K. 1963. Annual Rev. of Nucl. Sci. 13 191.

Goldman, L.H. 1968. Phys. Rev. 165 1203.

Goswami, A. and Sherwood, A.I. 1967. Phys. Rev. 161 1232.

Goulding, F.S., Landis, D.A., Carry, J. and Pehl, R.H. 1964. Nucl. Instr. and Meth. 31 1.

Griffiths, R.J., Knight, K.M., Candy, C.J. and Cole, J. 1962. Nucl. Instr. and Meth. 15 309.

Hjorth, S.A. and Cohen, B.L. 1964. Phys. Rev. 135 B930.

Holt, J.R. and Young, C.T. 1950. Proc. Phys. Soc. (London) A63 835.

Houdayer, A. 1972. Ph.D. Thesis, McGill University (Unpublished).

Johansson, S.A.E. 1965. Nucl. Phys. 64 147.

Kim, H.J., Robinson, R.L. and Johnson, C.H. 1971. Nucl. Phys. A167 65.

Kim, H.J., Robinson, R.L., Johnson, C.H. and Raman, S. 1970. Nucl. Phys. A142 35.

Kisslinger, L.S. and Sorensen, R.A. 1960. Kgl. Danske Videnskab. Selskab. Mat.-Fys. Medd. 32 No. 9.

Kisslinger, L.S. and Sorensen, R.A. 1963. Revs. Mod. Phys. 35 853.

Kozub, R.L. and Youngblood, D.H. 1970. Phys. Rev. C4 535.

Kunz, P.D. 1969. University of Colorado Report No. c00-535-606.

Landau, L.D. 1944. J. Phys. USSR 8 201.

Lane, A.M. 1953. Proc. Phys. Soc. (London) A66 977.

Lederer, C.M., Hollander, J.M. and Perlman, I. 1967. Table of Isotopes (John Wiley & Sons, New York).

Legg, J.C. 1963. Phys. Rev. 129 272.

Lindmayer, J. and Wrigley, C.Y. 1965. Fundermentals of Semiconductor Devices (Van Nostrand, Princeton).

Li, T.Y. and Mark, S.K. 1969. Nucl. Phys. A123 1.

Lin, E.K. 1965. Phys. Rev. 139 B340.

MacFarlane, M.H. and French, J.B. 1960. Revs. Mod. Phys. 32 567.

Maples, C., Goth, G.W. and Cerny, J. 1966. Nucl. Data Vol. 2, No. 5-6.

Mark, S.K. and Moore, R.B. 1966. Nucl. Instr. and Meth. 44 93.

Mark, S.K. and Standing, K.G. 1965. University of Manitoba, Cyclotron Laboratory Annual Report (1965).

McDonald, J. and Bäcklin, A. 1971. Nucl. Phys. A162 365.

McGrath, R.L., Cue, N., Hering, W.R., Lee, L.L. Jr., Liebler, B.L. and Vager, Z. 1970. Phys. Rev. Letts. 25 682.

Marrion, J.B. and Young, F.C. 1968. Nuclear Reaction Analysis (North-Holland, Amsterdam).

Morton, J.M., Davies, W.G., McLatchie, W., Darcey, W. and Kitching, J.E. 1971. Nucl. Phys. A161 228.

Ohnuma, H. and Yntema, J.L. 1968. Phys. Rev. 176 1416.

Perey, F.G. and Saxon, D.S. 1964. Phys. Letts. 10 107.

Phelps, M.E. and Sarantites, D.G. 1971. Nucl. Phys. A171 44.

Picard, J. and Bassani, G. 1969. Nucl. Phys. A131 636.

Picone, J.M., Coker, W.R. Fitch, J.F. and Moore, C.F. 1972. Phys. Rev. C6 1972.

Rabin, E. 1971. M.Sc. Thesis, McGill University, Montreal (Unpublished).

Riley, P.J., Horton, J.L., Hollas, C.L., Zaidi, S.A.A., Jones, C.M. and Ford, J.L.C. Jr. 1971. Phys. Rev. C5 1864.

Satchler, G.R. 1954. Proc. Phys.Soc. (London) A67 471.

Satchler, G.R. 1964. Nucl. Phys. 55 1.

Satchler, G.R. 1965. In Lecture in Theoretical Physics 1965, edited by P.D. Kunz, D.A. Lind and W.E. Britten (The University of Colorado Press, Boulder) p. 73.

Satchler, G.R. and Tobocman, W. 1960. Phys. Rev. 118 1566.

Schiffer, J.P. 1969. In Isospin in Nuclear Physics, edited by Wilkinson, D.H. (North-Holland, Amsterdam) p. 655.

Schiffer, J.P., Morrison, G.C., Siemssen, R.H. and Zeidman, B., 1967. Phys. Rev. 164 1274.

Sharpey-Schafer, J.F. 1968. Phys. Letts. 26 B652.

Smith, W.R. 1967. Atlas Laboratory Programme Library Report No. 7.

Stokes, R.H., Northrop, J.A. and Boger, K. 1958. Rev. Sci. Instr. 29 61.

Talmi, I. and Unna, I. 1960. Nucl. Phys. 19 225.

Tobocman, W. 1961. Theory in Direct Nuclear Reactions (Oxford University Press, New York).

Tucker, A.B. and Hein, W.W. 1970, Nucl. Phys. A155 129.

Turkiewicz, I.M., Beuzit, P., Delaunay, J. and Fouan, J.P. 1970. Nucl. Phys. A143 641.

Vervier, J. 1966. Nucl. Phys. 75 17.

Von Ehrenstein, D. and Schiffer, J.P. 1967. Phys. Rev. 164 1374.

Vourvopoulos, G., Shoup, R., Fox, J.D. and Ball, J.B. 1969. In Nuclear Isospin, edited by J.D. Anderson, S.D., Bloom, J. Cerny and W.W. True (Academic Press, New York) p. 205.

Wahlin, L. 1961. Nucl. Instr. and Meth. 14 281.

Wapstra, A.H. and Gove, N.B. 1971. Nucl. Data Tables A Vol. 9, No. 4-5.

Wilkinson, D.H. 1960. In Nuclear Spectroscopy, Part B, edited by F. Ajzenberg-Selove (Academic Press, New York) p. 859.

Williamson, C. and Boujot, J.P. 1962. Table of Range and Rate of Energy Loss of Charged Particles of Energy 0.5 to 150 MeV (CEN, Saclay).

Williamson, C., Boujot, J.P. and Picard, J. 1966. Centre d'Etudes Nucleaires de Saclay, Report No. CEA.-R3042.

Wolfe, B., Silverman, A. and Dewire, J.W. 1955. Rev. Sci. Instr. 26 504.

Yoshida, S. 1961. Phys. Rev. 123 2122.

Zurstadt, D. 1968. University of Colorado Report No. CYC-6742.

Zurstadt, D. 1969. University of Colorado Report No. CYC-6833.

APPENDIX

Low-Lying States of ^{80,82}Br from (d,p) Reactions

Published in Nuclear Physics A193 (1972) 225-235.

Appendix not microfilmed for reasons

of copyright.

ERRATA

"Low-Lying States of ^{80,82}Br from (d,p) Reactions" by Cheung *et al.*, Nucle. Phys. A193 (1972) 225:-

Page 231, line 21: $\left[(2p_{3/2})^{\pi}\,(1g^{3}_{9/2},\ v = J = 7/2)^{\nu}\right]_J$ should be $\left[(2p_{3/2})^{\pi}\,(1g^{5}_{9/2},\ v = 3,\ J = 7/2)^{\nu}\right]_J$.

Page 234, table 6: Entries in the column 'J^{π}' of the (d,p) reaction,

$(1,2)^{+}$ should be $(1,2)^{+}$, $(3,4,5,6)^{-}$, for E_x = 377 keV;

$(6,5,4,3)^{-}$ should be $(0,1,2,3)^{+}$, for E_x = 771 keV;

$(1,2)^{+}$ should be deleted for E_x = 845 keV.